University of Oslo
Department of Geosciences

Thermal Effects of Basaltic Sill Emplacement in Source Rocks on Maturation and Hydrocarbon Generation

Jørnar Heggsum Hubred

Cand.Scient-thesis

24th April 2006

URSO MAIORI - CUM GRATIIS MAXIMIS

"The stoneage did not end because we ran out of stones, the oil age will not end because we run out of oil" [1]

"Oil Isn't Going Away. The real threat is the ever-rising challenge of meeting global demand." [2]

"It is not possible to be a scientist unless you believe that it is good to learn... that it is of the highest value to share your knowledge... with anyone who is interested... that the knowledge of the world, and the power which this gives, is a thing which is of intrinsic value to humanity" [3]

[1] Sjeik Ahmed Zaki Yamani, oil minister Saudi Arabia 1962 - 1986, first secretary-general of OPEC, currently leader of Center for Global Energy Studies, London.

[2] Lee Raymond CEO ExxonMobil

[3] J. Robert Oppenheimer

Acknowledgments

I wish to thank my parents who have always encouraged me to pursuit with education. Without their efforts I would never have got this far. A big thanks also go to my grandfather Johan Heggsum who always was and will be a great example of how to live your life.

I am indebted to my supervisor Dr. Dag Karlsen who suggested this project and provided the data. Thanks to him also for his continuing interest in this work and for guidelines in preparing this manuscript. Kristian Baker Owe helped me at the lab and participated in many fruitful discussions. The people at the geology library provide a very good service fulfilling every literature request.

Thanks to Birger Dahl and Egil Rasmussen for allowing me to use the software PeGIS. Thanks to Ragnar Knarud, Norsk Hydro for encouragement and for borrowing me background literature on the Svalbard geology. Thanks to Nowell A. Briedis at ExxonMobil in Stavanger for reading through the orginal semester paper and give valuable feedback on the content (the semester paper has now grew into this thesis). Thanks to Jørgen Storvol at Store Norske Spitsbergen Kullkompani for the loan of the company Sodiak rubber boat.

Thanks to Realistforeningen and Akademisk Skytterlag for being the backbone of my social life during studies.

Thanks to the Department of Physics and especially to Dr. Torfinn Lindem for allow me to use one of their reading room places and encouragement during the last part of my thesis. Thanks to Senior Engineer Olav Borebekk for allow me to have my own computers connected to the Department of Physics IT network.

Thanks also to my friends that have encourage me and keep me going despite all adversity. A special thanks to those of you who have read through various parts of the thesis and given me feedback on both language and the content. You all know who you are. Thanks a lot!

At last, but equally important thanks to my sweetheart Chi Kwan Kwong for encouragement, morally support and patience.

This is the thesis for the Candidatus Scientarium degree at the Department of Geosciences, University of Oslo, Norway.

Oslo, April 2006

Jørnar Heggsum Hubred

Abstract

In sedimentary basins sills have a tendency to become emplaced in litholgies of lower mechanical competence, like shales, which can possess source rock qualities.

In this study has the thermal effects of thick sills on sedimentary rock units at Svalbard, Norway, been investigated. This study should be directly relevant for sills in large scale sedimentary basins. If sills were emplaced in contact with the source rocks at great burial depth, a "source rock on a hot plate" type of situation could arise with, a temperature-heat history quite unlike that of small dikes in shallow, water-rich sediments. An additional effect could be related to a regional increase in heat flow if the sills are in a sense "symptoms" of massive ingenious activity as known from other regions.

It is well proven that thin sills and dikes can locally mature source rocks, increase biomarker ratio in extractable compounds and at the same time cause systematic increases in kerogen maturity parameters. Few organic geochemistry results on large scale sills has been published. It is therefore not clear if massive sills simply could be viewed as a upscaling phenomena of the smaller dike and sill systems.

Samples were collected from eight different profiles with sills. The Triassic Botneheia black shale source rock formation, with dominantly marine kerogen, were collected from the hills of Botneheia (Central Spitsbergen), Teistberget (eastern Central Spitsbergen), Krefftberget and Høgrinden (Barentsøya Island). Samples were also collected from the Jurassic Janusfjellet black shale (with dominantly terrestrial kerogen) from Domen (eastern Central Spitsbergen) and the Wilhelmøya Island. Samples from identical black shale units in nearby sections not thermally affected by the sills were also collected and used for comparison.

Vitrinite reflectance, kerogen description, Rock Eval, TC and TOC were determined on all 170 samples, whereas EOM, Iatroscan TLC-FID, GC-FID and isotopic studies of C and O (in carbonates, kerogen and extracts) were conducted on 48 selected samples.

Results from this study would not only be relevant for sill intruded sedimentary basins but would possibly also be relevant for deep water exploration e.g. the Atlantic volcanic margin were sediments have experienced increased heat flows due to magmatic underplating.

Contents

Chapter 1

Introduction

This chapter describes the scope of work and briefly introduces sills, source rocks and the motivation for this study.

1.1 Motivation and Method

It is well known that sills in sedimentary basins have a tendency to become emplaced in litholgically weak zones, like organic rich shales, which have source rock qualities.

It is still debated, to what extent sills in sedimentary basins may affect the generation of hydrocarbons (HCs) from source rocks. Even more debated is the type of HCs that will be generated, i.e. the GOR of the petroleum. This issue is particularly important for exploration of oil in shallow basins, which depend upon sills for potential source rock maturation. Such basins exist in many regions, e.g. offshore Norway, on the shelf off South America and Africa.

1.1.1 Data samples

The samples which are the basis of this study were collected in 1995. Most of the analytical work was also completed in 1995. This work was a collaboration between the University of Oslo and the Norwegian Petroleum Directorate.

For various reasons the project ended before the results had been fully interpreted. None of the results have so far been published apart from a poster at the 19th International Meeting on Organic Geochemistry in Istanbul, 1999 by Dr. Dag A. Karlsen. The results from the 1995 study had basically lied untouched with regards to a deeper systematic review and interpretation until I asked Dr. Dag A. Karlsen for the possibility to do a Cand. Scient. project based on this material with him as supervisor.

1.1.2 Motivation

A lot of analytical work had been done in 1995. However, only initial interpretations of the data had been performed. It was therefore agreed that I, concerning

my thesis, should work through all the data from 1995, gather them into a database and use the data to address the following topics/questions:

- Vitrinite reflectivity is known to increase around intrusions. What is the relationship between the dimension of the intrusive body and the measurable thermal aureole? Is this higher maturity, indicated by vitrinite reflectance, also found by other maturity indicators?
- If maturity is shown to increase around sills also for maturity indicators other than vitrinite reflectance, is this sill maturation seemingly of the same type as maturation in normal subsiding basins, only faster?
- Can this study be utilized to evaluate the common rules of thumb concerning the extent of the aureole around a sill, one sill/dike thickness (Bostick, 1973) or two sill/dike thicknesses (Dow, 1977)?
- The importance of time on maturation and generation of oil is a topic extensively discussed in the literature. Can this study tell us something about the role of time as a factor for oil generation?

1.1.3 Methods

The samples had been microscopically examined and various geochemical analysis had also been performed. It was agreed that I should look at the results of the kerogen description, vitrinite reflectance, Rock Eval, Iatroscan TLC-FID, GC-FID and stable carbon- and oxygen-isotopes. A description of the analytical technics behind these results is included in the appendices together with the results.

The laboratory work was conducted partly at the University of Oslo and partly at the Institute for Energy Technology (IFE), Kjeller, Norway.

The results from the laboratory studies performed at UIO were obtained from Rock-Eval, Iatroscan TLC-FID and GC-FID analysis. The results from the laboratory studies done at IFE contained data on vitrinite reflectance, kerogen description and carbon isotopes. Much effort was spent making the data uniform in order to perform calculations on the whole dataset.

A few additional samples on the sill itself at the Botneheia site were collected by the author in 2002. These samples have been microscopically and analytically examined using GC-FID and GC-MS.

1.1.4 Interpretation of the data

Interpretations are to a large extent based on the use of plots taken from the literature. In Chapter 2, literature that deals with the same or adjacent themes to those relevant to this thesis is discussed. There the reader will find the original plots and a discussion of their relevance for this study.

To highlight special characteristics and results from the data in this study, plots not derived from plots in the literature have been made where considered appropriate by the author.

1.2 Key definitions

1.2.1 Source rocks, organic matter

Sedimentary rocks that are, or may become, or have been able to generate petroleum are *source rocks* (Tissot and Welte, 1984).

A rock, rich in *organic matter* (OM), if heated sufficiently, will generate oil or gas. Typical source rocks, usually shales or limestones, contain at least 0.5% total organic carbon (TOC), although a rich source rock might contain as much as 10% or more TOC. Source rocks of marine origin tend to be oil-prone, whereas terrigeneous source rocks (such as coal) tend to be gas-prone. Preservation of organic matter without degradation is crucial for a good source rock, and necessary for a complete petroleum system.

1.2.2 Maturity

Temperature affects chemical bonds in OM, causing them to break progressively at higher temperatures and deeper burial. *Maturity* reflects this temperature development and the state of a source rock with respect to its level of generating oil and gas. As a source rock begins to mature, the temperature driven reactions convert OM to oil, wet gas, and finally to dry gas and pyrobitumen. Thermally *immature* OM has been affected by chemical, biological and physical changes to OM during and after deposition of sediment prior to reaching burial temperatures greater than about 60° - 80 °C and without a pronounced effect of temperature. Thermally *mature* OM is (or was) in the *oil window* and has been affected by thermal processes covering the temperature range that generates oil; 60° - 150 °C. Thermally *post mature* OM is in the wet and dry gas zones (gas window) and has been heated suficiently (about 150° - 200 °C) to have been reduced to a hydrogen-poor residue, capable of generating only small amounts of hydrocarbon gases (temperature intervals and OM *maturity* definitions (Tissot and Welte, 1984)).

Virgin values

When discussing maturity later in the thesis the term *virgin* will be used for maturity measurements on samples thought to be unaffected by sills.

1.2.3 Kerogen

The term *kerogen* was applied for the first time in the description of shales in Scotland where it was used to refer to the organic mineraloid of indefinite chemical composition (Baker, 1972). In recent years, however, this term has been applied not only to organic matter in oil shales, but also to carbonaceous matter in a wide range of rocks regardless of their oil generating potential (Tissot and Welte, 1984). In this thesis the term kerogen is therefore used to describe the disseminated organic matter which is non-soluble in non-oxidizing acids, bases and organic solvents. Kerogen thus constitutes a complex mixture of structural

and amorphous phytoclasts of different aquatic and terrestrial origin, with contrasting chemical structures and hydrocarbon potential (Dow, 1977; Espitalie et al., 1977).

1.2.4 Intrusions

Igneous rocks are divided into 2 groups, extrusive and intrusive. *Extrusive rocks* form when magma reaches and flows onto the surface of the earth or floor of the ocean through deep cracks or fissures at volcanic vents, and then cools and hardens. *Intrusive rock* results when magma is forced into cracks or between layers of preexisting rocks and solidifies beneath the earth's surface. In general, extrusive rocks have a finer grained texture than intrusive rocks due to more rapid cooling; intrusive rocks vary from thin sheets to huge, irregular masses. Discordant intrusions that are vertical, or nearly so, are called *dikes*. Concordant intrusions that are horizontal, or nearly so, are called *sills*. These terms will be further defined in the next chapter.

1.3 Organization of the text

Known theory and results from other studies are presented in chapter 2. Chapter 3 introduces the reader to the large scale geological framework of Svalbard, leading to chapter 4 which deals with the field work done here in 1995. In chapter 5, all main results are shown and discussed. A summary of conclusions and a list of further work are featured in the final chapter (chapter 6).

Analytic technique descriptions, measured values and calculated parameters that are interdependent is grouped into chapters in the appendix.

Please consider the abstract for, and the poster presented at the 22nd International Meeting on Organic Geochemistry (IMOG 2005) included in appendix J.

Among the appendices I have also included the compulsory semesterpaper which I did as a prestudy before I started working on this thesis. The semesterpaper is a summary of the development of organic geochemistry and a discussion of how organic geochemistry results can be utilized in basin modeling, which at that time was foreseen as an important part of my thesis (appendix L).

Data CD-rom This thesis and all the analytical results from this study are included on the CD following the printed version of this thesis. The CD also includes software for viewing these results. A program for browsing the content of the CD will start automatically under Windows 2000/XP.

Chapter 2

Fundamental geological understanding of intrusions and maturation. Geochemical methods used in this study

In this chapter basic geological terms and theory on volcanic systems are presented. This basis of understanding is taken from a multitude of published sources and will be of importance as the potential generation of hydrocarbons next to sills are discussed in later chapters.

2.1 Volcanic systems

Volcanic systems are not limited to the sterotype form, cone-vulkanos and massive intrusive bodies, but characteristically include small intrusions, often in such large numbers as to rival the volume of the volcano. Intrusions having a narrow sheet-like form predominate. Propagation of sheet-like intrusions by hydraulic fracturing occurs very readily.

The nomenclature of sheet-like intrusions is slightly confusing, because it is based on two different criteria, namely dip or whether the intrusion are concordant or discordant to the countryrock bedding. Discordant intrusions that are vertical, or nearly so, are called dikes. Concordant intrusions that are horizontal, or nearly so, are called sills.

2.1.1 Sills

Sills underlie many flood-basalt regions. They can have large individual volumes, comparable with flood-basalt lava flows. Sill swarms can rival flood-basalts in total volume (Walker and Poldervaart, 1949)

Sills mostly intrude thick sedimentary rock sequences that, at the time of sill intrusion, were young and poorly consolidated. It has been interfered that levels of neutral buoyancy exists between well- and less well-consolidated sediments,

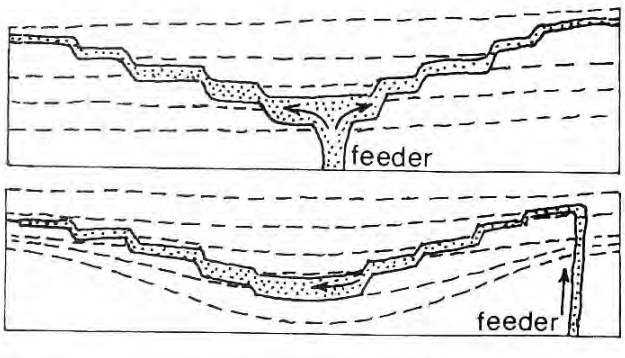

Figure 2.1: *Saucer-shaped sills; dashed lines are countryrock stratigraphic horizones; Upper figure: magma injected at the low-point (Carey, 1958). Lower figure: magma injected at a high level and accumulating at bottom of sedimentary basin (Francis, 1982).*

or alternatively that the sill magma simply flows under loose sediment. Bradley (1965) recognized that if magma is denser than the rock it intrudes, the roof of countryrock may effectively float on the magma. This is, however, an oversimplification of the situation since the magma has the capability of reaching the surface and building a volcano there.

Sills characteristically transgress across the countryrock bedding. Carey (1958) investigated this transgression in a Tasmanian sill by constructing isostratigraphic lines on a map connecting points where the sill is in contact with the same stratigraphic horizon and demonstrated that the sill has the overall form of a lowangle inverted cone saucer relative to the stratigraphy. He inferred that magma was injected at the low point of the cone down into the sedimentary basin. Francis (1982) found a similar pattern of isostratigraphic lines for the Whin Sill and observed that the sill systematically thickens toward the low-point (Figure 2.1).

It is probable that sills can form without surface volcanism. A possible example may be the sills penetrated by drillholes in the Fastnet Basin (Caston et al., 1981) where coeval volcanism appears to be absent.

2.1.2 Dikes

Bruce and Huppert (1990) showed that narrow dikes can travel only a short distance before they are blocked by rapid cooling. The number and total width of dikes injected in a given time interval therefore decrease strongly with distance outward from a volcanic center (Walker and Blake, 1988). Dikes injected within a given time interval therefore constitute a wedge tapering downrift. Their injection sets up localized stress in the central region that are relieved by the formation of intrusions approximately orthogonal to the general trend. Asymmetric addition of dikes to one side of a rift zone can cause originally collinear rift zones to become noncollinear.

Lateral dike-injections from a high-level magma chamber are thought to be

important near volcanic centers, but farther away dikes may commonly be vertically upward from a deep reservoir (Gautneb and Gudmundsson, 1992).

2.2 Alteration of Organic Matter

Diagenesis refer to all chemical, biological and physical changes to OM during and after deposition of sediment prior to reaching burial temperatures greater than about 60° - 80 °C. The quantity and quality of organic matter preserved and modified during diagenesis of a sediment ultimately determine the petroleum potential of the rock.

Catagenesis can be divided into the *oil zone*, which corresponds to the *oil window*, where liquid oil generation is accompanied by gas formation, and the more mature *wet gas zone*, where light hydrocarbons are generated through cracking and their proportion increases rapidly (Tissot and Welte, 1984). *Wet gas* (<98% methane) contains methane and significant amounts of ethane, propane, and their heavier hydrocarbons. The *gas window* corresponds to the interval from the top of the wet gas zone to the base of the dry gas zone.

Metagenesis corresponds to the *dry gas zone* where dry gas is generated . *Dry gas* consists of 98% or more methane (Tissot and Welte, 1984).

Maturity

For source rocks the diagenesis state of the rock is measured as *source rock maturity* as long as it has not passed over into greenshist metamorphism. Please see the definition for *maturity* in the Introduction chapter, section 1.2 on page 3 and section 2.3, this chapter.

2.2.1 Intrusions and their impact on maturity

Contact metamorphism affects the maturity of OM in intruded rocks to a distance which depends on various factors including; 1) the temperature difference between the sill/dike and the invaded rock; 2) the depth of emplacement; 3) water content of the host rock/sediment and 3) the rate of cooling. A traditional rule of thumb is that the distance or the thermal aureole extends to about one and two times the thickness of the intrusive body (Peters et al., 1978).

2.3 Methods used in this study to determine maturity

Maturity is a measurement about whether or not a source-rock has expelled hydrocarbons or not, and if hydrocarbons have been expelled, the degree of expulsion. One of the goals for this thesis was to see if or not, a sill emplaced into a source-rock, is able to mature the source-rock, sufficient for it to expel its hydrocarbons. In the following subsections I will shortly explain the maturity measurement methods utilized in this thesis study.

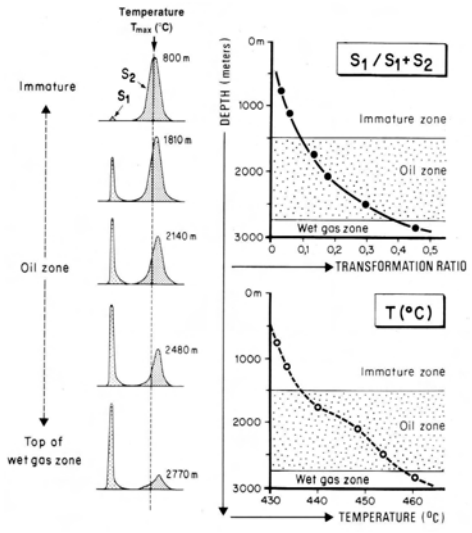

Figure 2.2: *Characterization of source-rock maturity by the pyrolysis methods. Figure shows how S_1, S_2 and* $\mathbf{T}_{textmax}$ *changes with increasing maturity.* $\mathbf{T}_{max}$ *approaches higher values with increasing maturity because activation energies for remaining kerogen increases with maturity (Tissot and Welte, 1984).*

2.3.1 TOC

TOC (wt. %), describes the quantity of organic carbon in a rock sample. TOC includes both kerogen and bitumen. The TOC measurement is used as an indicator of petroleum potential, but is not a clear indicator of this potential since e.g. graphite is essentially 100% carbon, but will not generate petroleum. This is why the use of hydrogen index (HI) is used in conjunction with TOC, see below.

Applied to estimating maturity close to sills/dikes, a decrease in TOC is expected when approaching the sill/dike.

2.3.2 Rock Eval

Pyrolysis is defined as heating of organic matter in the absence of oxygen, to yield organic compounds. In Rock-Eval pyrolysis, pulverized samples are gradually heated in an inert helium atmosphere. This heating distills the free organic compounds (free hydrocarbons; $C_1 - C_{25}$, Karlsen and Larter (1989)). It then cracks kerogen to yield pyrolytic products from the insoluble organic matter (kerogen).

- $\mathbf{S}_1$ measures at 300°C the free hydrocarbons that can be volatilized out of the rock without cracking the kerogen (mg HC/g rock). S_1 increases at the expense of S_2 with maturity.
- $\mathbf{S}_2$ measures the petroleum yield from cracking of kerogen (mg HC/g rock) and heavy hydrocarbons. S_2 represents the existing potential of a rock to

generate petroleum. S_2 is a more realistic measure of source-rock potential than TOC because TOC includes "dead carbon" incapable of generating petroleum.

- $\mathbf{S_1 + S_2}$ is a measure of genetic potential or the total amount of petroleum that might be generated from a rock.

Production index

[PI = $S_1/(S_1+S_2)$] gradually increases with depth for fine-grained rocks, as thermally labile components in the kerogen (which will in analysis be denoted S_2) are converted to free hydrocarbons (S_1). Reservoir rocks show anomalously high PI values compared to adjacent fine-grained rocks. For $\mathbf{T_{max}}$ values of <435°C and $\mathbf{T_{max}}$ in the range 435° - 445° C, **PI** values exceeding 0.4, respectively, are considered anomalous.

Approaching sills we would expect the production index to increase.

Hydrogen index

[HI =(S_2/TOC) x 100, mg HC/g TOC]is proportional to the amount of hydrogen in the kerogen and thus indicate the potential of the rock to generate oil. High hydrogen indices indicate greater potential to generate oil. **HI** values are readily convertable to geologically usefull figures e.g. a **HI**=700 means that 70% of the **TOC** can be converted to oil and gas.

Although **HI** versus **OI** plots are generally reliable indicators of kerogen type, gas-prone coals and coaly rocks can give anomalously high **HI** values that must be confirmed by elemental analysis (Peters, 1986). The average **HI** in a rock interval is best determined from the slope of a regression line on a graph of S_2 versus TOC (Langford and Blanc-Valleron, 1990).

Approaching sills we would expect the hydrogen index to decrease.

Petroleum potential	TOC (wt. %)	S_1 (mg HC/g rock)	S_2 (mg HC/g rock)
Poor	0-0.5	0-0.5	0-2.5
Fair	0.5-1	0.5 -1	2.5-5
Good	1-2	1-2	5-10
Very good	2-4	2-4	10-20
Excellent	>4	>4	>20

Table 2.1: *Geochemical parameters describing source-rock generative potential. Values taken from Peters and Cassa (1994).*

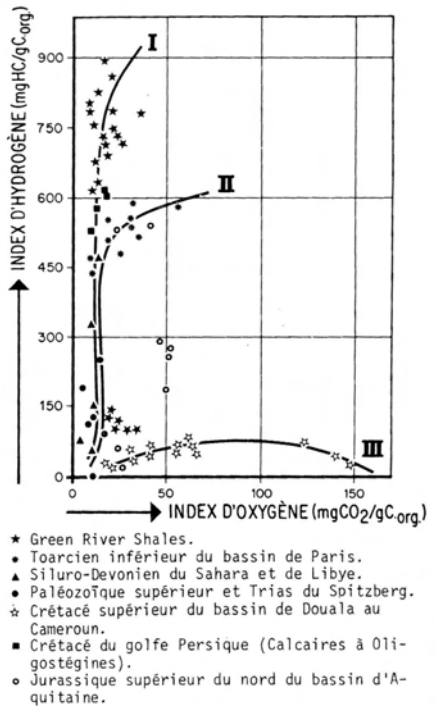

(a) The "modified" Van Krevelen diagram

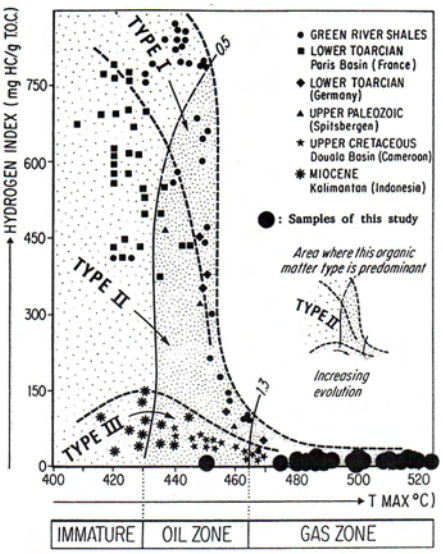

(b) The "modified modified" Van Krevelen diagram

Figure 2.3: *The modified van Krevelen diagrams. The first diagram was described by Espitalie et al. (1977) in the first article describing the use of the Rock-Eval instrument. The second Figure 2.3(b) was described in Espitalie et al. (1984) as a substitute plot for the 2.3(a) in situations were the S_3 results are suspected unreliable because of interference from thermally labile carbonate minerals or kerogen oxidation resulting from pulverizing the sample.*

Oxygen index

[OI = (S_3/TOC) x 100, mg CO_2/g TOC] is related to the amount of oxygen in the kerogen. In general, the S_3 measurement is not as reliable as other Rock-Eval parameters, partially because of interference of carbonate minerals or kerogen oxidation resulting from pulverizing the sample. Alternatively one can determine **OI** When S_3 results are suspected to be unreliable, **HI** versus $\mathbf{T_{max}}$ (Espitalie et al., 1984) can be substituted for the **HI** versus **OI** plot (Figure 2.3).

Approaching sills we would expect the oxygen index to decrease.

$\mathbf{T_{max}}$

measures thermal maturity and corresponds to the Rock-Eval pyrolysis oven temperature (°C) at maximum S_2 generation. $\mathbf{T_{max}}$ should not be confused with geologic temperatures. $\mathbf{T_{max}}$, is partly useless for type I kerogens due to their

narrow activation energy distribution (Peters, 1986). $\mathbf{T_{max}}$ values and generally accepted maturity levels are given in Table 2.2.

Approaching sills we would expect $\mathbf{T_{max}}$ to increase.

The HI-OI and HI-T_{max} diagrams

Elemental analysis shows that carbon and hydrogen are the main atomic constitutes in all types of kerogen. For 1000 carbon atoms, hydrogen varies between 500 and 1800 atoms depending on the type and evolution of the organic matter. The atom next in abundancy, oxygen amounts to only 25 to 300atoms (Tissot and Welte, 1984). Kerogen in immature source-rock samples will have a higher H/C and O/C ratio compared to samples of the same source-rock which have been buried deeper and hence have experienced higher pressure and temperature. This decrease of H/C and O/C ration in more mature samples is due to the generation and release of hydrocarbons. Hence the kerogen type is not entirely independent of maturity and kerogen will become increasingly "coaly" with increasing maturity (Section 2.4.2).

Using Rock-Eval data, the type of kerogen is characterised by two indicies: the *hydrogen index* ((S_2/organic carbon)×100) and the *oxygen index* ((S_3/organic carbon)×100). The indicies are independent of the abundance of organic matter and are strongly related to the elemental composition of kerogen. In particular there is a good correlation between the hydrogen index and H/C ratio, and between the oxygen index and O/C ratio, respectivly (Figure **??** on page ??).Thus the two indices can be plotted in place of the normal van Krevelen diagram, and interpreted in the same way (Figure 2.3).

2.3.3 Extractable organic matter (EOM)

Saturated hydrocarbons/aromatic hydrocarbons

The saturated hydrocarbons/aromatic hydrocarbons ratio (SAT/ARO) mainly reflect source-rock quality and maturity (Cornford et al., 1983; Clayton and Bostick, 1986). The ratio increase with increasing thermal maturity, but will also increase in the gas-phase of phase-fractionated petroleum during the migration to shallower depths.

Approaching a sill an increase in this ratio is expected as the remaining kerogen itself becomes aromatized.

$T_{max} < 425°C$	immature
$T_{max} < 435°C$	just mature
$T_{max} 435° - 465°C$	mature
$T_{max} > 465°C$	over mature

Table 2.2: $\mathbf{T_{max}}$ *values and generally accepted maturity levels*

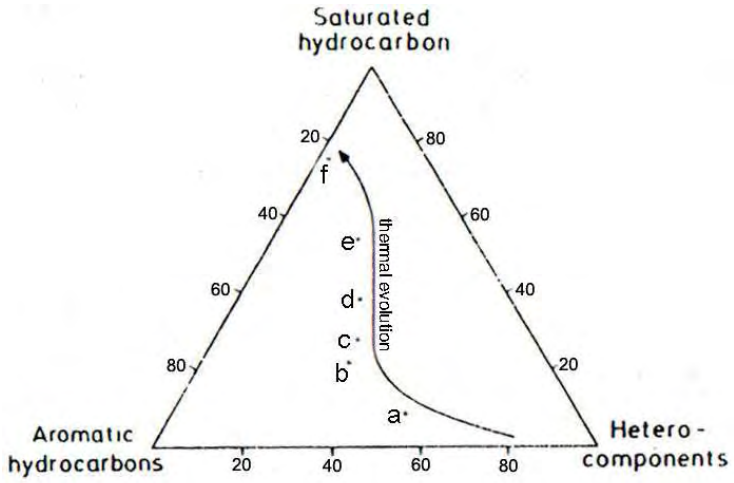

Figure 2.4: *Relative distribution of saturated hydrocarbons, aromatic hydrocarbons and polar components in extracts. Asphaltenes and evaporative losses during preparation are excluded. Increassing thermal alteration is indicated on the diagram a: 177868, b: 177840, c: 177839, d: 177838, e: 177836, f: 177834 (Schiener and Perregaard, 1981).*

Polar compounds relative to the amount of saturated hydrocarbons

Schiener and Perregaard (1981) reported a thermal evolution from polar to saturated hydrocarbons (Figure 2.4). I will come back to this in Chapter 5.

2.3.4 GC-FID

Gas-chromatographic analysis is used for quantification of individual hydrocarbon components and is usually carried out on whole oils, total extracts or saturated and aromatic hydrocarbon fractions of crude oils and bitumens. The GC-FID instrument, Figure C.1 on page 192, was used for detailed geochemical facies and maturity characterization by use of the n-alkanes and isoprenoid distributions.

Carbon Preference Index (CPI)

CPI was first introduced by Bray and Evans (1961) and can be used to indicate the thermal maturity of an oil or extract. Immature source rocks with significant input of land plant organic matter (terrestrial organic matter) are dominated by odd-carbon-numbered n-alkanes. High molecular weight alkanes derived from marine organic matter tend to have little or no carbon-number preference, or in the case of some hypersaline carbonate and evaporite source-rocks, a slight preference for even-numbered n-alkanes. In all cases, carbon-number preference approach 1.0 with increasing maturity. This trend is attributed to a combination of the thermal generation of n-alkanes from kerogen derived from different biological precursors and from thermal cracking of early diagenetic hydrocarbons

creating a product with no odd/even preference that volumetrically overwhelms the pre-existing alkanes. Hence, while high CPI indicates low maturity and land plant input, oils and source-rocks with CPI~1 may arise from a predominance of marine input and/or thermal maturation of any type of organic matter.

Approaching a sill we would expect values to become closer and closer to 1.0.

The n-Pristane/n-Phytane ratio

Pristane and phytane are isoprenoid isoalkanes and are, according to the traditional view, derived from the phytyl side-chains in chlorophyll (Tissot and Welte, 1984). Whether the phytyl transforms into pristane or phytane is determined by the degree of anoxia in the environment of deposition. Under anoxic conditions in sediments, the phytyl side chain is cleaved to yield phytol, which is reduced to dihydrophytol and then phytane. Under oxic conditions, phytol is oxidized to phytenic acid, decarboxylated to pristene and then reduced to pristane.

In samples of low thermal maturity, Pr/Ph ratios are not recommended to describe paleoenvironment. For samples within the oil-generative window, high Pr/Ph ratios (Pr/Ph < 3) indicates terrestrial organic matter under oxic conditions and low values (Pr/Ph < 0.6) typify anoxic, commonly hypersaline environments. Low wax oils from marine source-rocks often have a Pr/Ph ratios in the range 1 to 3. For samples showing Pr/Ph in the range 0.8 to 2.5 it is however not recommended that Pr/Ph its being used as an indicator of paleoenvironment without corroborating data (Peters and Moldowan, 1993).

The ratio can also be used as a maturity indicator because it typically increases with increasing maturity (Alexander et al., 1981), but because pristane and phytane, during diagenesis, can be derived from sources other than phytol e.g. bacterial membranes (ten Haven et al., 1987), the ratio should be used together with other parameters.

Approaching a sill an increase of this ratio is expected.

Isoprenoid/n-paraffin ratios

Pristane/n-C_{17} and Phytane/n-C_{18} ratios are used in addition to other parameters to determine source-rock facies, maturity and the level of biodegradation of hydrocarbons. Low ratios indicate a more mature sample, because the isoprenoids will break down earlier than n-alkanes during maturation. This is because tertiary carbon-carbon bonds have lower stability than primary and secondary carbon bonds. The ratios can be used together with other parameters to rank related, nonbiodegraded oils and bitumens based on thermal maturity. Still, care should be taken because organic input and biodegradation may affect the ratio (Peters and Moldowan, 1993).

Plotted together Shanmugam (1985) and others showed Pr/n-C_{17} vs. Ph/n-C_{18} to give information about sedimentological depositional environment and degree of maturation/biodegration (Figure 2.5).

Approaching a sill a lovering of these ratios is expected.

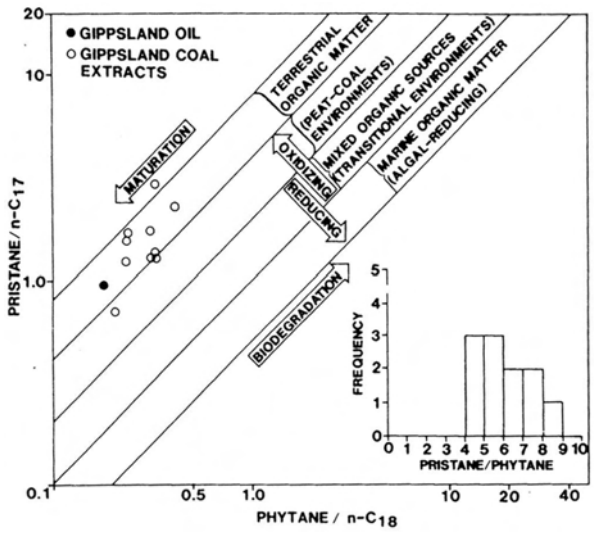

Figure 2.5: *Plot of pristane/n-C_{17} vs. phytane/n- C_{18} showing terrestrial source for hydrocarbons. (Histogram shows pristane/phytane ratio of oil and coal extracts) (Shanmugam, 1985).*

2.3.5 Vitrinite

Optical reflectance of vitrinite can be measured in a microscope and is frequently used as an maturity indicatior. Vitrinite reflectance (R_o) increases during thermal maturation due to complex, irreversible aromatization reactions. Approximate R_o values have been assigned for the beginning and end of oil generation (Table 2.3). R_o versus depth plots generally show linear trends on a semi-log scale. Dow (1977) showed how these plots can be used to support the existence of faults, intrusion, and changes in geothermal gradient and how to estimate the thickness of a section lost at an unconformity.

Applied to estimating maturity close to sills/dikes, an increase in vitrinite reflectance is expected when approaching the sill/dike.

2.4 Measurements not primary focusing on maturity which have been used in this study

2.4.1 Carbon isotopes (the ^{13}C contents)

The carbon isotopic composition of any naturally synthesized organic compound depends on (1) the carbon source utilized, (2) isotope effects associated with assimilation of carbon by producing organism, (3) isotope effects associated with metabolism and biosynthesis, and (4) cellular carbon budgets (Hayes, 1993).

The isotopic composition of the molecule can indicate the isotopic composition of the parent organism and that in turn, can reveal the carbon source util-

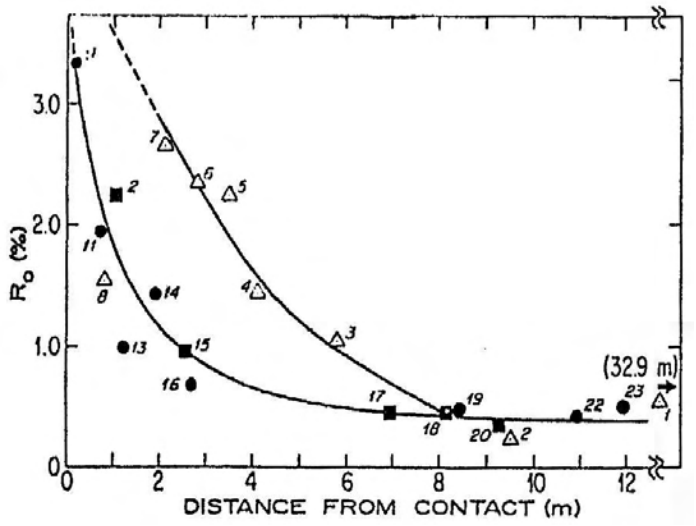

Figure 2.6: *R_o values plotted versus distance above (△) or below (■) sill. Below-sill data (•) from Baker et al. (1977) (Peters et al., 1978).*

ized by the producer and thus its position within the ancient ecosystem. Because these factors are in turn dependent on environmental conditions, the distribution of ^{13}C among natural products is a sensitive paleoenvironmental indicator that can provide much information about ancient biogeochemical processes.

The plots of the isotope values of separate compounds in EOM will permit grouping of different families and the variation in the source of these hydrocarbons can easily be recognized. Thereby, isotope values can be used to identify the different source kitchens involved in generating the hydrocarbons.

The values are presented relative to the standard PeeDee Beleminite (PDB).

$$\delta^{13}C‰ = \frac{(^{13}C/^{12}C)\text{sample} - (^{13}C/^{12}C)\text{standard}}{(^{13}C/^{12}C)\text{standard}} \times 1000 \qquad (2.1)$$

Equation 2.1 found in Tissot and Welte (1984).

The carbon isotope composition of petroleum hydrocarbons appears to be largely independent of maturation or migration processes (Fuex, 1977). Therefore it has been used as a indication of genetic relations between petroleum hydrocarbons. (The $\delta^{13}C$ value of kerogen will be slightly inflected by maturity. Hence kerogen will become a little isotopic heavier as isotopic light carbon is removed from the system in the form of petroleum and gas (Galimov, 1980)).

2.4.2 Kerogen description

Kerogen characterization and the distinction between its various types are essential for source-rock evaluation. This is because different types of organic matter have contrasting chemical structures, and, consequently, different hydrocarbon potentials. Qualitative and semi-quantitative assessment of kerogen

$R_o < 0.5$ to 0.7%	diagenesis stage	source rock is immature
0.5 to 0.7% $< R_o <$ 0.7 to 1.3%	catagenesis stage	main zone of oil generation
$ca.1.3\% < R_o < 2\%$	catagenesis stage	zone of wet gas and condensate
$R_o > 2\%$	metagenesis stage	dry gas zone

Table 2.3: *Vitrinite values, generally accepted diagenesis stages and maturity levels.*

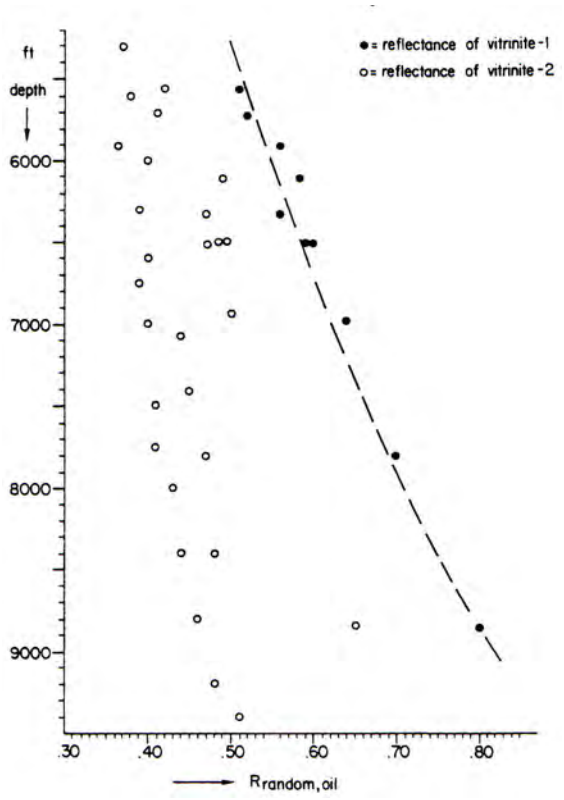

Figure 2.7: *A well-plot showing the importance to select vitrinite phytoclastes of type 1 when conducting temperature studies (Buiskool Toxopeus, 1983).*

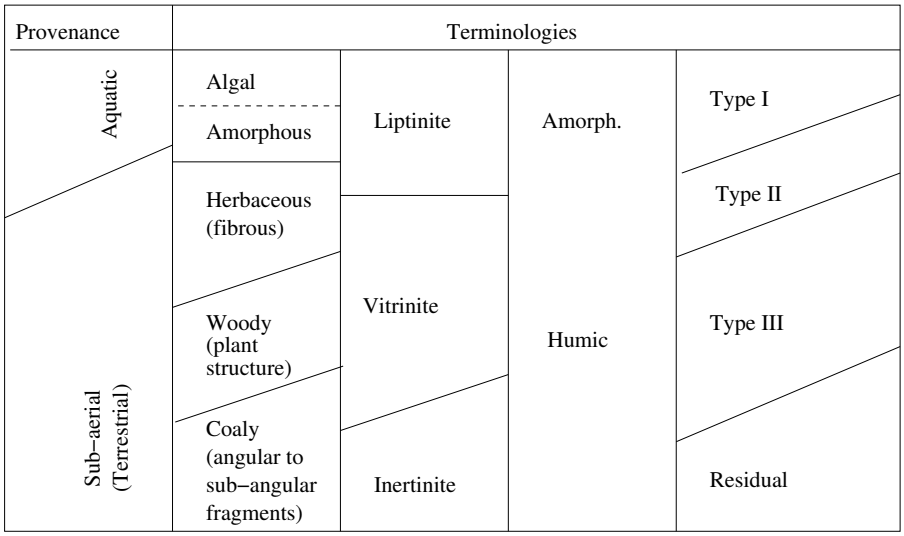

Table 2.4: *Approximate equivalence of various terms used in kerogen description. Table redrawn from original in Tissot and Welte (1984)*

concentrates offer a geochemical basis for the evaluation of potential source-rocks. This has been shown to be successful in following the maturation of kerogen.

Kerogen description is a visual estimate of the percentage amount of a kerogen type.

A general classification based on optical examination was proposed by Combaz (1980), who first characterized the individual organic constitutes and then grouped them in major classes: remnants of terrestrial plants (spores and pollen grains, vegetal fragments); algae and related microflora (acritarcs, leiosphaeridaceae and tasmanaceae, dinoflagellates, colonial and benthic algae); microfauna (chitinozoa, gigantostraceae, graptolites, scolecodontes and microforaminifera); and the amorphous fraction (aggregates, granular, subcolloidal, pellicular, gelified). Based on their occurrence and and association, it becomes possible to define *palynofacies*, which can be compared with the types of organic mater defined upon chemical analysis of kerogen (Combaz, 1980).

More general terms are normally used by petroleum geologists who usually distinguish between five types of kerogen:

- **Algal kerogen (AL):** is the amount of algal material as percentage of total kerogen. Determined from visual analysis of the concentrated kerogen fraction. Algal kerogen is generally regarded as being "oil prone" and may generate both oil and gas upon maturation.

- **Amorphous kerogen:** is the amount of amorphous or nonstructured kerogen as percentage of total kerogen. Determined by visual analysis of the concentrated kerogen fraction. Amorphous kerogen is generally regarded as being "oil prone" and may generate both oil and gas upon maturation. In

Appendix G, where the results from this study are listed, amorphous material is further subdivided in **FA**, which is fluorescing amorphous material, and **HA**, which is non-fluorescing amorphous material. **FA** is regarded oil-prone whereas **HA** is not believed to have any hydrocarbon potential or at best a little potential for gas (Tissot and Welte, 1984).

- **Herbaceous kerogen (HE):** is the amount of herbaceous kerogen (i.e. membranous plant materials) as percentage of total kerogen. It is determined from visual analysis of the concentrated kerogen fraction. Herbaceous kerogen is generally regarded as "oil prone" and may generate both oil and gas upon maturation.

- **Woody kerogen (WO):** is the amount of woody kerogen as percentage of total kerogen. Determined by visual analysis of the concentrated kerogen fraction. Woody kerogen is thought to generate primarily gas upon maturation.

- **Coaly kerogen (CO):** is the amount of coaly kerogen as percentage of total kerogen. It is determined by visual analysis of the concentrated kerogen fraction. Coaly kerogen is thought to generate primarily gas upon maturation.

This division of the kerogen types is based upon Burgess (1974). For a approximate equivalence of the various terms used in kerogen description see Table 2.4.

Thermal alteration index (TAI)

The thermal allteration index is based on visual comparision of the colour of kerogen concentrates relative to a standard. Organic particles become brown and eventually black with increasing maturity (Bostick, 1971; Tissot and Welte, 1984).

2.4.3 Volumetric calculation of generated petroleum

To calculate the potential, for the source rocks of this study, to generate petroleum we used the calculation approach proposed by Schmoker (1994), Figure 2.8(a).

The outline of this approach is as follows:

1. The source-rock is identified and its boundaris are defined.

2. The mass of organic carbon in the source-rock is calculated.

3. The mass of hydrocarbons generated per unit mass of organic carbon is estimated.

4. The total mass of hydrocarbons generated is determined by multiplication of these data.

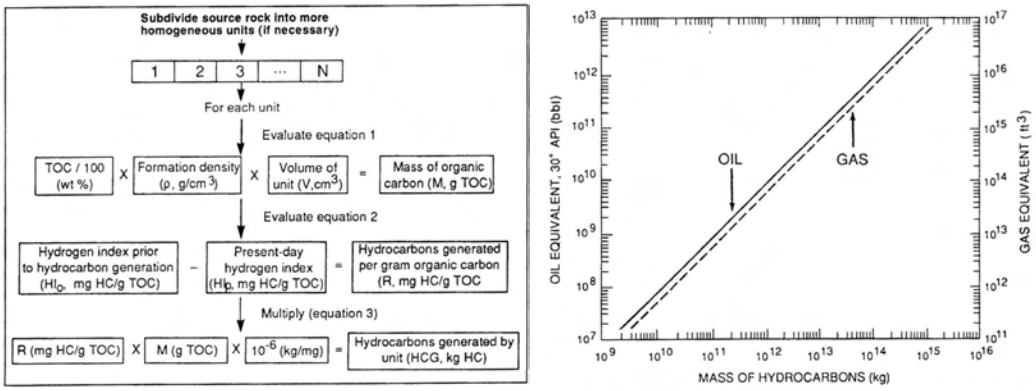

(a) Flow diagram of method for approximate calculation of mass hydrocarbons generated.

(b) Graph to convert mass of hydrocarbons to equivalent barrels of oil or cubic feet of methane

Figure 2.8: *Figures from Schmoker (1994).*

Description of claculation method

In its initial step, the source-rock is identified, and if necessary, subdivided into mapable units of more homogenous physical and geochemical properties. The calculation of hydrocarbons generated is then caried out for each source-rock unit and the results summed up to give a total for the petroleum system.

In the next step, the mass of organic carbon, M (g TOC), in each source rock unit is determined. The data neded to calculate M are the average TOC (wt. %), average formation density, ρ (g/cm^3) and volume, V (cm^3), of the unit. Multiplication of these three parameters gives the mass of organic carbon in the source-rock unit:

$$M(\text{g TOC}) = [\text{TOC (wt. \%)}/100] \times \rho(\text{g/cm}^3) \times V(\text{cm}^3) \tag{2.2}$$

In the third step, the mas of hydrocarbons generated per unit mass of organic carbon, R (mg HC/g TOC), for each source-rock unit is determined. The data needed to calculate R are the present-day hydrogen index, HI_p(mg HC/g TOC), and the original hydrogen index, HI_o(mg HC/g TOC), of the source-rock prior to any petroleum generation. The difference between these two indices approximates the mas of hydrocarbons generated per gram TOC:

$$R(\text{mg HC/g TOC}) = HI_o\,(\text{mg HC/g TOC}) - HI_p\,(\text{mg HC/g TOC}) \tag{2.3}$$

This equation gives the decline in generation potential to hydrocarbons actually generated. HI_p is derived from pyrolysis analysis; HI_o can be derived from pyrolysis analysis of thermaly immature samples if it is geologically reasonable to assume no variations in kerogen type. Alternatively, HI_o can be estimated from the genetic trends of van Krevelen-type diagrams (e.g., 2.3).

In the final step, the total mass of hydrocarbons generated, HCG (kg HC) is calculated:

$$HCG(\text{kg HC}) = R(\text{mg HC/g TOC}) \times M(\text{g TOC}) \times 10^{-6}(\text{kg/mg}) \qquad (2.4)$$

Volumetric hydrocarbon units (bbl of oil or ft^3 of gas) may be more familiar than the mass units of Equation 2.4. Figure 2.8(b) provides a graph to convert kilograms of hydrocarbons to equivalent barrels of oil or cubic feet of methane.

2.5 Other factors examined which is important for understanding intrusions

2.5.1 Time

In regionale coalification process, time is accepted as having a significant role in causing rank increase, when relatively low temperatures (T≈100-200°C for the formation of bituminous coals and anthracites) are maintained over many millions of years. In contrast, when magmaes are intruding at temperatures possibly exceeding 1000°C, temperature is conventionally held to be predominant in producing the molecular alterations of minerals and organic matter. There, time is of only minor importance.

This generalization oversimplifies the complicated relationship that exists between temperature level and length of exposure to elevated temperatures. It also ignores other factors such as the original maturation level of the organic matter before intrusion and the degree of lithification of the country rocks, their porewater content and porosity at the timespan of the intrusion activity.

2.5.2 Temperature

The temperature of intrusions varies greatly depending on their magma composition. So do also the intrusion volume and the timespan during which magma flows. These factors largely determine the time-period and increased level of temperature the country rock adjacent to the intrusion is raised to above the regional background temperature. Although these time-periods are short compared to the time-scale associated with with regional coalification process, a doubling of the time, must produce differences in the resulting organic products.

2.5.3 Heat flow modeling

The cooling of dike like igneous bodies using heat flow theory was initially addressed by Lovering (1935). Loverings's model did not consider the latent heat of crystallization, which, at about 400000 J/kg of melt, is an important factor that can increase estimated temperatures within the dike contact aureole on the order of 100°C (Jaeger, 1957). Bostick and Pawlewicz (1984) showed that $T_{\max}$ estimated from R_{v-r} and a vitrinite-reflectance geothermometer calibrated with laboratory heating experiments is generally 50-100°C higher than what is calculated by the model of Lovering (1935). Implying that the effects of latent

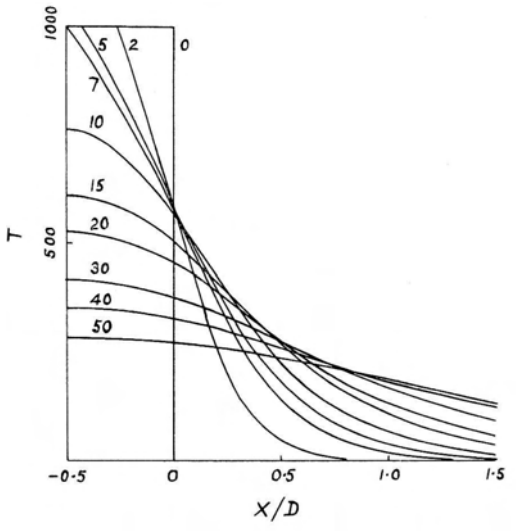

Figure 2.9: *Temperature T, as a function of the distance X (meters) from the margin of a sill/dike. D is the thickness of the sill/dike in meters. The sill/dike has a melting point of 1000° C intruded into wet sediments of porosity 0.2 in which the boiling point of water is 200° C. The numbers on the curves are times in multiples of $10^{-3}D^2$ years (Jaeger, 1959).*

heat should be included when calculating temperatures next to dike like igneous bodies.

Heat flow models that consider the effects of latent heat and pore fluids have been developed by, Jaeger (1957), Jaeger (1959), Jaeger (1964), Delaney (1982), Delaney and Pollard (1982) and Delaney (1987).

Time-dependent heat transfer is described by the partial differential equation:

$$\partial T/\partial t = \kappa \nabla^2 T - \nu \nabla T + A/pC \tag{2.5}$$

(Jaeger, 1959) which in one-dimension, with z = depth, reduces to:

$$\partial T/\partial t = \kappa \partial^2 T/\partial z^2 - \nu_z \partial T/\partial z + A/pC \tag{2.6}$$

where

T = temperature [K]

t = time [s]

κ = thermal diffusivity [m^2/s]

x = depth [m]

ν = velocity of the medium [m/s]

ν_z = velocity of the medium in the z-direction [m/s]

A = volumetric heat production $[W/m^3]$

C = specific heat $[J/(kgK)]$

p = density $[kg/m^3]$

Equations 2.5 and 2.6 define the change in temperature over time as functions of different types of heat transfer: Heat conduction, heat advection, and heat sources and sinks represented by the three termes on the right side of the equation, respectively.

The left-hand side of Equation 2.6 defines temperature change over time during contact metamorphism caused by the terms on the right side: conduction, convection and heat sinks and sources respectively. The first term on the right-hand side of the heat transfer Equation 2.6 describes how heating of a rock by conduction is dependent on the thermal diffusivity, κ, and the second spatial derivative of temperature. The second term describes heat transfer by convection which is proportional to the velocity of the pore fluid and the geothermal gradient. The third term on the right-hand of the equation describes the contribution of the heat source and sinks to the heat transfer. During contact metamorphism by dike or sill, an important source of heat is that released during crystallization of the magma.

The use of Equation 2.6 in a numerical model requires thermal diffusivity, magma temperature, host rock temperature and the latent heat of crystallization of the magma to be fixed. To quantify the effect of latent heat of crystallization on temperature estimates, the temperature interval over which crystallization occurs and the degree of crystallization at the moment of intrusion must be measured or specified (Spear and Peacock, 1989). Thermal diffusivity (κ), is defined by the relationship:

$$\kappa = K/pC \tag{2.7}$$

where

K = thermal conductvity

p = bulk density

With Equation 2.6 Carslaw and Jaeger (1959) calculated that for a sill intrusion of basic composition, with a center magma of 1000°C, the country rock 10 cm from the contact will only lie above T=350°C for approximately 1.5 years if the intrusion is 5 m thick. If the intrusion is 50 m thick the country rock at the same distance will be held above T=350°C for as long as 150 years. Even 10 m from the contact of a 50 m thick sill intrusion would the country rock be at T=350°C as long as 90 years after emplacement of the intrusion. Figure 2.9.

2.6 Other investigations of maturity caused by intrusion

The thermal effects of igneous intrusions have been studied in numerous investigations.

A list of some of the published articles discussing the results from such investigations is presented here and forms the background for my own investigations:

- Thermal alteration of clastic organic particles as an indicator of contact and burial metamorphism in sedimentary rocks. (Bostick, 1971)
- Electron paramagnetic resonance study of thermal alteration of kerogen in deep-sea sediments by basaltic sill intrusion. (Baker et al., 1977)
- Vitrinite reflectance-temperature determinations for intruded Cretaceous black shale in the eastern Atlantic. (Peters et al., 1978)
- Thermal maturation of organic matter by a thick basaltic sill in Upper Cretaceous shales, Svartenhuk Halvø, central West Greenland. (Schiener and Perregaard, 1981)
- Thermal alteration of Cretaceous black shale by diabase intrusion in the Eastern Atlantic-II. Effects on bitumen and kerogen. (Simoneit et al., 1981)
- Programmed pyrolysis of Organic Matter from Thermally Altered Cretaceous Black Shales. (Peters et al., 1983)
- Igneous intrusions in the North-West Canning Basin and their Impact on Oil Exploration. (Reeckmann and Mebberson, 1984)
- The effect of igneous intrusive bodies on sedimentary thermal maturity. (Wang et al., 1989)
- Molecular disordering in natural cokes approaching dike and sill contacts. (Khorasani et al., 1990)
- The interrelationship of biological marker maturity parameters and molecular yields during contact metamorphism. (Bishop and Abbott, 1993)
- Vitrinite reflectance and molecular geochemistry of Jurassic sediments: the influence of heating by Tertiary dikes (northwest Scotland). (Bishop and Abbott, 1995)
- Thermal effects of igneous intrusions on maturity of organic matter: A possible mechanism of intrusion. (Galushkin, 1997)
- Fluid inclusion and vitrinite-reflectance geothermometry compared to heat-flow models of maximum paleotemperature next to dikes, western onshore Gippsland Basin, Australia. Barker et al. (1998)

Chapter 3

The geological setting

The purpose of this chapter is to place the sample set used in a geological frame work. This is not a comprehensive description of Svalbards complex geological history, merely a short introduction ment for the reader to better understand the geological setting.

3.1 The geology of Svalbard

The geological history of Svalbard has great relevance for exploration of the Barents and northern Norwegian shelf areas. In a wider perspective, these areas form a critical link in the chain of proven and potential petroleum provinces which extend from the pre-Urals of Russia in the south east, and the Norwegian Sea in the west, through the Sverdrup Basin to the North Slope of Alaska (Figure 3.1). Svalbard has much to contribute concerning a better understanding of the evolution of the Artic Basin and the gigantic shelf areas which encircle the basin.

The stratigraphical succession of Svalbard contains rocks from all geological timeperiods, from the late Precambrium through to the Tertiary (Figure 3.2).

3.1.1 Tectonic setting

From Lithostratigraphic Lexicon of Svalbard (Dallmann et al., 1999): At the North of Svalbard, 50-100 km from the shore, a steep passive continental margin with slopes up to 10° (average 4°) forms the boundary relative to the Eurasian Basin of the Arctic Ocean. Offshore west of Svalbard, a 40-80 km wide shelf separates the coast of the main island, Spitsbergen, from a structural complex oceanic area, the Knipovich Ridge (Talwani and Eldholm, 1977). The central part of this ridge is a spreading axis, which is segmented by a transform fault system, the Spitsbergen Fracture Zone to the north, and the Greenland Fracture Zone to the south (Figure 3.2).

The nortwestern shelf corner borders the Yermak Plateau, the northern part of which may be the result of an Early-Tertiary shoulder uplift along the rifted margin of the developing Arctic Ocean, and subsequent transform movements

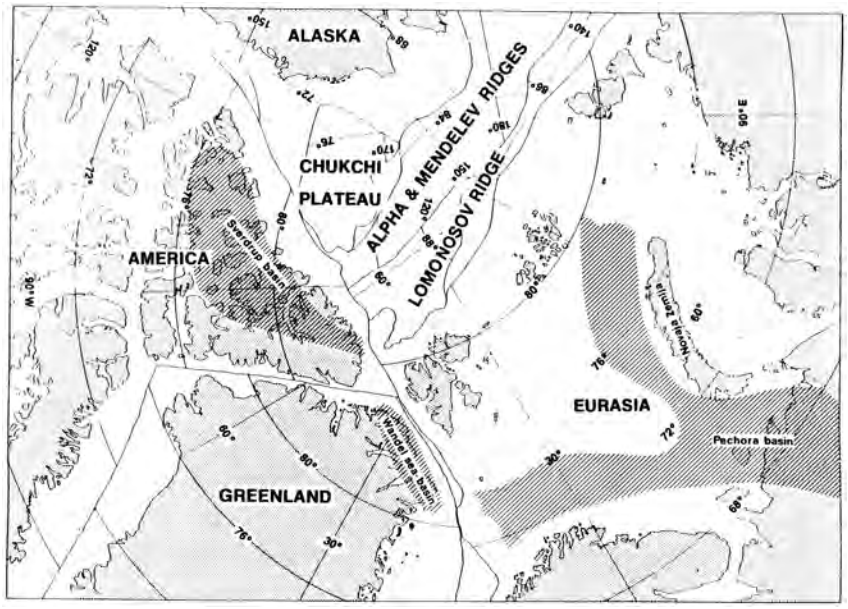

Figure 3.1: *A tentative paleocontinental reconstruction of Svalbard's relation to adjacent sedimentary basins at the Paleozoic/Mesozoic transition. (Steel and Worsley, 1984)*

in a periodically transpressive regime along the western margin may all have their share in explaining the uplift of the archipelago.

3.1.2 Paleozoicum

Two main deformation phases divides the Paleozoic sediments into three main groups:

1. Geosynklinale sediments deposited from late Precambrium to early Silurian (Scrutton et al., 1976) being folded by the Ny Friesland deformation.

2. Late Silurian and Devonian sediments being folded during the Svalbardian (Late Caledonian) deformation phase, which started at the end of the Devonian (Harland, 1974). An erosion- and angular unconformity marks the Svalbardian deformation and separates the Devonian sediments from the younger strata.

3. In the Carboniferous the sedimentation was controlled by vertical movements along old NNW-SSE trending lineaments resulting in formation of block/trough makings. The distribution of Carboniferous sediments suggests deposition of sediments in three approximately north-south trending troughs with intermediate blocks (Figure 3.3).

   The sediments in the three troughs are of Lower Carboniferous age and consist of coarse, continental conglomerates and sandstones with intermediate sequences of shales and coals (Gjelberg and Steel, 1979). On the blocks, Carboniferous rocks are missing today. The reason for this is

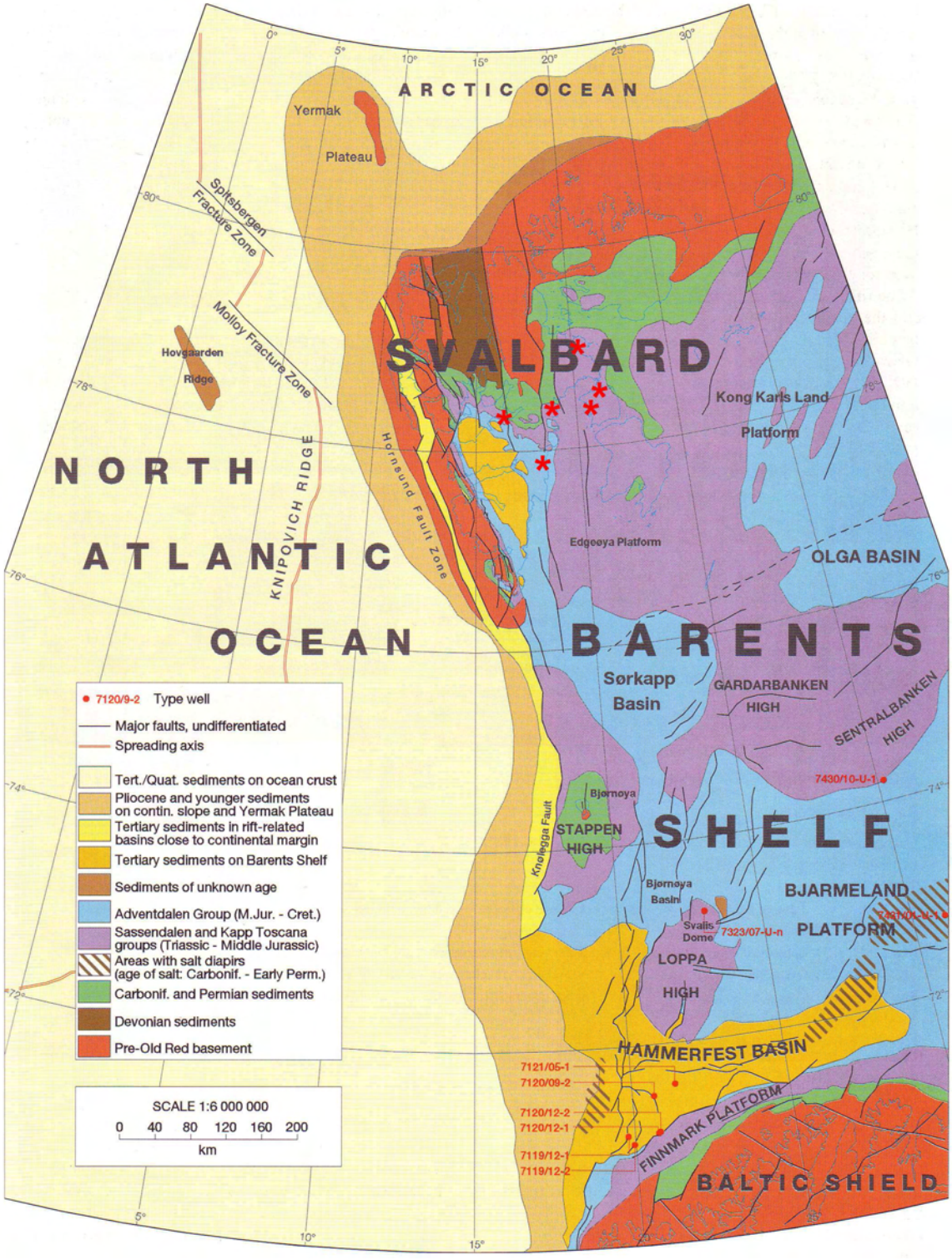

Figure 3.2: *Geological overview map of Svalbard and the western Barents Sea Shelf showing the position of major tectonic elements. (Dallmann et al., 1999) Red (*) indicate sample locations of this study.*

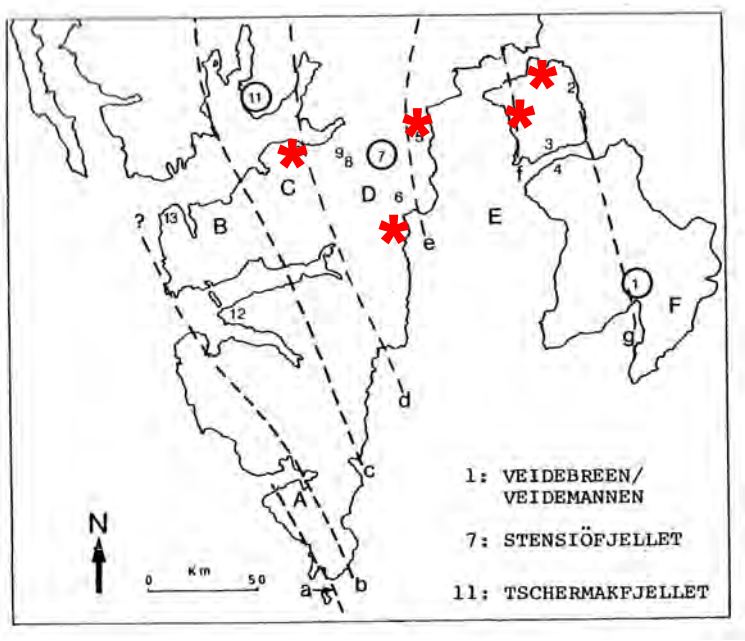

Figure 3.3: *Main structural elements that seems to have influenced sedimentation paterns at Svalbard in Upper Paleozoic and Mesozoic sediments (Forsberg, 1980). Red (*) indicate sample locations of this study.*

probably both the lack of deposition and subsequent erosion (Cutbill and Challinor, 1965). Gjelberg and Steel (1979) interpret the climate in the Lower Carboniferous as humid equatorial.

During the Middle Carboniferous the region undervent major changes. Faulting and regional sea level changes occurred at the same time as the climate changed from humid to arid and Svalbard drifted north. These changes caused deposition of continental "red beds" in alluvial fans alongside the blockedges. The Upper Carboniferous was characterized by declining tectonic activity. Since the regional sea level change continued, gradually the sedimentation in the troughs became dominated by marine carbonates.

The Carboniferous/Permian border is marked by a comprehensive transgression over a relief where the block/trough formation comes to a halt (Cutbill and Challinor, 1965). The carbonate sediments being deposited after this transgression, become more dolomitic upwards in Lower Permian and lowering of the sea level little by little created evaporates. These are believed to represent repeated sabkha-cycles (Lauritzen, 1981).

Angular unconformity and erosional contacts between Lower Permian and Upper Permian deposits at Hornsund suggest tectonic movements during the Lower Permian along the Hornsund-Sørkap High. Over the rest of Svalbard the block/trough constellation was more or less rubbed out. The Upper Permian deposits consists mainly of dark chert with varying interblending carbonate- and sandstone sequences (Hellem, 1980).

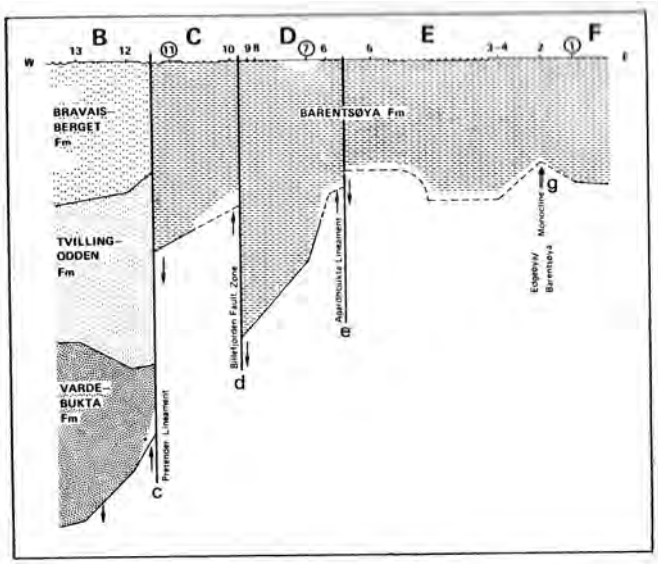

Figure 3.4: *Scheme that shows thickness relationship between the formation units in the Sassedalen Group, approximatly west - east traverse, Figure 3.3 (Forsberg, 1980)*

3.1.3 Mesozoicum

During Permian time, Svalbard moved farther north and the clastic sequences in the Triassic are supposedly deposited in open marine settings on a wide epicontinental platform. This platform was situated in the North-tempered-climatic-zone (Mørk and Worsley, 1978). Differences in thickness of strata belonging to the Lower and Middle Triassic suggests that the deposition pattern was influenced by the old block/trough system with slightly rotated faultblocks (Figure 3.4)

with sediment supply mainly from the west. In the Upper Triassic this pattern breaks down and deltaic systems are being build into the Triassic depositional basin from north and east (Edwards, 1976; Lock et al., 1978; Knarud, 1980).

The border between Triassic and Jurassic is marked by condensed strata deposited in the Upper Triassic to Middle Jurassic, ending with a thin sandstone with a polymict transgressional conglomerate. The conglomerate consists among other things of phosphate clasts with remaniéfauna of Upper Jurassic age (Bäckström, 1971), followed by a dark mudstone deposited under the transgression.

Tectonic activity followed by intrusion activity has been related with a hiatus that covers the entire Jurassic/Cretaceous border (Parker, 1966). The Lower Cretaceous deposits start with a dark shale which is the basis for an upward coarsening deltaic sequence (Steel et al., 1979). Above this unit follow cyclical, marine sediments thickening towards the south (Moe, 1980). Uplift and erosion of the northern areas during the Upper Cretaceous is assumed to be the reason for this pattern (Nagy, 1970). The uplift of the northern areas and the accompa-

nying erosion were considerable and Upper Cretaceous sediments are missing all over Svalbard.

3.1.4 Cenozoicum

Basal Tertiary deposits (Early Palaeocene) lie with erosion- and angular unconformity on increasingly older Lower Cretaceous rocks towards the north (Moe, 1980). Steel et al. (1979) divides the Tertiary deposits into three stages. In the first stage sediments were being transported into the Tertiary basin mainly from the northeast and north. During the second stage, sediment supply came both from the west and north implying uplift also in the west. The last stage began with fast subsidence followed by massive sediment supply from the uplifted areas in the northwest. The development of the Spitsbergen trough is linked to transform-movements between the Greenland and Eurasian plates inconnected with the opening of the Norwegian Sea (Figure 3.5). These movements caused deformation and development of the Tertiary foldbelt along the west coast of Spitsbergen (Talwani and Eldholm, 1977; Dallmann et al., 1993).

After the Tertiary folding and thrusting the region was partly peneplaned and later uplift and erosion has probably given the configuration of islands and fjords of today (Major and Nagy, 1972). The area was covered with ice during the Pliocene glacial ages. Pre Holocene the ice started to move back, at the same time as the land uplifted due to isostatic rebound (Hoppe, 1970). This uplift still continues. In the post-glacial period there has also been minor climatic changes with the mildest climatic conditions during Atlantic and Subboreal time (Feyling-Hanssen, 1955).

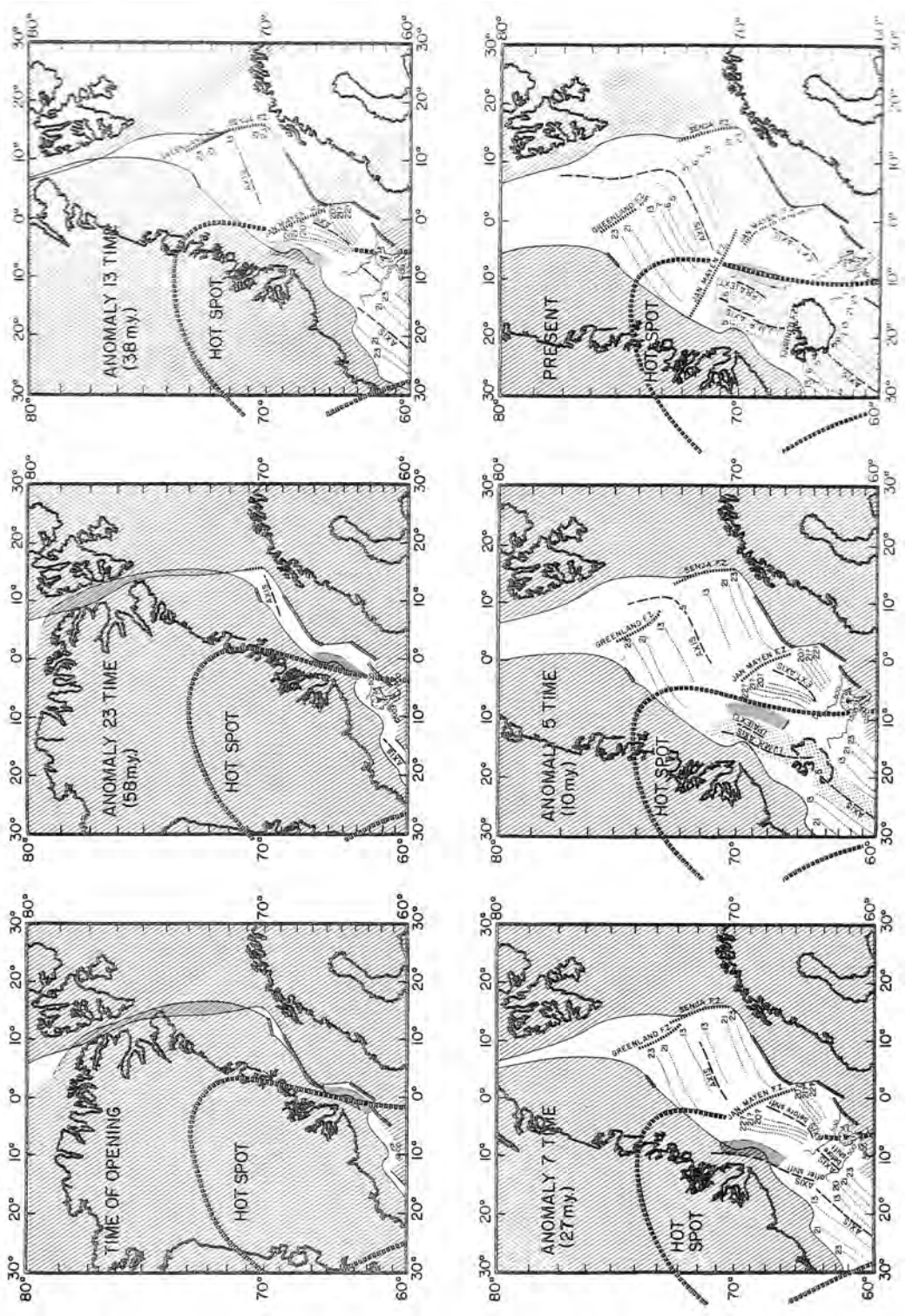

Figure 3.5: *Schematic model showing the creation of the Norwegian Sea and the ocean between Svalbard and Greenland. White areas are newly created sea floor whereas shaded areas represent old sea floor. (Talwani and Eldholm, 1977)*

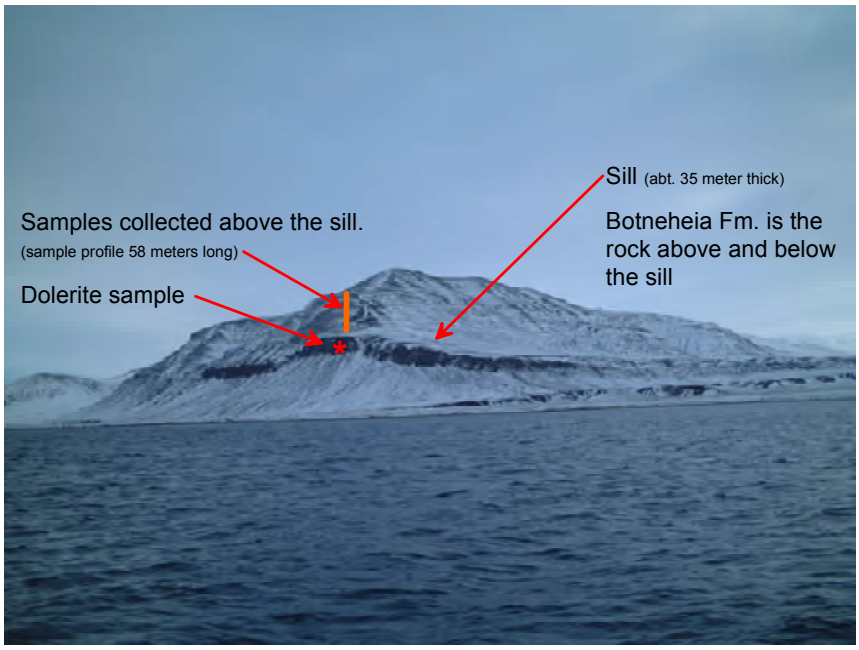

Figure 3.6: *Picture showing the Botneheia source-rock covered with snow, the dark pronounced cliff is the sill emplaced into the lithologically weak shale of the Botneheia Fm., Botneheia Spitsbergen. (Photo by the author, 2002)*

3.2 Geology of the source-rocks in this study

3.2.1 Botneheia Formation

Depositional age: Middle Triassic
Main Lithologies: Mudstone, calcareous siltstone

The Botneheia Formation (in the rest of the thesis, just noted Botneheia Fm.) is part of the Sassendalen Group, defined in 1965 as comprising three formations (Botneheia, Sticky Keep and Vardebukta). The formations are primary and they constitutes a group. There is no difficulty in distinguishing the three formations in the original section south of Sassendalen in the east, and in the Festningen section in the west. The upper two are best exposed south of Sassendalen and the lower one in the Festningen section. The names of these formations were accordingly taken from these localities (Harland, 1997; Worsley and Mørk, 1978).

The Botneheia Fm. itself forms a coarsening upward succession where basal mudstones grade into siltstone. The formation consists mainly of black shale with abundant small phosphate nodules. Thin to medium thick carbonaceous siltstone beds occur throughout the unit. The upper part is highly calcitic due to numerous thin-shelled bivalves, and these beds form a staking out cliff (Blanknuten Member). The top is marked by a siltstone bed with phosphate nodules, and is overlain by grey shale with purple weathering siderite nodules of the Tschermarkfjellet Formation (Figure 3.7).

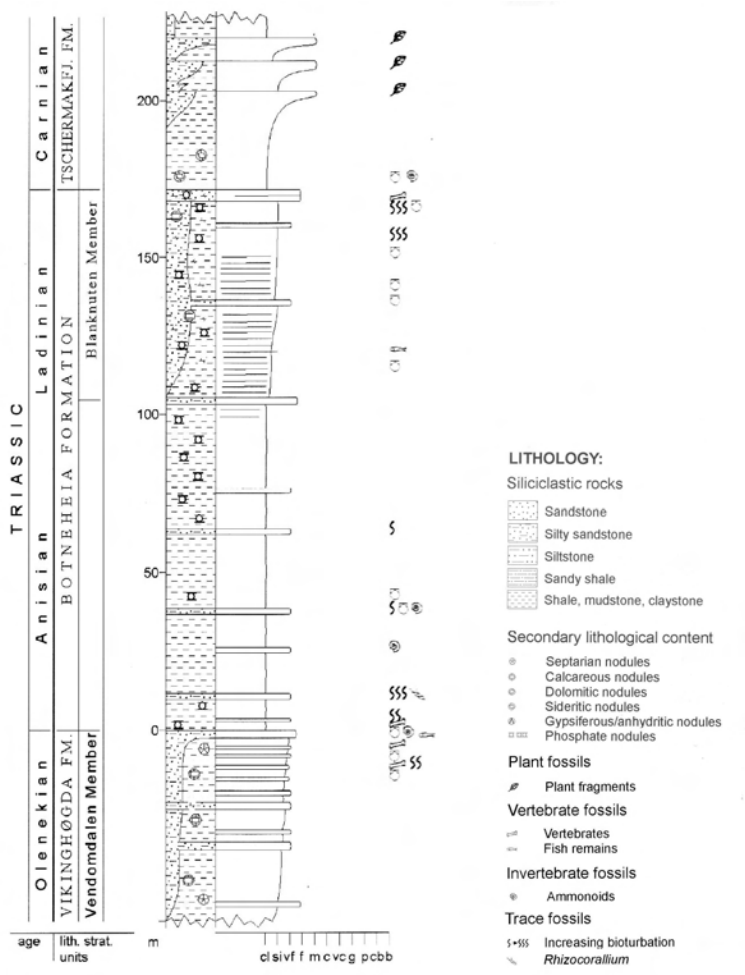

Figure 3.7: *Middle Triassic stratigraphical section. Stereotype for: Botneheia Formation. Locality: Stikey Keep (Mørk et al., 1982; Dallmann et al., 1999)*

The Botneheia Formation is interpreted as a deltaic influenced, regressive shelf deposit, with partly restricted environments in terms of water circulation and oxygen content (Mørk et al., 1982; Mørk et al., 1999).

3.2.2 Janusfjellet Subgroup

Depositional age: Late Juurassic - Early Barremian
Main Lithologies: Shale, siltstone, sandstone

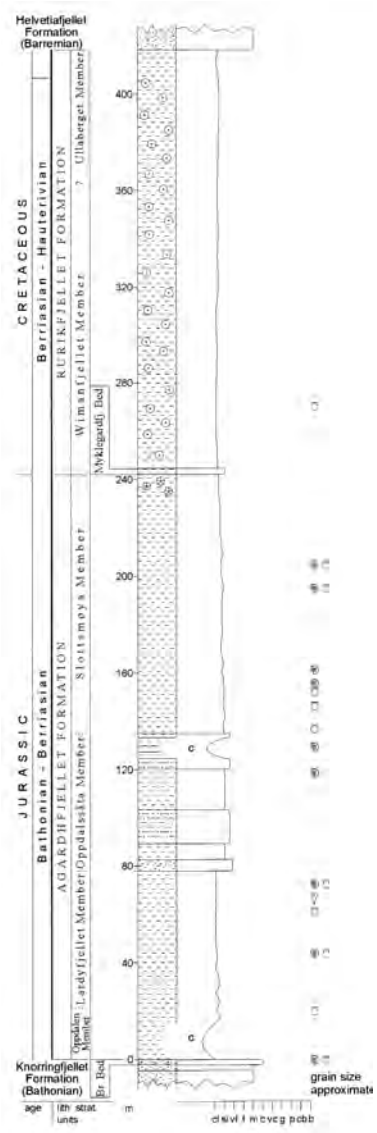

Figure 3.8: *Jurassic - Cretaceous stratigraphical section. Stereotype for: Janusfjellet Subgroup, Agardhfjellet and Rurikfjellet Formations. Locality: Agardhfjellet. Legend, see Figure 3.7 (Dallmann et al., 1999)*

The Janusfjellet Subgroup is defined in the Svalbard area, where it mainly consists of bituminous black shales and siltstones that pass into sandstones in the uppermost part.

The subgroup comprises the Agardhfjellet and Rurikfjellet formations. The subgroup is an easy mappable unit. The distinction between the two is difficult to impossible in many tectonised areas of western Spitsbergen. For this reason it has often been referred to as the Janusfjellet "Formation" in previous geological literature. The subgroup is of marine shelf origin (Figure 3.8).

3.3 The Svalbard Dolerites

Magmatic activity was intense during the platform episode in the evolution of Svalbard. Dolerite sills and dykes are typical and widespread in the sedimentary sequence spanning from Cambrian to Upper Jurassic sediments (Burov et al., 1975).

The petrography was described by Tyrell and Sandford (1933) who distinguished four main classes:

Normal medium- to fine grained facies constitute the main bulk of occurences with a plexus of ophitic texture with plagioclase laths in a bacground of pyroxene and skeletal crystals of iron ore. The rocks are typically non-porphyritic and contain patches of imperfectly crystallised mesostasial matter. The large feldspars are bytownite and the smaller ophitic laths are An_{55} acid laboradorite. The pyroxenes approximate to enstatite-augite or pigeonite. Irregular areas of red non-pleochroic serpentine indicate formerolivine. The skeletal ores are of titaniferous magnetite. The mesostasial matter is a fine complex of plagioclase laths quartz, chlorite and pyroxene altered to brown hornblende and biotite with needles of apatite in an ill-defined base of alkali feldspar.

Corase gabbroic and pegmatitic varieties exhibit fresh olivine and micropegmatite which may culminate in a pegmatite, of quartz, hornblende and biotitt with a nearly colourless pyroxene. These late-formed groundmass pyroxenes are enriched in iron (towards hypersthene) and magnesium (towards enstatite). There is evidence of transformation from olivine to pyroxene and the olivine coexists with quartz. Reddish biotite and deep greenish hornblende occur at the margins of the micropegmatite.

Marginal varieties Towards contacts with country rock of sills and dyke ophitic texture is lost in favour of an intergranular and finely intersertial texture. Feldspar phenocrysts may develop and olivine disappear.

"White trap" modification sills penetraiting Triassic and Jurassic rocks prefer carbonaceous strata. The result is of fine magnesian minerals and even feldspars by carbonates of calcium, magnesium and iron.

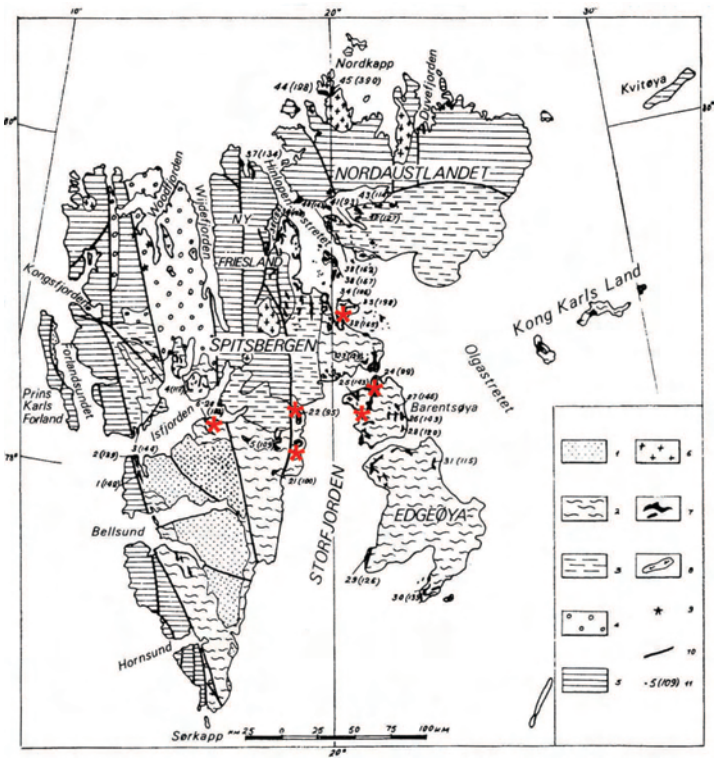

Figure 3.9: *Map of dolerite intrusions at Svalbard (on geologic-tectonic base). Structural-formational complexes of the platform cover: 1 Paleogene complex; 2. Mesozoic complex; 3. Upper Paleozoic complex; 4. Devonian orogenic (postgeosynclinal) complex; 5. Caledonian and pre-Caledonian fold structures; 6. Caledonian granites; 7. Mesozoic dolerites; 8. Late Mesozoic basalt flows; 9. Holocene volcanos; 10. Major faults. (Of special interest in this thesis;) 11. Ordinal number of sample and its K-Ar date (Burov et al., 1975). Red (*) indicate sample locations of this study.*

The above descriptions of the four main dolerite classes at Svalbard was taken from Harland and Kelly (1997) on page 377 and 378.

The sills of this study is of the first and the fourth class. Pictures of the sill at Botneheia is shown in figure 3.6 and 3.10. A picture of the sill at Teistberget is shown in figure 4.2.

3.3.1 Age

Publications on the geology of Svalbard usually speculate as to the time of intrusion. Before K-Ar dating of the dolerites were done in the late 1960's, Nathorst (1911) among others suggested that the intrusions were Late Jurasic-Early Cretaceous in age, while others Harland (1961) suggested them to be off Late Cretaceous age.

Isotopic determinations were first attempted by Gayer et al. (1970). The data however, had to low precision to have stratigraphic significance. The principal study by Burov et al. (1975) yielded 45 determinations from Isfjorden, Storf-

(a) The sill at Botneheia

(b) Closeup picture of the sill

Figure 3.10: **A** *Picture showing the sill at Botneheia standing out as a dark pronounced cliff from the lithologically weak shale of the Botneheia Fm. covered by snow.* **B** *Closeup picture of the dolorite sill at Botneheia. (Photos by the author, 2002)*

jorden, Barentsøya, Edgeøya, Wilhelmsøya and Nordaustlandet. Quartz-dolerites are typical of ages around 140Ma and younger olivine-dolerites range around 110 Ma. Burov et al. (1975) concluded two maxima, one at 144±5 and the other at 105±5 Ma. Their results show the older intrusion to occur on Spitsbergen and the younger on Edgeøya, Barentsøya and Nordaustlandet.

Age of the sills intruded into the source-rocks of this study

Location	Sill Ages (m.y.)	Sample nr. in Burov et al. (1975)
Botneheia	90±15	2865
Kreftberget	99	3389
Høgrinden	143	3390
Teistberget	n.a	n.a.
Domen	95±2	3382
Keisarkampen	165	3397

Table 3.1: *Sill ages at the sample locations, taken from The age of Spitsbergen Dolerites by Burov et al. (1975)*

From fig 1 and Table 1 in Burov et al. (1975) we selected 5 age readings, which we believe to be relevant for the sills that intruded the source-rocks of

this study (Figure 3.9, Table 3.1).

We can of course not be absolutely sure that the samples used for the time measurements were taken from the same sills that intruded into the source rocks of this study. What is certain is that the sills of this study and the sills sampled for the study of Burov et al. (1975) are located in the same areas. Burov et al. (1975) also show that the sills located in the same areas on Svalbard show approximately the same time readings. We therefore feel confident with respect to the significance of the dated sills in Table 3.1 concerning the time for emplacement and source-rock maturation of the samples in this study.

Chapter 4

The sample set

This chapter describes where and when the samples were collected.

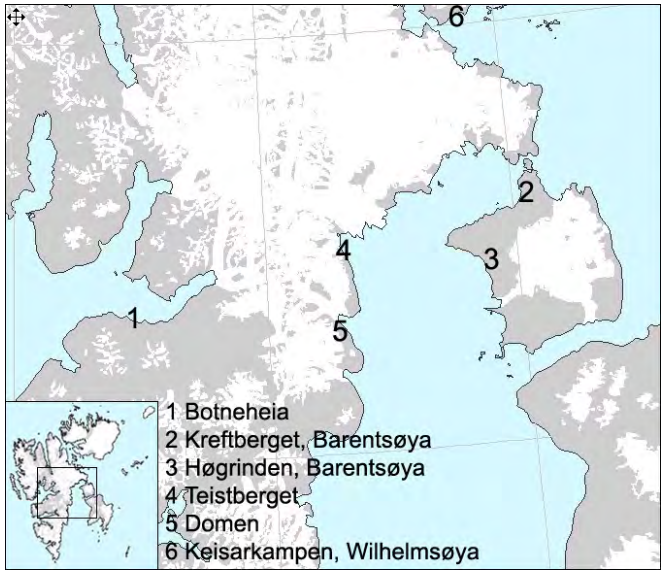

Figure 4.1: *Locations of the samples.*

4.1 Localities

The samples needed for this study where collected from source-rock outcrops on locations at Svalbard were a sill(s) are known to cut through the source rock.

Eight different places at Svalbard with sill intruded into source-rock were selected for sample collection. Samples were collected from profiles with sills in the organic rich Triassic Botneheia Fm. black shale. The formation contains mainly, marine kerogen. These samples was collected at the hills of Botneheia (Central Spitsbergen), Teistberget (eastern Central Spitsbergen), Kreftberget and Høgrinden (Barentsøya Island). From the Jurassic Janusfjellet black shale (with

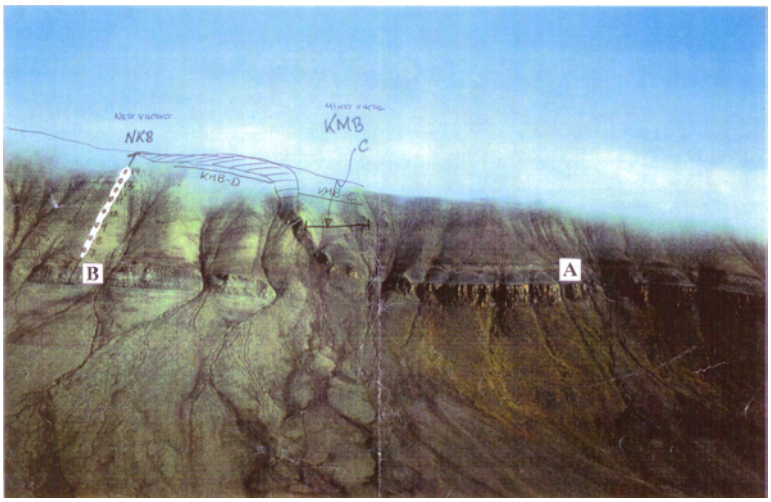

Figure 4.2: *Picture showing Kreftsberget, Barentsøya, the dark pronounced cliff is the sill emplaced into the lithologically weak shale of the Botneheia source rock. Drawings on the photo shows were samples were collected. A marks where the samples for the sample series KRB was collected, B markes where the samples for the sample series NKB was collected. (Photo and drawings by Sven Dahlgren, 1995)*

dominantly terrestrial kerogen) samples was collected at Domen (eastern Central Spitsbergen) and the Wilhelmøya Island. Samples from identical black shale units in nearby sections, not thermally affected by the sills, were used for comparison, i.e. what is the "virgin" geochemical parameters like TOC, HI and T_{max}.

4.2 Collecting samples

Samples were collected during the summer 1995 by Svein Dahlgren, Norwegian Petroleum Directorate. Figure 4.1 shows the sample locations. All samples were collected as hand specimens taken from solid rock using sledge hammers to obtain "deep" samples to reduce weathering effects. Distance from sill was measured in meters with measuring tape. The angel out from the sill was unfortunately not measured. Because of this the exact distance form sill can not be calculated, meaning that the distance from sill can be shorter/longer than what is recorded (Figure 4.3).

Additional samples were also collected by the author during a short trip to the hills of Botneheia during the autumn 2002, when the photograph in Figure 3.6 on page 32 was taken.

Weathering effects on the samples? As stated in above: "All samples were collected as hand specimen taken from solid rock using sledge-hammers to reduce the chance for weathering effects". Thus, care was taken when the samples were collected.

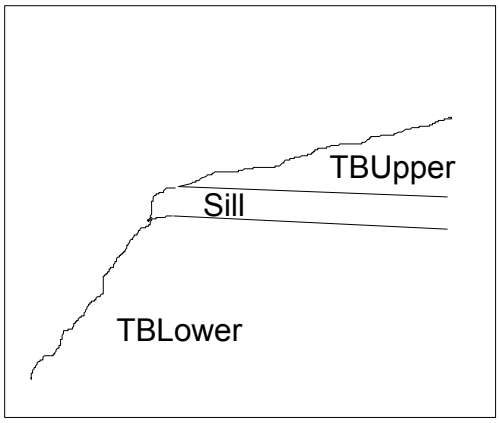

Figure 4.3: *Drawing showing the approximately angel between ground and sill at one of the collection sites; Teistberget. Adapted from original sketch by Sven Dahlgren.*

Forsberg and Bjorøy (1983) made a detailed study on the weathering effects in the Botneheia Fm. and found that surface weathering had no influence on TOC (Total Organic Carbon), but EOM (Extractable Organic Matter) was slightly affected, with an average loss of 10%. Aromatic hydrocarbons were more affected by weathering than the saturated hydrocarbon fraction.

Results from Rock-Eval analysis of Botneheia samples (Forsberg, 1980) shows that neither-nor the Hydrogen Index was influenced by weathering.

Care were undertaken when the samples were collected. A previous study (Forsberg, 1980) on samples collected from the same stratigraphically unit as examined in this study showed no weathering effects. Thus we see no reason to fear weathering effects on the samples taken from close to sills in the Botneheia Fm. The Janusfjellet Subgroup was not examined by Forsberg and Bjorøy (1983) but must be considered to have undergone the same climatic conditions and weathering effects as Botneheia Fm. since they both are located at the relatively small geographic area Svalbard. Therefore it seems reasonable to assume that weathering effects also can be ignored for the samples collected close to sills in the Janusfjellet Subgroup.

BH1	Botneheia East, Central Spitsbergen; Profile with only a minor sill
BH2	Botneheia East, Central Spitsbergen; Profile above sill
KRB	Kreftberget, Barentsøya: Profile above sill
NKB	Northern Kreftberget, Barentsøya; Profile without sill
KMB-C	Northern Kreftberget, Barentsøya; Along a single horizon
KMB-D	Northern Kreftberget, Barentsøya; Parallel to sill
HØB1	Høgrinden South, Barentsøya
HØB2	Høgrinden South, Barentsøya
HØB3	Høgrinden South, Barentsøya; sampled laterally along a single horizon
TBU	Teistberget, Eastern Spitsbergen; Profile above sill
TBL	Teistberget, Eastern Spitsbergen; Profile below sill
DOM	Domen, Eastern Spitsbergen; Profile above sill
WØU	Keisarkampen, Wilhemsøya; Profile above sill
WØL	Keisarkampen, Wilhemsøya; Profile below sill

Table 4.1: *Sample locations and their abbreviations used in figures and tables in the following chapters and the appendix*

Location	**Sill Thickness**
Botneheia	35m
Kreftberget	25m
Høgrinden	5-7m
Teistberget	17-18m
Domen	7-8m
Keisarkampen	not determined

Table 4.2: *Sill thicknesses at the sample locations reported by Svein Dahlgren, 1995*

Chapter 5

Results and discussion

Analytical data on the samples is found in the Appendix. There the reader will also find the majority of the different diagrams made of the analytical results. This chapter contains the interpretation of the analytical data in the form of figures and detailed description of variations in analytical results within each sample series as the sill is approached. The figures in this chapter present to the reader the general effects of what happens when a sill intrudes into source-rocks. For details concerning each sample series and individual samples, the reader is advised to look at figures and tables in the Appendix.

5.1 General results

As sedimentation and subsidence continue, in a normal subsiding basin, temperature and pressure increase. In this changing physical environment, the structure of the immature kerogen is no longer in equilibrium with its surroundings. Rearrangements will progressively take place to reach a higher and more stable, degree of ordering.

This constant adjustment of kerogen to increasing temperature and pressure results in a progressive elimination of functional groups and of the linkages between nuclei. A wide range of compounds is formed, including medium to low molecular weight hydrocarbons, carbon dioxide, water and hydrogen sulfide. Therefore the petroleum generation seems to be a necessary consequence of the drive of kerogen to adjust to its new surroundings by gaining a higher degree of order with increasing overburden (Tissot and Welte, 1984).

In this study the samples, according to vitrinite reflectance values for the samples most remote to the sills, reflect burial to approximately 1500 meters depth. The diagenesis stage of maturation of kerogen is normally taken to start at a vitrinite reflectivity between 0.5 and 0.7 corresponding to around 1500 to 2000 meters depending on the local geothermal gradient. The increasing vitrinite reflectance values observed in this study when approaching the sills must therefore mainly be attributed to the heat caused by the sill intrusion.

Generally, it seems that the sill intrusion has had its effect on all parameters measured in this study, see Figure 5.1. The n-alkane patterns clearly shifts from a “normal” decrease in peak height with increasing carbon number on samples

unaffected by sill(s) to an “heavy-end-biased” pattern with increasing concentrations of n-alkanes in the high carbon number side on samples close to a sill (Figure 5.10). Vitrinite reflectance increase when approaching the sill, so do also the production index (Figures 5.1(a) and 5.2).

5.2 The effect of sills on maturation

Investigations of sill maturation usually consider very few geochemical maturation parameters and usually concentrate on vitrinite reflectance and heat theory. This study considers in addition to vitrinite reflectance and heat theory also isotope measurements, kerogen description, hydrogen index, oxygen index, T_{max}, TOC, saturated/aromatic ratios, n-alkane patterns, pristane/phytane ratios and CPI. GC-MS analysis of the samples has also been conducted, but the results have not been examined in this thesis. This study considers more maturity parameters than what is common in sill inquires published in literature.

5.2.1 Microscope investigations

Optical microscopy can only be used to describe that part of the organic matter of a sediment occurring in particles large enough to be visible in an optical microscope (about 1 μm or larger). (Some finer “amorphous” organic matter can be identified, using transmitted light or fluorescence techniques). In this study kerogen description and vitrinite reflection have been determined using microscopic techniques. For details on how the measurements were conducted, please see Appendix F and G.

Vitrinite

The response of vitrinite reflectance values towards an intrusion contact seem to follow a general pattern (Figure 5.1(a)). As the heat influence grows to give vitrinite reflectance values above ca. 1.5 $\%R_o$, the vitrinite begins to restructurate into very small bonds. This form of Vitrinite is in the report from IFE refered to as "matrix vitrinite". There may still be measurable vitrinite fragments still, but often it is hard to decide whether the matrix vitrinite has the same reflectance as the fragments. There is a possibility that the fragment population is pseudovitrinite with slightly higher reflectance than ordinary vitrinite. Because of this uncertainty, these samples are classified by IFE as P (poor quality sample), see Tables F.1 to F.11. In Figure 5.1(a) only “Good” and “Medium” quality samples are plotted. For some of the sample series this unfortunately excludes several measurements. In Figures F.1 to F.8 in the Appendix I have not subdivided between “Good” and “Medium” quality samples, they are both plotted as “Pop1”, “Poor” sample quality measurements is plotted as “Pop2”.

Towards the intrusion contact, the vitrinite reflectance value increase dramatically. The organic material gets more uniform and polyaromatic. Thereby the number of populations decrease. At about 25-50% sill thickness from the contact, the vitrinite seem to reach a maximum reflectance value. Closer to the

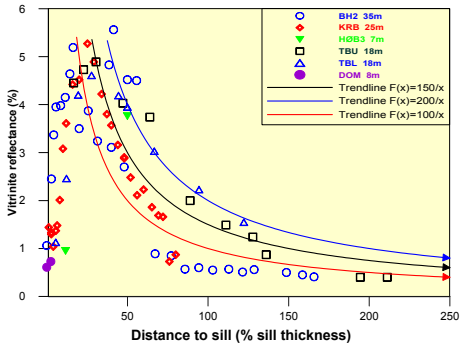

(a) Vitrinite

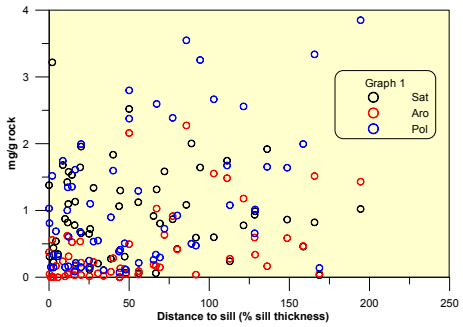

(b) Sat, Aro and Pol

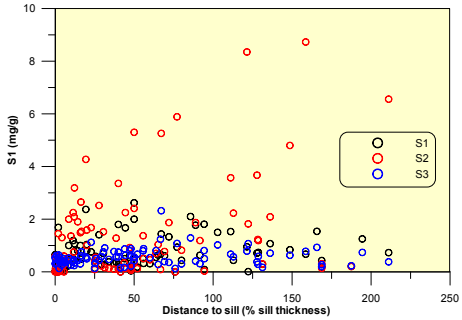

(c) S_1, S_2 and S_3

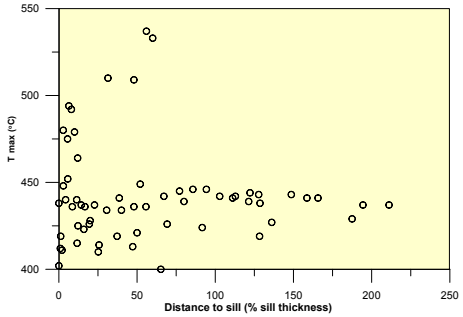

(d) T_{max} (°C)

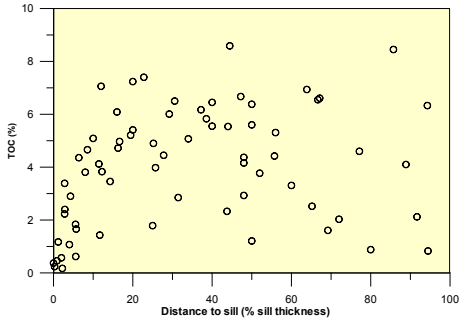

(e) TOC

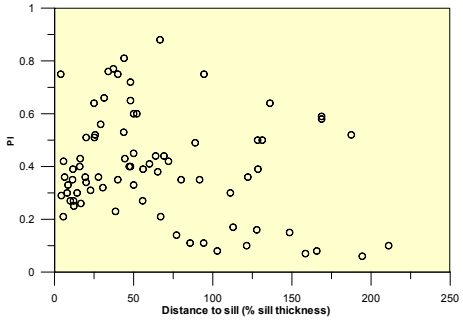

(f) Production index

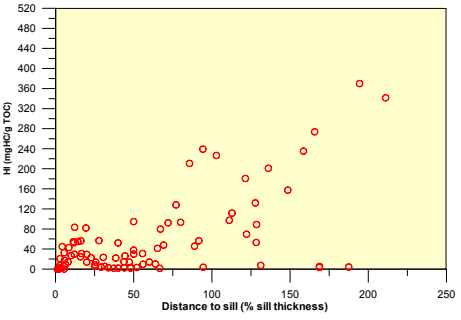

(g) Hydrogen index

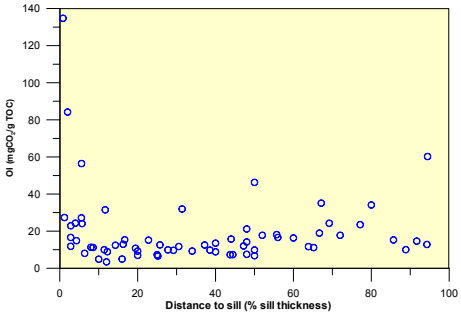

(h) Oxygen index

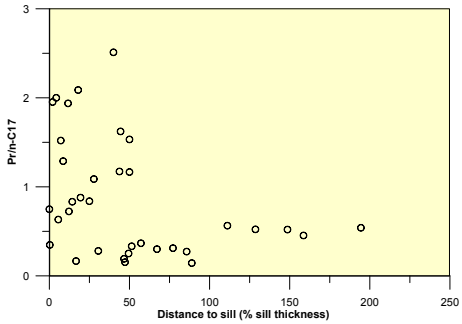

(i) Pristane/n-C_{17}

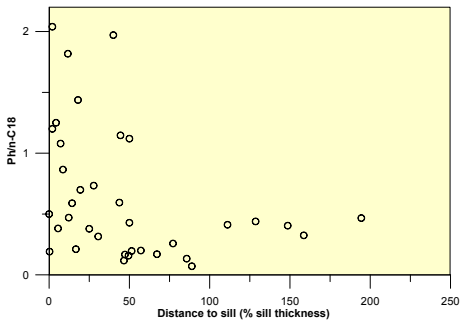

(j) Phytane/n-C_{18}

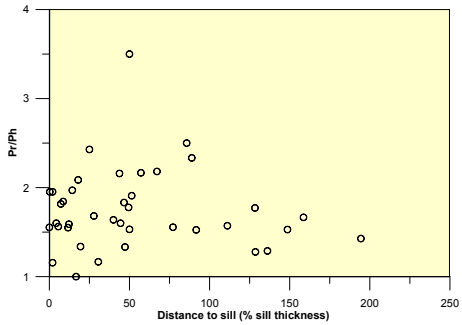

(k) Pristan/Phytan

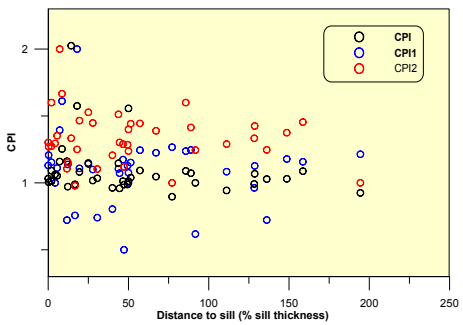

(l) CPI (see section 5.2.4 for formula)

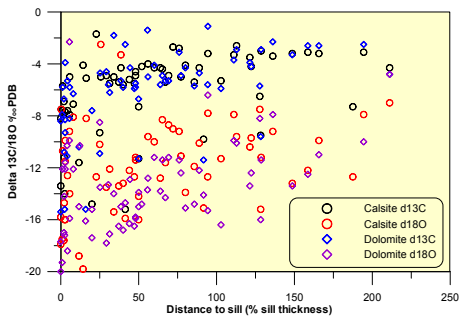

(m) Calsite and Dolomite

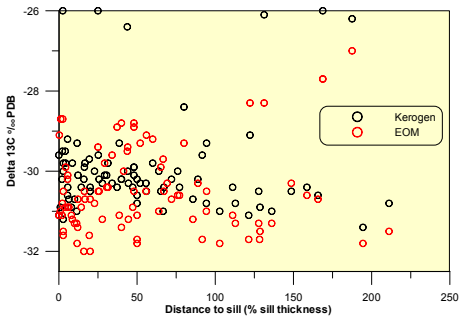

(n) Kerogen and EOM

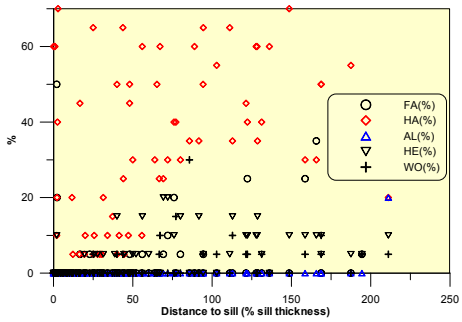

(o) % Kerogen types

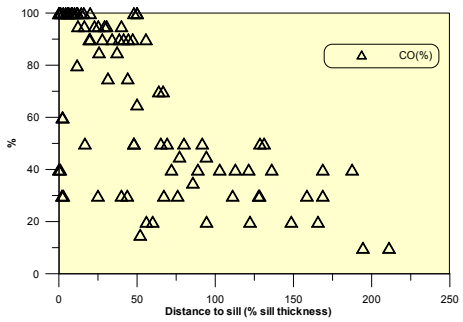

(p) % Coaly Kerogen

Figure 5.1: *Distance-to-sill plots for different parameters measured and calculated from geochemical and microscopic measurements on samples from seven profiles. Distance from sill is recalculated from meters measured to % sill thickness.*

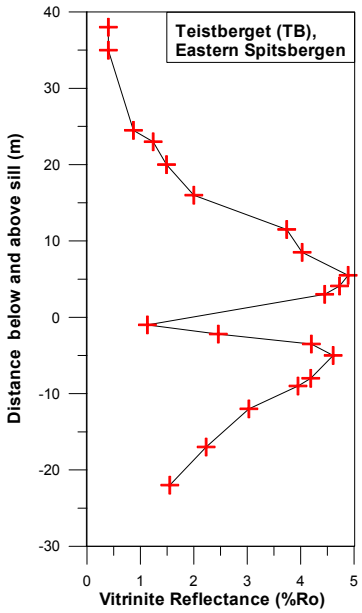

Figure 5.2: *Vitrinite plotted versus distance to the sill for the samples collected at Teistberget, Eastern Spitsbergen.*

contact, the vitrinite reflectance value drops significantly, down to 10-30% of the maximum reflectance value. Parallel to the drop in reflectance value, the organic material morphologically "splits up" in several populations. The vitrinite seem to appear in 2-3 reflectance populations, which may reflect different levels of the same process. At this point, the vitrinite is yellowish grey, often with white (oxidised?) rims.

This effect of R_o reversal close to the sill is well known in the litterature and is related to “cocking” and structural rearangement of the OM (Simoneit et al., 1981; Khorasani et al., 1990). That the heat influence process started and then retarded for the samples closer than 25% sill thickness is not likely. A second explanation may be a reaction between organic matter and steam at the contact, which results in formation of carbon monoxide. This reaction may be associated with the vitrinite reflectance reversal (Bishop and Abbott, 1995).

The reversal of the trend can be seen very well on Figure 5.2. This figure shows vitrinite reflectivity below and above the 17 - 18 meter thick sill at Teistberget. For location see Figure 4.1 on page 39.

This reversal is not observed on any of the other maturity indicators examined in this study.

Figure 5.3 show the vitrinite maturity values plotted alongside the generally accepted “oil-window” diagram. The lowest values in each series represent the “background” vitrinite reflectance. Coupled to the depth values in the “oil-window” diagram the samples “furthest-from-sill” give us the approximate burial level for each sample series. This maximum burial depth for each sample series can have been reached before, at or after the sill intrusion. From this it is given that the higher vitrinite reflectance values are the consequence of the

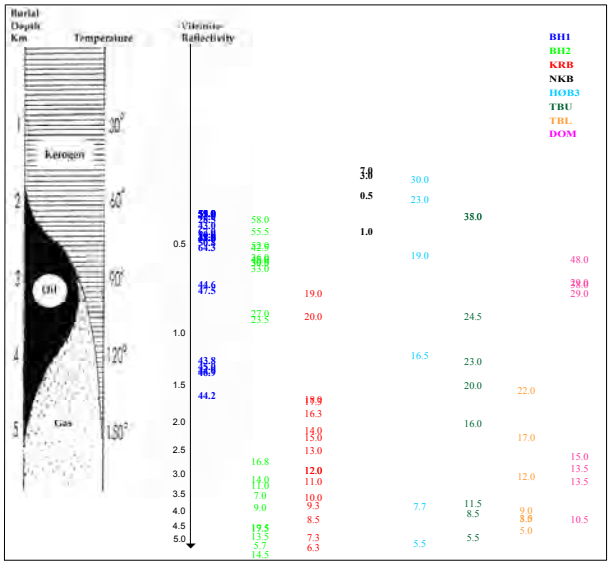

(a) Samples and maturity. Sample Label = distance from sill measured in meter

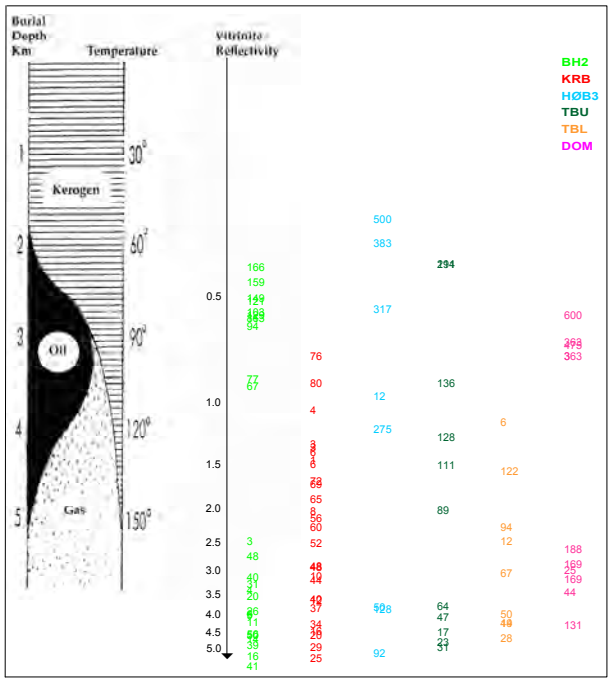

(b) Samples and maturity. Sample Label = distance from sill measured in %sill thickness

Figure 5.3: *Vitrinite reflectance values plotted in the "oil-window diagram". The depth and temperature scales, respectively refer to the depth and temperature at which samples normally reach the same maturity levels. The label for each sample is a number that reflects the distance from the sill where the sample was collected. Note that no sill is present for the NKB series and that this sill is located at approximately 45m for the BH1 series. The immature samples for all series indicate that the source rock has been buried to between 1500 - 2000 meter depth, asuming a geothermal gradient of 30° C pr. km. In a another study by Throndsen (1977) the Botneheia Fm. at Botneheia was, also, found to have been buried between 1500 and 2000 meters.*

heat caused by the sill intrusion. The figure shows that all samples must have been buried to between 1500 to 2000 meters before, at or after the sill intrusion. At approximately 80 %sill thickness all samples are well within the oil window, indicating that the source-rock from here and closer to the sill should have generated oil. At approximately 25 %sill thickness vitrinite reflectance reaches its maximum and all samples seem to be within the gas zone meaning that all the source-rocks potential for generating oil is realized, but with some remaining potential for generating of gas. Closer to the sill than 25 %sill thickness the vitrinite values drops (better observed in Figure 5.1(a)) see discussion above.

The drawing to the left of the Figure 5.3 is based upon Tissot et al. (1974).

Vitrinite changes within each sample series:

BH1, Botneheia East, Central Spitsbergen The BH1-series (Table F.1) were uncomplicated with a small sill around 45-46m from the base of the Botneheia Fm. (Figure F.1).

BH2, Botneheia 2, Central Spitsbergen In the BH2-series (Table F.2) there is a major problem with the quality of the the vitrinite. All the samples BH2-17 - BH2-1 were dominated by matrix vitrinite. BH2-13 - BH24 have a population of matrix vitrinite, which has fairly stable vitrinite reflectance values of 2.0-2.7%Rm. These values are likely to be too low and not representative. In Table F.2 an alternative fragment population of vitrinite or pseudovitrinite is added were possible. This population is of poor quality for most of the samples, and may only tentatively indicate the maturity level (Figure F.2).

KRB, Kreftberget, Barentsøya The KRB-series (Table F.3) is a good example of the vitrinite maturation process with increasing reflectance values to a maximum value of 5.27 $\%R_o$ at 6.3 m from the intrusion contact. It then drop to 1.44 $\%R_o$ at 0.3 m from the contact. KRB-4 and KRB-5 have been noted with 2 and 3 populations respectively in Table F.3. These populations seem to be vitrinite at different maturity levels (Figure F.3).

TBU and TBL, Teistberget, Eastern Spitsbergen The TBU- and TBL-series (Tables F.4 and F.5) represent the profiles above and below a sill. Note the comparable vitrinite reflectance values in corresponding distance above and below the sill. TBL-3 and -4 contain 2 populations, both seem to be vitrinite at different maturity levels (Figure 5.2 (this chapter), Figures F.4 and F.5).

DOM, Domen, Eastern Spitsbergen The DOM-series (Table F.6) were fairly uncomplicated with respect to analytical data. Most of the matrix vitrinite was not measurable. DOM-1 and DOM-2 are noted with 2 populations which both seem to be vitrinite at different maturity levels (Figure F.6).

FA	Fluorescing amorphous material
HA	Non-fluorescing amorphous material
AL	Algal material and dinocysts
HE	Herbaceous material, spores, pollen
WO	Woody material
CO	Coal

Table 5.1: *Abbreviations used in kerogen description*

HØB3, Høgrinden South, Barentsøya The HØB3-series were fairly uncomplicated to analyse. HØB3-2 is noted with 2 populations in Table F.9, both seem to be vitrinite (Figure F.7).

NKB, Northern Kreftberget, Barentsøya The NKB-series (Table F.4) were uncomplicated and without intrusion heat influence. NKB-14 though, is remarkably more mature compared to samples NKB-13 to NKB-1 (Figure F.8). This is seen both by vitrinite reflectance analysis and kerogen description. This is because the samples at the end of the NKB sample series, as discussed in Subsection **??**, are actually not far away from the Kreftberget sill.

KMB-C and KMB-D (Tables F.7 and F.8) were poor in vitrinite and difficult to analyse. No distance to sill was provided for these samples, but they seem to be close to intrusion contacts because of yellowish grey vitrinite and light (oxidised?) rims. They are both close to the Kreftberget sill (Figure 4.2).

JR-1 and SR-1 The Norwegian Petroleum Directorate standard samples was also analytical examined to prevent systematic analytical errors. The standard sample JR-1 were poor in vitrinite, had a high content of pyrite and was generally a bad quality sample. The standard sample SR-1 was of moderate quality with a relatively high content of pyrite. The sample was rich in vitrinite and it was possible to establish the maturity level for this sample (Table F.11).

Kerogen description

The kerogen description results can be looked at in detail in Appendix G on page 263.

In kerogen description, the samples are described by sorting the organic material found into six main groups by percent. These groups are: Fluoramorphinite (FA), Hebamorphinite (HA), Algal organic matter (AL), Herbaceous organic matter (HE), Woody organic matter (WO) and Coaly organic matter (CO). These definitions are summarized in Table 5.1.

Generally, the kerogen description results are shown in the Figures 5.1(o) and 5.1(p) were the percentage amount of each distinguishable kerogen type is plotted versus distance to the sill. From this figures it can be seen that the background amount (values on samples far from the sill) of coaly kerogen is

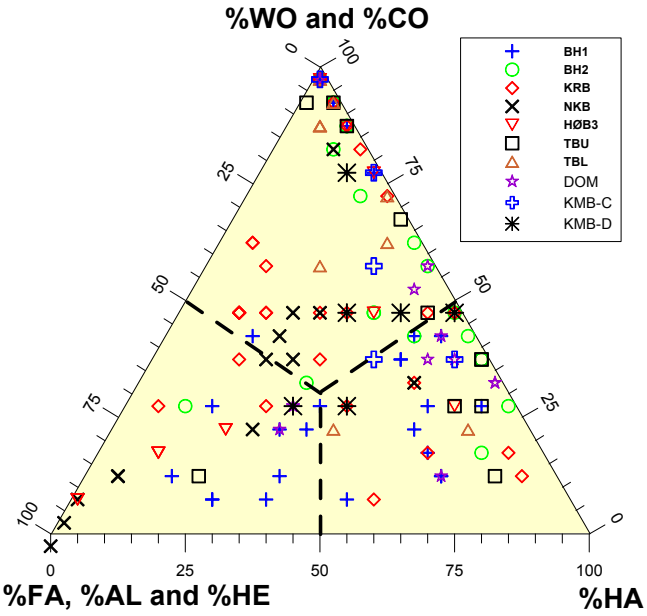

Figure 5.4: *Kerogen description results plotted in a ternary plot describing results in terms of oil - gas potential. The abbreviations used in the figure are defined in Table 5.1. FA, AL and HE kerogen are believed to be oil prone, versus WO and CO which mainly give potential for gas. HA is regarded as dead carbon with no potential for neither oil nor gas.*

approximately 30%. At a distance of 80% to 100% sill thickness away from the sill the amount of coaly kerogen starts increasing in amount and often (there is quit a bit of scatter in the data-points) reaches 100% at distances up to 50% of the sill thickness.

An increasing amount of the identified kerogen particles are identified as coaly when approaching the sill. This is natural since the H/C and O/C ratio in kerogen will become increasingly lower with increasing maturity. This occures as a consequence of generation and release of hydrocarbons, see also Section 2.4.2 on page 15.

The general pattern from the kerogen description is accordingly that the samples become more and more coaly and “coke-like” i.e. the aforementioned and structural rearangement of vitrinite at extreme heat when approaching the sill at distances less than one sill thickness. Although this is the general pattern, Figure 5.1(o) show that especially non-fluorescing amorphous material (HA) can be quite abundant in the samples even at short distances from the sill. All the other kerogen types described disappear at distances less than 20% sill thickness (with one exceptions; TBL-2 (FA=20%)).

The stability on the other kerogen particles, based on this study, is summarized in Table 5.2

Ternary plots In addition to kerogen composition plots it was chosen also to make ternary plots, (Figures 5.4 and G.2). Abbreviations The first corner is the

Parameter	Behaviour (trend) during sill approachment
FA	stable until one sill thickness.
HA	stable until one half sill thickness.
AL	can not be determined based on this study due to only a few of the samples containing AL kerogen.
HE	stable until 1/3 sill thickness.
WO	stable until 2/3 sill thickness.
CO	end product, stabile more or less all the way.

Table 5.2: *Stability off the kerogen particles based on this study and their abbreviations used in this chapter*

sum of FA, AL and HE, the top corner is sum WO and CO and the third corner is HA. The thought behind this subdivision is that the first corner is "oil-prone", the second corner is "gas-prone" and the third corners has no potential. Plotting the frequency for each sample in this diagram will give an indication of the sample being oil-prone, gas-prone or having no potential for oil/gas.

This plot was made after reading about kerogen in Tissot and Welte (1984). I have not seen the plot used in the literature but I am confident as to the plot's usability for indicating oil potential. My only doubt about the plot is the placement of CO. For the samples of this study, CO would maybe have been better placed together with HA, i.e. in the no potential corner. For general use, however, CO can have good potential for gas and is therefore grouped together with WO.

Kerogen changes within each sample series:

BH1, Botneheia East, Central Spitsbergen The BH1-series (Table G.1, Figures G.1(a) and G.2(a)) has a sill located within the sampled section. The distance measurements are from the base of the Botneheia formation. The kerogen description is in agreement with the vitrinite reflection data, namely that the sill must be located at approximately 45 meter from the base of Botneheia Fm. The sample collected at 45 meter contains 100% coaly kerogen, the sample collected at 46,8 meter also contain 100% coaly kerogen. Both samples are noted "poor" in the IFE report. A sample collected at 46,9 meter (above the sill) contains 50% HA, 5% HE and only 45% CO. The sample at 52 meters contains 30% FA, 15% HA, 5% AL, 10% HE, 10% WO and 35% CO. All samples at this distance from the sill and the samples farther away from the sill contain more than 30 % FA. Below the sill we have a similar development. FA together with AL and HE are believed to be the most "oil-prone" kerogen types, it is therefore natural that FA disappear close to the sill. The temperature from the sill has caused generation and release of petroleum close to the sill and it follows that these kerogen types are not to be found close to the sill.

In Figure G.2(a) we see that the gross composition plots in the FA, AL and HE corner, for the samples most distant to the sill. Closer to the sill HA dominates. Samples collected close to the sill plots in the WO and CO corner. To evaluate

this plot it is also necessary to have an eye on Figure G.1(a). From looking at Figure G.1(a) we see that there are three kerogen types dominating; FA, HA and CO. As we move closer to the sill FA expel its oil and becomes HA. WO is coalified and becomes CO. I therefore would interpret from this plot that the Botneheia Fm. has a good potential for oil and some potential for gas.

BH2, Botneheia 2, Central Spitsbergen In the BH2-series (Table G.2, Figures G.1(b) and G.2(b)), we observe the same increase in coaly kerogen as the sill is approached. In this series there is a reversal close to the sill were HA is even more abundant than in the samples farthest-from-sill. This reversal occur in the same samples as described earlier. For the kerogen description overall this retreat is only observed in this sample series alone and it is therefore difficult to be conclusive.

Figure G.2(b) show that the source-rock at this location has a far less source rock potential compeared to the source-rock at the BH1 sample series, even though both sample series were collected at Botneheia in the same source rock, the Botneheia Fm. A explanation for this could be that the sill at the BH2 sample series is rather thick (35 meter) whereas the sill for the BH1 sample series is thin (on the order of 1 meter). Heat from the sill changes FA into HA. Since the sill is thin at the BH1 sample series, it affected only a few of the samples. For the BH2 sample series, the thicker sill affected almost all the samples and only one sample plot in the oil potential part of the diagram. Surprisingly, this is sample BH2-1, one of the samples collected closest-to-sill (0.7 meter). From looking at Figure G.1(b) the reason for this sample to plot here is a considerable amount of FA kerogen. Normally I would have expected this to change into HA so close the sill.

KRB, Kreftberget, Barentsøya Table G.3, Figures G.1(c) and G.2(c). In the samples most distant to the sill several contain 25% WO. It seems that WO kerogen is easy influenced by temperature and therefore seldom occurs at distances shorter than one sill thickness. In the most distant from the sill samples we also have FA kerogen which totally disappears when approaching the sill. In two samples we observe some AL kerogen. From Figure G.1(c) it also seems likely to suggest that when FA experiences heat, it is first transformed into HA and then are stable to about one half sill thickness.

Figure G.2(c) shows an overweight of HA and CO kerogen with CO increasing as the sill is approached. The samples most distant to the sill show some oil potential but the potential is considerably lower for these samples compared with the samples belonging to the BH1 sample series. From Figure G.1(c) we can see that the amount of WO kerogen is also considerably higher than in the BH1 and BH2 series. This means that the Botneheia source-rock at Kreftberget probably have been deposited in an environment closer to land than the BH1 and BH2 series. The amount of HE kerogen is higher than in the BH2 series, but comparable to the BH1 series.

TBU and TBL, Teistberget, Eastern Spitsbergen The TBU- and TBL-series (Tables G.7 and G.8, Figures G.1(d), G.2(g), and G.2(h)), represent the profiles above and below the 18 meter thick sill at Teistberget. The pattern of the kerogen constituents are very similar to the BH1 sample series were we also have a sill in the middle of the sample series. WO kerogen is stable until one half sill thickness. HE kerogen is stable until between 1/4 and 1/3 sill thickness. FA kerogen is stable until one sill thickness, then changing to HA that remains stable until 4/3 to one sill thickness.

Figure G.1(d) show how CO kerogen increase on both sides of the sill as the sill is approached.

Figures G.2(g) and G.2(h) could have been plotted as one plot. As they now appear as two different plots it is, however, very clear that the source-rock intruded is of the same type above and below the sill with a predominance of HA an CO kerogen.

DOM, Domen, Eastern Spitsbergen The DOM-series (Table G.9, Figures G.1(e) and G.2(f)), are the only sample series were kerogen description have been done and the source-rock is not the Botneheia Fm. The source-rock in this sample series is the Janusfjellet subgroup or more precisely the Agardhfjellet Fm. which is equivalent to the Hekkingen Fm. in the Hamerfest Basin, in the Barents sea. Here FA is stable at 3 sill thicknesses but disappears closer to the sill. WO kerogen is still present at 1/4 sill thickness. HE kerogen disappears at 1 sill thickness. Even though the sill is thin (8 meter), AL kerogen is not present even in the most distal samples.

Figure G.2(f) show that the DOM series source-rock most have been deposited in an environment very similar to the environment for the Botneheia source-rock. A little more WO kerogen indicating a more proximal environment than the average for the Botneheia samples described in the BH1 and BH2 series, but not more than what would be described for the Botneheia NKB sample series further down. (Especially the frequency plot of the DOM series reflects the BH2 sample series Figures G.2(b) and G.2(f)). This is in agreement with what is being stated in Chapter 3 on page 25 were both are listed as being shelf deposits. Botneheia being deltaic influenced and Janusfjellet just listed as being of marine shelf origin.

HØB3, Høgrinden South, Barentsøya The HØB3-series (Table G.6, Figures G.1(f) and G.2(e)), are together with the BH1 sample series, the only that have more than one sample containing AL kerogen. All three samples in the HØB3 sample series with AL kerogen have a possible 20% content of algae. This is significantly lower than the content of Al kerogen in SR-1 (Table G.12 and Figure G.1(j)). It is thus, on the basis on this study, difficult determine the stability for AL kerogen. The most-close-to-sill sample were AL kerogen is found is 16,5m. away from the sill. With a sill thickness of 7 meters at HØB3 this means that AL kerogen may be stable until two sill thicknesses away from the sill. The HØB3 samples most distant from the sill are also the ones that bears the closest resemblance to the SR-1 sample. The FA kerogen content is significant on the farthest away

from the sill samples. The closest-to-sill samples contain some HA kerogen, but the sample at 3m. from the sill contains only CO kerogen. Sign of a possible reversal, as observed and discussed for the BH2 sample series?

Figure G.2(e) together with Figure G.1(j) show that this sample series have a higher amount of AL and HE kerogen than any of the other sample series in this study. This does not necessarily mean that the HØB3 sample series have been deposited under other conditions than the other sample series. It could simply be because we in the HØB3 sample series have an much thiner sill. The samples that have be collected far from the sill in term of sill thickness in the HØB3 series, would be less influenced by the sill than samples in the other sample series, who have been collected at the same distance in term of meter, but much closer to sill in term of sill thickness. AL and HE kerogen are both easily influenced by the heat of the sill. As, the samples in the HØB3 series were less influenced by the the sill (they are located much farther away from the sill in term of sill thickness) more AL and HE kerogen have been preserved in the "most-far-from-sill" samples in this series.

KMB-C and KMB-D The series KMB-C was collected along a single horizon away from the Kreftsberget sill and the KMB-D series was collected parallel to the same sill. See picture 4.2 on page 40. The measurements, see Tables G.10 and G.11, Figures G.1(g) and G.1(h), show that the KMB-D samples that where collected parallel to the sill are close to homogeneous with respect to the maturity parameters. The KMB-C series show a shift versus more coaly samples, but since no distance to sill is given for these samples it is difficult to be conclusive.

Figure G.2(i) show that the samples becomes increasingly coalified as the sill is approached. Figure G.2(j) illustrate the same as Figure G.1(h), and underlines that the horizon is not as homogeneous as expected.

The difference between the relatively unaffected samples of the NKB sample series, where no sill is present, and samples from the KMB-C and KMB-D sample series is noticeable. Despite this the picture in Figure 4.2 show all these samples to stem from a rather small area.

NKB, Northern Kreftberget, Barentsøya When samples were collected at the NKB-series (Table G.5, Figures G.1(i) and G.2(d)), samples were assumed to be unaffected by any sill. The samples with highest sample number are, however, clearly more mature than the samples where sampling began, which have lower sample numbers. At first this was surprising, until we analyzed the picture shown in Figure 4.2. On this picture the actual sampling profiles for the sample series NKB, KMB-C and KMB-D are indicated. From the drawing and the picture we can conclude that the end of the NKB sample series is not far from the Kreftberget sill. This explains the higher vitrinite maturity measured measurements and changes in the kerogen content. As background values for the kerogen description components, only, the first samples in this sample series can be used. Unfortunately, because of the sill, this sample series can not be used for describing the variability of kerogen in a totally unaffected sample series. What the series does tell us is that the Botneheia source-rock contains a high amount

of FA kerogen in the samples most distant to the sill, and the data are similar to those of the SR-1 standard.

Figure G.2(d) show that unaffected samples of Botneheia Fm. has a strong predominance of FA kerogen. Botneheia source-rocks should therefore be a promising potential source-rock in regions if buried sufficiently deep.

JR-1 and SR-1 The Norwegian petroleum directorate (NPD) has two standard source-rocks available for laboratories throughout the world for calibration of instruments. Table G.12 and Figure G.1(j), show the results of these two standards being measured the same way as the other samples in this study. Interesting for this study is that the source-rock SR-1 (abbreviation for Svalbard Rock 1) is actually a sample of the Botneheia Fm., the same source-rock as has been intruded by the sill in most of the sample series in this study. SR-1 contains more AL-kerogen than any of the samples in this study (Table G.12). We do not know exactly were the SR-1 sample was been collected, but assume the SR-1 to have been sampled at a place were no sill or dike has been observed.

In the SR-1 sample, AL kerogen is abundant. In the samples of this study, hardly any AL kerogen is present. This could mean that AL kerogen is very sensitive to heat changes and that the samples of this study simply have not been collected far enough away from the sills to see this virgin background amount of AL kerogen. Also interesting is that the SR-1 sample does not contain HA kerogen, but 40% FA kerogen. This support my previous observation in the sample series that FA kerogen seem to change to HA kerogen under the heat influence of the sill.

The JR-1 standard source-rock (abbreviation for Jet Rock 1) has been sampled on the north east cost of England and is not that interesting for this study other than its use for calibrating our measurements. The measurements both for SR-1 and the JR-1 are in accordance with the values listed in NIGOGA 2000 (Weiss et al., 2004).

5.2.2 Rock Eval and related results

The Rock-Eval values are listed in the Table A.1 on page 142 to Table A.9 on page 147. Geochemical logs based on, and calculated from, the Rock Eval data can be viewed in Figures A.2 to A.8. The geochemical log figures were constructed using the Petroleum Geoscientific Interpretation System (PeGIS) software developed by Dahl and Rasmussen (2003). PeGIS is developed for applications in the petroleum industry were most data are connected to depth in a drilled well. The samples in this study has a measurement in meters from a sill. “Depth” in the geochemical logs of this study means, consequently, distance from the sill, above or below (noted in the figure text).

Figures 5.1(c), 5.1(d) and 5.1(e) show S_1, S_2, S_3, T_{max} and total organic carbon (TOC) plotted versus distance to sill in %sill thickness.

TOC was determined on the LECO instrument and, all other chemical parameters treated in this part of the thesis were measured on a Rock-Eval II. For details, see Appendix A on page 139.

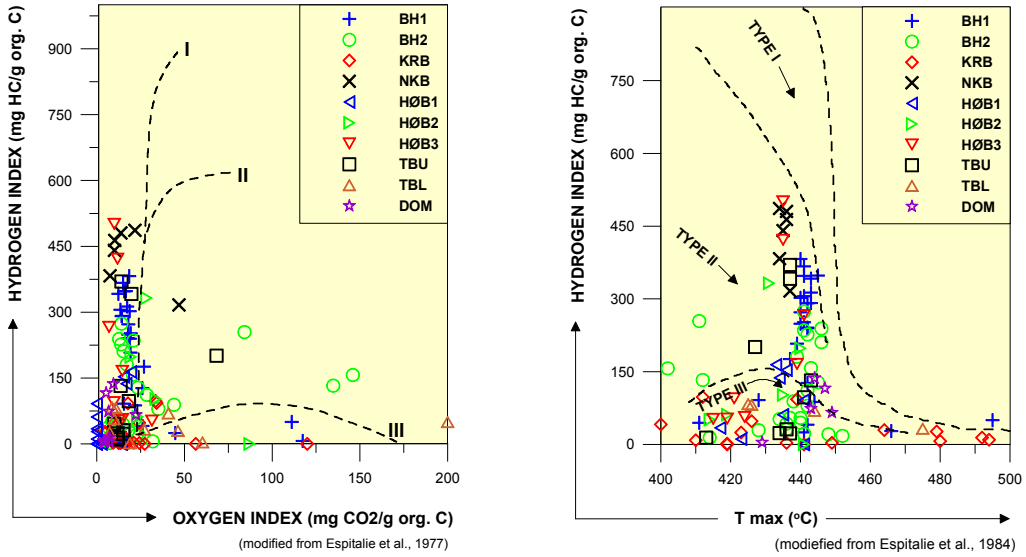

(a) Hydrogen Index - Oxygen Index

(b) Hydrogen Index - T_{max}

Figure 5.5: *"van Krevelen" type diagrams of the Svalbard data series.*

Figure 5.5(a) show the hydrogen index (HI) plotted versus the oxygen index (OI). This figure show that the samples of this study follow a thermal evolution of the organic matter along an oil-prone Type II pathway as the sill is approached (Espitalie et al., 1977). Samples approach higher levels of thermal maturity nearer to origo of the plot. The information is approximately the same in Figure 5.5(b). This figure also indicates a thermal evolution of the organic matter along a oil-prone Type II pathway (Espitalie et al., 1984). These figures are used only for rapid, qualitative description of the organic matter and the approximate level of organic maturity. In this study both the HI-OI and HI-T_{max} plots have been constructed for all the sample series. This assures the interpretation of the data to be correct and possible inaccuracy in the S_3 measurement with consequences for the OI index and following misinterpretation is avoided (Section 2.3.2).

The interpretation from pyrolysis is in agreement with Dallmann et al. (1999) were the Botneheia Formation is interpreted as a deltaic influenced, regressive shelf deposit with partly restricted environments in terms of water circulation. As we can see from the figure, there is agreement between the results obtained with Rock-Eval and the interpretation done by geologists in the field, namely that we have a marine environment with Type II kerogen/source-rock. We also have kerogen of Type III that indicate terrestrial organic material as we typically would expect in an deltaic environment (Tissot and Welte, 1984).

The relatively low production index (PI $\leqslant$ 0.3) until a distance of two sill thicknesses from sill indicates that little hydrocarbon generation has occurred before or after sill emplacement (Figure 5.1(f)). The PI is the ratio of free or distillable compounds to the total amount of organic compounds generated from a

sample by pyrolysis ($S_1/[S_1+S_2]$). At the same distance from sill, high HI and OI values indicate significant hydrocarbon generative potential (Figures 5.1(g) and 5.1(h)). The accompanying vitrinite reflectance study confirms this conclusion with vitrinite reflectance values only around 1 at the same distance from sill (Figure 5.1(a)).

At shorter distances to the sill the kerogen becomes more mature. This is reflected in the increased HI seen in most samples at distances equivalent to 1.5 sill thickness away from the contact and approaching the sill. Surprisingly, T_{max} does not assume higher values before at a distance from contact of only one half sill thickness. At the contact the highest recorded T_{max} values are just below 500°C. At greater distances, T_{max} remains almost constant at 440°C. At 50% sill thickness in the BH2 series there are two T_{max} values above 500°C, Sample BH2-13 and BH2-17. The S_2 peaks are clearly defined in both these sample. The explanation for these abnormally high T_{max} temperatures we find in the kerogen description, Appendix G on page 263. Sample BH2-13 contain 20%HA kerogen, 5% HE kerogen and 75% CO kerogen. Sample BH2-17 contain 100% CO kerogen. Both samples contains ~100% kerogen which may only yield gas if any hydrocarbons at all. The Rock-Eval analyses of the two samples show that they have a potential for gas, but only at very high temperatures.

Rock-Eval data are often used to determine the richness and quality of source-rock candidates. Only samples with TOC > 1wt% are regarded as source-rock candidates in this thesis albeit values as low as 0.3 to 0.5wt% have traditionally been used (Tissot and Welte, 1984). Increased maturity of a source-rock sample decrease the petroleum potential. A plot of the measurements of TOC versus S_2 is often used to evaluate this. Commonly accepted limit values are given in Figure 5.6.

In most series the samples most far away from the sills show the greatest potential, wereas the closest-to-sill samples only show fair potential. This is why increased maturity of source-rock samples decrease the petroleum potential. Generally, the Botneheia Fm. seem to have good to rich potential as a source-rock for hydrocarbons.

Total organic carbon (TOC)

From locking at the geochemical logs on Figures A.2 to A.8 it appears to me that for some of the series, TOC values seem to increase when approaching the sills. This was, and is, disturbing since the TOC content was thought to be homogeneous throughout the sample profiles before sill emplacement took place, opening for the possibility that the TOC would be decreasing as the sill is approached.

Instead, in some of the sample series, the opposite is recorded by the LECO TOC determination instrument (Figure 5.7).

The sill itself is an igneous rock, and at the temperatures it had when intruding the source-rock there is no way the sill itself can bring organic matter to the surrounding rock. The increased TOC values close to where the sill is emplaced must therefore have a lithological explanation. The sill should cause a lowering of the TOC when hydrocarbons are formed and transported away from the sill,

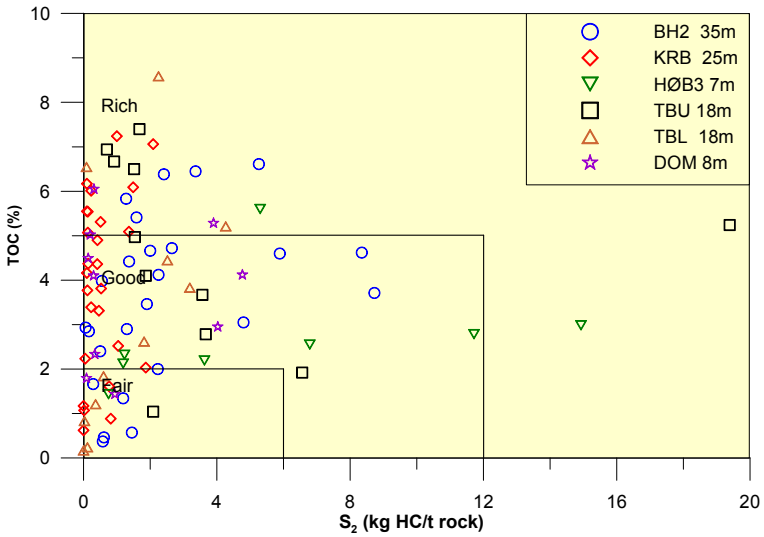

Figure 5.6: *Values for TOC (%wt of total carbon in source-rock) and S_2 (source-rock petroleum potential, mg petroleum pr. g TOC) indicate the richness and quality of source-rock candidates. Only samples with TOC > 1wt% are regarded as source-rock candidates. Increased maturity of source-rock sample decrease the petroleum potential.*

at emplacement and some time after. This is because of the high temperatures and violent mobilizations of water and organic and inorganic gases e.g. CO_2 around the sill immediately after sill emplacement and the subsequent cooling of the sill. A lovering of the TOC is also visible from 25% sill thickness and approaching the sill. The increased TOC content in some of the sample series seem to start at 100% sill thickness, but lowered from 25% sill thickness.

If the hydrocarbons are not able to escape the source-rock, generated hydrocarbons would probably backmigrate when the sill cools down. Generated hydrocarbons would gather in cracks and pore volume available. The sill intrusion event would have made the rock around the sill "dry", evaporating the water in a radius around the sill. The high temperatures could also cause cracks to be made in the surrounding rock. Generated hydrocarbons could also leave open pores behind if they are able to escape. When the sill cools down, generated hydrocarbons may have backmigrated to fill the holes and cracks caused by the sill emplacement. This can, however, not explain the observed increase in the TOC content when approaching the sill.

The question is not really why the TOC content increases. As already stated, this must be due to lithological changes within the rock. The question is maybe rather why does the sill seem to be emplaced within the rock were measurements show that the TOC content is at its maximum.

Could it be that the high TOC content also is associated with low shear strenghts within the rock? Studies on fold and thrust belts have shown these to be located within organic rich shale formations with low shear strenghts. Hydrocarbon generation is believed to further lower shear strenghts and favour formation of faults where organic content is high (Andresen, 2005). I therefore

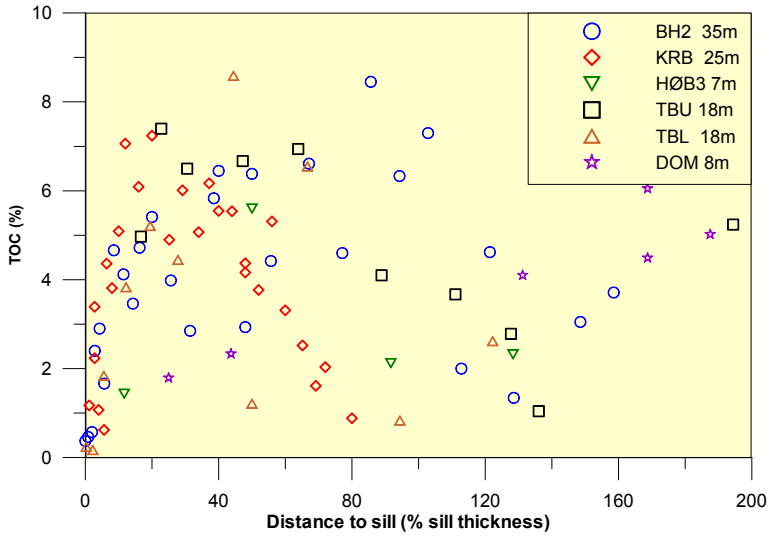

Figure 5.7: *TOC values increase for some of the sample series towards the sill but fall back to lower values at the contact. See explanation in the text.*

find it possible that the sill is located were the TOC content is at its maximum because this would be the easiest place for the sill to penetrate into the the source-rock.

The change in organic content towards a sill determined with Rock-Eval and Leco is summarized in Table 5.3.

Rock-Eval and TOC changes within each sample series:

BH1, Botneheia East, Central Spitsbergen For the BH1 series, the sill is located at approximately 45 - 46 meter from the base of the Botneheia formation where sampling began, according to vitrinite reflectance values, see Section 5.2.1. This is clearly reflected in the geochemical log (Figure A.2). S_1 which are free hydrocarbons in the rocks porespace is at its highest level at 47.5 meter. This is slightly above the level were the sill is expected to be. Around 45 meter we also observe a decrease in S_2 and HI values (which are related via TOC). OI is at its highest levels at 44.96 and 46.9 meters. T_{max} is at its highest at 44.96m which corresponds to the sill border below the sill. This is expected since the sill at this short distance should have matured significantly the source-rock. The activation energy needed to crack kerogen into hydrocarbons is interconnected with maturity. When running Rock-Eval the kerogen remaining in the rock during the temperature program progressively has higher activation energies. Hence the peak of S_2 generation is occuring later for mature than for immature samples. TOC is at its highest at 47.5 meter, slightly above the sill. At what appears to be the sill border at 44.96 and 46.9 meters we have the lowest values of TOC. But at the next sample, TOC is back to what is average through the series. That TOC seems to be little affected by the sill means that the hydrocarbons generated by the sill is still present in the porevolumes of the rock. That the sill caused

Parameter	Behaviour (trend) during sill approachment
TOC Total Organic Carbon	seems to increase approaching a sill, then decrease towards sill from 15% sill thickness
$\mathbf{S}_1$	stable until one half sill thickness (50%).
$\mathbf{S}_2$	stable until one sill thickness (100%).
HI Hydrogen Index	stable until one sill thickness (100%).
OI Oxygen Index	stable, then increases towards sill from 15% sill thickness.
PI Production Index	stable until one sill thickness (100%).
$\mathbf{T}_{max}$	stable, then increases towards sill from 15% sill thickness.

Table 5.3: *Change/stability in organic content towards a sill determined with Rock-Eval and Leco on the samples in this study*

generation of HC is evident because of the higher S_1 and the lower S_2 around where the sill is located. PI also reaches its highest values around were the sill is located and is in agreement with the expectations. See also Table A.1.

Both the HI-OI, Figure A.10(a), and the HI-T_{max}, Figure A.10(b), show a thermal evolution of the organic matter along an oil-prone Type II pathway. Two samples just above the sill show high OI values. These values are probably not reliable because of the very low TOC values for these samples. The kerogen in the BH1 samples series is therefore interpreted as Type II kerogen.

The BH1 samples are collected at the place that has given the Botneheia Fm its name. The samples examined here should therefore give the best evaluation of the Botnheia Fm. potential as a source-rock at its type locality. Figure A.10(c) show that both the TOC and S_2 contents are high in most samples. Samples at more than 2 meters from the sill on both sides all plot in the “Good” potential area. At a slightly larger distance from the sill, all samples plot in the “High” potential region. The Botneheia Fm. should therefore be regarded as a promising source-rock with a high potential for generating petroleum.

BH2, Botneheia 2, Central Spitsbergen The geochemical log for the BH2 series (Figure A.3) starts at the sill/source-rock contact. Samples were collected above the sill, so the depth in the geochemical log are in reality meters above sill. The S_1 values in the BH2 series are all lower than the values for the BH1 series. S_1 values at the sill/source-rock border are higher than at 5 meter from the sill but not as high as farther away from the sill. It is difficult to see any trend for the S_1 values. For the S_2 values on the opposite side, the values drop clearly at approximately 30 meters. This corresponds to approximate one sill thickness. This drop is also reflected in the HI index. Since TOC drops, HI increasses the last 5 meter towards the sill. It reaches virtually the same levels as at 30 meter from the sill. The OI shows low values all the way but increases the last 5 meters (because of the low TOC content). As already mentioned, TOC drops at the last 5 meters. PI is slightly higher than what appears to be the average for the last 20

meters, which is approximately 2/3 sill thickness away from sill. T_{max} values are reasonably uniform at values between 440 - 450°C. It is not possible to observe any change in T_{max} close to the sill for this series.

Both the HI-OI, Figure A.11(a), and the HI-T_{max}, Figure A.11(b), show a thermal evolution of the organic matter mainly along an oil-prone Type II pathway. Some of the samples have have high OI values. The same samples have T_{max} values close to 400°C indicating that we also have samples in this series with mainly Type III kerogen. What we have seem to be a mixture of Type II and Type III kerogen. This is common. The Type I, II and III pathways on the HI vs. OI diagram are only generalized; many samples plot between the kerogen evolution pathways. Kerogen evolution paths on an HI vs. OI diagram are actually broad bands (Peters, 1986).

Figure A.11(c) show that both the TOC and S_2 content are high in most samples. The description given for the BH1 sample series could have been used for this sample series as well. The difference seem to be that this series has slightly fewer samples with high S_2 values. The potential must be regarded as "Good" to "Rich". We observe that the increased maturity close to the sill are decreasing the petroleum potential in the same interval.

KRB, Kreftberget, Barentsøya The KRB sample series are like the BH2 series sampled above a sill. This means that depth in the geochemical log (Figure A.4) is in reality meters above sill. In general, the S_1 values in this sample series are low. When approaching the sill the S_1 values lie between 0.5 and 0.25 (values are higher in the most distant to the sill samples). At approximately 5 meter, from the sill the S_1 value suddenly increase to 1, and is then gradually reduced to 0.20 in the sample closest-to-sill. S_2 values decrease until 5 meters from sill then increase until 3 meters from sill and then decrease again. The decrease and increase are probably due to lithology since this is not observed in the other sample series. But the decrease from 5 meter to the sill/source-rock border is probably caused by the sill. HI that is closely related to S_2 follows the same pattern. OI seem rather uniform at values of ~15 but increases the last two meters. TOC gradually increase until 3 meters from sill and then decrease quickly. The gradual increase are probably caused by lithology changes. PI seems to wary a bit because of lithology changes then have some higher values at the last 3 meter before the sill. T_{max} values are uniform around 440°C +/- 10°C (two exceptions). T_{max} has values above 450°C the last 4 meters before the sill.

The sill at Kreftsberget is approximately 25 meters thick. Unfortunately, samples have not been collected more than 20 meters away from the sill. All samples are therefore probably affected by the heat from the sill emplacement. Background maturity values are probably not recorded in this sample series.

Figure A.12(a) show that both HI and OI values are low. The distribution of T_{max} values, Figure A.12(b) suggest Type III kerogen. When examine the S_2 tops on the Rock-Eval printouts, a great many of the low and some of the high T_{max} values become questionable. Probably are the kerogen in the samples of this series also a mixture of Type II and Type II. Compared with the BH1 and BH2 sample series, NKB may be a little biased towards Type III kerogen.

Figure A.12(c) show that the TOC content is high in most samples. The S_2 and HI values for all samples are, however, low and the PI is values are generally high. I therefore would regard this sample series potential as "Good" at the best for generating oil and "Good" to "Rich" for generating gas.

TBU and TBL, Teistberget, Eastern Spitsbergen The TBU- and TBL-series (Tables A.4 and A.5, Figures A.6 and A.7), are sampled above and below the Teistberget 18 meter thick sill.

Above the sill, all TOC values are high (higher than 2, except 1). Below the sill, most TOC values are high. But we observe the normal decrease from 15% sill thickness away from the sill. Above the sill HI seem to steadily decrease from one sill thickness away from sill The farthest-from-sill samples have very high HI values (above 300). OI seem to be rather uniform around 12 to 16 above sill. Below the sill, none of the HI values are higher than 100. HI decrease for the last three meters towards sill. S_1 and S_2 also decrease the last two meters. Above the sill T_{max} is rather uniform at values above 430°C. Below the bsill T_{max} values are above 340°C, but increase to above 400°C from 3 meters away (approximately 15% sill thickness). OI is very high at the closest-to-sill samples in the TBL series, but those abnormal values are not too likely because of the very low TOC content.

The reason for the differences in measured values above and below the Teistberget sill is probably the fact that samples from above the sill were in fact closer to the sill than the depth measurements indicate. See explanation at Figure 4.3.

Kerogen type, maturity and HC potential for the TB series are subdivided into the series TBU (Teistberget upper) above sill; Figure A.13 and TBL (Teistberget lower) below sill; Figure A.14. I will here threat them individually at first, then sum up my impression of them both.

Figure A.13(a) show a thermal evolution of the organic matter mainly along an oil-prone Type II kerogen pathway. One sample has a high OI values. The same samples has a mature T_{max} value at close to 440°C. At the same time three of the samples have low T_{max} values but have also low HI and OI values, see Figure A.13(b). The kerogen type is interpreted as a Type II, maybe with some Type III for one of the samples.

Figure A.13(c) show that the TOC content is "High" in most samples. The S_2 values are rather good for all samples. I would therefore regard this sample series potential as "Good" for generating oil and "Good" to "Rich" for generating gas.

Both Figure A.14(a) and Figure A.14(b) show results that can be interpreted as thermal evolution of the organic matter mainly along a Type III pathway. None of the samples have a high HI values although the TOC content its good for most samples. The difference in HI values from above the sill is noticeable. That the organic matter might be of another type below the sill is feasible but not likely. The kerogen type of the samples below sill has therefore been interpreted as mixture between Type II and Type III kerogen, maybe with slightly more Type III than above sill.

Figure A.13(c) show that the TOC content is "Good" in most samples. The S_2

values for most samples are between 2 and 3 kg HC/t rock. This is a little less than we would want for a oil-prone source-rock. I would therefore regard this sample series potential as "Fair" for generating oil and "Good" for generating gas.

Samples seem more influenced by the sill and show a higher thermal maturity below than above it. Maybe water steam created at the contact easier could escape above sill than below. This would make the sill cool down faster on the top. The "dry" rock on the top off the sill could also have an isolating effect on the rock at a little distance from the sill. Water has a much better heat conductivity than dry rock. Below the sill the stagnant steam from contact reaching out in the rock would heat up the rock at distances farther away from the sill.

DOM, Domen, Eastern Spitsbergen The source-rock in which the DOM-series (Table A.6, Figure A.8), was collected is rather organic rich. Samples have a TOC content on 2% wt or above. From around one sill thickness and closing in to the sill, the TOC content gradually falls. The HI index seem to be reduced from 300% sill thickness towards the sill. The PI increases in the same interval. S_1 and S_2 also decreases from 300% sill thickness and closing in towards the sill. S_3 increases causing also the OI to increase when closing in to the sill.

In general, the DOM series show the same pattern as the other series, although the DOM series is from another stratigraphic unit, namely the Janusfjellet subgroup. The other series are collected close to sills in the Botneheia formation. This means that what is being described in this investigation is probably universal for all sill emplacement into source-rock situations.

Figure A.15(a) show results that can be interpreted as thermal evolution of the organic matter mainly along a Type II pathway. Figure A.15(b) has some low T_{max} values, but they are related to low S_2 values. The samples of the DOM series are interpreted as a series dominated by a Type II mixed with Type III kerogens.

Figure A.15(c) shows that the TOC content is "Good" in most samples. The S_2 values for most samples are between 1 and 2 kg HC/t rock. This is less than what we would want for an oil-prone source-rock. I therefore would regard this sample series potential as "Fair" for generating oil and "Good" for generating gas.

HØB1, HØ2 and HØB3, Høgrinden South, Barentsøya (Tables A.7, A.8 and A.9 and Figure A.5).

These are actually three series. Unfortunately, distance to sill is only noted for the HØB3 series. A geochemical log is then consequently only constructed for the HØB3 series. It is difficult to say anything about the sill interaction for the HØB1 and HØB2 since the distance to sill is not noted.

Noticeable for the HØB1 series (Table A.7) are the very low S_1, S_2 and S_3 at low sample numbers, meaning close to the sill. TOC seems to be rather uniform throughout the series, but seems to increase a bit at lower sample-numbers. $CACO_3$ is also very stable, indicating the same lithology in the entire series. T_{max} is rather uniform at values between 420°C and 450°C. For samples with

low sample-numbers T_{max} values can not be trusted since no S_2 peaks have been recorded.

The HØB2 series (Table A.8), like the HØB1) series, have very low S_1, S_2 and S_3 values for samples with low sample numbers. OI is very high in the samples with low sample numbers but this is not likely as TOC is only 0.31 wt. %. HI decrease in the samples as the sample-number became lower indicating that we approach a sill. OI is rather uniform when not considering the samples with low sample-numbers. T_{max} is uniform around 420°C to 440°C when not considering samples with low sample-numbers. It seem therefore clear that the HØB2 sample series has been collected next to a sill.

For the third of the Høgrinden sample series, HØB3 (Table A.9 and Figure A.5), distance to sill has been noted. Additionally, it is noted that the samples have been collected laterally along a single horizon. Laterally should mean that the samples with increasing sample number at least moves away from the sill, but not necessary at a 90 degree angle. TOC decrease slowly from 2.98% wt. at 30 meters away from the sill (500% sill thickness away) to 1.43% wt. 0.7 meters away from the sill. The sill is 6 meters thick. S_1 decreases slowly when closing in towards the sill. S_2 decrease from 14,93 at a distance from sill equal to 500% sill thickness to 0.75 at 5.5 meters (equals approximately one sill thickness). HI decreases and OI increases. PI increases from 0.1 to 0.39. T_{max} values are pretty uniform at values between 420 and 440.

In the HØB1 sample series most samples have very low OI values because S_3 is 0 or close. HI is not very high neither. T_{max} values lie around 430 to 450°C (except for one sample). Interpretation of kerogen type is therefore a bit uncertain but the samples seem to follow a Type II pathway (Figures A.16(a) and A.16(b).

Figure A.16(c) shows a very low TOC content. The potential for this source-rock is therefore only “Fair”.

The HØB2 sample series has two samples with HI values higher than 150 mg HC/g org C. Samples seem to follow a Type II kerogen pathway. See Figure A.17(a). The HI-T_{max} diagram also gives results that has to be interpreted as a Type II kerogen pathway.

Figure A.16(c) has the lowest TOC content of all the sample series, but none of the samples has a TOC contents lower 1.0 % wt. The petroleum potential for the HØB2 is therefore, as for the HØB1 sample series, only “Fair”.

The HØB3 sample series contain considerably better samples compared with the HØB1 and HØB2 sample series. Figures A.18(a) and A.18(b) both show that the kerogen is probably of Type II and show higher maturity as we approach the sill.

The petroleum potential for the HØB3 samples is also considerably better than for the HØB1 and HØB2 samples. Most samples have a TOC content above 2 % wt. S_2 values are also good. I regard the potential to be “Good” for for gas and a bit lower, but still “Good”, for oil.

NKB, Northern Kreftberget, Barentsøya The NKB-series (Table A.10, Figure A.9), were, as already mentioned in Section 5.2.1, sampled under the assump-

tion that the samples should not be under the influence off any sill. Vitrinite description and kerogen description showed however this not to be true. For the Rock eval results, however, the samples seem to be little affected by the sill, at least for the samples most distant to the sill. Values rather closely follow the TOC and $CaCO_3$ content. Differences between the samples can then be explained as differences in lithology. T_{max} is uniform at approximately 435°C for all the samples. PI is low for all the samples (mean value 0.09).

The NKB sample series were sampled where no sill was thought to have influenced maturity. As previously interpreted from the vitrinite and kerogen description data, this has been showed not to be correct. The thermal maturity difference is also reflected in the Rock Eval data, but not so clearly as for the vitrinite reflectance data. Figure A.12(a) shows results that can be interpreted as thermal evolution of the organic matter mainly along Type II pathway. There is a bit of variation in the HI values, but generally they become less pronounced the closer we get to the sill. Figure A.12(b) also show that the kerogen is of a typical Type II. All T_{max} values are between 434 and 434 °C.

Figure A.15(c) show that both TOC and S_2 content is high for all samples except one. The potential for the source-rock plots in the "Rich" area of the TOC-S_2 diagram. This source-rock should have a great potential as a source-rock for both oil and gas.

5.2.3 Extractable organic matter (EOM)

The results obtained from Iatroscan analysis of the extracts are presented in this subsection. Tables B.1 to B.11 in the Appendix B lists the gross composition in terms of absolute yield and relative percentages of saturated hydrocarbons, aromatic hydrocarbons and polar compounds. Figures B.1 to B.10 show the composition for all the samples.

Each sample series have been closely examined by looking at the total yield and percentage of the saturated, aromatic and polar components. When looking at the sample series as a hole, the general picture is that the total yield is lowering when the sill is approached (disregarded a few samples most likely having higher values because of lithological changes). For the percentage distribution of the individual components, the aromatics are the only ones that clearly decrease when the sill is approached. Polars seem to decrease and saturates seem to increase in some sample series as observed by Schiener and Perregaard (1981). In this study the opposite is also observed in other sample series. We therefore find the claimed thermal evolution from polar to saturated compounds by Schiener and Perregaard (1981) doubtful, see Figures B.1(d) to B.10(d) were the number next to plot-mark tells how far we are from the sill (in meters). The evolution lines of Schiener and Perregaard (1981) have therefore not been added to the Figure 5.9.

For the sat/aro ratio, however, there seem to be a connection to maturity as claimed by Cornford et al. (1983) and Clayton and Bostick (1986) for the samples in this study. In Figures B.1(c) to B.10(c) the sat/aro ratio increase when a sill is approached. In many of the series the sat/aro ratio stabilizes at ~ 1 when we came at a certain distance from the sill. Taking the sill thickness

Parameter	Behaviour (trend) during sill approachment
SAT Saturated	decreases in yield, increases in %
ARO Aromatic	decreases in yield, decreases in %
POL Polar	decreases in yield, no change in %
SAT/ARO	increases (from one sill thickness (?) (100%))

Table 5.4: *Change/Stability in organic content towards a sill determined with Iatroscan TCL-FID on the samples in this study*

into account this seem to happen at approximately on sill thickness away from sill, meaning that the sill is capable of influencing the saturated, aromatic and polar components at a distance equal to its own thickness, but not further away (Figure 5.8).

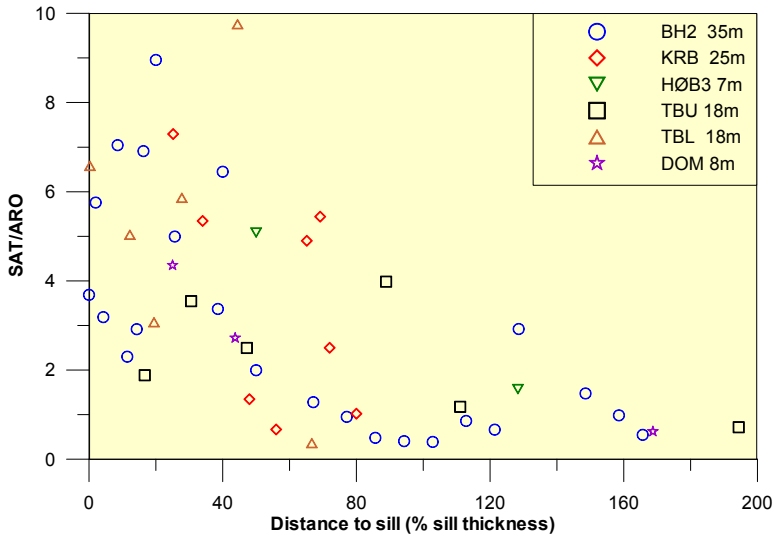

Figure 5.8: *SAT/ARO values increase when approaching the sill.*

The change in organic content towards a sill, determined with Iatroscan analysis is summarized in Table 5.4.

Description of the iatroscan results for each sample series:

BH1, Botneheia East, Central Spitsbergen Also on Iatroscan data the location of the sill on the BH1 sample series is easily detected, although not as clearly as on the Vitrinite and Rock-Eval data, see Table B.1 and Figure B.1.

The total yield, Figure B.1(a), is clearly less than the other samples on the sample nearest to the sill at 46.9 meter. On the other side of the sill the total yield falls in all samples except the sample nearest to the sill (at 44.65 meter).

On the diagram showing the percentage of saturated hydrocarbons, aromatic hydrocarbons and polar compounds (resins and asphaltens) the effect of the sill

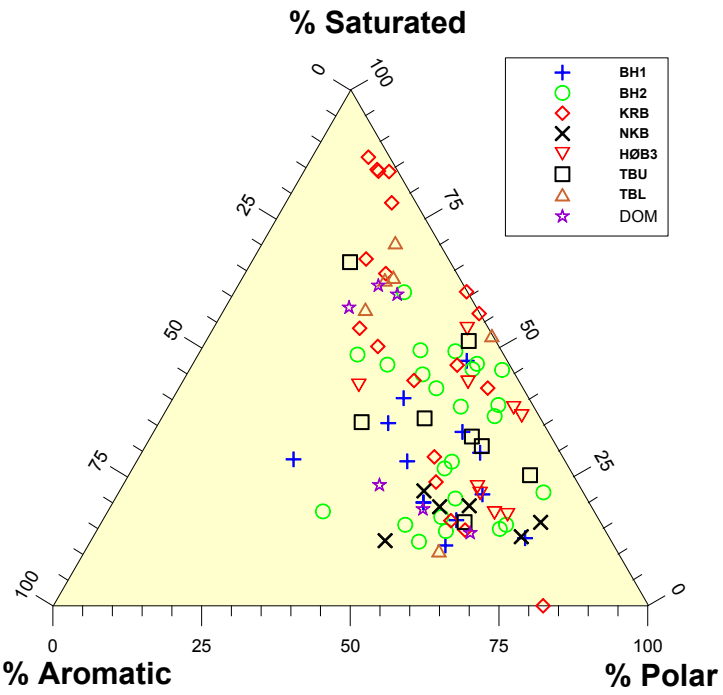

Figure 5.9: *A ternary plot of saturated, aromatic and polar compounds of the 48 selected samples*

is less clear (Figure B.1(b)). It looks like the percentage amount of aromats falls on each side of the sill.

The decrease in aromats and combined increase in percentage of saturated compounds leads to an increase also in the sat/aro ratio. This is expected with increasing maturity (Figure B.1(c)).

On the ternary plot, no trend is clear (Figure B.1(d)). The most mature samples show a higher amount of saturated compounds than the least mature that show an higher amount of polar compounds. Since the percentage of aromatic compounds varies quite a bit, the picture becomes rather chaotic. The trend reported by Schiener and Perregaard (1981), from polar to saturated compounds, can not be seen on the BH1 sample series although the samples also here seem to be increasingly richer in saturated compounds.

BH2, Botneheia 2, Central Spitsbergen For the BH2 sample series, where the sill is below the sample series, the same pattern as for the BH1 sample series is recognized (Table B.2 and Figure B.2). In fact maybe a little easier here since the sill is located on the bottom of the sample series, not within.

Despite some scatter the trend for the total yield is clearly a decrease for all the compounds (Figure B.2(a)). For the individual compounds, polars and aromats decrease whereas saturated seem to increase a bit.

When it comes to percentages (Figure B.2(b)) saturated compounds clearly increase. Polars and aromats decrease. The decrease in amount for polars and

aromats seem to occur through the hole sample series, no sample seems unaffected by the sill. If it is true that the sill at the BH2 sample series is 35 meters thick, it affects the amounts of saturated, aromats and polar compounds at at least 1.6 times the sill thickness (the most far away from sill sample is collected at 58 meters from sill).

The sat/aro ratio increases from around 1 for the samples most far away to around 5 for the samples close to the sill. One sample, at 19,5 meters from sill, has a, for this series anomalously high sat/aro ratio. Since the values presented here are the average of two sample runs at the Iatroscan the value should be correct or at least any wrong values should be detectable. The reason for the low amount of aromats at 19.5 meter is unknown, but one sample can not affect our interpretation of the general development within the sample series.

The ternary plot (Figure B.2(d)) shows no obvious trends. Generally the most mature samples have a little less amount of polar and aromatic compounds and amounts of polar compounds increase with maturity. No sample reaches more than 50% in saturated compounds even at the shortest distances to the sill.

KRB, Kreftberget, Barentsøya The KRB sample series is also located above a sill. The results for vitrinite reflectance show a very good, and increasing reflectance profile when approaching the sill (Figure F.3). The pattern shown by the Iatroscan results is not so regular (Table B.4 and Figure B.3). In fact, Figure B.3(a) almost looks as if we have not one but two sills in the profile. Well, we only have one sill here and that sill is located next to the sample collected at 0.1 meters from sill. Here at 0.1 meters from the sill, there samples was collected (KRB-1A , KRB-1B and KRB-1C). The Iatroscan analyzes of these there samples show quite different results. Especially the results from sample 1C is questionable. I therefor choose to ignore them for the interpretation of these results.

As mentioned above it almost looks as if we have two sills present. One at 0 meters and a small one at approximately 11 meters. Since this is not reflected in vitrinite reflectivity and no sill is reported here in Sven Dahlgren's report, there should not be any. The kerogen description shows high amounts of CO and AH kerogen for the samples at 11, 12 and 14 meters away from the sill (Table G.3). The low total yields for these are therefore probably lithology related.

When ignoring the lowering of the total yield at around 11 meters from the sill the pattern shown in this sample series is as for the BH1 and BH2 sample series. Total yield is lowered when approaching the sill (Figure B.3(a)). The percentage and total amount of saturated hydrocarbons increase when approaching the sill (except for the samples closer than 1 meters from sill). Aromatic hydrocarbons and polar components are reduced both in total amount and percentage when approaching the sill (Figure B.3(b)).

The sat/aro ratio increases when approaching the sill. At the last meter, before the sill we have no saturated and no aromatic hydrocarbons in the samples. Consequently the sat/aro ratio for these samples is zero (Figure B.3(c)).

The ternary plot, Figure B.3(d) shows that the samples all plot close to the polar - saturated line. Polar components are closest in resemblance with virgin

kerogen. A maturity line, as reported from polar components versus saturated hydrocarbons as reported by Schiener and Perregaard (1981), therefore should exist. This sample series is the best we in this study came to the proposed maturity line by Schiener and Perregaard (1981). The samples closest-to- sill clearly plot closer to the Saturated corner of the ternary plot than the most farthest-from-sill samples that plot closer to the polar corner. There are, however, also samples collected at a distance of 16 meters from the sill (equivalent 2/3 sill thickness) that show as which as 70% saturated hydrocarbons. As previously concluded for the BH1 and BH2 sample series, there is a trend here, but this is not so clear as the sat/aro relationship.

TBU and TBL, Teistberget, Eastern Spitsbergen At Teistberget, TBU (upper) and TBL (lover) we have sample series both from above and below the sill. The vitrinite reflectance values reflect each other on each side of the sill. For the Iatroscan data, the trends are also reflected, but the yield values are quite different (Tables B.5 and B.6, Figures B.4 and B.5).

At the first glance on Figures B.4(a) and B.5(a) it seems like the analytic determined parameters are equal at coperable distances above and below the Teistberget sill. Then it becomes important to also look at the label for each sample which for these figures in the Appendix *Iatroscan* all represent the distance to the sill, in meters. When comparing the sample at 3.0 meters from the sill in Figure B.4(a) with the sample at 3.5 meters from the sill in Figure B.5(a), we see that the sample from above the sill yields far less than the sample from below. If we compare the sat/aro ratio for the same samples we see that the sample from below the sill is most mature.

That the yield above sill is significantly lower than below the sill can be explained by the distance above the sill probably being shorter than the measured value given as distance to the sill. See discussion in the Chapter 4, Section 4.2

With the discussion above in mind the main trend on both sides of the Teistberget sill is the same as for the already described sample series. The total yield decreases when approaching the sill. At least for the below sill sample series the sat/aro ratio increases, see Figure B.5(c). For the samples above the sill it can be seen that they increase in value from the most furthest-from-sill samples, but seem almost constant from the sample at 16 meters away to the sample at 5.5 meters away. This observation indicates that we for these three samples are at approximately the same distance from the sill (Figure B.4(c)).

The ternary plots look like a shotgun shot for the above sill series (Figure B.4(d)). No trends at all are visible in this plot.

For the below sill samples (Figure B.5(c)) we could have confirmed the findings of Schiener and Perregaard (1981) with the maturity trend from polar to saturated. In this plot it actually looks like we have this trend. But if we had had more samples, the picture would have been more like the other ternary plots shown in this thesis.

DOM, Domen, Eastern Spitsbergen The DOM sample series follows the same main pattern (Table B.7 and Figure B.6) as described for all the previous series

although the source-rock here is not the Botneheia Fm., but the Janusfjellet Subgroup.

The total yield gradually decreases as the sill is approached, see Figure B.6(a). The sample at 48 meters gives a significantly higher yield than the others. Unfortunately we do not have more samples for this series. The sill is only 8 meters thick. Maybe the sample at 48 meters from the sill represents the background, virgin, yields but since we do not have any more samples before reaching 29 meters from the sill (which gives far less, yield), this could be only a sample with anomalously high yield for the Janusfjelet source-rock or it could represent the virgin background values. If it represents the virgin background, the effects of the sill are visual in Iatroscan data up to 3.6 times the sill thickness away from sill (the sample at 29 meter).

When it comes to percentages, saturates and especially polars increase but the aromatics decrease (Figure B.6(b)). This is also reflected in the ternary plot were the furthest-from-sill samples plot close to the polar corner of the diagram whereas the closest-to-sill samples plot closer to the saturated corner of the diagram (Figure B.6(d)).

In the iatroscan maturity plot (Figure B.6(c)) the ratio is highest for the closest-to-sill samples.

HØB1, HØB2 and HØB3, Høgrinden South, Barentsøya For the HØB1 and HØB2 no distance to a sill is given. It is also unclear whether these samples are collected above or below a sill, if close to a sill at all.

HØB1 See Table B.8 and Figure B.7. No distance to a sill is given for this series. Compared with the other sample series it is, however, likely that a sill is not far from the sample with the lowest sample numbers. E.g. the total yield for sample 6 is much lower than for samples with higher sample numbers, e.g. sample 11 (Figure B.7(a)).

Percentages for saturated, aromatic and polar components also follow the pattern found for the other series with a known distance to a sill (Figure B.7(b)). Aromatic and polar components decrease whereas saturates increase (in percentage). For the sat/aro ratio the picture is also the same as for the other series close to a sill. The samples with low sample numbers have high values but the samples with high sample numbers have values at approximately 1 (Figure B.7(c)).

Within the ternary plot, see Figure B.7(d), the samples plot in two groups. One group where the samples plot close together and show a rather high content of polar components. The other group that has fewer polar components and does not plot so close together. I suggest that the first group has not been affected by the sill, whereas the other group shows increasing maturity and therefore does not plot close to the first one. See also Figure B.7(c).

To conclude I find it likely that a sill is located close to sample 6 or at least closer to sample 6 than to sample 13. Since no distance to a sill is given for these samples, it is difficult to use them for anything other than a general rule on how the composition of saturated, aromatic and polar components changes when

approaching sills. Since I do not know for sure that the samples are collected with increasing distance to a sill, I will not make use of this sample series when making conclusions for this sill study.

HØB2 See Table B.9 and Figure B.8. No distance to a sill is given for this series. As for the HØB1 series, the HØB2 series also seems to be located with the lowermost sample numbers close to a sill whereas the highest sample numbers seem to be samples collected further away from the sill.

Total yield is lowest for what probably are the closest-to-sill samples (those with the lowest sample numbers) (Figure B.8(a)).

Percentages of saturated, aromatic and polar components also follow the pattern of the other series (Figure B.8(b)). Aromatic and polar components decrease whereas saturates increase (in percentage). The sat/aro ratio picture is also the same as for the other series. The samples with low sample numbers have high values while the samples with high sample numbers have values at approximately 1 (Figure B.8(c)).

Based upon what I have seen for the other sample series, it looks like samples unaffected by sill(s) have a sat/aro ratio at approximately 1. None of the samples in the HØB2 sample series have a sat/aro ratio ~ 1 (Figure B.8(c)). What we see in Figure B.8(d) therefore represents difference in maturity or distance to the sill.

All measurements of Iatroscan values for the HØB2 sample series indicate that these samples also must have been collected with different distances to a sill. But, since I do not know for sure that the samples are collected with increasing distance to a sill, I will not make use of this sample series when making conclusions for this sill study.

HØB3 See Table B.10 and Figure B.9. For the HØB3 series, distances to a sill is noted, thus it also can be used for making rules on how compositions of saturated, aromatic and polar components change when approaching sills.

For the total yield measurements, the closest-to-sill sample at 0.7 meter gives the lowest yield, as expected. More disturbing is the sample at 3.0 meters, which has the highest of all the yields in this series. It is, however, no doubt that the total yield is lowered as the sill is approached, if we disregard the sample at 3.0 meters (Figure B.9(a)).

For the percentage distribution of saturated, aromatic and polar components the change when approaching the sill is as expected. Aromatic components decrease whereas saturates increase (in percentage). polar components decrease at first for the furthest-from-sill samples when approaching the sill from 7.7 meters, however, the polar components start increasing again. The sat/aro ratio also changes as expected with increasing values when approaching the sill (except for one sample at 5.5 meter) (Figure B.9(c)). All the samples from 7.7 meters and further out have a sat/aro ratio ~ 1. If we regard these samples as unaffected by the sill, it means that the sill has affected the surrounding rocks equal to one sill thickness (the sill at Høgrinden is noted to be 5-7 meter thick).

In the ternary plot, see Figure B.9(d), all the samples with a sat/aro ratio ~ 1 plot at approximately the same spot in the diagram (expect the sample from 7.7

meter). The other samples plot close to polar - saturated line (In this series, the amount of polar components does not decrease when approaching the sill as it does in the HØB1 and HØB2 series).

NKB, Northern Kreftberget, Barentsøya As mentioned before, the NKB sample series were thought to be unaffected by sills when sampled. Both the kerogen description, vitrinite reflectance and Rock-Eval data have shown this to not be true. Samples with high sample numbers are clearly more thermally mature than the samples with low sample numbers. The sampling for the samples of this series started at the base of the Botneheia Fm. and not at a sill/source rock border as for the other series.

For the Iatroscan results, see Table B.11 and Figure B.10, the total yield increases with decreasing sample number/distance to base, except for the two samples closest to base (Figure B.10(a)). The sat/aro ratio, however, is approximately 1 for all the samples, indicating no increase in maturity with higher sample number/meter value (Figure B.10(c)). The percentage plot (Figure B.10(b)) does not show the decrease in aromats as observed in series close to sills.

To conclude, the Iatroscan data for the northern Kreftberget series, NKB, gives no indication of higher maturity for the samples with high sample numbers/meter value as shown in vitrinite reflectance and kerogen description. Iatroscan or more precisely the sat/aro ratio therefore seems to be less sensitive to maturity changes than vitrinite and kerogen description analysis results.

The scatter in Figure B.10(d) is therefore most likely due to lithology changes and the fact that the kerogen precursor for the oil in these rock samples is a mixture of Type II and Type III kerogen.

5.2.4 Composition of hydrocarbons

GC-FID analysis of extracts has been used to analyse C_4 - C_{30} alkanes with the emphasis placed on the C_{15+} compounds. The n-alkane distribution together with n-C_{17}, n-C_{18}, pristane and phytane (Figure 5.10) can give valuable information about source and depositional facies, maturity and biodegradation. For this study, where the source is not questioned, maturity determination has been the main focus.

n-alkane pattern

The n-alkane patterns can be used to classify chromatograms, giving valuable information about the facies and maturity of the samples (Peters and Moldowan, 1993).

In this study we are generally interested in maturity and hydrocarbon generation, the facies of the Botneheia and Janusfjellet Formations have been examined in many other studies. Generally the pattern for the n-alkane GC-FID chromatograms is like the two chromatograms in Figure 5.10. Close to the sill(s) the chromatograms are biased; n-alkanes concentrate predominantly on the high carbon number side, like Figure 5.10 A.

Peak name	Identity
n-C_{17}	n-Heptadecane
n-C_{18}	n-Octadecane
pr (C_{19})	Pristane
ph (C_{20})	Phytane
n-C_{23}	n-Tricosane
n-C_{24}	n-Tetracosane
n-C_{25}	n-Pentacosane
n-C_{26}	n-Hexacosane
n-C_{27}	n-Heptacosane
n-C_{28}	n-Octacosane
n-C_{29}	n-Nonacosane
n-C_{30}	n-Triacontane
n-C_{31}	n-Ettriacontane
n-C_{32}	n-Dotriacontane
n-C_{33}	n-Tritriacontane

Table 5.5: *Identified peaks from the GC-FID chromatograms*

Far away from the sill, where the sill has not affected the samples, or at places were no sill is present the n-alkane pattern shows a decrease in peak height with increasing carbon number, creating a concave curve in the chromatogram like in Figure 5.10 B.

Carbon Preference Index (CPI)

In this study the CPI was calculated using the following equation (the Bray and Evans 1961 method):

$$CPI = \frac{1}{2}\left(\frac{C_{25}+C_{27}+C_{29}+C_{31}}{C_{24}+C_{26}+C_{28}+C_{30}} + \frac{C_{25}+C_{27}+C_{29}+C_{31}}{C_{26}+C_{28}+C_{30}+C_{32}}\right) \tag{5.1}$$

For comparision CPI was also calculated on the easier Philippi (1965) method:

$$CPI_{\text{Philippi}} = \frac{2C_{29}}{C_{28}+C_{30}} \tag{5.2}$$

In Figure 5.11 all calculated CPI values are plotted versus distance to the sill at Teistberget. CPI and CPI_{Philippi} follow each other closely, and the interpretation of both is the same. The CPI_{Philippi} is, however, more sensitive to errors since fewer parameters are used for the calculations. CPI_{Philippi} was a faster method to calculate CPI values in the time before computers became common. Today with computers available to perform these calculations, both methods take equally long time. Since errors can more easily appear with the CPI_{Philippi} method, we feel most comfortable with using the first CPI by Bray and Evans (1961) even though both have been used successfully in numerous publications.

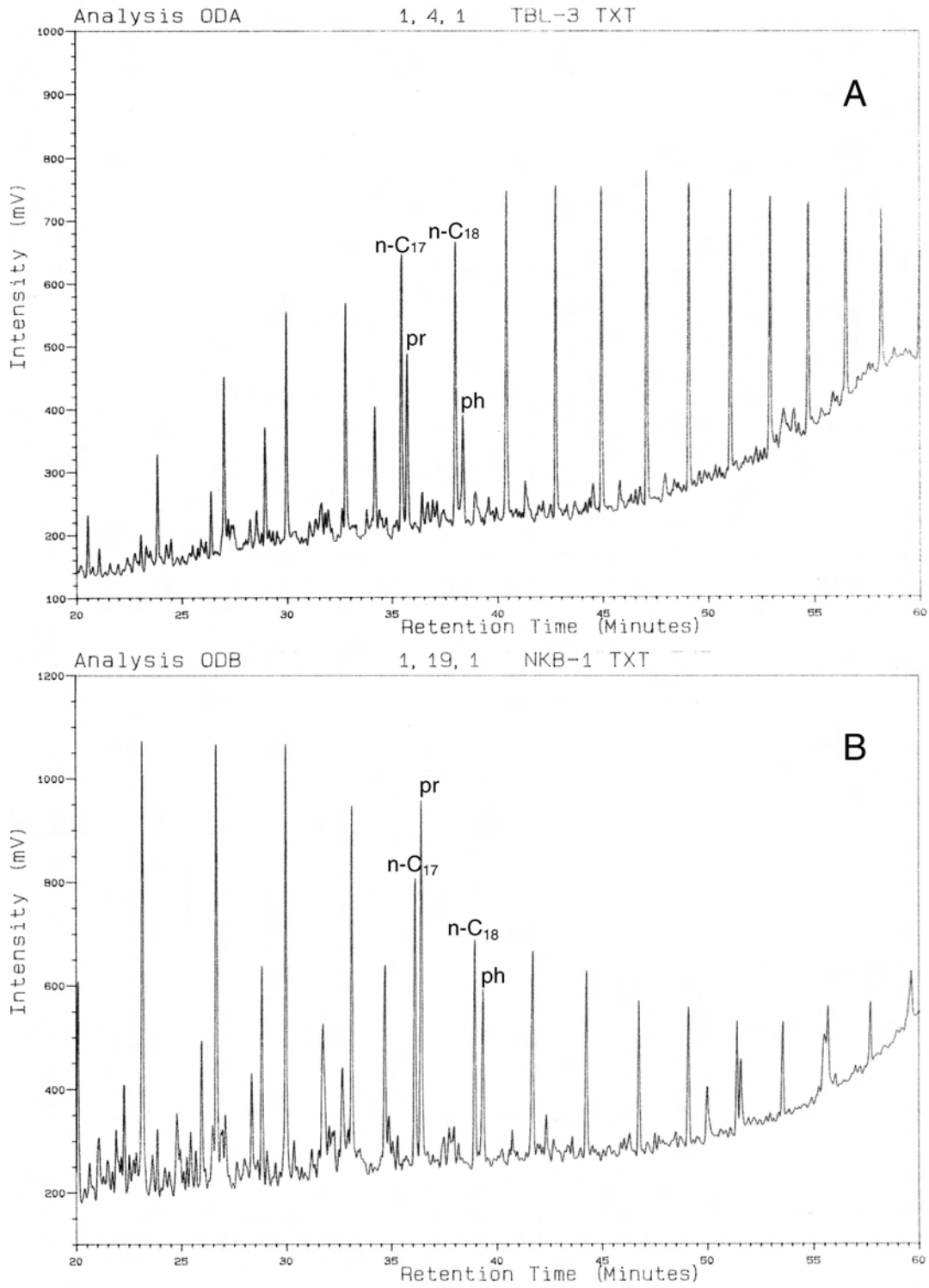

Figure 5.10: *Typical GC-FID traces from this study. Note the difference in the n-alkane pattern for the mature, close to sill sample A, compared to sample B, a sample taken where no sill is present. Both samples were taken from the Botneheia source-rock formation and have both been buried to approximately the same depths in the past (and therefore experienced the same temperature histories before the sill intruded).*

To evaluate if the extracts had the same odd/even distribution for both short and longer chained n-alkanes two further CPI values were calculated:

$$CPI_1 = \frac{C_{23} + C_{25}}{C_{24} + C_{26}} \tag{5.3}$$

$$CPI_2 = \frac{C_{27} + C_{29} + C_{31}}{C_{28} + C_{30} + C_{32}} \tag{5.4}$$

The plot of the different CPI parameters versus distance to a sill, Figure 5.1(l), shows differences in value. The explanation is, as we also have seen by other measurements on the samples that the organic sources for the Botneheia Fm. and the Janusfjellet Subgroup are a mixture of marine Type II kerogen and terrestrial Type III. Marine Type II kerogen will predominantly produce normal hydrocarbons in the range n-C_{17} to n-C_{19}. Terrestrial Type III kerogen will predominantly produce terrestrial plant waxes in the range n-C_{27} to n-C_{33}. Terrestrial kerogen is found to produce odd number n-alkanes in abundance whereas marine Type II kerogen produces equal amounts of odd and even numbered n-alkanes (Bray and Evans, 1961). High CPI indicates low maturity and land plant input. Oils and source-rocks with CPI~1 may arise from a predominance of marine input and/or thermal maturation of any type of organic matter (see Subsection 2.3.4, Carbon Preference Index)). The difference on CPI_1 and CPI_2 can thereby be explained by terrestrial matter giving an odd carbon number preference. The terrestrial input most strongly affects the long chained n-alkanes represented by CPI_2.

n-C_{17}/n-C_{31} ratio

The ratio of n-C_{17}/n-C_{31} given in Tables D.1 to D.11, is a simplified parameter that is generally thought to reflect relative contributions of aquatic/marine and terrestrial n-alkanes.

Degradation of organic matter can alter the n-alkane distribution and thereby modify the source signal by enriching the more stable land-derived fraction through enhanced loss of the more labile aquatic lipids (Sinninghe et al., 2003).

The samples of this study have a predominantly marine signature in the n-alkane distribution for all samples at some distance from the sill. Approaching the sill, the n-alkane pattern changes (Figure 5.10). This change is due to emplacement of light hydrocarbones with warm water steam, orginating from the sill.

In this study the n-C_{17}/n-C_{31} ratio is therefore used to see how far from the sill the emplacement has altered the n-alkane distribution. (The thermal degradation of the samples closest to the sill becomes numerically evident using the n-C_{17}/n-C_{31} ratio).

Generally the overweight of n-C_{17} compared with n-C_{31} is reduced as the sill is approached (Figure 5.12). It is, however, difficult to determine how far the influence of the sill reaches based on this parameter. It is difficult, because of the considerable scatter in the results, that also is a problem for the samples furthest away from the sill .

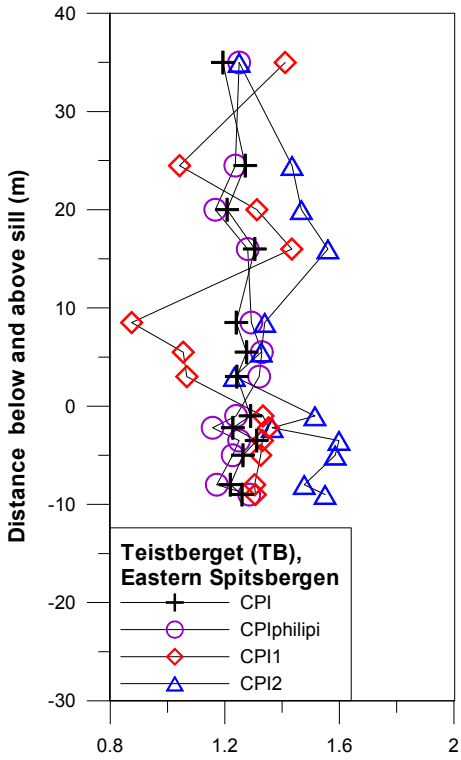

Figure 5.11: *CPI values versus depth for the Teistberget (TB) series. The figure shows the neglectable difference between CPI and* $CPI_{philippi}$.

Isoprenoids

Isoprenoids are hydrocarbons composed of, or derived from, polymerized isoprene units. Typical acyclic isoprenoids are pristane (C_{19}) and phytane (C_{20}).

Pristane/Phytane ratio This parameter is used as an indicator of organic facies and as a maturity indicator. In this study we are mostly focused on maturity. Based on published results from other studies we expect this ratio to increase with increasing maturity (see section 2.3.4 on page 12 The n-Pristane/n-Phytane ratio).

Figure 5.1(k) shows that an increasing number of samples have high values for this ratio, as the sill is approached. For some samples the measurements also give a lower value for this ratio, as the sill is approached. For many samples close to a sill the ratio has a value approximately the same as for a samples furthest-from-sill. The scatter in the plot does not, in our point of view, support an increase/decrease in this ratio. Something is happening as the sill is approached but it seem to us that it is too chaotic to suggest a trend.

The measurements of samples furthest-from-sill, and therefore regarded unaffected, have a ratio of approximately 1.5, supporting other measurements indicating a Type I/II kerogen and deposition of marine algae in anoxic environments. (Pr/Ph > 3 indicates Type III kerogen or coal and deposition of terrestrial material in a dysoxic environment).

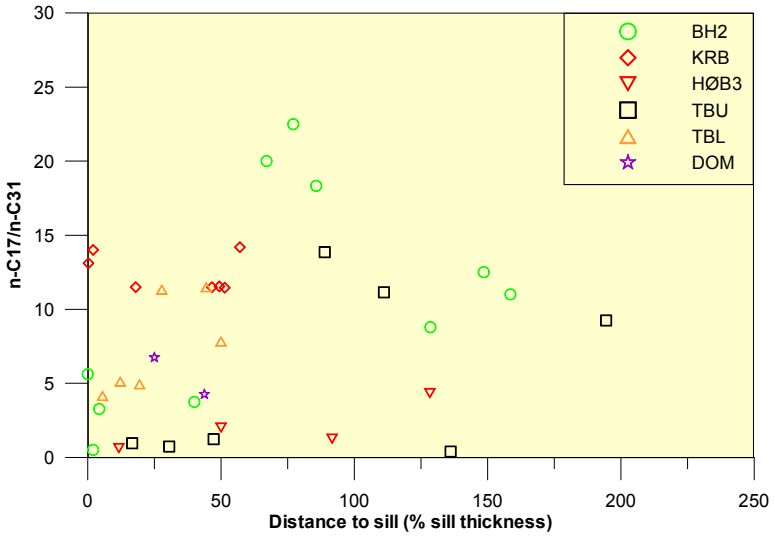

Figure 5.12: *nC_{17}/nC_{31} versus distance to sill in % sill thickness.*

Pristane/n-C_{17} and Phytane/n-C_{18} ratios The common view is that these ratios should decrease with increasing maturity (Peters and Moldowan, 1993). This is because isoprenoids will break down earlier than n-alkanes during maturation and because the amount of isoprenoids will decrease, as maturation of the kerogen and cracking of longer chained n-alkanes subsequently will outnumber the isoprenoids (Section 2.3.4 on page 12 Pr/n-C_{17} and Ph/n-C_{18}).

In this study, these ratios both follow the same pattern (Figures 5.1(i) and 5.1(j)). At a distance to sill equal to one sill thickness (100%) the values of these ratios are lowered as expected. From a distance about one half sill thickness (50%) the picture is more complicated. Most samples now give a value for the ratios that is higher than for the furthest-from-sill samples (opposite from what is expected), but there is a lot of scatter in the plot and some samples also give the expected low values.

This scatter makes it difficult to conclude, but is indicating that sill maturation can not be directly compared with natural burial maturation, which compared with sill maturation, is much more time consuming. I will come back to this in the conclusions chapter.

Pristane/n-C_{17} ratio versus Phytane/n-C_{18} ratio Shanmugam (1985) showed that when Pristane/n-C_{17} is plotted vs. Phytane/n-C_{18}, it gives information about the depositional environment and about the degree of maturation/biodegradation. In Figure 5.13 we have plotted the corresponding pristane/n-C_{17}, phytane/n-C_{18} values for the samples of this study. The diagram has been divided into areas, to represent different depositional environments, as found by Shanmugam (1985). As we can see, almost all samples plot within the field of "Mixed organic sources (Transitional Environments)". The plotting of the values

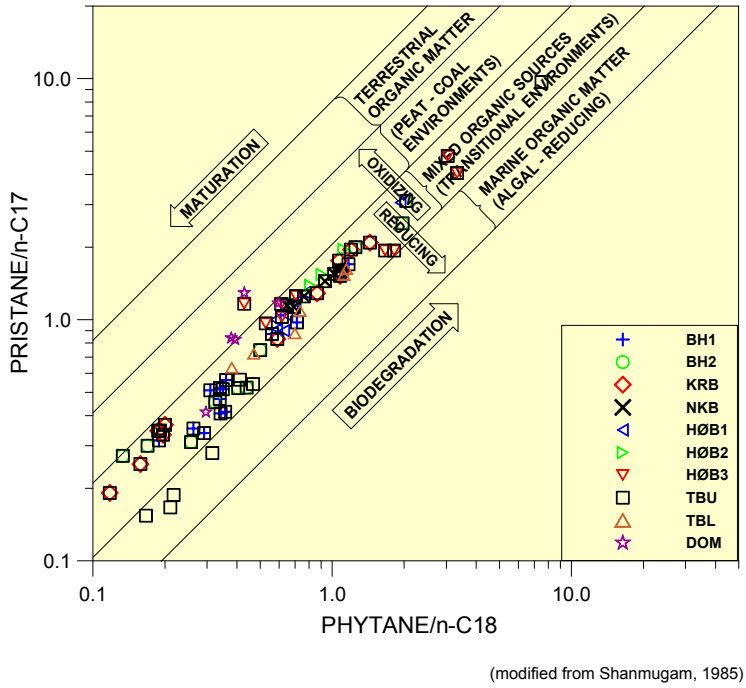

Figure 5.13: *Pristane/nC_{17} plotted versus Phytane/nC_{18}.*

for each series also shows increasing maturity, as the sill is approached.

CPI versus Pristane/Phytane ratio Figure 5.14 show CPI (see equation 5.1) plotted versus the pristane/ phytane-ratio. This plot is meant to indicate type of source rock for immature samples and maturity differences among samples. The closest-to-sill samples are expected to show the highest maturites with values around 1 for CPI and plot on the right-hand side in the diagram for pristane/phytane ratio (Figure 5.14).

The reason why we have put three of these figures beside each other is to clearly show the differences between the three calculated CPI-values.

*CPI*2 (see equation 5.4) is calculated for the the n-alkanes C_{27} to C_{32} and shows a clear odd-over-even preference indicating terrestrial matter as main source for these n-alkanes. *CPI*1 (see equation 5.3) is calculated on the n-alkanes C_{23} to C_{26}. These n-alkanes also show an odd-over-even preference but not as clearly as the calculation for the n-alkanes in *CPI*2. The conclusion that can be drawn from this is that the organic matter in the Botneheia Fm. and Janusfjellet Subgroup must have a significant terrestrial input during sedimentation and that the kerogen type therefore is a mixture of marine Type II and terrestrial Type III (Figures 5.14(b) and 5.14(c)).

Terrestrial kerogen will predominantly yield n-alkanes in the range C_{27} to C_{33} with an odd-over-even preference. Marine kerogen will predominantly yield n-alkanes in the range C_{17} to C_{19} with no carbon number preference.

The plot for the *CPI* value (Figure 5.14(a)), featuring both short and long

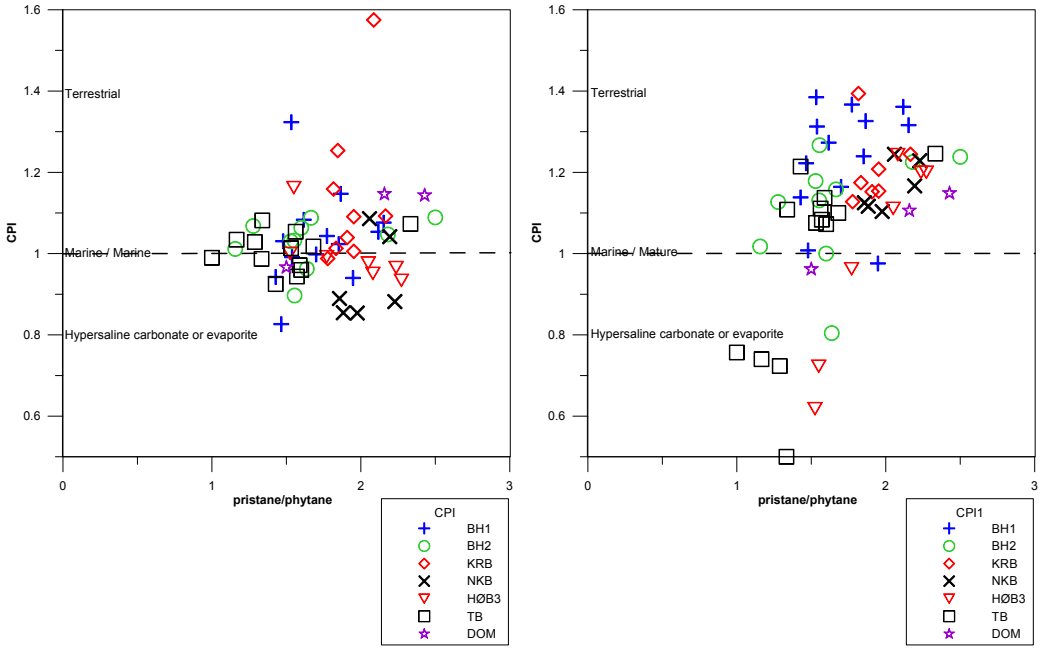

(a) *CPI* see equation 5.1

(b) *CPI*1 see equation 5.3

(c) *CPI*2 see equation 5.4

Figure 5.14: *CPI calculated for different parts of the n-alkane distribution*

Parameter	Behaviour (trend) during sill approachment
$\mathbf{nC_{17}/nC_{31}}$	decreases (?%)
pr/ph	increasingly scattered
$\mathbf{pr/nC_{17}}$	increases at 50% sill thickness distance
$\mathbf{ph/nC_{18}}$	increases at 50% sill thickness distance
CPI	no change
$\mathbf{CPI_1}$	no change
$\mathbf{CPI_2}$	no change

Table 5.6: *Change/Stability in organic content towards a sill determined with GC-FID on the samples in this study.*

chained n-alkanes, shows that most samples have a carbon preference around 1. This means that the samples are mostly rather mature and/or of marine origin.

Figure 5.14 also shows that the pristane/phytane ratio is strongly affected by the sill. The pristane/phytane ratio is known to be affected by maturity. This is, because phytane has one more carbon atom than pristane and this is slightly less degradable than pristane. The samples of this study plot in the range 1.0 to 2.6. This is a rather wide range and is probably maturity related/related to the sill emplacement. The pristane/phytane ratio reflects the origin of the contributed OM, and therefore is commonly used in oil source rock studies. The findings in other studies indicate that oils and condensates from nonmarine source rocks had a pristane/phytane ratio in the range 5 to 11, while low wax oils from marine source rocks had pristane/phytane ratios from 1 to 3 (Peters and Moldowan, 1993). Our results are in agreement with the results in these other studies (Both Botneheia Fm and the Janusfjellet Subgroup are thought to be mainly marine). Anyhow, we were surprised over the wide range the pristane/phytane ratio had in this study. We therefor stress that the pristane/phytane ratio must be used together with other parameters, when doing oil-source rock correlations.

The changes in th OM towards a sill, determined with GC-FID are summarized in Table 5.6.

The GC-FID results change within each sample series:

BH1, Botneheia East, Central Spitsbergen The samples closest to the sill (determined with the vitrinite measurements and other data of this study), sample BH1-17 and BH1-18, have not been extracted and analyzed on the GC-FID (Table C.1). (Only samples believed to give good results, indicated by TLC-FID, were analyzed on GC-FID). The closest to sill samples that have been extracted and analyzed on the GC-FID, Sample BH1-15 and Sample BH1-19 show a slightly higher yield for each n-alkane measured than the rest of the samples, but in total the yield is approximately the same for all the samples measured. The sill presence is not easy to see on the n-alkane pattern alone.

Looking at the plots of parameters, calculated on the GC-FID, data the sill presence in the sample series is more clearly marked (Table D.1). From this

we have found that the sill is, as also showed by other measurements and analysis, located approximately 45 meters from the base off the Botneheia Fm. CPI, $CPI1$, pristane/n-C_{17} ratio and phytane/n-C_{18} ratio "jump" in sample BH1-19 (Figures D.2(a) and D.2(b)). Pristane/phytane ratio values decline for the samples close to and below the sill. The ratio of the sample above the sill rises in value but not as fast as in the samples below. The furthest-from-sill sample (BH1-1) has a pristane/phytane ratio value only a little higher than the closest-to-sill samples and this is comparable with the sample furthest-from-sill sample above (BH1-27). The BH1-1 sample is approximately 45 meters below the sill. The BH1-27 sample is approximately 22 meters above the sill. It therefore seems that there is a difference in the sill's influence of the pristane/phytane ratio below and above the sill. The strongest influence is below the sill.

Figure D.2(c) shows CPI, $CPI1$ and $CPI2$ plotted versus pristane/phytane ratio. Mature samples should have CPI~1 and plot on the right hand side of the diagram (pristane/phytane ratio would slowly increase with increasing maturity). How the different CPI-values and the pristane/phytane ratio change when approaching the sill in this series, is described above. What this figure shows us is that longest chained n-alkanes, calculated as $CPI2$, group around a CPI2~1.4. The shorter n-alkanes, calculated as $CPI1$, group around a CPI1~1.2. The CPI for all the measured n-alkanes is calculated as CPI and groups around CPI~1.0.

The number below each measurement is the distance to base Botneheia in meters. Samples around 45 meters should be most mature, since other measurements have shown the sill to be located there. For the calculated CPI values: CPI plots close to 1.0 whereas samples furthest-from-sill on both sides plot in the range 0.8 to 1.15. This suggests, as expected, the most close to sill samples to be the most mature. For the pristane/phytane ratios, however, there does not seem to be a connection between distance-to-sill and the ratio, as it plots randomly from 1.4 to 2.2. $CPI2$ is calculated for the n-alkanes C_{27} to C_{32} and shows a clear odd-over-even preference, indicating terrestrial matter as main source for these n-alkanes. $CPI1$ is calculated on the n-alkanes C_{23} to C_{26}. These n-alkanes also show an odd-over-even preference but not as clearly as the calculation for the n-alkanes in $CPI2$ does. The conclusion that can be drawn from this is that CPI measurements also indicate the kerogen most likely to be a mixture of marine Type II and terrestrial type III. Terrestrial kerogen will predominantly yield n-alkanes in the range C_{27} to C_{33} with an odd-over-even preference. Marine kerogen will predominantly yield n-alkanes in the range C_{17} to C_{19} with no carbon number preference.

The last plot made on the GC-FID data for the BH1 sample series is Pristane/n-C_{17} ratio versus Phytane/n-C_{18} ratio (Figure D.2(d)). All samples plot within the "Mixed Organic Sources" field which agrees with the results from other measurements e.g. the HI-OI plot, based on the Rock-Eval analyses. Pristane and phytane are less resistant to thermal breakdown than their neighbor n-alkanes, in the gas chromatograms, n-C_{17} and n-C_{18}. As the sill is approached, both these ratios therefore should decrease. But, as for the pristane/phytane ratios, there does not seem to be any connection in this series. (The sample at 45 meter, is the sample having the highest values, in contrary to what is expected).

BH2, Botneheia 2, Central Spitsbergen The yield is by no doubt highest for the closest-to-sill sample, sample BH2-1. The yield then subsequently decreases moving away from the sill. The sill in proximity to the BH2 sample series is 35 meters thick. From sample BH2-21, which is located at 27 meter from the sill (less than one sill thickness), samples seem uninfluenced by the sill, when moving away from it. The yield for these furthest-from-sill samples is comparable with the yields in the unaffected series, the NKB series. (Table C.2).

Using the n-C_{17}/n-C_{31} ratios we got approximately the same result. These ratios suggest sample BH2-20 and all samples further away from the sill to be uninfluenced by the sill. Sample BH2-20 is located 23.50 meters away from the sill, which equals ~70% of the sills thickness (Table D.2).

CPI values are approximately stable at distances above 30 meters from sill. Closer to the sill, values fall as the sill is approached. This fall in CPI value as the sill is approached, is most evident for the longest chained n-alkanes. The $CPI2$ calculation shows a fall from 1.6 at approximately 30 meter from sill to 1.25 at the sill/source-rock border. $CPI1$ also moves from an odd to a more even carbon number preference with a value of 1.2 at 30 meters from sill and values ~1 at the sill/source-rock border. CPI changes little in this sample series but has a little odd preference for the samples more than 30 meters from the sill (Figure D.3(a)).

Moving to the isoprenoid ratios, the influence of the sill is evident for the same samples as for the carbon number preference. The ratios for pristane/n-C_{17} and phytane/n-C_{18} are both stable from sample BH2-20 at 23.50 meters from the sill and all samples further away from the sill. In sample BH2-15, which is the next sample in which the GC-FID measurements have been conducted, the ratio increases in value and higher values than what seem to be the background continue all the way to the sill/source-rock border. The pristane/phytane ratio is expected to increase as the sill is approached. But except for four samples this ratio is stable at values ~1.5. Close to the sill, sample BH2-3 at 0.70 meter, actually has a lower value: 1.16. Two samples has values higher than ~1.5; these are sample BH2-20 (ratio=2.18) and BH2-22 (ratio=2.50) at 23.50 and 30.00 meters respectively (Figure D.3(b)).

Figure D.3(c) shows the difference in CPI value for all measured n-alkanes (CPI), the short chained n-alkanes ($CPI1$) and the longest chained ($CPI2$). This figure shows the same grouping s in the BH1 series. As with the BH1 series the connection with pristane/phytane ratio and maturity seems poor.

Figure D.3(d) gives the same picture as the BH1 series did in the same plot. All samples plot within the “Mixed organic sources” part of the plot. Strangely, the most close to sill samples plot as being far less mature than the more distant samples, as also observed for the BH1 sample series.

KRB, Kreftberget, Barentsøya In this sample series, the n-alkane yield is actually highest for some of the most distant from sill samples. Sample KRB-22 to KRB-24 show the highest yields (The yield is also good for sample KRB-1c). The sill, where these samples were collected, is 25 meters thick. The sill influence is not easy to see on the n-alkane pattern (Tables C.3 and C.4).

Using the n-C_{17}/n-C_{31} ratios, the sills influence becomes visible for the BH1 and BH2 sample series. For the KRB sample series, however, this ratio changes little if at all, while approaching the sill. We have very high values in the middle of the series (samples KRB8 to KRB11), but those must be related to something else than sill proximity (Table D.3 and Figure 5.12).

Moving to the plots of the calculated CPI values, changes within the series, that maybe can be related to sill nearness, are clearly visible (Figure D.4(a)). Samples KRB-3a, KRB-8, KRB-9 and KRB-11 have a clear odd carbon number preference, presuming that samples KRB-22, KRB-23, KRB-24 and KRB-26 represent the virgin background. Note the strong odd preference for the short chained n-alkanes ($CPI1$) in sample KRB-11 and KRB-12, which is stronger than for the longer chained n-alkanes ($CPI2$) in these samples. As the sill is approached, maturity is expected to increase. For CPI values, increasing maturity should reduce any carbon number preference. The CPI value should be ~1 for mature samples. The CPI results for the KRB series therefore are difficult to interpret as sole consequence of sill proximity. (When approaching a sill, we would expect any carbon number preference to disappear). For the KRB sample series, however, four of the closest-to-sill samples show a very clear odd carbon number preference. The CPI number does not increase as the sill is approached in any of the other sample series of this study. I therefore conclude that the observed increase in CPI number for the KRB sample series, despite in closing sill proximity, can not be explained.

The pristane/n-C_{17} and phytane/n-C_{18} ratios behave as in the other sample series. Approaching the sill, these calculated ratios at first increase in value, then fall to the same values as for the samples furthest-from-sill at the sill/source-rock border. This is, as noted for the BH1 and BH2 series, not to be expected. These ratios should decrease with increasing maturity according to the traditional view (Peters and Moldowan, 1993). Approaching a sill, however, the opposite, an increase in these ratios, seems to be the rule. The sill is 25 meters thick at where the KRB sample series was collected. Unfortunately no GC-FID measurements on the samples between 6.3 meters and 16.3 meters from sill were conducted. The sample collected at 6.3 meters, sample KRB-12, seem to be influenced by the sill. The sill's influence thus extends at least over 25% of its own thickness.

Figure D.4(c) shows the difference in CPI value for all measured n-alkanes (CPI), the short chained n-alkanes ($CPI1$) and the longest chained ($CPI2$). The figure shows approximately the same grouping for the CPI parameters calculated as the figure for the BH1 and BH2 sample series (Figure D.2(c) and D.3(c)). The spread in pristane/phytane ratio is the most narrow of all sample series. The pristane/phytane ratio does not seem to be connected with maturity, at least the influence of the sill on the pristane/phytane ratio seems minimal).

Figure D.4(d) gives the same picture as the BH1 and BH2 sample series did in the same plot. All samples plot within the "Mixed organic sources" part of the plot. Strangely, the most closest-to-sill samples plot as being far less mature than more distant samples, as also observed for the BH1 sample series.

TBU and TBL, Teistberget, Eastern Spitsbergen Above the sill, sample series TBU (Table C.5) the yield for the short chained n-alkanes first increase as we move away from the sill (until sample TBU-7) then the yields fall in the two last samples, examined on GC-FID, sample TBU-9 and TBU-10. The sill at Teistberget is 17 to 18 meters thick. Based on other measurements from this series, it is possible that these two last mentioned samples give us the virgin values, for GC-Fid yield. Below the sill the sample examined on GC-FID furthest-from-sill, TBL-8, is only 9 meters away from the sill (Table C.6). The yields on the samples below the sill vary with the lowest yield present in sample TBL-8. It is, as with the other series, difficult to see trends just looking at the yield numbers on either side of the sill.

With the n-C_{17}/n-C_{31} ratios it is easier to see a trend in the data, at least for the TBU series (Table D.5). In the TBU series the n-C_{17}/n-C_{31} ratios falls as the sill is approached, telling us that the amount of short chained n-alkanes decreases compared with the long chained. For the TBL series we have the same trend (Table D.6).

CPI is rather stable in all samples below and above the sill (at ~1). *CPI*1 is stable at ~1.1 below the sill. Above the sill it first falls to 0.65, showing an even number n-alkane preference for the first 10 meters, then it has a value ~1.1 and odd number n-alkane preference for the rest of the samples (except one, sample TBU-9). *CPI*2 is also approximately stable below the sill with values ~1.4. Above the sill the value falls to ~1.1 for the examined samples up to sample TBU-4 at 8.5 meters above the sill. For the next examined sample, TBU-6 at 16 meters above the sill, the value increases to ~1.3. Then the value is stable at ~1.2 on the examined samples until 24.5 meters above sill. The furthest-from-sill sample at Teistberget, TBU-10 at 35 meters above sill, shows a *CPI*2-value of 1.0. As with the other series it is difficult to prove, whether the variations of the calculated CPI values are related to the sill influence (Figure D.5(a)).

In the BH2 and KRB sample series the ratios for pristane/n-C_{17} and phytane/n-C_{18} is increasing as the sill is approached. For the two Teistberget series, above and below the sill, these ratios decrease as the sill is approached (Figure D.5(b)). This decrease is as originally expected but a little surprising since this was not the case for the two first examined series. The decrease is particularly easy to see below the sill where pristane/n-C_{17} ratio falls from ~1.5 to ~0.2 and phytane/n-C_{18} falls from ~1.1 to ~0.2. Above the sill the values increase as we move away from the sill, but not as fast as below the sill. (The samples above the sill are in fact closer to the sill than the distance in meters indicates, see Subsection **??**).

Figure D.5(c) shows the difference in CPI value for all measured n-alkanes (*CPI*), the short chained n-alkanes (*CPI*1) and the longest chained (*CPI*2). The figure shows the same grouping as in the other sample series in this study where the samples have been collected in the Botneheia Fm. As with the other series, the connection with pristane/phytane ratio and maturity seems poor.

Figure D.5(d) differs from the other figures of the same type in that the data has been divided in two, for samples above sill (TBU) and samples below sill (TBL). More importantly, this figure also differs from the others as being the only one where some of the samples plot within the “Marine Organic Matter”

part of the diagram. The samples below the sill all plot within the "Mixed organic sources" part of the plot and the samples also follow the expected maturity trend rather well. The samples above the sill, however, also plot in the "Marine Organic Matter" part of the diagram. This change in organic facies could explain the previously described higher TOC values in TBU compared with TBL (See Subsection 5.2.2).

DOM, Domen, Eastern Spitsbergen For the DOM sample series only four samples have been examined with GC-FID. The DOM samples were collected going outwards from a sill in the Jurassic/Cretaceous Janusfjellet Subgroup, which is an organic rich source-rock believed, to have been deposited in similar conditions as the Botneheia Fm.

The n-alkane patterns for the examined samples show approximately the same yields for each individual n-alkane and it is not possible to see any changes that can be attributed to sill intrusion (Table C.7).

The n-C_{17}/n-C_{31} ratios for the other series have shown clear changes between the samples as the sill is approached. In this series variation between the samples is small except for the furthest-from-sill sample, sample DOM-11 (Table D.7). The sill at Domen is only 7 to 8 meters thick. Sample DOM-11 is located 48 meters from the sill. Compared with the other sample series influenced by a sill, we should also have detected a change in the close-to-sill samples. The difference in yield and n-C_{17}/n-C_{31} ratio for sample DOM-11 are not likely to be caused by the sill.

The calculated CPI values vary little with distance from the sill (Figure D.6(a)). It should be noted that the sample furthest-from-sill is most mature according to the CPI calculations (has the lowest values). Notice that $CPI1$ closely follows CPI and has a less odd carbon number preference, compared with the sample close to sills in the Botneheia Fm. CPI, however, shows a greater odd carbon number preference than in the Botneheia Fm sample series.

The isoprenoid ratios show no changes that can be related to the sill intrusion (Figure D.6(b)). The decrease in pristane/n C_{17} and phytane/n-C_{18} ratios between the two most close to sill samples (DOM-3 and DOM-4) can be related to the sill but we find it difficult to suggest a trend on the basis of a calculated difference between only two samples. The possibly sill caused difference between samples DOM-3 and DOM-4 can also be observed in the Pristane/Phytane ratio.

Figure D.6(c) shows the difference in CPI value for all measured n-alkanes (CPI), the short chained n-alkanes ($CPI1$) and the longest chained ($CPI2$). The figure shows that this sample series, the DOM series, has another grouping than the sample series which have been collected in the Botneheia Fm. CPI and $CPI1$ group together whereas $CPI2$ shows higher values.

As we move to the pristane/n-C_{17} ratio versus phytane/n-C_{18} ratio plot, indications by the CPI values become even more evident (Figure D.6(d)). This plot indicates that the Janusfjellet Subgroup has been deposited under more oxic conditions than the Botneheia Fm, as one sample very clearly plots within the "Peat - Coal" part of the diagram (sample DOM-9). Two other samples, DOM-3 and DOM-4, plot on the border between "Peat - Coal" and "Mixed organic

sources". This may also indicate that the organic input to the Janusfjellet Subgroup has had a stronger terrestrial input compared with the Botneheia Fm.

HØB, Høgrinden South, Barentsøya Here, three sample series have been collected. Distance to sill is, however, only noted for one of them, and only this sample series is treated in detail in this part of the thesis.

HØB1 Unfortunately, no distance to sill or other information is given for this series. The n-alkane pattern shows highest yields for the short-chained n-alkanes in all samples (Table C.8). The yields vary between the samples but it is difficult to see any trend in the data.

The n-C_{17}/n-C_{31} ratios show little variation and no trend. Neither can I see any trend in the calculated CPI values nor in the isoprenoid ratios (Table D.8).

I therefore conclude that there probably is no sill close to the samples examined in this series. If a sill is present, it has not influenced the n-alkane pattern in the samples measured on GC-FID. Sample HØB1-1 to HØB1-5 have not been examined. These samples are the ones most likely to be close to a sill, if present. Since so much is uncertain about this series, I will not discuss it any further.

HØB2 Unfortunately, no distance to sill or other information is given about this series either. As for the HØB1 sample series, samples with low sample numbers and possible proximity to a sill, have not been examined on GC-FID. The n-alkane pattern shows highest yields for the short chained n-alkanes in all the samples (Table C.9). The yields are approximately the same for all examined samples.

The n-C_{17}/n-C_{31} ratios show little variation and no trend. Neither can I see any trend in the calculated CPI values or the isoprenoid ratios (Table D.9).

I therefore conclude that there probably is no sill close to the samples examined in this series. If a sill is present, it has not influenced the n-alkane pattern in the samples measured on GC-FID. Since so much is uncertain about this series, I will not discuss it any further.

HØB3 For the HØB3 sample series, distance to sill is noted. Samples are also noted to have been sampled within a single horizon. For this sample series the presence of the sill is more evident. The short-chained n-alkanes, for example, increase in yield as we move away from the sill (decrease in yield as the sill is approached) (Table C.10).

Using the n-C_{17}/n-C_{31} ratios, they decrease in value as the sill is approached. This is a clear trend throughout the whole sample series (Table D.10). According to the measurements on a series without any sill (the NKB series), the virgin values for this ratio varies between 10 and 35. Taking that into account, the sill's presence is visible as to sample HØB3-5 at 7.7 meter from sill. The sill here is measured to be 5 to 7 meters thick. This indicates that the sill has influenced the adjacent strata to a distance equal to $\sim$ one sill thickness.

CPI values are relatively stable at distances greater than 7 meters from the sill. Closer to the sill values become unstable (Figure D.7(a)).

Considering the isoprenoid ratios, the influence of the sill is evident for the same samples as carbon number preference is (Figure D.7(b)).

Figure D.7(c) shows the difference in CPI value for all measured n-alkanes (CPI), the short chained n-alkanes ($CPI1$) and the longest chained ($CPI2$). The figure shows the same grouping as in the BH1 series. As with the BH1 series the connection with the pristane/phytane ratio and maturity seems poor.

Figure D.7(d) shows the HØB3 samples to plot as expected within the "Mixed Organic Sources" part of the diagram.

NKB, Northern Kreftberget, Barentsøya As mentioned earlier these samples were collected perpendicular to the bedding of the Botneheia Fm. The distance to any sill is sufficient for the samples to give representative virgin values for the examinations, conducted in this study.

Since no sill is present, the resulting values for each measurement conducted are expected to be approximately the same in every sample of this sample series. Any variations between the samples must be because of differences in sediment input.

When looking at the n-alkane pattern and the yields for each n-alkane, we see that the yields vary between the samples (Table C.11). However, compared with the series where a sill is present, the variation in this series is much smaller.

The n-C_{17}/n-C_{31} ratios varies a lot even in this series where no sill is present. This ratio must therefore be used with caution. The increase for one sample in the series, shows that we must have an up-going trend in more than one sample to use this ratio as an indicator of approaching a sill.

CPI values are uniform throughout the sample series except at the start (Figure D.8(a)). So are the isoprenoid ratios (Figure D.7(b)). No sill is reported close to this sample series, but if we were not aware of this, we would assume a sill to be located were the sample series begins. This tell us that variations in the isoprenoid ratios up to 0.5 are possible, even if no sill is present

Figure D.8(c) shows the difference in CPI value for all measured n-alkanes (CPI), the short chained n-alkanes ($CPI1$) and the longest chained ($CPI2$). The figure shows the same grouping as for all the other sample series, where the source-rock is the Botneheia Fm. The calculated CPI value in this series shows a lower value than it does in the other series. CPI will approach a value ~1.0 with increasing maturity. The samples in this series evidently are not very mature. $CPI2$ is closer to ~ 1 in this series than any other series, supporting the mainly marine origin of the organic matter for the Botneheia Fm. Regarding the maturity increase of pristane/phytane ratio, this figure indicates that we must have a relative change of more than 0.5 to relate to a sill, if present (Figure D.8(b)).

Figure D.8(d) places the samples and the Botneheia Fm. in "Mixed organic sources" part of the plot, as expected. The spread between the samples is noticeable.

5.2.5 Stable isotopes

See Figures 5.1(m) and 5.1(n).

There is a lot of scatter in the data, but looking at each individual series, a general pattern emerges: The calcite and dolomite isotope ratios get lighter, when approaching the sill. Kerogen and EOM isotope ratios get heavier, when approaching the sill

This is best observed in the individual data series. The descriptions of how the isotope values change while approaching the sill, is given below for each individual series. When reading these descriptions, it alsao supports the understanding to look at the isotope value plots in the Appendix (Figures E.1 to E.8 on page 244).

It is difficult to pinpoint exactly how far from the sill its emplacement has influenced the isotopic ratios. The changes in isotope ratio are very small for kerogen- and EOM-δ^{13}C. The changes in isotope ratio are bigger for calcite- and dolomite-δ^{13}C and δ^{18}O. The change for calcite- and dolomite-δ^{13}C and δ^{18}O goes more gradually in contrast to the more immediate but small, changes observed in kerogen- and EOM-δ^{13}C.

The kerogen and EOM δ^{13}C values seem split into two groups, with one group of samples most close to sill and the second group with the rest of the samples. Within each group the isotopic ratio value is approximately the same for each sample.

For the small sills (up to 10m thickness) the emplacement of the sill seems to have influenced the isotope ratios up to a distance equal one sill thickness. For the thicker sills the influence does not seem to reach farther than one half of the sill's own thickness. Due to this difference of influence between thin sills and thick sills, it is impossible to formulate a general rule of sill influence on the isotopic composition, based on the sills own thickness.

Isotope changes within each sample series:

BH1, Botneheia East, Central Spitsbergen See Table E.1. The isotope values for Calcite δ^{13}C and δ^{18}O, Dolomite δ^{13}C and δ^{18}O are all falling (becoming isotopically lighter) around the sill, which we previously have located at approximately 45 meter from base Botneheia Fm. For the Kerogen δ^{13}C isotope measurements there is a change to more heavy isotope values for the two samples closest to the sill (see Figure E.1). The isotope measurements of the EOM δ^{13}C show no significant change. The amount of mg EOM is falling towards the sill (mg EOM/g rock).

BH2, Botneheia 2, Central Spitsbergen See Table E.2 and Figure E.2.

The isotope values for Calcite δ^{13}C and δ^{18}O, Dolomite δ^{13}C and δ^{18}O are all falling (becoming lighter) approaching the sill. There seems to be no change for kerogen δ^{13}C and EOM δ^{13}C, as the sill is approached.

Sample BH2-16 has low Calcite δ^{13}C and δ^{18}O, Dolomite δ^{13}C and δ^{18}O values at the same time as having a heavy kerogen δ^{13}C value (for one of two measurements). This could indicate that we may have a small sill located within

the sampled sequence. However, no sill has been reported by the sampling geologist and lack of measurements on the nearby samples makes this difficult to state/prove. We therefore just note that there is a possibility for a small sill here. Also for vitrinite reflectance, sample BH2-16 separates from the others (see Table F.2).

The amounts of mg EOM are good for most samples, and are not significantly lowered for the most close to sill samples.

KRB, Kreftberget, Barentsøya See Table E.4 and Figure E.3.

Due to this sample series complexity, concerning the isotopic measurements, we have subdivided the description into the various compounds measured:

Calcite δ^{13}C Sample 36 to 24 have rather fluctuating isotope values. The reason for this is difficult to interpret, but could be due to differences in the sediment input. For samples 23 to 13 isotope values are stable between 4 - 5 δ^{13}C‰PDB. Samples 7 - 1 (approaching sill) show a lowering in value as we also have found in the previous BH1 and BH2 series.

Calcite δ^{18}O Samples 36 to 26 show low values. We don't know the reason for this other than what has been suggested above for the Calcite δ^{13}C values. Samples 25 to 19 have heavier values. Values decrease in samples 18 to 13 and increase again, in the samples 7 to 1B.

The Calcite δ^{18}O for the KRB sample series is difficult to understand. Differences in sediment input could be a reason, but this is not supported by the kerogen description (see Figure G.1(c)).

Dolomite δ^{13}C High values are present in samples 35 to 23. They vary between 4 - 5 in samples 23 to 11. The lowest values are found in samples 6 to 1. For the measurement series at whole we have a lowering, approaching the sill.

Dolomite δ^{18}O Low values are found in samples 35 to 26. The values are stable between 10 and 11 for samples 25 to 21. Low values are present in samples 19 to 10. The value is $\sim$ 12 for samples 6 to 1.

Kerogen δ^{13}C The measured isotopic weights decrease in samples 36 to 24. Measurements stabilize at $\sim$ 30 on samples 23 to 1. Approaching the sill, an increase in the isotopic weight for kerogen δ^{13}C is expected. On samples 36 to 24 the opposite is happening.

Kerogen description (see Figure G.1(c)) shows that all kerogen types are almost equally distributed in the furthest-from-sill samples. The kerogen is for sure derived from a variety of biological precursors that would give different isotopic values if subdivided before measurement. As we can see from figure G.1(c), the kerogen content changes when approaching the sill. The decrease in isotopic value for kerogen δ^{13}C is coincident with the decrease in FA-kerogen (samples

36 to 24), but this seems to be accidental, since the same correlation is not retrieved for any other sample series.

EOM δ^{13}C The same pattern as for Kerogen δ^{13}C is shown in the measurement of EOM δ^{13}C. On samples 36 to 24 the measured isotopic weight decreases. For samples 23 to 1 the measured isotopic weight stabilizes at values between 29 - 31.

KRB isotopic values, conclusions The isotopic value is determined by sediment input, associated with assimilation of carbon by producing organism and to a lesser degree maturity. For the KRB sample series measurements on the isotopic value for carbon show no trend and the measurements vary a lot. The only explanation I find possible is that the sediment input has varied a lot during sedimentation. The differences in measured isotopic value therefore must be of stratigraphic origin.

TBU and TBL, Teistberget, Eastern Spitsbergen These are two sample series, above and below the same sill, at Teistberget. We first describe the two sample series by themselves, before looking at similarities/differences between the two:

TBU, Teistberget Upper See Table E.6 and Figure E.4.

Calcite δ^{13}C moves from values around -3 for the most distant samples to values around -5 close to the sill. A move to more isotopicallly light samples is observed, as the sill is approached. The calcite δ^{18}O values also move to lighter values, from $\sim$ -7 to -12.7. The jump between sample 7 and 6, from -7.9 to -10.1 should be noted. The sill is approximately 18 meters thick so this jump happens at exactly one sill thickness distance away from sill, a jump in the Calcite δ^{18}O at one sill thickness distance away from sill is also observed for the HØ3 series (see Table E.11). The isotope quantities for dolomite δ^{13}C and dolomite δ^{18}O are both going towards lighter values, as the sill is approached.

For kerogen δ^{13}C no clear change in the isotopic value is observed. A small change towards a more heavy composition is possible, but probably related to small changes in the sediment input (Figure E.4).

Also for EOM δ^{13}C the isotopic values seem unaffected by the sill. Small changes are probably also related to sediment input (Figure E.4).

TBL, Teistberget Lower See Table E.7 and Figure E.5.

For calcite δ^{13}C there only are few measurements, but these suggest a move to lighter values, as the sill is approached. There are, unfortunately, few measurements of the calcite δ^{18}O for this series, but as for calcite δ^{13}C, a lowering of the measured values is observed.

The measurements of dolomite δ^{13}C show very “heavy” values on sample 3, 4 and 10. Disregarding these measurements, the values move towards lighter values, as the sill is approached. The dolomite δ^{18}O goes towards lighter values as the sill is approached.

Except for sample TBL1, which is significantly heavie than the other measurements of kerogen δ^{13}C in this sample series, no change in the isotopic value is observed. For the EOM δ^{13}C no change in the isotopic value that can be related to approaching the sill, is observed.

Similarities/differences between TBU and TBL On both sides of the sill the measured isotopic values for calcite δ^{13}C, calcite δ^{18}O, dolomite δ^{13}C and dolomite δ^{18}O are lowered when approaching the sill. The measured isotopic values for kerogen δ^{13}C and EOM δ^{13}C seem to be unaffected by the sill.

DOM, Domen, Eastern Spitsbergen See Table E.8 and Figure E.6.

Unfortunately only a few of these samples gave results, when the Calcite and Dolomite δ^{13}C and δ^{18}O contents were measured. Sample DOM-10 is the only sample at some distance from the sill (38 meters) with results on all isotopic values investigated in this study. The results (sample DOM-10) all show low values for calcite δ^{13}C, calcite δ^{18}O, dolomite δ^{13}C and dolomite δ^{18}O. The next sample (sample DOM-3, 2 meters from sill) that has values for both Calcite and Dolomite isotope values, has considerably more heavy isotope content. The closest-to-sill samples thereafter (DOM-2 and DOM-1 at 0.2 meter 0.0 meter from sill, respectively) are the isotopically lightest samples in this sample series. As with most other series in this study, the DOM sample series becomes isotopically lighter, when approaching the sill when regarding calcite δ^{13}C, calcite δ^{18}O, dolomite δ^{13}C and dolomite δ^{18}O.

For kerogen δ^{13}C the measurements suggest a stable isotope ratio for the samples at approximately -26 ‰PDB, with the closest-to-sill sample (sample DOM-1) with a lower value of -29.6 ‰PDB.

EOM δ^{13}C shows rather stable values until a distance approximately equal one sill thickness away from sill (Sample DOM-5 at 10.5 meters from sill). Then values decrease from approximately -27 ‰PDB down to -29 ‰PDB (samples become isotopically lighter).

KMB-C and KMB-D These two sample series differ from the others as the samples are not collected perpendicular to a sill. Because of this, no distance to sill is given for these sample series.

KMB-C See Table E.9 and the photo in Figure 4.2.

From Sven Dahlgren's photo it seems likely to me that the samples have been collected in one single layer, where the sill cuts through the strata. The samples therefore have the sill both on their left side and also, the same sill, below them.

There are few isotope measurements done on this sample series. For calcite δ^{13}C and calcite δ^{18}O we only have measurements for sample KMB-C-1. The measurement on calcite δ^{13}C resembles samples at between 20 to 7 meter from the sill in the KRB sample series that have been sampled close by. If sample KMB-C-1 is sampled close to the sill, I would have expected a lighter value (when comparing with the other sample series). For calcite δ^{18}O, however, the measured value is as expected.

For kerogen δ^{13}C and EOM δ^{13}C we have more measured values. We find it hard, however, to see any trend for these measurements, because we have very few samples and do not have any distance to sill quoted. There may be a trend for lighter values for EOM δ^{13}C, but as EOM also is very low in these samples, we would not trust these measurements too much.

KMB-D See Table E.10and the photo in Figure 4.2.

This sample series is, according to Sven Dahlgren's photo, sampled in one horizon parallel to the sill at Kreftsberget. If the distance to the sill is approximately the same for all these samples, the values of measured parameters should be approximately the same for all the samples in this series.

The measured values, however, show a decrease with increasing sample number, for all the isotope ratios determined (calcite δ^{13}C, calcite δ^{18}O, dolomite δ^{13}C, dolomite δ^{18}O, kerogen δ^{13}C and EOM δ^{13}C).

If these measurements really represent the natural variation within a single layer, the interpretation of the isotope measurements in the other sample series of this study certainly becomes difficult, Great care must be taken before suggesting trends and makeing conclusions.

HØB3, Høgrinden South, Barentsøya See Table E.11 and Figure E.7.

The isotopic ratios for calcite δ^{13}C, calcite δ^{18}O, dolomite δ^{13}C and dolomite δ^{18}O are all decreasing, which means that the samples become isotopicly lighter, as the sill is approached.

For kerogen a small increase is possible for the closest-to-sill samples, indicating that the isotopic weight is increasing when approaching the sill.

Also for EOM a small increase is possible for the closest-to-sill samples, indicating that the isotopic weight is increasing when approaching the sill.

mgEOM is good in all samples expect Sample HØB3-1.

NKB, Northern Kreftberget, Barentsøya See Table E.12 and Figure E.8.

No sill should be present close to the samples in this series. However, as we have written tedious times now, the Kreftberget sill is located not far from the samples with high sample numbers. This has been visible in most of the other measurements done on the samples in this series.

As with the other measurements, the presence of the sill can be seen in the isotope measurements of the samples with high sample numbers.

Measurements of calcite δ^{18}O, dolomite δ^{13}C and dolomite δ^{18}O all decrease, as the sample number increases. This is in agreement with what is observed, when approaching a sill in the other sample series.

The decreasing is however not so clear for calcite δ^{13}C, where the isotope ratio gets heavier as the sill is approached.

For kerogen δ^{13}C and EOM δ^{13}C the samples split into two groups. The lightest samples are sample NKB-1 to sample NKB-7, whereas sample NKB-8 to sample NKB-14 are isotopically heavier. This is also reflected in EOM, where the isotopic heavy group has less mgEOM/g rock than the light samples.

NPD, Standard samples See Table E.13.

Weiss et al. (2004) enlist acceptance criteria and reference samples for both Norwegian standard JR-1 and SR-1. The values, enlisted for the JR-1 EOM δ^{13}C permissible range, are -31.6 to -31.3 with -31.3 as the most likely value. The values enlisted for the SR-1 EOM δ^{13}C permissible range, are -32.7 to -32.3 with -32.6 as the most likely value.

The values IFE measured therefore seem to be a bit low for both JR-1 and SR-1, if we compare with the NIGOGA (Weiss et al., 2004) most likely values with the measured values in Table E.13. The values are also outside the permissible range, meaning that the instrument would have been adjusted if the measurements had been performed today. The samples of this study were, however, measured before the NIGOGA standards for geochemical studies were made and IFE can not be blamed for this. The only implication this has is that all measurements of this study are probably 0.7 too low (meaning that 0.7 should be added to all the measurements).

We have choosen to not correct for this, since it has no implication on our interpretations of the data.

5.3 Source-rock facies

Facies is the sum of total features such as sedimentary rock type, mineral content, structures, etc., which characterizes a sediment as having been deposited in a given environment. Facies, which are particularly characterized by rock type are referred to as lithofacies, whereas rocks particularly characterized by organic content are referred to as organic facies.

Organic- and lithofacies of the source-rock units of this study have been determined in a number of investigations. We see no reason to doubt these results (Section 3.2 on page 32).

Anyway, we have made facies plots as a part of this thesis. It is done as a control of the analytical results. If the facies plots show the same results as those obtained in other studies, it confirms the validity of our data. Then we can also trust the maturity parameters, being calculated on the basis of these data. Since maturity is the main concern in this thesis, it is imperative that we can trust these results.

5.3.1 Organic source-rock facies

All source-rocks capable of generateing petroleum contain organic matter (OM), called kerogen. In sedimentary basins we primarily find kerogen Type II, because this kerogen type represent marine OM and marine basins are by far the most common.

Kerogen Type I -	Lacustrine OM
Kerogen Type II -	Marine OM
Kerogen Type III -	Terrestrial OM

Parameters	Marine OM	Terrestrial OM	Lacustrine OM
Pr/Ph	≤2	≥3	1≤Pr/Ph≤3
Pr/n-C_{17}	<0.5	>0.6	-
Ph/n-C_{18}	<0.5	>0.6	-

Table 5.7: *Parameters used to decide organic source-rock facies (Peters and Moldowan, 1993)*

Organic compound	$\delta^{13}C_{PDB}$ (‰)
Marine Plants	(-20) - (-10)
Plankton	(-30) - (-20)
Land Plants (C_4)	(-18) - (-10)
Land Plants (C_3)	(-30) - (-20)

Table 5.8: *Variations in range of stable carbon isotope ratios (Versus PDB standard for different organic compounds) (Peters and Moldowan, 1993)*

Additionally, we can have OM that is mixed from different sources, making the decision of the organic facies difficult.

Table 5.7 shows three parameters that are used to determine organic source-rock facies (many more parameters can be used, but these where the only ones that could be used in this study, based on the analytical results available). The parameters have been described in Chapter 2 on page 5.

From these parameters we have made two cross plots, shown in Figures 5.13, and 5.15. The first, Figure 5.13, we have described in the Subsection 5.2.4. We will here not repeat anything other than that all sample series plot within the Mixed-Organic-Sources part of the diagram. Sample series HØB3 and TBU also plot in the Peat-Coal and Marine-Organic part of the diagram. The source-rocks in this study, the Botneheia Fm. and the Janusfjellet Subgroup, are both interpreted as shelf deposits by sedimentology geologists. On a shelf OM would typically be mixed, as this plot indicates.

In the series TBU, however, most of the samples plot as Marine, indicating that these series has been deposited further away from land than the other series in this study.

Additionally, we made a cross plot of Pristane/nC_{17} versus Pristane/Phytane (Figure 5.15). Adding the limit values from Table 5.7, we defined areas for the OM types. Terrestrial OM is top right and marine OM is in the opposite corner. Source-rocks with a mixed OM (OM that consists of marine and terrestrial input) plot in a transition zone, marked with the two 45° lines. Especially Pristane/nC_{17}, but also Pristane/Phytane, are maturity dependent. The value for Pristane/nC_{17} will fall with increasing maturity. In this study, with source-rock samples collected close to a sill, we can clearly see from the plot that the Pristane/nC_{17} value falls with increasing maturity. The furthest-from-sill samples plot as Marine or Marine-Terrestrial OM. Close-to-sill samples plot as Lacustrine OM. The sill presence make this plot difficult to use for OM de-

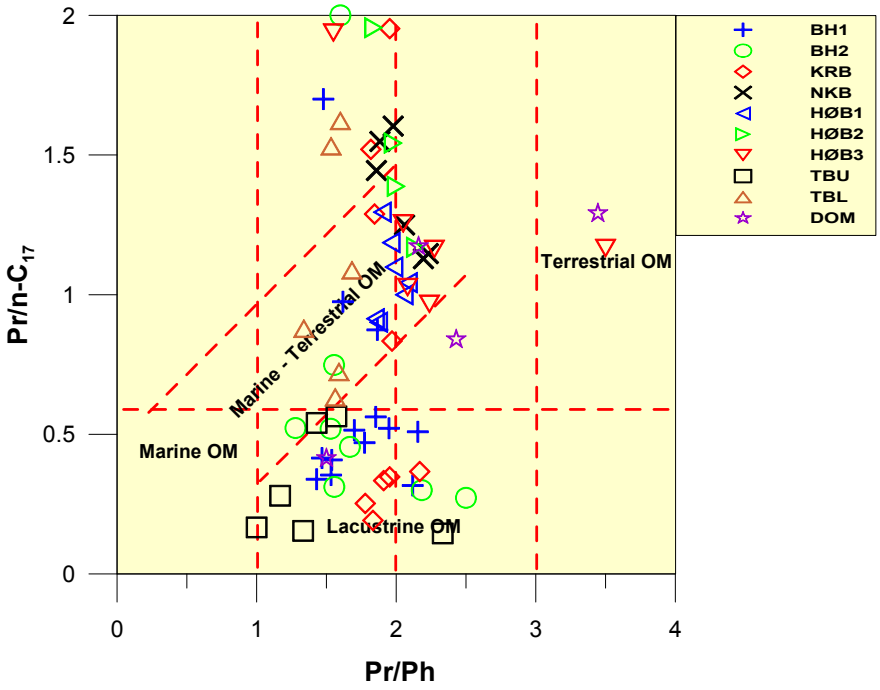

Figure 5.15: *Pristane/nC_{17} versus Pristane/Phytane*

termination. From this we conclude that this plot must be used with extreme caution in sedimentary basins where intrusions, e.g. sills, are known to exist. Secondly, the values for Pristane/nC_{17} in Table 5.7 should not be used as proof of the origin of an oil. (Plots as this should never be used alone as prof on the origin of an oil, but must be suported by other plots made on other parameters).

The unaffected-by-sill series in this study, the NKB series, plotS as Marine and Marine-Terrestrial. For all series, consisting of samples from the Botneheia FM., source-rock, this is correct, according to published sources.

Detailed plots for each sample series are included in the Appendix (Figure D.9).

The last organic facies plot we made is the Pristane/Phytane-versus-δ^{13}C EOM plot (Figure 5.16). From Table 5.8 we see that terrestrial OM can have higher δ^{13}C values (being isotopic heavier) than marine OM.

Additionally, under generation of hydrocarbons we would get isotope fractioning. The oil/gas that is generated would have more light δ^{13}C values than the remaining kerogen (Subsection 2.4.1).

The DOM-sample series is according to other measurements on the samples the series with the highest amount of terrestrial OM. As we can see from figure 5.16 is the isotopic values for the Dom-series slightly more heavier than the values for the other sample series and accordingly in agreement with the interpretation of the other measurements.

Figure 5.16 indicates, as the other interpretations, that the OM in samples of this study are of marine or mixed marine-terrestrial origin. The Dom-series is

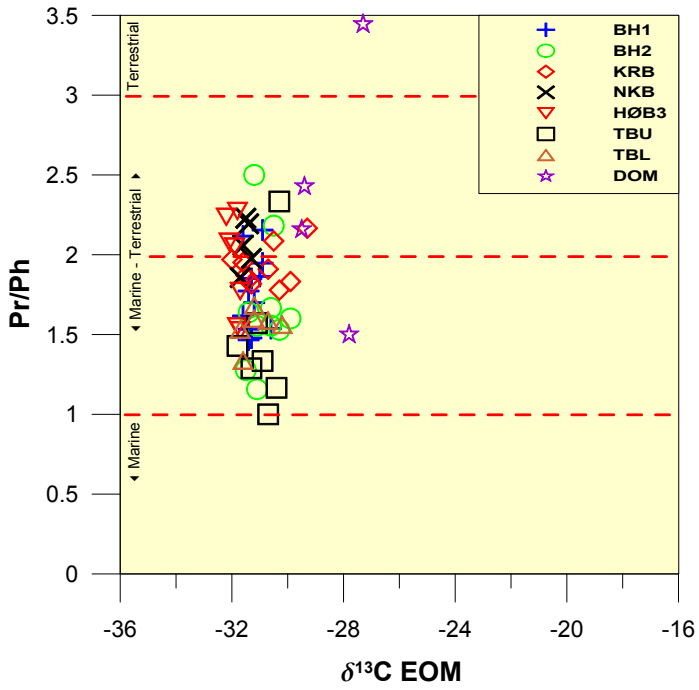

Figure 5.16: *Pristane/Phytane versus $\delta^{13}C$ EOM*

more terestrial influenced than the others.

Figure 5.13 also indicates that the OM in the samples of this study is of mixed Marine-Terrestrial origin. Together these plots (Figure 5.13 and Figure 5.16) strongly support this last interpretation.

Detailed plots for each sample series are included in the Appendix (Figure E.9).

Kerogen type A well established method for determing the kerogen type is plotting the HI-index versus the OI-index determined from the results on Rock-Eval analysis of whole-rock-samples. The kerogen type is directly related to OM, and the HI-index versus the OI-index plot therefore may act as a control of other facies plots or vice versa. Additionally, HI-index versus T_{max} (also determined using Rock-Eval) can be made to confirm the results of the HI-index versus the OI-index plot. Or it is an alternative if the OI-index values can not be relied on(Subsection 1.2).

Figure 5.5(a) indicates mainly a kerogen of Type II that corresponds to a marine source of the OM. Figure 5.5(b) indicates a mixture of Type II and Type III kerogen. Type III kerogen would mean terrestrial, land-sourced organic content.

The indication of kerogen type above is in agreement with the sedimentological interpretation of the Botneheia Fm., suggesting a deltaic influenced, regressive shelf deposit, which would yield a kerogen of both marine type II and terrestrial Type III (Subsection, Botneheia, 3.2.1).

The interpretation is also valid for the Janusfjellet Subgroup samples (the

DOM series) where Figure 5.5(a) and Figure 5.5(b) also indicate a mixture of Type II and Type III kerogen. The sedimentological interpretation of the Janusfjellet Subgroup is Marine shelf deposit, which as for the Botneheia Fm., would yield a mixture of Type II and Type III kerogen (Subsection, Janusfjellet Subgroup, 3.2.2).

5.3.2 Lithologic source-rock facies

The freshly deposited unfastened sediment at the seafloor contains organic matter (OM) and inorganic matter (IM). In clastic sediments the IM consists of e.g. clay minerals. In carbonate sediments the IM consists of calcium carbonate ($CaCO_3$), magnesite ($MgCO_3$) and dolomite ($CaMg(CO_3)_2$). The differences in mineralogy will affect i.a. the pH value and to some extent also Eh in the sedimentary column.

Table 5.9 shows three parameters that are used to determine lithologic source-rock facies (many more parameters can be used, but these were the only ones that could be used in this study, based on the analytical results available).

Parameters	Shale facies	Carbonate facies
CPI (C_{22}-C_{32})	≥ 1	≤ 1
Pr/Ph	≤ 2	≥ 3
Ph/n-C_{18}	Low (≤ 0.3)	High (≥ 0.3)

Table 5.9: *Parameters used to decide lithological source-rock facies (Peters and Moldowan, 1993)*

In this study we have made one cross plot of two of these parameters, CPI versus Pristane/Phytane ratio (Figure 5.14). As CPI with increasing maturity would approach values closer to 1 with increasing maturity, this parameter is useless for mature samples. The samples of this study are clearly affected by maturity, but as we see, especially the long-chained n-alkanes have values ≥ 1, indicating shale-facies. In this study, having the rock samples, we know this to be correct.

No cross plots were constructed using the Phytane/n-C_{18} parameter since this parameter, is strongly affected by maturity. The presence of a sill close the samples, taken in this study made the Phytane/n-C_{18} parameter unsuitable for lithofacies determination

The Phytane/n-C_{18} parameter must therefore be used with extreme caution in sedimentary basins were intrusions, e.g. sills are known to exist. The values for Phytane/n-C_{18} in Table 5.9 should not be used as indicator for the origin of an oil.

5.4 Temperature

When a sill intrudes into a source-rock, the most dramatic change is the increase in temperature next to the sill. Moving away from the border of the sill into the

surrounding rock, the temperature decreasses. The rised temperature is the most important factor for the changes in the source-rock around the sill.

5.4.1 Calculated heat

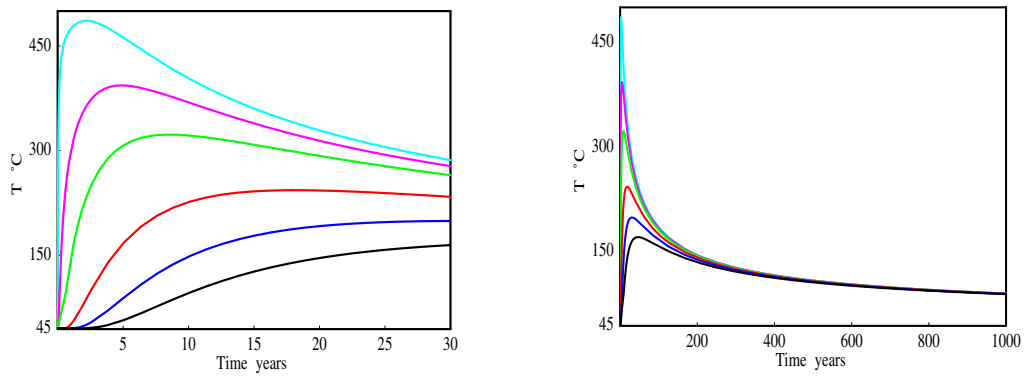

(a) 30 years

(b) 1000 years

Figure 5.17: *Calculated theoretical temperatures versus time for 6 different distances away from a 30 meter thick sill at 1500 meter depth. The uppermost curve in both plots is for a distance 1 meter (m) from the sill. The following curves represent respectively 5, 10, 20, 30 and 40 meters away from the sill.*

Since we can not be present when a sill intrudes a source-rock at e.g. 1500 meter depth (which must be considered shallow), the temperatures at the sill border and within the source-rock when moving away from the sill must be calculated theoretically. In Section 2.5.3 we have discussed the theory used when making calculations on the temperature at the sill border and within the source-rock at the moment when the sill intrudes and the subsequent cooling before reaching the normal temperatures at the depth considered.

In Figure 5.17 temperature-time curves have been calculated for increasing distance to a sill that is 30 meter thick sill and buried at 1500 meters depth. The curves have been calculated using the equation modified from Lovering (1935):

$$T = T_0 + \frac{T_m - T_0}{2}\left[\operatorname{erf}\left(\frac{L-x}{2\sqrt{\kappa t}}\right) + \operatorname{erf}\left(\frac{L+x}{2\sqrt{\kappa t}}\right)\right] \tag{5.5}$$

where

T = temperature [K],

T_0 = normal rock temperature at the depth of intrusion [K],

T_m = magma temperature [K],

L = one-half the thickness of the sill [m],

x = distance [m],

κ = thermal diffusivity [m^2/s],

t = time [s], and

erf = error function [defined in equation 5.6].

$$\mathrm{erf}(x) = \frac{2}{\sqrt{\pi}} \int_0^x e^{-\zeta^2} d\zeta \tag{5.6}$$

Lovering (1935) calculations of heat next to a sill do not consider the latent heat of crystallization, which at about 400000 J/kg of melt, is an important factor that can increase estimated temperatures within the dike contact aureole in the order of 100 °C (Jaeger, 1957) (see discussion in Section 2.5.3). The reason why we chose Lovering's model for making the heat curves in Figure 5.17 is because of its simpleness. The purpose of the figure is just to give an idea about the temperatures that can be reached around a sill and for how long these temperatures remain sufficiently high to possibly mature the source-rock around the sill.

From Figure 5.17 it can be seen that approximately the first 8 meters next to the sill reach the pyrolysis temperature of 350 °C. 30 meters on each side of the sill the rock reaches 150 °C. At 1 meter temperatures higher than 150 °C are reached almost instantaneously. At 30 meters it takes 30 years before a temperature of 150 °C is reached, and at 30 meters this also is approximately the maximum sill induced temperature at this distance from the sill.

5.4.2 Time

The temperature calculations show that the intensified temperature caused by the sill (30 meters thick at 1500 meters depth) exists only for about 200 years. Due of the form of the function this simple description of heat development will never return to the start temperature (T_0). When discussing oil formation, the term oil window is often referred to. The oil window starts at 60 °C and ends at 150 °C. Normal burial depths for this temperature interval would be from 2 km to 5 km, depending on the geothermal gradient. At 40 meters away from the sill the end temperature for the oil window, 150 °C is barely reached. At 30 meter from the sill (one sill thickness) a temperature above 150 °C is kept for approximately 130 years but it never exceeds 180 °C. At 20 meters distance the temperature last approximately the same time but reaches 200 °C. At 10 meters distance the time above 150 °C is approximately 150 years but here the temperature reaches 300 °C. At 5 meters from the sill, temperatures reach 380 °C and the time above 150 °C is approximately 180 years. 1 meter from the sill temperatures reach more than 400 °C almost instantaneously and temperatures remain above 150 °C for 200 years. (All temperatures and times mentioned in the text here are approximate values based on the heat calculations, showed in figure 5.17).

The data of this study has not been extensively compared to the calculated data. Other investigations, e.g. Bostick and Pawlewicz (1984), showed that $T_{\max}$ estimated from R_{v-r} and a vitrinite-reflectance geothermometer calibrated

with laboratory heating experiments is generally 50-100 °C higher than what is calculated by the model of Lovering (1935).

In any case, it is clear that sill emplacement is a rather short and temporary heating event.

5.5 Source-rock potential

The amount of hydrocarbons generated can be calculated using the simple calculation method described by Schmoker (1994), see volumetric calculation of generated hydrocarbons, subsection 2.4.3 on page 18.

To do the calculations we used equations 2.2, 2.3 and 2.4 and the values in the upper part of Table 5.10. To determine the density at 1500 meter depth we used the density for a solid shale and subtracted for the porosity. The density of a solid shale is 2675 kg/m^3 (SImetric, 2005). The porosity in shale at 1500 meter depth is approximately 15% (Tissot and Welte, 1984).

Parameter	**Botneheia Fm.**	**Agardhfjellet Fm.**
Shale density at 1500 m depth (g/cm^3)	2.27	2.27
Shale porosity 1500 m depth (%)	15	15
Sourcerock extent (presumed) (km^2)	9	9
Thickness (m)	90	250
TOC immature sample (% wt)	8.10	4.12
TOC mature sample (% wt)	0.50	1.79
S_2 immature sample (kg HC/t rock)	35.47	4.23
S_2 mature sample (kg HC/t rock)	1.00	0.10
HI_0 (immature sample) (kg HC/t org C)	438	103
HI_p (mature sample) (kg HC/t org C)	200	5.59
$M(gTOC)$	1.49×10^{14}	2.10×10^{14}
$R(mgS_2/gTOC)$	238	97
$HCG(kgHC)$	3.54×10^{10}	2.04×10^{10}
Botneheia/Agardhfjellet	1.73	
Botneheia/Agardhfjellet pr. unit rock	4.81	

Table 5.10: *Petroleum potential for Botneheia Fm. versus Agardhfjellet Fm. Although Agardhfjellet Fm. is 2.5 times thicker, Botneheia Fm. would generate 1.7 times more oil.*

The thickness of the Botneheia Fm. and the Janusfjellet Subgroup at central Spitsbergen is approximately 90 and 420 meters, respectively (Dallmann et al., 1999). For the Janusfjellet Subgroup, however, only the lower part, the Agardhfjellet Fm. is regarded as a potential sourcerock and we have, therefore, only used the thickness of this unit in our calculations. This unit is approximately 250 meters thick in central Spitsbergen.

The "volumetric calculation of hydrocarbons generated" method of Schmoker (1994) uses the Rock-Eval HI index as a basis for its calculations. In our calculations we used a HI value that was an average of the HI values determined on

samples regarded to be unaffected by any sill to account for HI prior to hydrocarbon generation. To account for the HI index after hydrocarbon generation we used an value that was an average of HI values determined on samples close to a sill.

The results of the calculations are listed in the lower part of Table 5.10. ($M(gTOC)$ is the mass of organic carbon calculated from TOC, density and volume. $R(mgS_2/gTOC)$ is hydrocarbons generated per gram organic carbon, calculated using the HI index for immature and mature sourcerock. $HCG(kgHC)$ is hydrocarbons generated by the sourcerock unit found by multiplying $M(gTOC)$ and $R(mgS_2/gTOC)$.)

Based on this calculation method we see that although the Agardhfjellet Fm. is 2.5 times thicker, the Botneheia Fm. would generate 1.7 times more oil if the area of matured source rock is the same. Per unit rock the Botneheia Fm. generates 4.8 times more hydrocarbons than the Agardhfjellet Fm.

Using the graph in Figure 2.8(b), we converted the weight of hydrocarbons into equivalent barrels of oil or cubic feet of methane. The Botneheia Fm. yield equals 3.54×10^8 barrels of oil (bbl) or 3.54×10^{12} gas equivalent (ft^3). The Agardhfjellet Fm. yield equals 2.04×10^8 barrels of oil (bbl) or 2.04×10^{12} gas equivalent (ft^3). (See Figure 2.8(b)).

This calculation method has its limits and should be used with caution. We can, however, determine that the Botneheia Fm. has a greater potential as a sourcerock than the Agardhfjellet Fm. The calculations for the Botneheia Fm. are based on Rock-Eval measurements of outcrop samples at five locations. The calculations for the Agardhfjellet Fm. are based on samples from only one outcrop. The Agardhfjellet Fm. should be further investigated prior to determination of its potential. For these calculations we also presumed the sourcerock to be totally mature and to have expelled all its hydrocarbons. This rarely happens in nature. Furthermore, we used theoretical values for porosity and density at 1500 meters depth. 1500 meters depth is at the very beginning or shortly before the oil window starts. The reason for using these values is that this seems to be the maximum depth the samples of this study have been buried (based on vitrinite reflectance).

5.5.1 Petroleum generated next to a sill

Petroleum generation next to a sill depends on the thermal aureole around the sill, which in turn depends on the thickness of the sill, thermal conductivity of the shale next to the sill, burial depth of the rock intruded, porosity of the rock intruded, etc.

To resolve the size of the thermal aureole both theoretical heat calculations and direct or indirect measurement of maturity indicators have been used and described in the literature. When using maturity parameters one must have samples collected on each side of the sill and have information about at what distance to the sill each sample is collected. Preferably the thickness of the sill should also be known. Sourcerock samples with known distance to sill can be obtained from boreholes or outcrop profiles.

Sill thickness (m)	30
Presumed sill extent (km^2)	9
Shale density at 1500 m depth (g/cm^3)	2.27
TOC immature sample (% wt)	8.10
TOC mature sample (close to sill) (% wt)	0.50
S_2 immature sample (average) (kg HC/t rock)	35.47
S_2 mature sample (average) (kg HC/t rock)	1.00
HI_0 (immature sample) (kg HC/t org C)	438
HI_p (mature sample, close to sill) (kg HC/t org C)	200
$R(mgS_2/gTOC)$	238
Matured source rock (heat calculations)	1.33 sill thickness
Matured source rock (vitrinite reflectance)	0.75 sill thickness
Matured source rock (T_{max})	0.25 sill thickness
$M(gTOC)$ (based on heat calculations)	1.32×10^{14}
$M(gTOC)$ (based on vitrinite reflectance)	7.45×10^{13}
$M(gTOC)$ (based on T_{max})	2.48×10^{13}
$HCG(kgHC)$ (based on heat calculations)	3.14×10^{10}
$HCG(kgHC)$ (based on vitrinite reflectance)	1.77×10^{10}
$HCG(kgHC)$ (based on T_{max})	5.90×10^{9}

Table 5.11: *Upper part: Values used for calculating the petroleum yield next to a sill intruded into the Botneheia Fm. at 1500 meters depth. Middle part: Aureole size estimated with heat calculations, vitrinite reflectance and T_{max}. Lower part: Results. Note the big difference in yield estimates. This is caused by different estimates for the volume of sourcerock (its kerogen) the sill has transformed to petroleum.*

In order to discuss generation of petroleum next to sills and get numerical results that can be compared, we have in the following used distances from sill where the kerogen, according to heat calculation or measured maturity parameter, is completely transformed to petroleum. The aureole around the sill will in nature be bigger, but outside these distances to the sill the kerogen would be less and less affected by the sill and generation of petroleum will end (at least the generation caused by the sill will end when we reach a certain distance to the sill). Because of this, the numerical calculation for petroleum yield next to sills in this subsection is/are a little smaler than it would be in nature given that the size of the aureole is correct.

As with all other theoretical or semi theoretical calculations in this study, we have assumed that the sill intruded into the rock when it was buried at approximately 1500 meters depth. We therefore used porosity data for this depth to calculate the density of the rock.

As the sill matures the source rock on each side, we must multiply the affected distance to sill by a factor of 2 to account for the petroleum generated on both sides.

To calculate a numerical value for the amount of petroleum that can be generated next to a 30 meter thick sill, we used the same equations as when calculating the total potential for the Botneheia Fm. and the Agardhfjellet Fm. For

simplicity and for comparison we also used the same area (9 km^2) as when doing the calculations on the entire formations.

Aureole size based on heat calculations In the previous section we have calculated the temperatures reached next to a 30 meter thick sill at different times and distances (section 5.4). These calculations indicate that temperatures as high as 150 °C is reached as far away from the sill as 40 meter when the sill itself is 30 meter thick. At 150 °C we have passed through the entire "oil-window" and reached the catagenesis stage. If temperature alone can causes kerogen to be transformed to petroleum we can use this distance to calculate how much petroleum is being formed by the sill. The raised temperatures, according to these calculations, has bean above 100 °C at distances much longer than 40 meters. Petroleum yield would therefore, in nature, be bigger than in our calculations if this estimation of the size where full transformation takes place is correct. Hydrocarbons in the form of gas would be generated at higher temperatures than 150 °C. According to the general opinion petroleum would form at temperatures as low as 60 °C. Nevertheless, we selected 150 °C as our lower temperature that must be reached when estimating the size of the aureole where all the kerogen is transformed into petroleum, using calculated heat values.

The petroleum yield, based on heat calculation to determine the size of the aureole and by that the volume of matured source rock, is given in the lower part of table 5.11.

Aureole size based on maturity measurements Maturity is commonly used to determine if a rock has expelled its hydrocarbons, if it is still in the phase of expelling or if it has not reached the phase of expelling hydrocarbons yet.

In this study we have studied samples collected from outcrops with sills. The maturity of each sample has been determined using different maturity indicators. The different maturity indicators give various answers to the question of how far the aureole extends on each side of the sill.

Since the maturity indicators determined in this study give various answers to the question of how far the aureole reaches on each side of the sill, the amount of expelled hydrocarbons next to a sill would be different, depending on which maturity indicator is applied. Below we have discussed two of the maturity indicators determined on the samples in this study and their indication of the size of the aureole. Furthermore, we have done calculations of how much oil would be expelled, indicated by the two maturity indicators.

Vitrinite Using vitrinite reflectance to determine the size of the aureole around a sill indicates that hydrocarbons could have been formed and expelled from the sourcerock as far away as 1.5 times the sill thickness as a consequence of the sill intrusion. Further away from the sill R_o values are all bellow 0.7%. To have comparable results between the estimates used, we above selected the lower temperature for the catagenesis stage (zone of wet gas and condensate). Vitrinite reflectance values for the catagenesis stage is accepted to be in the

range 1.3%<R_o<2%. Accordingly, the aureole stretches from the sill until R_o decrease to values below 1.3%. From Figure 5.1(a) we determined the aureole to reach as far from the sill as 0.75 of the sills own thickness.

We then used the same equations as when calculating the total potential for the Botneheia Fm. and the Agardhfjellet Fm.

The results are given in the lower part of Table 5.11. The results, when using vitrinite reflectance to determine the size of the aureole, is 1.77×10^{10} $kgHC$ which equals 1.77×10^8 barrels of oil (bbl) or 1.77×10^{12} gas equivalent (ft^3).

T_{max} When determining the aureole size based on T_{max}, we used the same approach as with vitrinite reflectance above. The catagenesis stage is accepted to have been reached when T_{max} values are above 435 °C. Using figure 5.1(d) we determined the aureole to reach as far from the sill as 0.25% of the sills own thickness. (This estimation is very uncertain as many of the measured T_{max} values within this distance to sill is lower than 435 °C.)

The size obtained for the aureole when applying T_{max}, is only $1/5$ of the size as when using heat calculations to determine the aureole size. Compared with vitrinite reflectance, of many concerned to be the best parameter to determine aureole size, T_{max} estimates an aureole size which is $3/5$ the size determined by vitrinite reflectance.

The calculated amount of formed hydrocarbons is, thus, $1/5$ as much as what was calculated when using heat calculations, or $3/5$ as much as when using vitrinite reflectance to decide the size of the aureole.

The results are given in the lower part of Table 5.11. The results, when using T_{max} to determine the size of the aureole, are 5.90×10^9 $kgHC$, which equals 5.90×10^7 barrels of oil (bbl) or 5.90×10^{11} gas equivalent (ft^3).

5.5.2 Commercial oil find?

Whether or not an oil find is commercial, depends on factors like where the oil is found: on land, at sea, close to existing infrastructure or in the middle of the wilderness. Depth, i.e. how far you must drill to reach the oil, and the oil price would also be limiting factors for a minor discovery.

When all of these factor have been summed up, it concludes with the question of how much hydrocarbons can be recovered from the reservoir. For one of the smallest fields offshore Norway, the Glitne field, there are only 45.2×10^6 barrels of recoverable oil (corresponds to 4.5×10^9 kgHC). The development consists of the floating production, storage and offloading vessel, Petrojarl 1, which is tied back to four production wells and a water injection well. The oil is exported using shuttle tankers.

An even smaller field development offshore Norway is the Skirne field. Here there are 10.1×10^6 barrels of oil and 6.7×10^9 standard cubic meter gas (236.51×10^9 ft^3) of recoverable hydrocarbons (corresponds to 3.3×10^9 kgHC). This field is, however, tied back with a pipeline to another field (Heimdal) for processing. Data on the Glitne and Skirne fields were found in the Norwegian Petroleum Directorate publication Facts (2005).

Giant oil fields are fields containing more than a billion barrels of recoverable oil.

Above we have discussed how much oil will be formed if a 9 km^2 part of the sourcerocks in this study matures and expels all its hydrocarbons. 9 km^2 is not a big area when operating on a sedimentary basin scale.

Comparing our calculated results for the Botneheia Fm. and the Agardhfjellet Fm. (Janusfjellet Subgroup) we see that both these source rocks are capable of generating commercial accumulations for a small offshore field. But this is if all the hydrocarbons formed are able to escape the source rock, migrate through carrier beds and reach a trap without migration losses. According to England (1994) only a small portion of the generated hydrocarbons will reach commercial accumulations. The amount depends especially on the lithology and faulting of the carrier system, whereas the migration distances is of minor importance. Since we in our study do not have a complete petroleum system with source rock, carrier beds and a trap, estimation of migration efficiency and the size of migration losses would have to rely entirely on speculations.

If we do speculate and estimate that 10% of the generated hydrocarbons in our calculations reach a trap and is recoverable we see that both Botneheia Fm. and the Agardhfjellet Fm., if fully matured, could produce accumulations comparable with the small fields above. From the calculations where the source rock is matured by sills, and where the aureole size is determined with heat calculations (fully theoretical) and by vitrinite reflectance, we see that generated amounts for the Botneheia Fm. could produce commercial accumulations. For the sill calculations where we used T_{max} to determine the aureole size the generated amounts would probably be to low for commercial offshore accumulations). For the Agardhfjellet Fm. none of the calculations for sill maturation produces sufficient amount for commercial offshore accumulations (values for Agardhfjellet Fm. are not shown in Table 5.11).

That 10% of the total generated hydrocarbons is recoverable, is probably a best guess. If only 5% of the generated hydrocarbons reaches a trap and is produceable, none of our calculations of hydrocarbons next to sills will produce commercial offshore accumulations!

In the discussion above we have compared our calculated amounts for generated hydrocarbons next to sills with commercial accumulations offshore Norway. If prospecting on land, especially in the USA, also the Agardhfjellet Fm. could have expelled enough oil to create commercial accumulations if the reservoir is not to deep. In the USA the infrastructure with refineries to receive oil from even very small producers exists. An oil well in the USA is commercial at production rates as low as a few barrels a day (10-20) and with expectations of producing oil for a year or two.

The calculations for expelled hydrocarbons next to a sill naturally give a yield that is less than when the whole sourcerock unit expels its hydrocarbons. Sills can be interbedded in a sourcerock for many kilometers, but will normally break through the bedding of the rock it intruded, moving upwards to the surface after some time (Figure 2.1). The amounts of hydrocarbons generated by a sill we therefore regard as unlikely to yield offshore commercial accumulations when we also account for migration losses. On land, however, and especially, as noted

above, in the USA, sills may generate oil in sufficient quantities for commercial accumulations.

Chapter 6

Summary and Conclusions

This chapter summarizes the findings and conclusions of the previous chapters. It also suggests future work and publications.

In the Introduction, Chapter 1, four questions were asked:

- Vitrinite reflectivity is known to increase around intrusions. What is the relationship between the dimension of the intrusive body and the measurable thermal aureole? Is this higher maturity, indicated by vitrinite reflectance, also found by other maturity indicators?
- If maturity is shown to increase around sills also for maturity indicators other than vitrinite reflectance, is this sill maturation seemingly of the same type as maturation in normal subsiding basins, only faster?
- Can this study be utilized to evaluate the common rules of thumb concerning the extent of the aureole around a sill, one sill/dike thickness (Bostick, 1973) or two sill/dike thicknesses (Dow, 1977)?
- The importance of time on maturation and generation of oil is a topic extensively discussed in the literature. Can this study tell us something about the role of time as a factor for oil generation?

In this thesis the aim has been to answer these questions. In the next section each of these questions will be addressed.

The conclusions presented in this chapter are valid only for the data sets; NKB, BH2, KRB, TBU, TBL and HOB3. The data from BH1, HOB1, HOB2, KMB-C, KMB-D, WØU and WØL are not complete in the sense that not all geochemical measurements have been carried out on these samples. For some of the data sets in the lather category fundamental measurements like distance to sill are also missing. This makes these data impossible to use for the purpose of this thesis.

6.1 Findings

The data being used as a basis for this thesis were gathered in 1995. The goal of the investigation in 1995 is unknown to the author, but I believe it was to answer

questions like the ones listed above. An attempt to answer the questions will be given below. The order of the answers will be slightly different than the order of the questions.

6.1.1 Sill aureole size

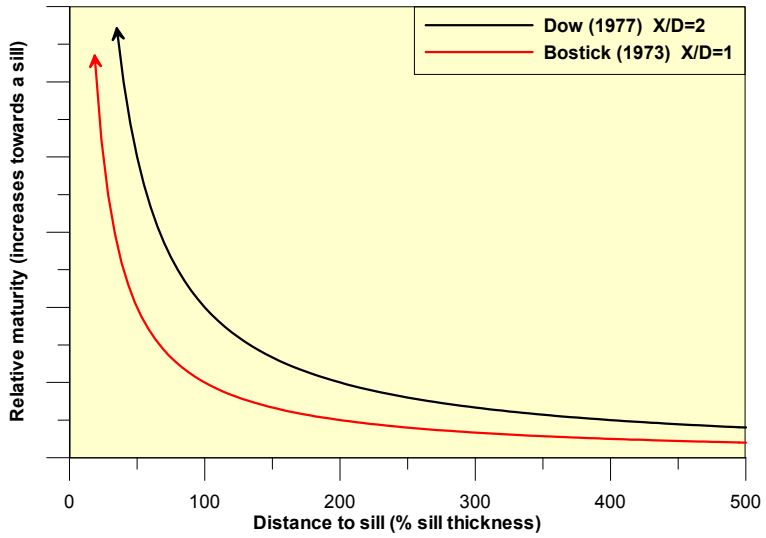

Figure 6.1: *The contact aureole in sedimentary rocks can be detected at a distance away from the sill/dike contact equal to one sill/dike thickness ($X/D = 1$; Bostick (1973)) or two sill/dike thicknesses ($X/D = 2$; Dow (1977).*

Question: Can this study be utilized to evaluate the common rules of thumb concerning the extent of the aureole around a sill/dike, one sill/dike thickness (Bostick, 1973) or two sill/dike thicknesses (Dow, 1977)?

Bostick's (1973) and Dow's (1977) observations seem to be too simple and is in the best case valid only for the parameters they were utilized (vitrinite). This conclusion is based on our measurements of maturity changes approaching sills summarized in Table 6.1.

But first, before giving the reason for our conclusion, we will briefly discuss what the rule of thumb concerning the extent of the aureole around a sill/dike really is. The position within a contact aureole of a sill/dike can be expressed as the ratio of the distance from the sill/dike margin (X) divided by the sill/dike thickness (D). X/D normalizes the distance from the sill/dike contact and makes this data comparable between sills/dikes of different thicknesses (Jaeger, 1959). The sill/dike rule is an empirical observation suggesting that the contact aureole in sedimentary rocks can be detected at a distance away from the sill/dike contact equal to one sill/dike thickness ($X/D = 1$; Bostick (1973)) or two sill/dike thicknesses ($X/D = 2$; Dow (1977)). See illustration in figure 6.1.

In Table 6.1 characteristics measured on the samples and parameters calculated on the base of the characteristics are listed. The distance-to-sill in which a change appears, is normalized as described above.

As can be seen in Table 6.1, only vitrinite reflectance (**%R$_o$**) is observed to change on a distance-to-sill > 1. **FA** kerogen, **S$_2$**, **HI** and **OI** are unchanged and stable until distance-to-sill = 1. **SAT/ARO** increases, but because of the considerable scatter it is difficult to conclude at exactly which distance the increase starts. **Pr/n-C$_{17}$** and **Ph/n-C$_{18}$** both increase from a distance-to-sill = 1/2. The rest of the parameters measured or calculated either shows no change as we approach the sill or change at even shorter distances to the sill.

Another observation from Table 6.1 is that the changes mainly occur in the kerogen-bound parameters. Changes in free hydrocarbons are more difficult to determine and the scatter in these results make them questionable.

As the majority of the characteristics measured and parameters calculated shows no change at distances above a distance equal to one sill thickness, we find Dow's (1977) observation ($X/D = 2$) not to be valid for this study. Bostick's (1973) observation ($X/D = 1$) seems to be valid as long as we measure characteristics and calculated parameters related directly to the kerogen. For characteristics measured on free-hydrocarbons it is difficult to see any pattern as the scatter in measured values is considerable. However, shortchained n-alkanes seem to decrease in number compared to long-chained n-alkanes, when approaching the sills.

6.1.2 Sill maturity

Two questions were asked regarding maturity around intrusions. They will here be addressed separately.

Maturity indicators

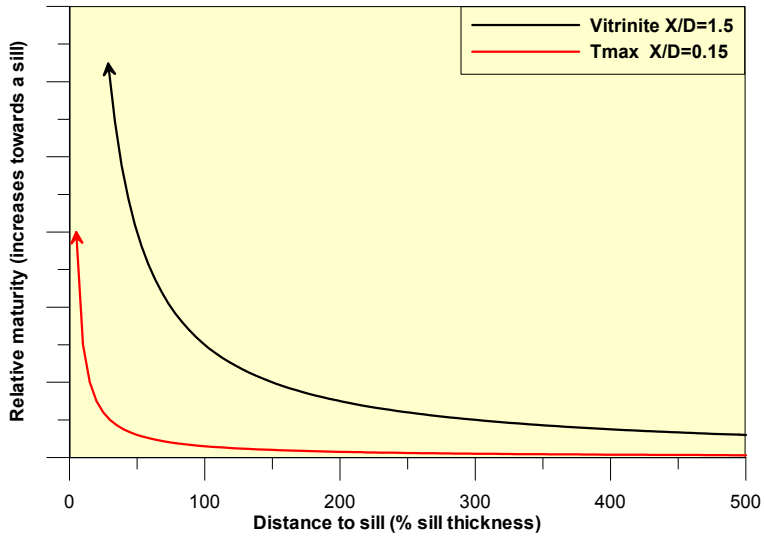

Figure 6.2: *An illustration of the measurable changes in two of the maturity parameters determined on the samples of this study. Black curve represent* **T$_{max}$** *X/D=1.5 and red curve represent* **%R$_o$** *X/D=0.15.*

MICROSCOPY	VR	$\%R_o$	stable until one 1.5 sill thickness ($X/D = 1.5$)
	KEROGEN	FA	stable until one sill thickness ($X/D = 1.0$)
		HA	stable until one half sill thickness ($X/D = 0.5$)
		AL	can not be determined based on this study
		HE	stable until one 1/3 sill thickness ($X/D = 0.33$)
		WO	stable until 2/3 sill thickness ($X/D = 0.66$)
		CO	end product, stable at all distances
GEO CHEMICAL	ROCK EVAL	TOC	seems to increase approaching a sill, then decreases towards sill from $X/D = 0.15$ sill thickness
		S_1	stable until one half sill thickness ($X/D = 0.5$)
		S_2	stable until one sill thickness ($X/D = 1.0$)
		HI	stable until one sill thickness ($X/D = 1.0$)
		OI	stable, then increases towards sill from $X/D = 0.15$ sill thickness.
		PI	stable until one sill thickness ($X/D = 1.0$)
		T_{max}	stable, then increases towards sill from $X/D = 0.15$ sill thickness.
	TLC-FID	SAT	decreases in yield, increases in %
		ARO	decreases in yield, decreases in %
		POL	decreases in yield, no change in %
		SAT/ARO	increases (from one sill thickness (?) ($X/D = 1.0$))
	GC-FID	$n\text{-}C_{17}/n\text{-}C_{31}$	decreases
		Pr/Ph	increasingly scattered
		$Pr/n\text{-}C_{17}$	increases at $X/D = 1.5$
		$Ph/n\text{-}C_{18}$	increases at $X/D = 1.5$
		CPI	no change
		CPI_1	no change
		CPI_2	no change

Table 6.1: *Change/stability in organic content/maturity towards a sill.*

Question: Vitrinite reflectivity is known to increase around intrusions. What is the relationship between the dimension of the intrusive body and the measurable thermal aureole? Is this higher maturity, indicated by vitrinite reflectance, also found by other maturity indicators?

The vitrinite reflectance ($\%R_o$) profiles show the typical inverted profile closer to the sills i.e. the vitrinite values are as low as 1.5% at 2 meters from a 25 meter thick sill, 5% at 5 meters, decreasing to 3.5% at 10 meters, before reaching the background value of 0.8% at a distance of about 20 meters from sill (Table F.3).

The only other direct measurement of kerogen maturity in this study is the measurement of Rock-Eval T_{max}. T_{max} should increase from values below 425 °C for immature samples. Just-mature samples should have values above 435 °C. Mature samples should have values of 435 to 465 °C. Over-mature samples should have values above 465 °C. The same samples observed to have a good, clear maturity trend in the vitrinite measurements ($\%R_o$) show no trend when it

comes to $\mathbf{T_{max}}$ (Table A.3). Figure 5.1(d) shows all the $\mathbf{T_{max}}$ measurements of this study. This figure shows that some samples have increasing $\mathbf{T_{max}}$ values as we approach the sill. The scatter within each series is, however, considerable. It is therefore difficult to conclude that $\mathbf{T_{max}}$ show an increasing maturity trend, approaching a sill.

Indirect measurements of maturity, e.g. kerogen-description results, show increasing maturity as the sill is approached (Figure G.2(c)). These results are, like the vitrinite reflectance results, obtained by microscopic measurements and are related directly to the kerogen and physical and/or chemical changes of the kerogen.

$\mathbf{T_{max}}$ is also directly related to the kerogen, as this is the temperature where the $\mathbf{S_2}$ peak has its maximum. $\mathbf{S_2}$ measures the petroleum yield from cracking of kerogen. As we approach a sill $\mathbf{T_{max}}$ should increase if the sill intrusion has generated hydrocarbons (remaining kerogen needs subsequently more heat to crack). The fact that $\mathbf{T_{max}}$ does not follow the same increasing maturity trends as vitrinite-reflectance and kerogen-description results is therefore surprising.

Moving over to maturity indicators measured on free-hydrocarbons (biomarkers), the picture of sill maturation as being of a different nature compared to maturity increase in a "normal" subsiding basin, is further amplified. No change is observed in measured **CPI** values, even though other measurements show the kerogen to be a mixture of both marine and terrestrial kerogen. Long-chained n-alkanes, derived from immature terrestrial kerogen, would have an odd-carbon-number preference. With increasing maturity any odd- or even-carbon-number preference would be wiped out. For the samples of this study we see no change in the **CPI** values when approaching the sills. The only change we observe in the free hydrocarbons are the ratios $\mathbf{Pr/n\text{-}C_{17}}$ and $\mathbf{Ph/n\text{-}C_{18}}$. These ratios both seem to increases from 1/2-sill-thickness distance away from the sill (Figures 5.1(i) and 5.1(j)). Normally these ratios are thought to decrease as maturity increases. What we observe in this study is an opposite trend, and there is no indication that biodegradation have occurred. However, looking at the values in each sample series we see that there is a lot of scatter in the data and the suggested trends are not always clear.

The isotope measurements show no change in the free-hydrocarbons δ^{13}**C EOM** approaching the sill. In the kerogen we see a slightly heavier δ^{13}**C KER** values indicating that some generation of hydrocarbons has occurred (the oil/gas that is generated should normally have lighter δ^{13}**C** values than the remaining kerogen).

Maturity around sills compared with maturity in a normal subsiding basin

Question: If maturity is shown to increase around sills also for maturity indicators other than vitrinite reflectance, is this sill maturation of the same type as maturation in normal subsiding basins, only faster?

As discussed above, the observed changes in maturity only seem to occur on characteristics and indicators directly related to the kerogen. For the free hydrocarbons we must go closer to the sill to observe any change, and the scatter in our measurements becomes considerable.

These results were in the beginning difficult to understand, but directed us to suggest that the generative process leads to strong mobilization of water at the same time as the generation of light hydrocarbons occured. We suggest that generated hydrocarbons were "flushed away" from the shale intervals closer to the sill. Later, low-maturity n-alkanes and biomarkers may have back-diffused from the lower-maturity, unaffected shales into the thermally affected shales, following cooling of the intrusion.

The composition of the generated hydrocarbons extracted from the rock samples indicates that hydrocarbon generation by sills may be a less-than-perfect analogy for normal hydrocarbon generation in subsiding basins. Thus both the **Pr/n-C_{17}** and the **Ph/n-C_{18}** ratios increases as we approach the sill. Normally these ratios are decreasing as maturity increases. What we observe in this study is an opposite trend.

An illustration of the processes involved when a sill intrudes a source rock at a depth of 1500 meters is given in Figure 6.3.

6.1.3 Importance of time

Question: The importance of time on maturation and generation of oil is a topic extensively discussed in the literature. Can this study tell us something about the role of time as a factor for oil generation?

Yes, "sufficient" time seems to be important for maturation and generation of oil. Our findings and reasons for this conclusion will be discussed below.

Calculation of the temperature at different distances from the sill shows that the anomalous high temperature caused by the sill (30 m thick at 1500 m depth) exists for about 200 years (section 5.4.2). (Anomalous high at this burial depth.) The start temperature for the oil window, 60 - 100 °C is reached as far from sill as a distance to sill ~ about twice the sill's own thickness. At a distance equal to 2/3 times the sill own thickness (from the sill), the temperature reaches 200 °C and stay there for approximately 130 years. At a distance equal to 1/3 times the sill own thickness (from the sill), the time above 150 °C is approximately 150 years, but here the temperature reaches 300 °C. At a distance from the sill equal to 1/6 times the sill own thickness, temperature reaches 380 °C and the time above 150 °C is approximately 180 years.

However, measurements of vitrinite reflectance on the samples used in this study indicates that hydrocarbons have not been formed on distances further away from the sill than 1.5 times the sills own thickness. Measurements of other maturity indicators indicate that the distance to sill were hydrocarbons have been formed is even shorter.

The T_{max} measurements show hardly any increase as we approach the sill. Only very few samples support the vitrinite reflectance measurements. The samples most close to sill have almost the same S_2 content as samples collected most distant to the sills.

To conclude, the temperatures, generally accepted as necessary for generating hydrocarbons, are reached when a sill intrudes a source rock. Measurement of vitrinite reflectance indicates high temperatures, and that hydrocarbons are

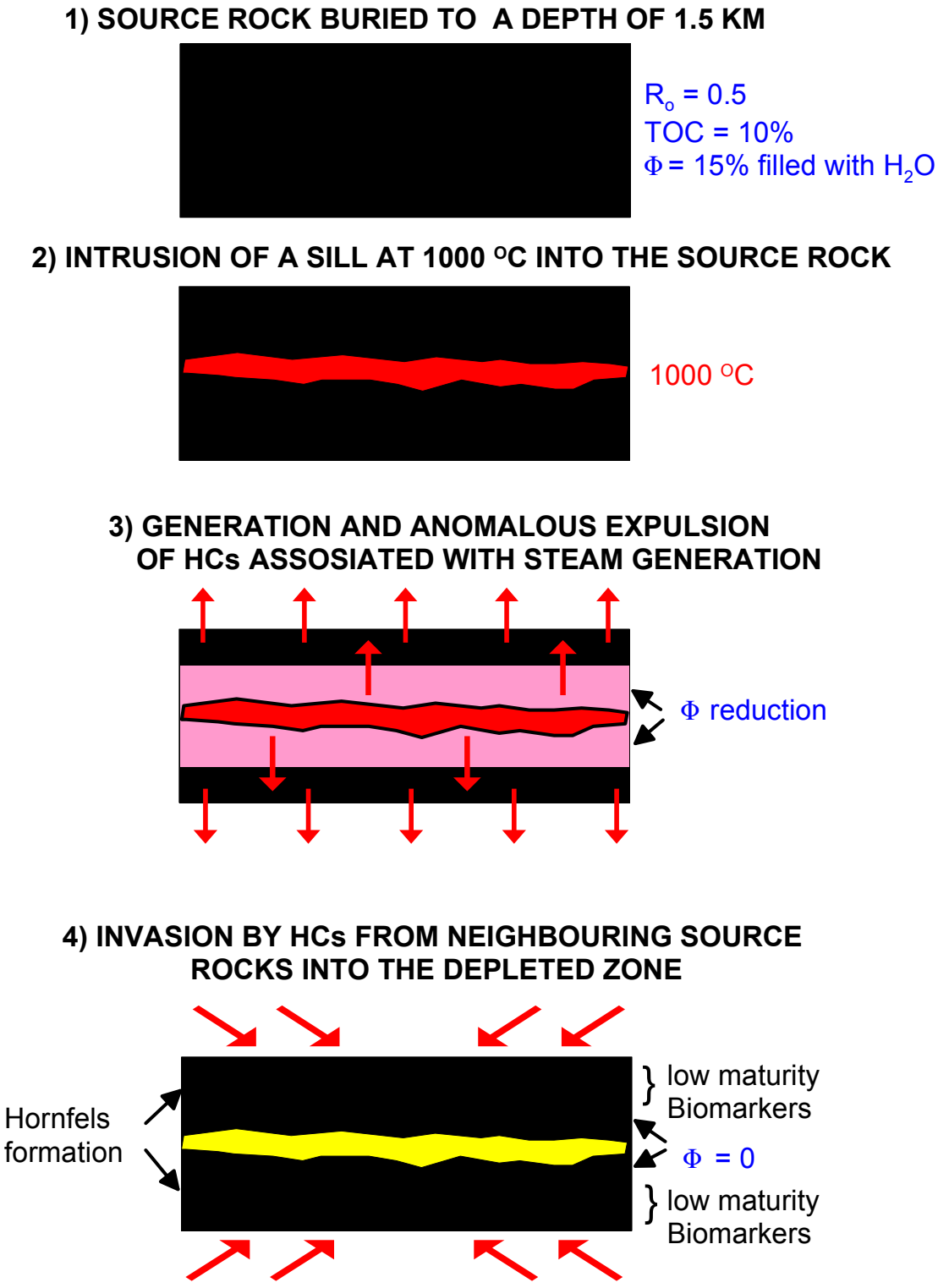

Figure 6.3: *An illustration of the processes involved when a sill intrudes a source rock at 1500 m depth*

formed around sills, but not as far from the sills as the heat calculations indicate. Measurements of other maturity indicators, generally accepted to give trustable results for indicating maturity, further reduces the distance to sill where hydrocarbons has been formed. That sills cause high temperatures in the rock around them is indisputable. Since the majority of maturity indicators measured in this study suggest far lower temperatures in the surrounding rock than the heat calculations show, we must conclude that the higher temperatures in the surrounding rock after sill emplacement do not exist for sufficient time for the maturity indicators to change. This shows that time is important for the maturity indicators to change. Hence, time is also probably important for the generation of hydrocarbons, including oil.

In other words, time is important for the generation of oil and gas, not only the temperature.

6.2 Implications of this study

Hydrocarbon exploration

This study shows that sills ~ about 30 meters thick emplaced in shallow buried source rocks are unlikely to have generated hydrocarbons in sufficient quantities for the formation of offshore commercial accumulations of oil and gas. On land, however, and especially in countries where the infrastructure to receive oil from even very small producers exists, sills may have generated enough petroleum for commercial accumulations to exist.

Oil - sourcerock correlation studies

Biomarker ratios like **Pr/n-C_{17}** and **Ph/n-C_{18}** seem to be strongly affected by sills and should therefore not be used as facies indicators in basins were intrusions are known to exist.

6.3 Perspective

As this study is concluded, work that could be done still remains.

GC-MS results

Detailed GS-MS analysis was carried out on 48 of the samples in 1996. These results should be interpreted within the context of the conclusions made in this thesis regarding free hydrocarbons next to a sill.

Basin modeling

Basin modeling could have been integrated as a part of this study. However, as the treatment of the data itself proved to be quite extensive, and more than enough for a Cand. Scient. thesis. Thus, basin modeling was not performed.

A basin model of sills emplaced into the Botneheia Fm. would depend heavily on the assumptions regarding the overburden formations' thicknesses and structures. This is something we would like to investigate further, and it could eventually lead to a future publication.

6.4 Further Publications

Thermal effects of basaltic sill emplacement in source rocks

The interest for the results presented at the IMOG meeting in Seville, Spain, 12-16th September 2005 (poster, Appendix J) indicates that the results of this study should be published.

Triassic oil, Svalbard

In the autumn 2002 a one-day excursion to Botneheia was conducted by the author during a stay at Svalbard. In addition to photographs of the sample site, some samples were collected. A sample collected from the sill itself later showed evidences of hydrocarbons when a gas sample was analyzed on the GC-FID. So far we have additionally analyzed an extract on the GC-MS and microscopically examined the sample. The results show liquid petroleum to be present in inclusions of the rock sample. The hydrocarbons found within the sill should be compared with the ones found in the surrounding source rock and with oil samples from the Barents Sea. Some of these data are included in Appendix K.

References

Alexander, R., R. I. Kagi, and G. W. Woodhouse (1981). Geochemical correlation of windalia oil and extracts of winning group (cretaceous) potential source rocks, barrow subbasin, western australia. AAPG Bulletin 65(2), 235–250.

Andresen, A. (2005). Private correspondance. Professor in Structural geology, University of Oslo, Norway.

Baker, D. R. (1972). Organic geochemistry and geological interpretations. In Papers on Low-Temperature Geochemistry., Volume 20; 5 of Journal of Geological Education, pp. 221–234. Lawrence, KS, United States: National Association of Geology Teachers.

Baker, E. W., W. Y. Huang, J. G. Rankin, J. R. Castano, J. R. Guinn, and A. N. Feux (1977). Electron paramagnetic resonance study of thermal alteration of kerogen in deep-sea sediments by sill intrusion. In J. Gardner and J. Herring (Eds.), Abidjan, Ivory Coast, to Malaga, Spain, February-April 1975., Volume 41 of Initial Reports of the Deep Sea Drilling Project, pp. 839–847. College Station, TX, United States: Texas A&M University, Ocean Drilling Program.

Barker, C. E., Y. Bone, and M. D. Lewan (1998). Fluid inclusion and vitrinite-reflectance geothermometry compared to heat-flow models of maximum paleotemperature next to dikes, western onshore gippsland basin, australia. In C. Crelling John (Ed.), 13th annual meeting of the Society for Organic Petrology., Volume 37; 1-2 of International Journal of Coal Geology, pp. 73–111. Amsterdam, International: Elsevier. 13th annual meeting of the Society for Organic Petrology. Carbondale, IL, United States. Sept. 15-19, 1996.

Bhullar, A. G., D. A. Karlsen, O. K. Backer, T. K. Le, E. Skalnes, H. H. Berchelmann, and J. E. Kittelsen (2000). Reservoir characterization by a combined micro-extraction–micro thin-layer chromatography (iatroscan) method; a calibration study with examples from the norwegian north sea. Journal of Petroleum Geology 23(2), 221–244.

Bishop, A. N. and G. D. Abbott (1993). The interrelationship of biological marker maturity parameters and molecular yields during contact metamorphism. Geochimica et Cosmochimica Acta 57(15), 3661–3668.

Bishop, A. N. and G. D. Abbott (1995). Vitrinite reflectance and molecular geochemistry of jurassic sediments; the influence of heating by tertiary dykes (northwest scotland). In J. Cardott Brian, L. Thompson Rizer Carolyn, and

R. Woods (Eds.), Collected papers from the Tenth annual meeting of the Society for Organic Petrology., Volume 22; 1 of Organic Geochemistry, pp. 165–177. Oxford-New York, International: Pergamon.

Bostick, N. H. (1971). Thermal alteration of clastic organic particles as an indicator of contact and burial metamorphism in sedimentary rocks. In American Association of Stratigraphic Palynologists, Proceedings, 2nd., Volume 3 of Geoscience and Man, pp. 83–92. Baton Rouge, LA, United States: Louisiana State University, School of Geoscience.

Bostick, N. H. (1973). Time as a factor in thermal metamorphism of phytoclasts (coaly particles). In Septieme Congres International de Stratigraphie et de Geologie du Carbonifere., Volume 7; 2 of Compte Rendu - Congres International de Stratigraphie et de Geologie du Carbonifere = International Congress on Carboniferous Stratigraphy and Geology., pp. 183–193.

Bostick, N. H. and M. J. Pawlewicz (1984). Paleotemperatures based on vitrinite reflectance of shales and limestones in igneous dike aureoles in the upper cretaceous pierre shale, walsenburg, colorado. In J. Woodward, F. Meissner Fred, and L. Clayton Jerry (Eds.), Hydrocarbon source rocks of the Greater Rocky Mountain region., pp. 387–392. Denver, CO, United States: Rocky Mt. Assoc. Geol.

Bradley, J. (1965). Intrusion of major dolerite sills. Royal Society of New Zealand Transactions 3, 27–55.

Bray, E. E. and E. D. Evans (1961). Distribution of n-paraffins as a clue to recognition of source beds. In Symposium on the chemical approaches to the recognition of petroleum source rocks., Volume 22; 1 of Geochimica et Cosmochimica Acta, pp. 2–15. Oxford, International: Pergamon.

Bruce, P. M. and H. E. Huppert (1990). Solidification and melting along dykes by the laminar flow of basaltic magma. In M. P. Ryan (Ed.), Magma transport and storage, pp. 87–101. Chichster: Wiley & Sons.

Buiskool Toxopeus, J. M. A. (1983). Selection criteria for the use of vitrinite reflectance as a maturity tool. In Petroleum geochemistry and exploration of Europe; International congress, Volume 12 of Special Publication, pp. 295–307. London, United Kingdom: Geological Society of London.

Burgess, J. D. (1974). Microscopic examination of kerogen (dispersed organic matter) in petroleum exploration. Geological Society of America - Spec. Paper. (153), 19–30.

Burov, J. P., s. A. A. Krasil, D. V. Firsov, and B. A. Klubov (1975). The age of spitsbergen dolerites (from isotopic dating). Årbok - Norsk Polarinstitutt 1975, 101–108.

Bäckström, S. A. (1971). Paleontologisk og sedimentologisk undersøkelse av Brentskardhaugen laget (jura) på Spitsbergen. Cand. real. thesis, University of Oslo.

Carey, S. W. (1958). The isostrat: a new technique for the analysis of structure of the Tasmanian dolerite. In Dolerite: a symposium, pp. 130–164. University of Hobart.

Carslaw, H. S. and J. C. Jaeger (1959). Conduction of heat in solids. Oxford: Clarendon Press.

Caston, V. N. D., R. Dearnley, R. K. Harrison, C. C. Rundle, and M. T. Styles (1981). Olivine-dolerite intrusions in the fastnet basin. Journal of the Geological Society 138, 31–46.

Clayton, J. L. and N. H. Bostick (1986). Temperature effects on kerogen and on molecular and isotopic composition of organic matter in pierre shale near an igneous dike. In D. Leythaeuser and J. Ruellkotter (Eds.), Advances in organic geochemistry, 1985; Part I, Petroleum geochemistry., Volume 10; 1-3 of Organic Geochemistry, pp. 135–143. Oxford-New York, International: Pergamon.

Combaz, A. (1980). Les kerogenes vus au microscope. In B. Durand (Ed.), Kerogen; insoluble organic matter from sedimentary rocks., pp. 55–112. Paris, France: Ed. Technip.

Cornford, C., J. A. Morrow, A. Turrington, J. A. Miles, and J. Brooks (1983). Some geological controls on oil composition in the u.k. north sea. In J. Brooks (Ed.), Petroleum geochemistry and exploration of Europe; International congress., Volume 12 of Special Publication - Geological Society of London, pp. 175–194. London, United Kingdom: Geological Society of London.

Cutbill, J. L. and A. Challinor (1965). Revision of the stratigraphical scheme for the Carboniferous and Permian rocks of Spitsbergen and Bjornoya. Geological Magazine 102(7), 418–439.

Dahl, B. and E. Rasmussen (2003). Petroleum geoscientific interpretation system (PeGIS). Software program developed for applications in the petroleum industry in order to optimize the use of available geological data and make interpreted results available for re-use.

Dallmann, W. K., A. Andresen, S. G. Bergh, H. D. Maher, and Y. Ohta (1993). Tertiary fold-and-thrust belt of Spitsbergen, Svalbard : compilation map, summary and bibliography. Oslo: Norsk Polarinstitutt.

Dallmann, W. K., K. Birkenmajer, H. Dypvik, J. G. Gjelberg, H. B. Keilen, A. Mørk, J. Nagy, A. Nottvedt, T. M. Pcelina, R. J. Steel, and D. Worsley (1999). Lithostratigraphic lexicon of Svalbard. Tromsø, Norway: Norsk Polarinstitutt.

Delaney, P. T. (1982). Rapid intrusion of magma into wet rock; groundwater flow due to pore pressure increases. JGR. Journal of Geophysical Research. B 87(9), 7739–7756.

Delaney, P. T. (1987). Heat transfer during emplacement and cooling of mafic dykes. In C. Halls Henry and F. Fahrig Walter (Eds.), Mafic dyke swarms; a collection of papers based on the proceedings of an international

conference., Volume 34 of Special Paper - Geological Association of Canada, pp. 31–46. Toronto, ON, Canada: Geological Association of Canada.

Delaney, P. T. and D. D. Pollard (1982). Solidification of basaltic magma during flow in a dike. American Journal of Science 282(6), 856–885.

Dow, W. G. (1977). Kerogen studies and geological interpretations. Journal of Geochemical Exploration 7(2, Application of geochemistry to the search for crude oil and natural gas), 79–99.

Edwards, M. B. (1976). Growth faults and associated structures in upper Triassic deltaic sediments, Svalbard, Norway. AAPG Bulletin 60(4, AAPG-SEPM annual meeting), 668.

England, W. A. (1994). Secondary migration and accumulation of hydrocarbons. In B. Magoon Leslie and G. Dow Wallace (Eds.), The petroleum system; from source to trap., Volume 60 of AAPG Memoir, pp. 211–217. Tulsa, OK, United States: American Association of Petroleum Geologists.

Espitalie, J., J. L. Laporte, M. Madec, F. Marquis, P. Leplat, J. Paulet, and A. Boutefeu (1977). Methode rapide de caracterisation des roches meres, de leur potentiel petrolier et de leur degre d'evolution. Revue de l'Institut Francais du Petrole et Annales des Combustibles Liquides 32(1), 23–42.

Espitalie, J., F. Marquis, and I. Barsony (1984). Geochemical logging. In J. Voorhees Kent (Ed.), Analytical pyrolysis techniques and applications., pp. 276–304. London, United Kingdom: Butterworth and Co.

Facts (2005). Facts 2005: The Norwegian petroleum sector. Oslo: Olje- og energidepartementet. http://www.npd.no/NR/rdonlyres/027B030F-38BE-4B2A-9F4F-CE39E9BD2F78/0/Fakta2005.pdf.

Feyling-Hanssen, R. W. (1955). Stratigraphy of the marine late-pleistocene of Billefjorden, Vestspitsbergen, Volume 107 of Norsk Polarinstitutt Skrifter. Oslo, Norway: Norsk Polarinstitutt.

Forsberg, A. and M. Bjorøy (1983). A sedimentological and organic geochemical study of the botneheia formation, svalbard, with special emphasis on the effects of weathering on the organic matter in shales. In M. Bjoroey, C. Albrecht, C. Cornford, K. de Groot, G. Eglinton, E. Galimov, D. Leythaeuser, R. Pelet, J. Rullkoetter, and G. Speers (Eds.), Advances in organic geochemistry, 1981., Volume 10 of Proceedings of the International Meeting on Organic Geochemistry, pp. 60–68. Chichester-New York, International: Wiley & Sons.

Forsberg, A. W. (1980). En sedimentologisk og organisk geokjemisk undersøkelse av Barentsøya formasjonen (Trias), Svalbard. Cand. real. thesis, University of Oslo.

Francis, P. W. (1982). Magma and sediment. I. Emplacement mechanism of Late Carboniferous tholeiite sills in northern Britain. Journal of the Geological Society 139, 1–20.

Fuex, A. N. (1977). The use of stable carbon isotopes in hydrocarbon exploration. Journal of Geochemical Exploration 7(2, Application of geochemistry to the search for crude oil and natural gas), 155–188.

Galimov, Y. M. (1980). $^{13}c/^{12}c$ in kerogen. In B. Durand (Ed.), Kerogen; insoluble organic matter from sedimentary rocks., pp. 271–299. Paris, France: Ed. Technip.

Galushkin, Y. I. (1997). Thermal effects of igneous intrusions on maturity of organic matter; a possible mechanism of intrusion. Organic Geochemistry 26(11-12), 645–658.

Gautneb, H. and A. Gudmundsson (1992). Effect of local and regional stress fields on sheet emplacemnets in west iceland. Journal of Voulcanology and Geothermal Research 51, 339–356.

Gayer, R. A., D. C. Gee, W. B. Harland, J. A. Miller, H. R. Spall, R. H. Wallis, and T. S. Wisnes (1970). Radiometric age determinations on rocks from Spitsbergen, Volume 137 of Norsk Polarinstitutt Skrifter. Oslo, Norway: Norsk Polarinstitutt.

Gjelberg, J. and R. Steel (1979). Middle Carboniferous sedimentation in relation of tectonic, climate and sea level changes on Bjoernoeya and Spitsbergen. Norwegian Sea Symp. Norw. Pet. Soc. NSS/27, 25.

Harland, W. (1997). The geology of Svalbard. London: Geological Society.

Harland, W. B. (1961). An outline structural history of spitsbergen. Geology of the Artic 1, 68–132.

Harland, W. B. (1974). The Billefjorden fault zone, Spitsbergen., Volume 161 of Norsk Polarinstitutt Skrifter. Oslo, Norway: Norsk Polarinstitutt.

Harland, W. B. and S. R. A. Kelly (1997). Jurassic-cretaceous history. In W. B. Harland, M. Anderson Lester, and D. Manasrah (Eds.), The geology of Svalbard., Volume 17 of Memoir - Geological Society of London, pp. 363–387.

Hayes, J. M. (1993). Factors controlling (super 13) c contents of sedimentary organic compounds; principles and evidence. In R. J. Parkes, P. Westbroek, and J. W. de Leeuw (Eds.), Marine sediments, burial, pore water chemistry, microbiology and diagenesis., Volume 113; 1-2 of Marine Geology, pp. 111–125. Amsterdam, Netherlands: Elsevier.

Hellem, T. A. (1980). En sedimentologisk og diagenetisk undersøekelse av utvalge profiler fra Tempelfjordengruppen (Perm) i Isfjordenområdet,Spitsbergen. Cand. real. thesis, University of Oslo.

Hoppe, G. (1970). The Wurm ice sheets of northern and arctic Europe. Acta Geographica Lodziensia 94, 205–215.

Jaeger, J. C. (1957). The temperature in the neighborhood of a cooling intrusive sheet. American Journal of Science 255(4), 306–318. Article.

Jaeger, J. C. (1959). Temperatures outside a cooling intrusive sheet. American Journal of Science 257(1), 44–54. Kline Geology Laboratory, Yale University. New Haven, CT, United States. 1959.

Jaeger, J. C. (1964). Thermal effects of intrusions. Reviews of Geophysics 2(3), 443–466. Article.

Karlsen, D. A. and s. Larter (1989). A rapid correlation method for petroleum population mapping within individual petroleum reservoirs: applications to petroleum reservoir description. In J. D. Collinson (Ed.), Correlation in Hydrocarbon Exploration, pp. 77–85. London: Graham & Trotman.

Karlsen, D. A. and S. R. Larter (1991). Analysis of petroleum fractions by tlc-fid; applications to petroleum reservoir description. Organic Geochemistry 17(5), 603–617.

Khorasani, G. K., D. G. Murchison, and A. C. Raymond (1990). Molecular disordering in natural cokes approaching dyke and sill contacts. Fuel (Guildford) 69(8), 1037–1046.

Knarud, R. (1980). En sedimentologisk og diagnostisk undersøkelse av Kapp Toscana formasjonens sedimenter på Svalbard. Cand. real. thesis, University of Oslo.

Langford, F. F. and M. M. Blanc-Valleron (1990). Interpreting rock-eval pyrolysis data using graphs of pyrolizable hydrocarbons vs. total organic carbon. AAPG Bulletin 74(6), 799–804.

Lauritzen, Ø. (1981). Undersøkelser i de sulfatførende sedimentene fra underperm i områdene nord for Isfjorden, Svalbard. Norsk Polarinstitutt Raport serie. Number 6, 1–21.

Lock, B. E., C. A. G. Pickton, D. G. Smith, D. J. Batten, and W. B. Harland (1978). The geology of Edgeoeya and Barentsoeya, Svalbard, Volume 168 of Norsk Polarinstitutt Skrifter. Oslo, Norway: Norsk Polarinstitutt.

Lovering, T. S. (1935). Theory of heat conduction applied to geological problems. Geological Society of America Bulletin 46(1), 69–94.

Major, H. and J. Nagy (1972). Geology of the Adventdalen map area, Volume 161 of Norsk Polarinstitutt Geological Map. Oslo, Norway: Norsk Polarinstitutt.

Moe, H. R. (1980). Sedimentologiske og diagenetiske undersøkelser i krittlagrekken på Svalbard. Cand. real. thesis, University of Oslo.

Mørk, A., W. K. Dallmann, H. Dypvik, E. P. Johannessen, G. B. Larssen, J. Nagy, A. Nottvedt, S. Olaussen, T. M. Pcelina, D. Worsley, and e. Stratigrafic Commitee for Svalbard (1999). Mesozoic lithostratigraphy. In W. K. Dallmann, K. Birkenmajer, H. Dypvik, G. Gjelberg John, B. Keilen Hilde, A. Mørk, J. Nagy, A. Nottvedt, M. Pcelina Tatjana, J. Steel Ron, and D. Worsley (Eds.), Lithostratigraphic lexicon of Svalbard; review and recommendations for nomenclature use; upper Palaeozoic to Quaternary bedrock., pp. 127–214. Tromsø, Norway: Norsk Polarinstitutt.

Mørk, A., R. Knarud, and D. Worsley (1982). Depositional and diagenetic environments of the Triassic and Lower Jurassic succession of Svalbard. In F. Embry Ashton and R. Balkwill Hugh (Eds.), Arctic geology and geophysics; proceedings of the Third international symposium on Arctic

geology., Volume 8 of Memoir, pp. 371–398. Calgary, AB, Canada: Canadian Society of Petroleum Geologists.

Mørk, A. and D. Worsley (1978). : The triassic stratigraphy of southern spitsbergen. Årbok - Norsk Polarinstitutt, 43–59.

Nagy, J. (1970). Ammonite faunas and stratigraphy of lower Cretaceous (Albian) rocks in southern Spitsbergen, Volume 152 of Norsk Polarinstitutt Skrifter. Oslo, Norway: Norsk Polarinstitutt.

Nathorst, A. G. (1911). Beitraege zur geologie der baeren-insel, spitzbergens und des koenig-karl-landes. Bulletin - Uppsala Universitet, Mineralogisk-geologiska Institut 10, 261–415.

Parker, J. R. (1966). Folding, faulting and dolerite intrusions in the Mesozoic rocks of the fault zone of central Spitsbergen. Årbok - Norsk Polarinstitutt 1964, 47–55.

Peters, K. E. (1986). Guidelines for evaluating petroleum source rock using programmed pyrolysis. AAPG Bulletin 70(3), 318–329.

Peters, K. E. and M. R. Cassa (1994). Applied source rock geochemistry. In B. Magoon Leslie and G. Dow Wallace (Eds.), The petroleum system; from source to trap., Volume 60 of AAPG Memoir, pp. 93–120. Tulsa, OK, United States: American Association of Petroleum Geologists.

Peters, K. E. and J. M. Moldowan (1993). The Biomarker guide. Interpreting molecular fossils in petroleum and ancient sediments. Prentice Hall.

Peters, K. E., B. R. T. Simoneit, S. Brenner, and I. R. Kaplan (1978). Vitrinite reflectance-temperature determinations for intruded cretaceous black shale in the eastern atlantic. In D. F. Oltz (Ed.), Symposium in geochemistry; Low temperature metamorphism of kerogen and clay minerals., pp. 53–57. Los Angeles, Calif., United States: Soc. Econ. Paleontol. and Mineral., Pac. Sect.

Peters, K. E., J. K. Whelan, J. M. Hunt, and M. E. Tarafa (1983). Programmed pyrolysis of organic matter from thermally altered cretaceous black shales. AAPG Bulletin 67(11), 2137–2146.

Philippi, G. T. (1965). On the depth, time and mechanism of petroleum generation. Geochimica et Cosmochimica Acta 29(9), 1021–1049.

Reeckmann, S. A. and A. J. Mebberson (1984). Igneous intrusions in the northwest canning basin and their impact on oil exploration. In P. G. Purcell (Ed.), The Canning Basin, W.A., pp. 389–399. Aust.Australia: Geol. Soc. Aust.. Perth, Australia | Pet. Explor. Soc.

Schiener, E. J. and J. Perregaard (1981). Thermal maturation of organic matter by a thick basaltic sill in Upper Cretaceous shales, Svartenhuk Halvø, central West Greenland. Grønlands geologiske undersøgelse Rapport(102), 1–17.

Schmoker, J. W. (1994). Volumetric calculation of hydrocarbons generated. In B. Magoon Leslie and G. Dow Wallace (Eds.), The petroleum system;

from source to trap., Volume 60 of AAPG Memoir, pp. 323–326. Tulsa, OK, United States: American Association of Petroleum Geologists.

Scrutton, C. T., W. T. Horsfield, and W. B. Harland (1976). Silurian fossils from western Spitsbergen. Geological Magazine 113(6), 519–523.

Shanmugam, G. (1985). Significance of coniferous rain forests and related organic matter in generating commercial quantities of oil, gippsland basin, australia. AAPG Bulletin 69(8), 1241–1254.

SImetric (2005). http://www.simetric.co.uk/si_materials.htm. www-document.

Simoneit, B. R. T., S. Brenner, K. E. Peters, and I. R. Kaplan (1981). Thermal alteration of cretaceous black shale by diabase intrusions in the eastern atlantic; ii, effects on bitumen and kerogen. Geochimica et Cosmochimica Acta 45(9), 1581–1602.

Sinninghe, D. J. S., M. M. M. Kuypers, S. Schouten, S. Schulte, and J. Rullkoetter (2003). The lycopane/ c (sub 31) n-alkane ratio as a proxy to assess palaeoxicity during sediment deposition. Earth and Planetary Science Letters 209(1-2), 215–226.

Sofer, Z. (1980). Preparation of carbon dioxide for stable isotope analysis of petroleum fractions. Analytical Chemistry 52, 1389–1391.

Spear, F. S. and S. M. Peacock (1989). Metamorphic pressure-temperature-time paths. Washington, D. C.: American Geophysical Union.

Steel, R. J., A. Dalland, K. Kalgraff, and V. Larsen (1979). An outline of the history of sedimentation of Svalbard's central Tertiary Basin. Norw. Sea. Symp. Pet. Soc. NSS/24, 29.

Steel, R. J. and D. Worsley (1984). Svalbard's post-caledonian strata; an atlas of sedimentational patterns and palaeogeographic evolution. In M. Spencer Anthony, O. Johnsen Sverre, A. Moerk, E. Nysaether, P. Songstad, and A. Spinnangr (Eds.), Petroleum geology of the North European margin., pp. 109–135. London, United Kingdom: Graham and Trotman.

Talwani, M. and O. Eldholm (1977). Evolution of the Norwegian-Greenland Sea. Geological Society of America Bulletin 88(7), 969–999.

ten Haven, H. L., L. J. W. de, J. Rullkoetter, and D. J. S. Sinninghe (1987). Restricted utility of the pristane/ phytane ratio as a palaeoenvironmental indicator. Nature (London) 330(6149), 641–643.

Throndsen, T. (1977). Sammensetning og termisk omdannelse av organisk materiale i Svalbards tertiær. Cand. Real. thesis, University of Oslo.

Tissot, B., B. Durand, J. Espitalie, and A. Combaz (1974). Influence of Nature and Diagenesis of Organic Matter in Formation of Petroleum. AAPG Bulletin 58(3), 499–506.

Tissot, B. and D. Welte (1984). Petroleum formation and occurrence. Springer Verlag.

Tyrell, G. W. and K. S. Sandford (1933). Geology and petrology of the dolerites of spitsbergen. 53, 284–321.

Walker, B. H. and A. Poldervaart (1949). Karroo dolerites of the Union of South Africa. Geological Society of Amerika Buletin 60, 591–706.

Walker, G. P. L. and D. H. Blake (1988). Three Hawaiian calderas: an origin through loading by shalow intrusions? Journal of Geophysical Research 93, 14,773–14,784.

Wang, X., I. Lerche, and C. Walters (1989). The effect of igneous intrusive bodies on sedimentary thermal maturity. Organic Geochemistry 14(6), 571–584.

Weiss, H. M., A. Wilhelms, N. Mills, J. Scotchmer, P. B. Hall, K. Lind, and T. Brekke (2004). NIGOGA The Norwegian Industry Guide to Organic Geochemical Analyses. Available from World Wide Web:<http://www.npd.no/engelsk/nigoga/default.htm>: Norsk Hydro, Statoil, Geolab Nor, SINTEF Petroleum Research and Norwegian Petroleum Directorate.

Worsley, D. and A. Mørk (1978). The Triassic stratigraphy of southern Spitsbergen. Årbok - Norsk Polarinstitutt 1977, 43–59.

List of Figures

[ ]

List of Tables

APPENDIX

Appendix A

Rock-Eval and TOC measurements

A.1 Rock Eval

Rock-Eval analysis was carried out at Institute for Geology, University of Oslo, Norway.

The purpose of Rock-Eval pyrolysis is to quickly obtain information on hydrocarbon generation potential, presence or absence of non-indigenous hydrocarbons, organic matter type and thermal maturity of a rock, requiring no special preparation other than grinding the rock. The method uses a special pyrolysis device (Figure A.1). The sample (ca. 100 mg) is progressively heated to 550°C under an inert atmosphere, using a special temperature program. During analysis, the hydrocarbons already present in the rock in a free or adsorded state will evaporate at a moderate temperature. The amount of these hydrocarbons is measured by a flame ionization detector (FID) and the corresponding peak on the pyrolysis record is termed/named the S_1 peak. Subsequently pyrolysis of kerogen results in generation of hydrocarbons and hydrocarbon-like compounds, responsible for the S_2 peak. The third peak on the record, the S_3 peak, is carbon dioxide. In addition water is also evaporated from the rock, but this is not recorded. The volatile compounds are spilt into two streams, one passing through a FID detector measuring S_2 and the other passing through a thermal conductivity detector measuring S_3. A good temperature program should always have good separation of the S_1 and the S_2 peaks on the FID detector. The S_3 measurement is however limited to a convinient temperature window in order to include the main stage of CO_2 generation from kerogen, and to avoid other sources of CO_2 (such as decomposition of carbonates, and particularly of siderite, which is the most labile carbonate). The forth parameter determined by the Rock-Eval instrument is T_{max} corresponding to the maximum of hydrocarbon generation during pyrolysis.

A.1.1 Analysis

The analytical equipment being used for the Rock-Eval analysis is a Rock-Eval II Multichrom CH 2.

- S1, S2, S3 = quantified peak areas (mg HC or CO_2/g rock)

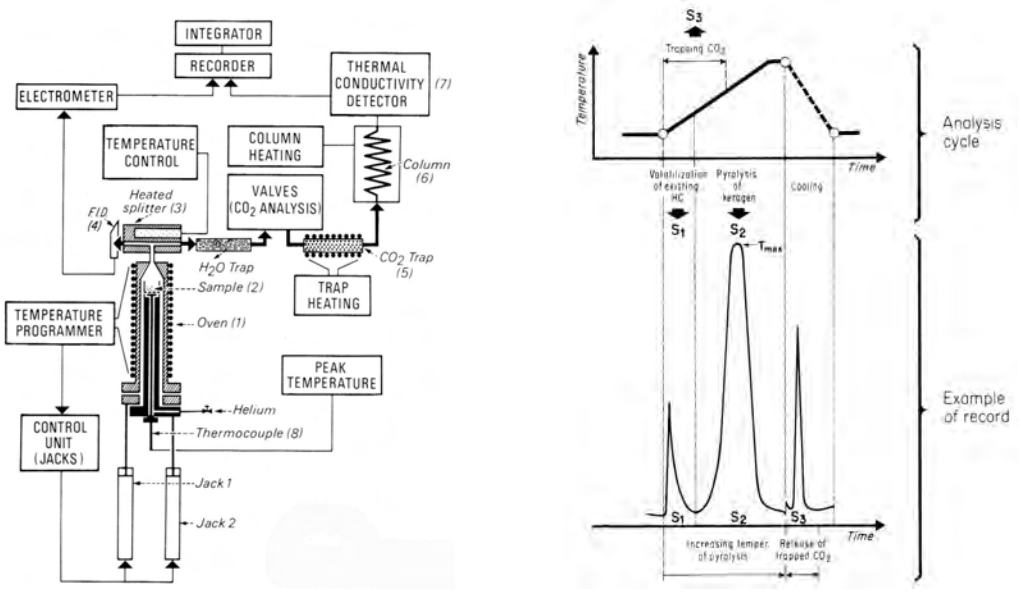

(a) Principle of the Rock-Eval pyrolysis device

(b) One analytical cykle and a example on a print-out from the recorder

Figure A.1: *Figures describing the Rock-Eval hole rock analysis. From Espitalie et al. (1977).*

- PP = petroleum potential (mg HC/g rock) = S1 + S2
- PI = production index (weight ratio) = S1/(S1+S2)
- Tmax (°C) = temperature at maximum of S2 peak at 25°C/min heating rate
- HI = hydrogen index (mg HC/g TOC) = 100*S2/TOC
- OI = oxygen index (mg CO_2/g TOC) = 100*S3/TOC

The samples must first be crushed, either in a centrifugal mill or if the sample is very small, crushed in a mortar.

An aliquot of the crushed sample is then weighted into a crucible and then is analysed on a bulk-flow pyrolysis-FID(/TCD) instrument (in this case a Rock-Eval II).

The sample weight must be adjusted to the expected pyrolysate yield of the sample in such a way that the obtained signal is within the linear part of the response curve of the detector. If overloading occurs, a smaller aliquot of the sample must be reanalysed.

Furthermore, a general rule is that at least one NGS reference sample is analysed as a control sample at the beginning and the end of each batch, and at least once every ten analyses.

For the Svalbard samples standard temperature program (Cycle 1) was used. On Rock-Eval II this cycle is as follows: 300°C (3 min.) - 25°C/min. linear temperature gradient - 600°C (1 min.) (Weiss et al., 2004).

A.2 Carbon measurements

A.2.1 Analysis

Total organic carbon (TOC) TOC was measured by the use of a LECO induction furnace with an IR detector. Prior to combustion the finely grounded rock samples were treated with HC to remove carbonate. Reproducibility was found to be better than 0.05% weight.

The calcite contents evaluated by combustion By taking the difference between total carbon, determined by combustion in the LECO induction furnace of finely grounded but acid untreated samples, and TOC, the amount of inorganic carbon in the sample is obtained. From this the weight % of carbonates can be calculated. Since it is suggested, based on X-ray analyses, that the quantitatively most important carbonate in the sample is calcite, the amount of calcite in the samples was calculated. The weight of $CaCO_3$ to carbon is $100.0892/12.011 = 8.333$. Thus this factor is used to calculate the amount of calcite from the amount of inorganic carbon as determined by the above mentioned procedure.

A.3 Results

On the following pages the results from the Rock-Eval and Carbon measurment analyses on the source-rock samples close to sills on Svalbard can be seen.

Figures A.2 to A.19 was prepared using the PeGIS software (Dahl and Rasmussen, 2003).

Table A.1: Rock-Eval. Botneheia East, Central Spitsbergen; Profile with only a minor sill

Sample	*Tmax*	*S1*	*S2*	*S3*	*HI*	*OI*	*PI*	*TOC %*	*TC%*	*CaCO3*
BH1-1	443	2	10.08	0.56	313.04	17.39	0.17	3.22	5.86	21.99
BH1-2	441	2.92	26.79	1.1	366.98	15.07	0.1	7.3	9.26	16.33
BH1-3	440	1.65	10.08	0.73	248.89	18.02	0.14	4.05	5.42	11.41
BH1-4	440	2.19	25.42	1.23	382.26	18.50	0.08	6.65	7.4	6.25
BH1-5	441	2.9	27.49	1.24	347.53	15.68	0.1	7.91	9.49	13.16
BH1-6	440	2.53	18.27	1.21	272.28	18.03	0.12	6.71	7.59	7.33
BH1-7	439	1.4	5.82	0.54	207.86	19.29	0.19	2.8	8.76	49.65
BH1-8	441	1.58	13.78	0.61	305.54	13.53	0.1	4.51	7.39	23.99
BH1-9	443	1.7	20.56	1.01	291.63	14.33	0.08	7.05	10.2	26.24
BH1-10	442	2.44	22.11	1.08	290.92	14.21	0.1	7.6	9.89	19.08
BH1-11	441	1.73	13.62	1.05	251.76	19.41	0.11	5.41	9.37	32.99
BH1-12	437	1.37	6.92	1.06	176.08	26.97	0.17	3.93	6.6	22.24
BH1-13	444	2.08	4.4	1.1	87.48	21.87	0.32	5.03	6.81	14.83
BH1-14	466	2.48	1.92	0.92	27.39	13.12	0.56	7.01	10.1	25.74
BH1-15	411	2.11	3.05	1.06	44.66	15.52	0.41	6.83	8.55	14.33
BH1-16	441	0.16	0.71	1.29	24.65	44.79	0.11	2.88	3.87	8.25
BH1-17	495	0.06	0.09	0.2	50.00	111.11	0.43	0.18	1.32	9.50
BH1-18	337	0.02	0.09	0.52	3.19	18.44	0.2	2.82	6.58	31.32
BH1-19	339	0.04	0.05	0.88	6.67	117.33	0.5	0.75	1.9	9.58
BH1-20	428	4.93	7.78	1.32	91.53	15.53	0.39	8.5	12.7	34.99
BH1-21	442	1.47	3.86	0.79	126.97	25.99	0.28	3.04	6.36	27.66
BH1-22	442	1.28	10.48	0.77	240.92	17.70	0.11	4.35	9.62	43.90
BH1-23	442	1.04	10.53	0.83	239.32	18.86	0.09	4.4	8.57	34.74
BH1-24	440	1.31	11.24	0.7	302.15	18.82	0.1	3.72	6.8	25.66
BH1-25	445	1.02	12.53	0.6	348.06	16.67	0.08	3.6	7.29	30.74
BH1-26	443	0.96	16.24	0.59	341.89	12.42	0.06	4.75	8.71	32.99
BH1-27	442	0.08	0.53	0.34	40.77	26.15	0.13	1.3	10.7	78.30

Table A.2: Rock-Eval. Botneheia East, Central Spitsbergen; Profile above sill

Sample	*Tmax*	*S1*	*S2*	*S3*	*HI*	*OI*	*PI*	*TOC %*	*TC%*	*CaCO3*
BH2-1	402	0.65	0.58	0.54	156.76	145.95	0.53	0.37	2.41	16.99
BH2-2	412	0.31	0.61	0.62	132.61	134.78	0.34	0.46	1.9	12.00
BH2-3	411	1.69	1.45	0.48	254.39	84.21	0.54	0.57	1.81	10.33
BH2-4	448	0.29	0.5	0.55	21.83	22.92	0.37	2.4	2.44	0.33
BH2-5	440	0.52	1.3	0.43	44.83	14.83	0.29	2.9	3.07	1.42
BH2-6	452	0.2	0.29	0.4	17.47	24.10	0.42	1.66	1.79	1.08
BH2-7	436	1	2	0.52	41.92	11.16	0.33	4.66	4.82	1.33
BH2-8	440	1.19	2.25	0.41	54.61	9.95	0.35	4.12	4.16	0.33
BH2-9	437	0.8	1.9	0.43	54.91	12.43	0.3	3.46	3.32	-1.17
BH2-10	385	0.49	2.65	0.61	56.14	12.92	0.43	4.72	4.66	-0.50
BH2-11	428	0.8	1.59	0.5	29.39	9.24	0.34	5.41	5.44	0.25
BH2-12	414	0.59	0.55	0.5	13.82	12.56	0.52	3.98	3.88	-0.83
BH2-13	510	0.29	0.16	0.91	5.61	31.93	0.66	2.85	3.59	6.16
BH2-14	441	0.37	1.28	0.57	21.96	9.78	0.23	5.83	5.59	-2.00
BH2-15	434	1.8	3.36	0.57	52.09	8.84	0.35	6.45	6.41	-0.33
BH2-16	352	0	0	0.15	n.d.	n.d.	0	n.d.	n.d.	n.d.
BH2-17	509	0.04	0.06	0.22	2.05	7.51	0.4	2.93	3.18	2.08
BH2-18	380	2	2.41	0.43	37.77	6.74	0.45	6.38	6.46	0.67
BH2-19	436	0.5	1.37	0.8	30.99	18.10	0.27	4.42	4.49	0.58
BH2-20	442	1.44	5.26	2.32	79.58	35.10	0.21	6.61	9.24	21.91
BH2-21	445	0.94	5.89	1.08	128.04	23.48	0.14	4.6	7.33	22.74
BH2-22	446	2.1	17.81	1.29	210.77	15.27	0.11	8.45	10.8	19.58
BH2-23	446	1.81	15.13	0.81	239.02	12.80	0.11	6.33	9.68	27.91
BH2-24	442	1.5	16.54	1.02	226.58	13.97	0.08	7.3	8.92	13.49
BH2-25	442	0.44	2.23	0.57	111.50	28.50	0.17	2	9.98	66.47
BH2-26	439	0.95	8.35	0.79	180.74	17.10	0.1	4.62	8.59	33.07
BH2-27	438	0.74	1.19	0.59	88.81	44.03	0.39	1.34	9.17	65.22
BH2-28	443	0.84	4.8	0.63	157.38	20.66	0.15	3.05	7.52	37.24
BH2-29	441	0.67	8.73	0.78	235.31	21.02	0.07	3.71	8.8	42.40
BH2-30	441	1.54	18.04	0.93	273.75	14.11	0.08	6.59	8.71	17.66

Table A.3: Rock-Eval. Krefftberget, Barentsøya: Profile above sill

Sample	*Tmax*	*S1*	*S2*	*S3*	*HI*	*OI*	*PI*	*TOC %*	*TC%*	*CaCO3*
KRB-1a	441	0.01	0	0.36	0.00	120.00	0.01	0.3	9.22	74.30
KRB-1b	308	0	0	0.26	0.00	16.88	0	1.54	9.35	65.06
KRB-1b (dupl)	n.d.	n.d.	n.d.	n.d.	n.d.	n.d.	n.d.	n.d.	n.d.	n.d.
KRB-1c	412	1.00	1.66	0.57	97.65	33.53	0.38	1.7	4.33	21.91
KRB-2	419	0	0	0.32	0.00	27.35	0	1.17	7.47	52.48
KRB-3a	480	0.15	0.23	0.4	6.78	11.80	0.39	3.39	3.44	0.42
KRB-3b	366	0.05	0.05	0.37	2.24	16.59	0.5	2.23	2.42	1.58
KRB-4	326	0.06	0.02	0.26	1.87	24.30	0.75	1.07	1.14	0.58
KRB-5	306	0.03	0	0.35	0.00	56.45	1	0.62	2.55	16.08
KRB-6	494	0.23	0.41	0.35	9.40	8.03	0.36	4.36	4.45	0.75
KRB-7	492	0.22	0.53	0.43	13.91	11.29	0.3	3.81	3.65	-1.33
KRB-8	479	0.5	1.36	0.25	26.72	4.91	0.27	5.09	5.18	0.75
KRB-8 (dupl)	n.d.	n.d.	n.d.	n.d.	n.d.	n.d.	n.d.	n.d.	n.d.	n.d.
KRB-9	464	0.76	2.09	0.24	29.60	3.40	0.27	7.06	7.23	1.42
KRB-10	423	1	1.49	0.3	24.47	4.93	0.4	6.09	6.64	4.58
KRB-11	393	1.04	1	0.5	13.81	6.91	0.51	7.24	7.5	2.17
KRB-12	410	0.43	0.42	0.32	8.57	6.53	0.51	4.9	5.28	3.17
KRB-13	355	0.29	0.23	0.58	3.83	9.65	0.56	6.01	7.09	9.00
KRB-14	341	0.38	0.13	0.47	2.56	9.27	0.76	5.07	5.43	3.00
KRB-15	419	0.31	0.1	0.77	1.62	12.48	0.77	6.17	6.44	2.25
KRB-16	375	0.27	0.1	0.75	1.80	13.51	0.75	5.55	6.63	9.00
KRB-17	296	0.5	0.13	0.87	2.35	15.70	0.81	5.54	7.48	16.16
KRB-17 (dupl)	n.d.	n.d.	n.d.	n.d.	n.d.	n.d.	n.d.	n.d.	n.d.	n.d.
KRB-18a	382	0.17	0.1	0.88	2.40	21.15	0.65	4.16	5.61	12.08
KRB-18b	436	0.33	0.14	0.62	3.20	14.19	0.72	4.37	5.89	12.66
KRB-19	449	0.18	0.12	0.67	3.18	17.77	0.6	3.77	4.75	8.16
KRB-20	537	0.32	0.51	0.88	9.60	16.57	0.39	5.31	6.57	10.50
KRB-20 (dupl)	n.d.	n.d.	n.d.	n.d.	n.d.	n.d.	n.d.	n.d.	n.d.	n.d.
KRB-21	533	0.31	0.46	0.54	13.90	16.31	0.41	3.31	6.05	22.82
KRB-22	400	0.64	1.04	0.28	41.27	11.11	0.38	2.52	6.9	36.49
KRB-23	426	0.61	0.77	0.39	47.83	24.22	0.44	1.61	8.57	57.98
KRB-24	393	1.33	1.87	0.36	92.12	17.73	0.42	2.03	6.03	33.32
KRB-24 (dupl)	n.d.	n.d.	n.d.	n.d.	n.d.	n.d.	n.d.	n.d.	n.d.	n.d.
KRB-25	351	0	0	0.13	n.d.	n.d.	0	n.d.	3.66	n.d.
KRB-26	439	0.44	0.82	0.3	93.18	34.09	0.35	0.88	9.09	68.39

Table A.4: Rock-Eval. Teistberget, Eastern Spitsbergen; Profile above sill

Sample	*Tmax*	*S1*	*S2*	*S3*	*HI*	*OI*	*PI*	*TOC %*	*TC%*	*CaCO3*
TBU-1	436	0.55	1.54	0.76	30.99	15.29	0.26	4.97	4.97	0.00
TBU-2	437	0.76	1.68	1.12	22.70	15.14	0.31	7.4	7.77	3.08
TBU-3	434	0.7	1.52	0.76	23.38	11.69	0.32	6.5	6.57	0.58
TBU-4	413	0.62	0.92	0.8	13.79	11.99	0.4	6.67	7.6	7.75
TBU-4 (dupl)	n.d.	n.d.	n.d.	n.d.	n.d.	n.d.	n.d.	n.d.	n.d.	n.d.
TBU-5	387	0.55	0.7	0.81	10.09	11.67	0.44	6.94	7.43	4.08
TBU-6	386	1.77	1.87	0.41	45.61	10.00	0.49	4.1	6.29	18.24
TBU-7	441	1.53	3.57	0.67	97.28	18.26	0.3	3.67	8.39	39.32
TBU-8	443	0.71	3.67	0.38	132.01	13.67	0.16	2.78	7.7	40.98
TBU-9	427	1.07	2.09	0.71	200.96	68.27	0.64	1.04	7.62	54.81
TBU-10	437	1.25	19.39	0.74	370.04	14.12	0.06	5.24	8.21	24.74
TBU-11	437	0.73	6.56	0.38	341.67	19.79	0.1	1.92	9.69	64.72

Table A.5: Rock-Eval. Teistberget, Eastern Spitsbergen; Profile below sill

Sample	*Tmax*	*S1*	*S2*	*S3*	*HI*	*OI*	*PI*	*TOC %*	*TC%*	*CaCO3*
TBL-1	389	0.13	0.12	0.48	50.00	200.00	0.54	0.24	0.7	3.83
TBL-1 (dupl)	n.d.	n.d.	n.d.	n.d.	n.d.	n.d.	n.d.	n.d.	n.d.	n.d.
TBL-2	233	0.01	0	0.64	0.00	376.00	0.01	0.17	0.4	1.92
TBL-3	475	0.16	0.6	0.5	32.61	27.17	0.21	1.84	1.92	0.67
TBL-4	425	1.06	3.19	0.34	83.29	8.88	0.25	3.83	4.07	2.00
TBL-5	426	2.37	4.27	0.56	81.96	10.75	0.36	5.21	5.19	-0.17
TBL-6	394	1.41	2.52	0.44	56.63	10.75	0.36	4.45	4.4	-0.42
TBL-7	379	1.67	2.25	0.63	26.19	7.33	0.43	8.59	8.64	0.42
TBL-8	346	0.53	0.36	0.56	29.75	46.28	0.6	1.21	4.98	31.40
TBL-9	294	0.67	0.09	1.24	1.371	18.93	0.88	6.55	6.51	-0.33
TBL-10	344	0.09	0.03	0.5	3.61	60.24	0.75	0.83	2.45	13.49
TBL-11	444	0.01	1.82	1.07	69.47	40.84	0.36	2.62	3.61	8.25

Table A.6: Rock-Eval. Domen, Eastern Spitsbergen; Profile above sill

Sample	*Tmax*	*S1*	*S2*	*S3*	*HI*	*OI*	*PI*	*TOC %*	*TC%*	*CaCO3*
DOM-1	438	0.02	0	0.31	n.d.	n.d.	1	n.d.	0.78	n.d.
DOM-2	342	0.05	0.02	0.13	n.d.	n.d.	0.83	n.d.	1.05	n.d.
DOM-3	267	0.14	0.09	0.13	5.03	7.26	0.64	1.79	1.82	0.25
DOM-3 (dupl)	n.d.	n.d.	n.d.	n.d.	n.d.	n.d.	n.d.	n.d.	n.d.	n.d.
DOM-4	390	0.37	0.34	0.17	14.59	7.30	0.53	2.33	2.42	0.75
DOM-5	392	0.29	0.3	0.17	7.32	4.14	0.5	4.1	4.12	0.17
DOM-6	306	0.43	0.31	0.27	5.13	4.46	0.58	6.05	6.07	0.17
DOM-7	319	0.19	0.14	0.2	3.12	4.45	0.59	4.49	4.44	-0.42
DOM-8	429	0.21	0.2	0.23	3.98	4.58	0.52	5.02	5.09	0.58
DOM-9a	447	0.8	4.77	0.22	115.78	5.34	0.14	4.12	4.34	1.83
DOM-9b	443	0.54	3.9	0.36	73.86	6.82	0.12	5.28	5.24	-0.33
DOM-10	449	0.31	0.94	0.32	65.73	22.38	0.25	1.43	4.82	28.24
DOM-11	444	0.7	4.03	0.28	136.61	9.49	0.15	2.95	2.89	-0.50

Table A.7: Rock-Eval. Høgrinden South, Barentsøya;

Sample	*Tmax*	*S1*	*S2*	*S3*	*HI*	*OI*	*PI*	*TOC %*	*TC%*	*CaCO3*
HØB1-1	441	0	0	0	0.00	0.00	0	1.55	10.7	76.22
HØB1-2	309	0	0	0.08	0.00	14.29	0	0.56	7.77	60.06
HØB1-3	219	0	0	0.05	0.00	2.75	0	1.82	10.3	70.64
HØB1-4	267	0	0	0	0.00	0.00	0	1.97	9.89	65.97
HØB1-5	220	0.01	0	0	0.00	0.00	0.01	1.25	10.2	74.55
HØB1-6	423	0.24	0.24	0	11.06	0.00	0.5	2.17	10.9	72.72
HØB1-7	384	0.22	0.16	0	28.07	0.00	0.58	0.57	11	86.88
HØB1-8	417	0.3	0.26	0	34.21	0.00	0.54	0.76	11.3	87.80
HØB1-9	435	0.34	0.41	0	61.19	0.00	0.46	0.67	11.1	86.88
HØB1-10	441	0.23	0.86	0	91.49	0.00	0.21	0.94	11.1	84.63
HØB1-11	434	0.38	2.44	0.3	137.08	16.85	0.13	1.78	11.2	78.47
HØB1-12	433	0.5	3.61	0.43	164.09	19.55	0.12	2.2	11	73.30
HØB1-13	436	0.34	2.97	0.3	153.09	15.46	0.1	1.94	11.1	76.30

Table A.8: Rock-Eval. Høgrinden South, Barentsøya;

Sample	*Tmax*	*S1*	*S2*	*S3*	*HI*	*OI*	*PI*	*TOC %*	*TC%*	*CaCO3*
HØB2-1	441	0	0	0.27	0.00	87.10	0	0.31	8.6	69.06
HØB2-2	359	0	0	0.18	n.d.	n.d.	0	n.d.	5.27	n.d.
HØB2-3	267	0	0	0.14	n.d.	n.d.	0	n.d.	3.84	n.d.
HØB2-4	419	0.53	1.05	0.4	61.40	23.39	0.34	1.71	9.04	61.06
HØB2-5	414	0.6	0.97	0.44	51.05	23.16	0.38	1.9	8.33	53.56
HØB2-6	435	0.6	1.37	0.45	102.24	33.58	0.31	1.34	9.91	71.39
HØB2-7	440	0.48	3.27	0.32	198.18	19.39	0.13	1.65	10.4	72.89
HØB2-8	431	0.81	5.98	0.51	332.22	28.33	0.12	1.8	10.2	69.97

Table A.9: Rock-Eval. Høgrinden South, Barentsøya; sampled laterally along a single horizon

Sample	*Tmax*	*S1*	*S2*	*S3*	*HI*	*OI*	*PI*	*TOC %*	*TC%*	*CaCO3*
HØB3-1	442	0	0	0.06	n.d.	n.d.	0	n.d.	1.42	n.d.
HØB3-2 (dupl)	n.d.	n.d.	n.d.	n.d.	n.d.	n.d.	n.d.	n.d.	n.d.	n.d.
HØB3-2	415	0.48	0.75	0.45	52.45	31.47	0.39	1.43	2.95	12.66
HØB3-3	421	2.62	5.3	0.55	94.64	9.82	0.33	5.6	6.66	8.83
HØB3-4	424	0.63	1.19	0.31	56.13	14.62	0.35	2.12	10.3	68.14
HØB3-5	419	1.21	1.23	0.29	53.02	12.50	0.5	2.32	9.41	59.06
HØB3-6	439	1.26	3.63	0.32	165.75	14.61	0.26	2.19	8.6	53.40
HØB3-7	441	1.07	6.79	0.18	266.27	7.06	0.14	2.55	9.33	56.48
HØB3-8	435	1.46	11.72	0.33	421.58	11.87	0.11	2.78	10	60.14
HØB3-9	435	1.59	14.93	0.3	501.01	10.07	0.1	2.98	9.65	55.56

Table A.10: Rock-Eval. Northern Kreftberget, Barentsøya; Profile without sill

Sample	*Tmax*	*S1*	*S2*	*S3*	*HI*	*OI*	*PI*	*TOC %*	*TC%*	*CaCO3*
NKB-1	437	0.36	2.5	0.37	316.46	46.84	0.13	0.79	6.87	50.65
NKB-2	436	2.6	31.71	0.91	480.45	13.79	0.08	6.6	8.41	15.08
NKB-3	434	4.39	49	0.97	382.81	7.58	0.08	12.8	13.6	6.66
NKB-4	436	3.5	39.73	0.88	463.59	10.26	0.08	8.57	10.6	16.91
NKB-5	435	3.41	40.17	0.92	440.94	10.10	0.08	9.11	10.2	9.08
NKB-6	434	0.75	16.73	0.75	486.33	21.80	0.04	3.44	9.57	51.06

Figure A.2: *Geochemical Log. Botneheia East, Central Spitsbergen; Profile with only a minor sill*

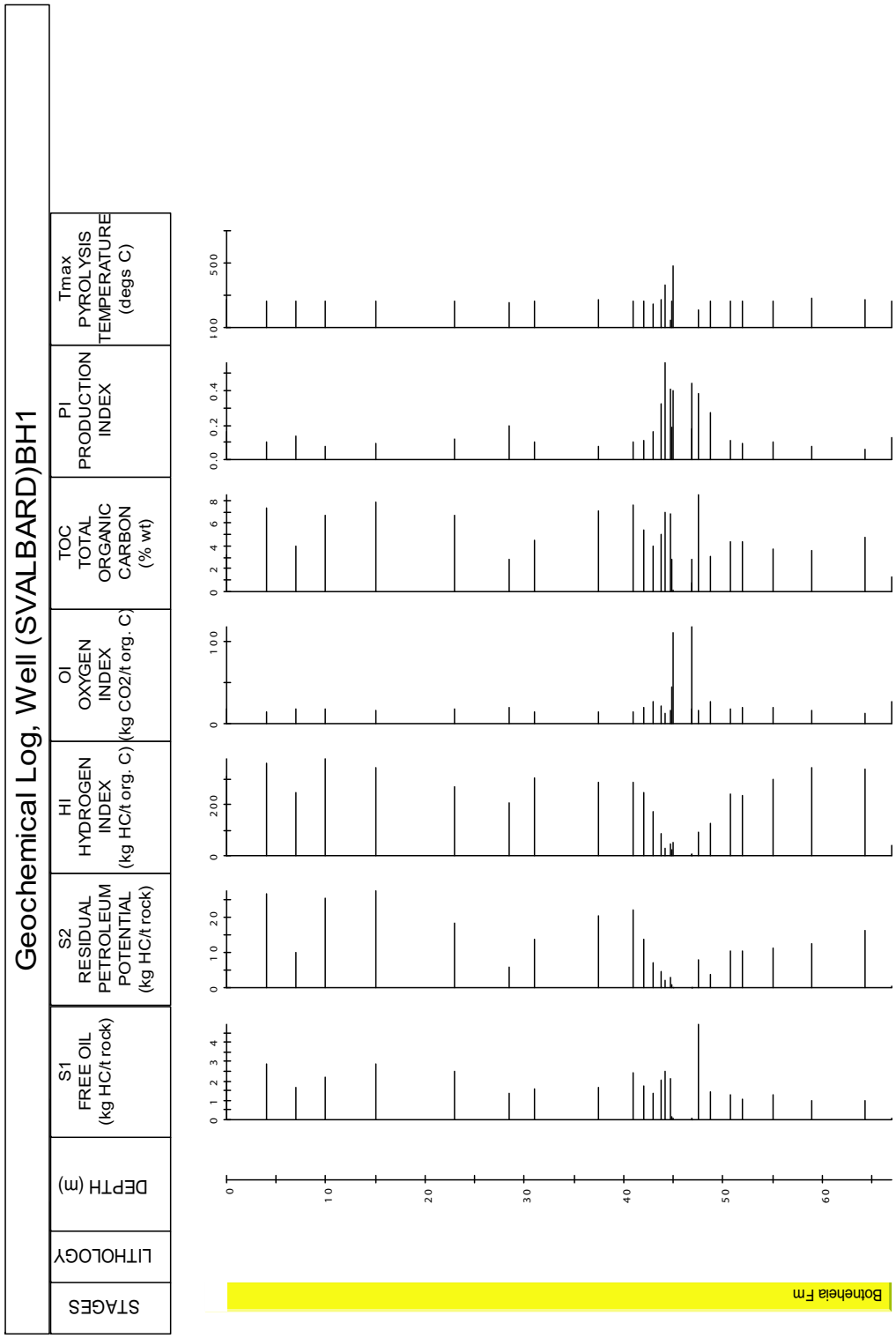

Figure A.3: *Geochemical Log. Botneheia East, Central Spitsbergen; Profile above sill*

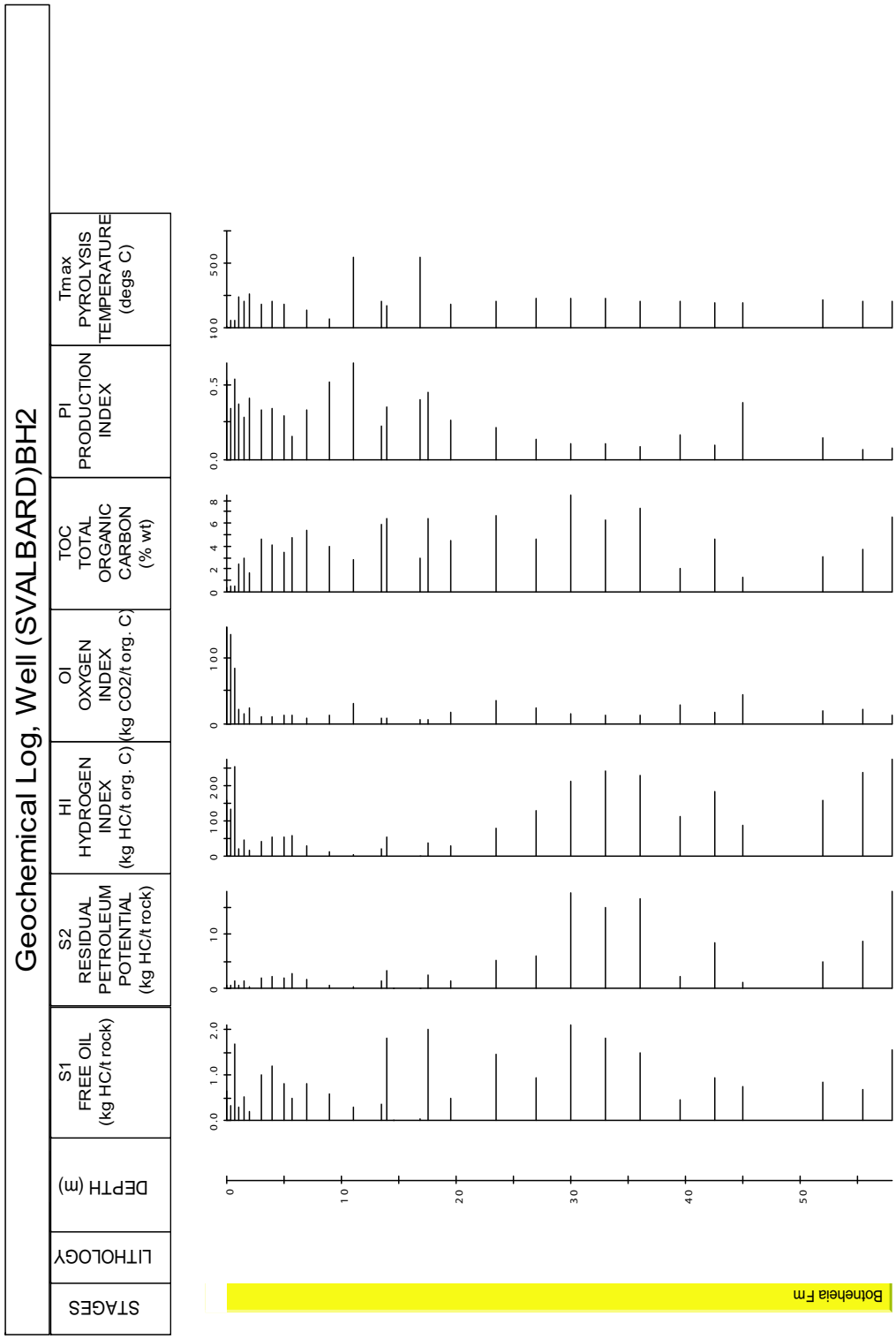

Figure A.4: *Geochemical Log. Krefftberget, Barentsøya: Profile above sill*

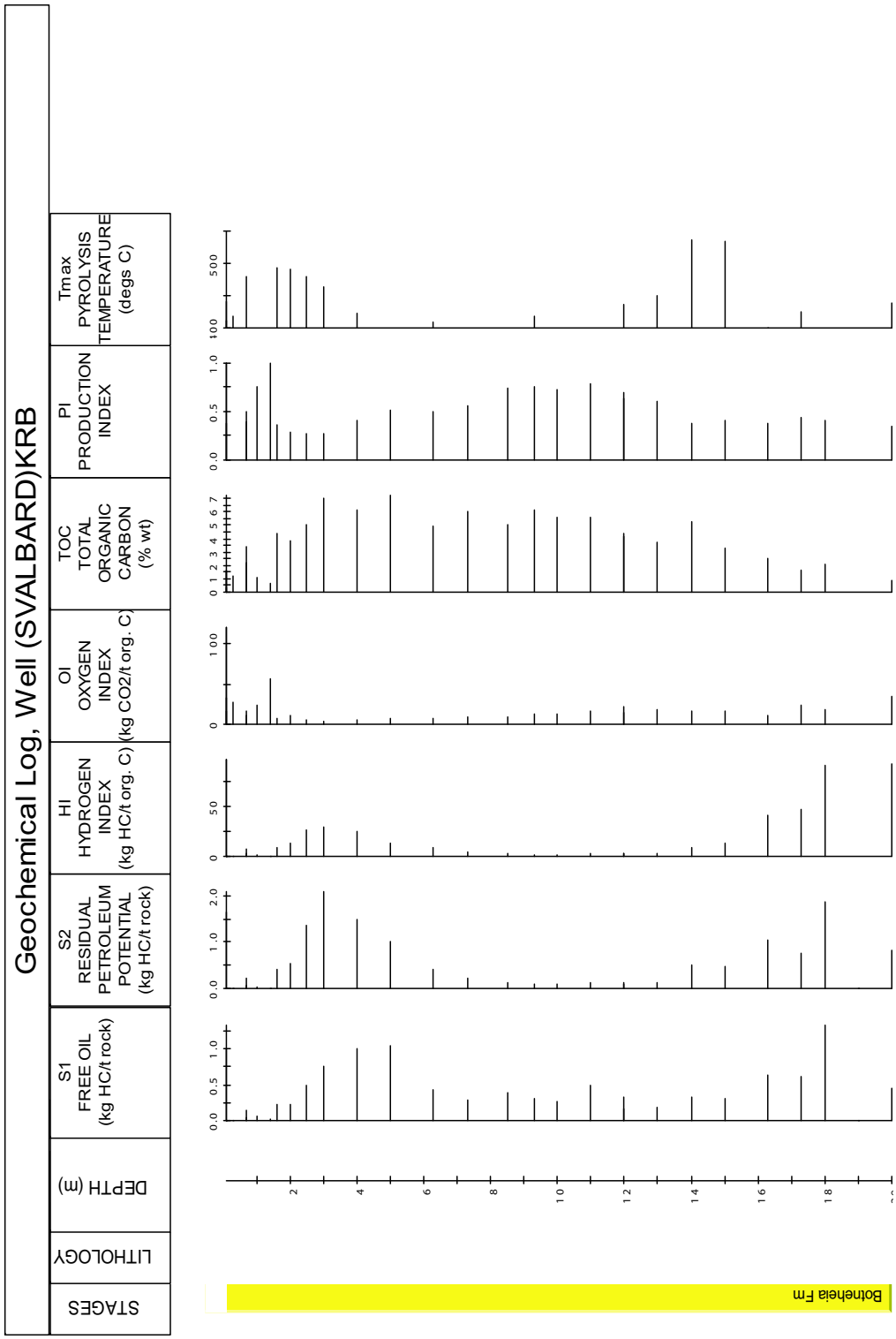

Figure A.5: *Geochemical Log. Høgrinden South, Barentsøya; sampled laterally along a single horizon*

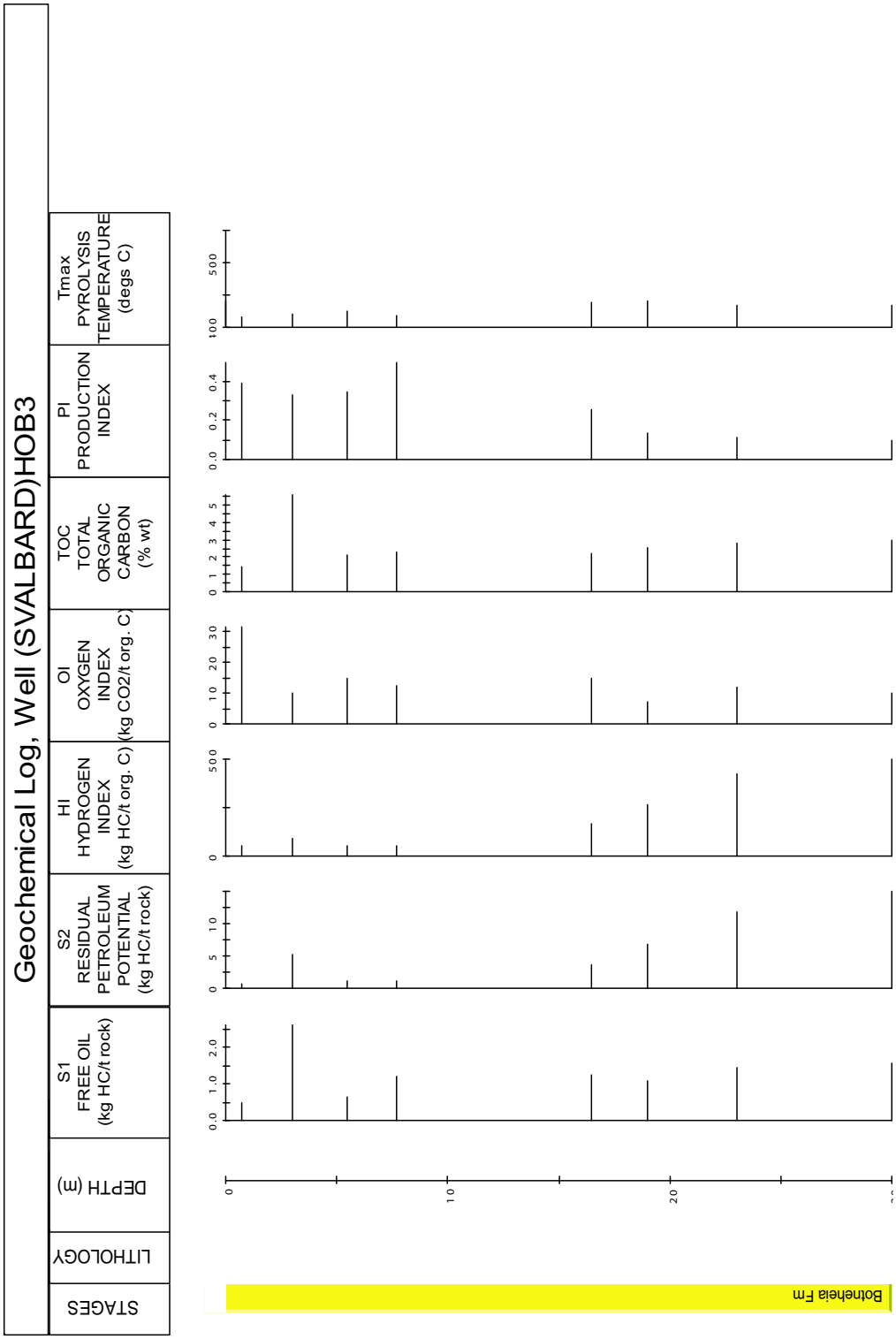

Figure A.6: *Geochemical Log. Teistberget, Eastern Spitsbergen; Profile above sill*

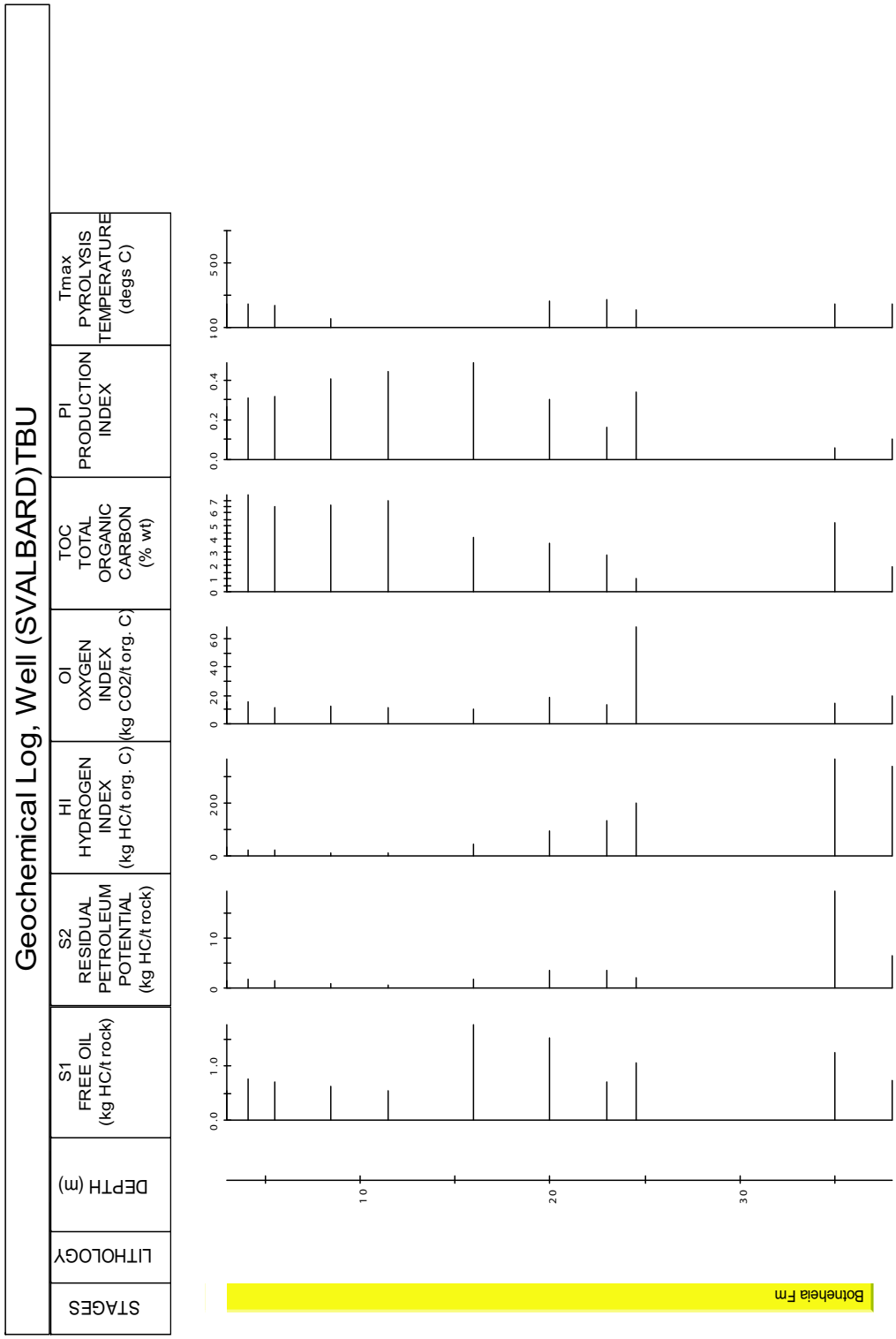

Figure A.7: *Geochemical Log. Teistberget, Eastern Spitsbergen; Profile below sill*

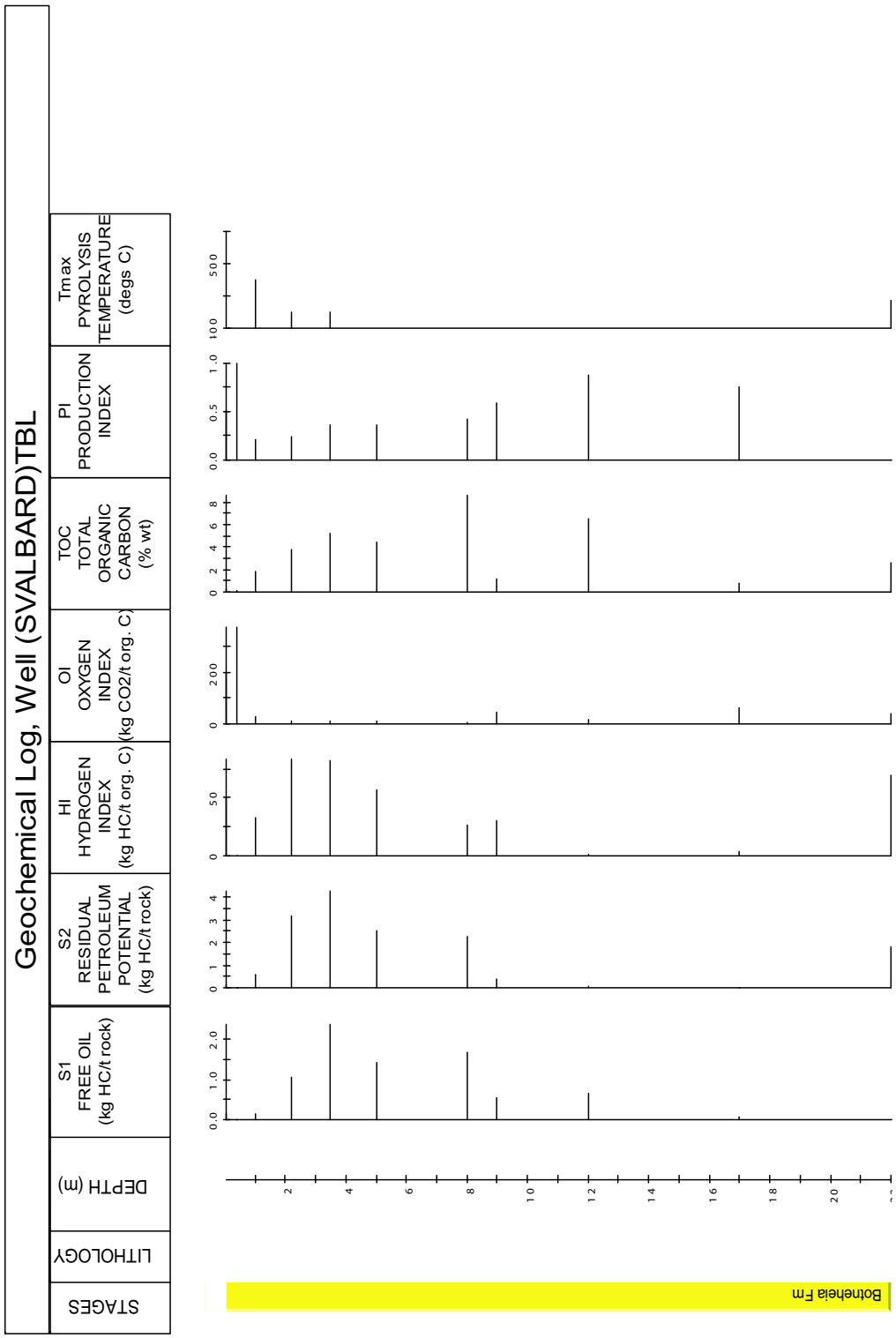

Figure A.8: *Geochemical Log. Domen, Eastern Spitsbergen; Profile above sill*

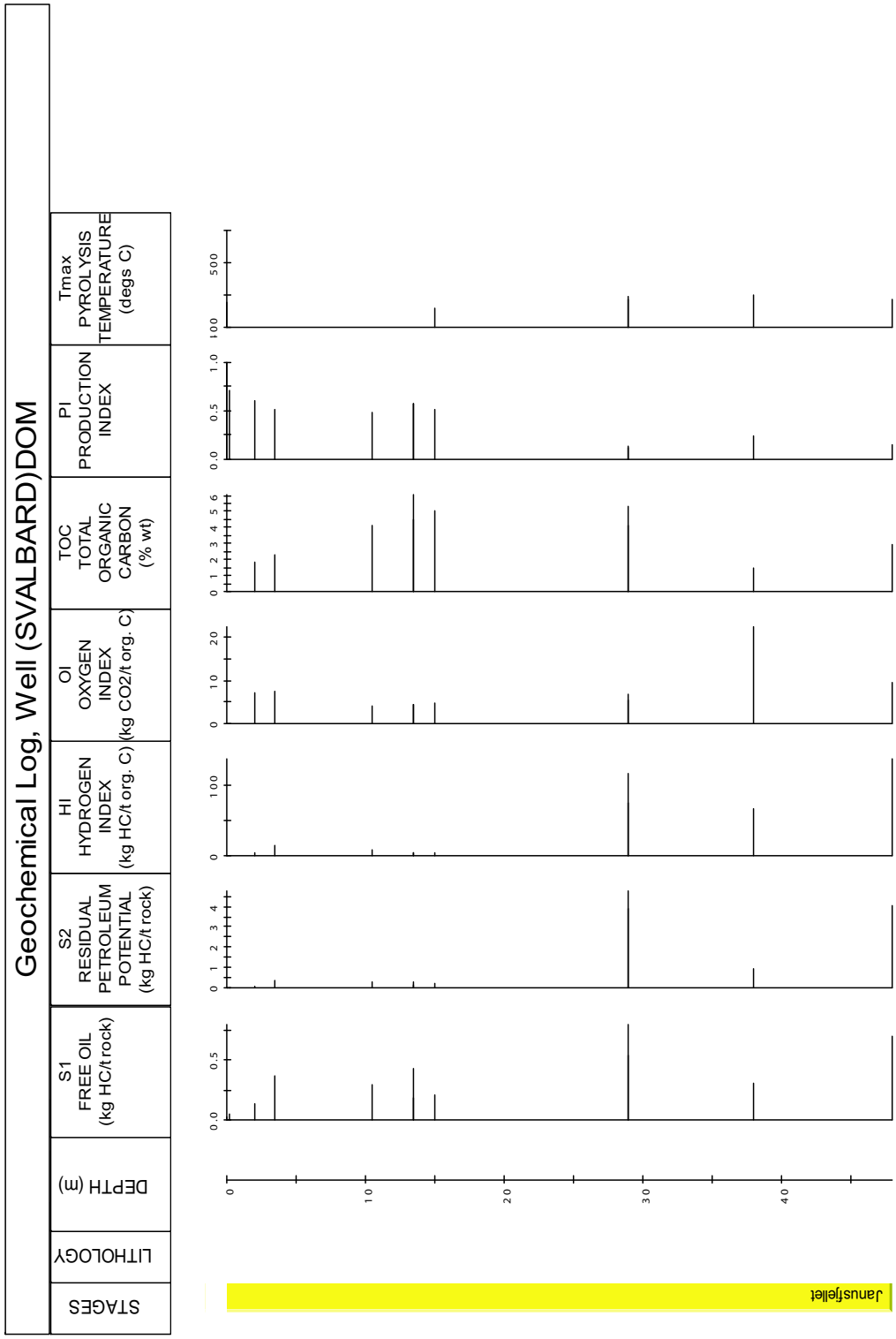

Figure A.9: *Geochemical Log. Northern Kreftberget, Barentsøya; Profile without sill*

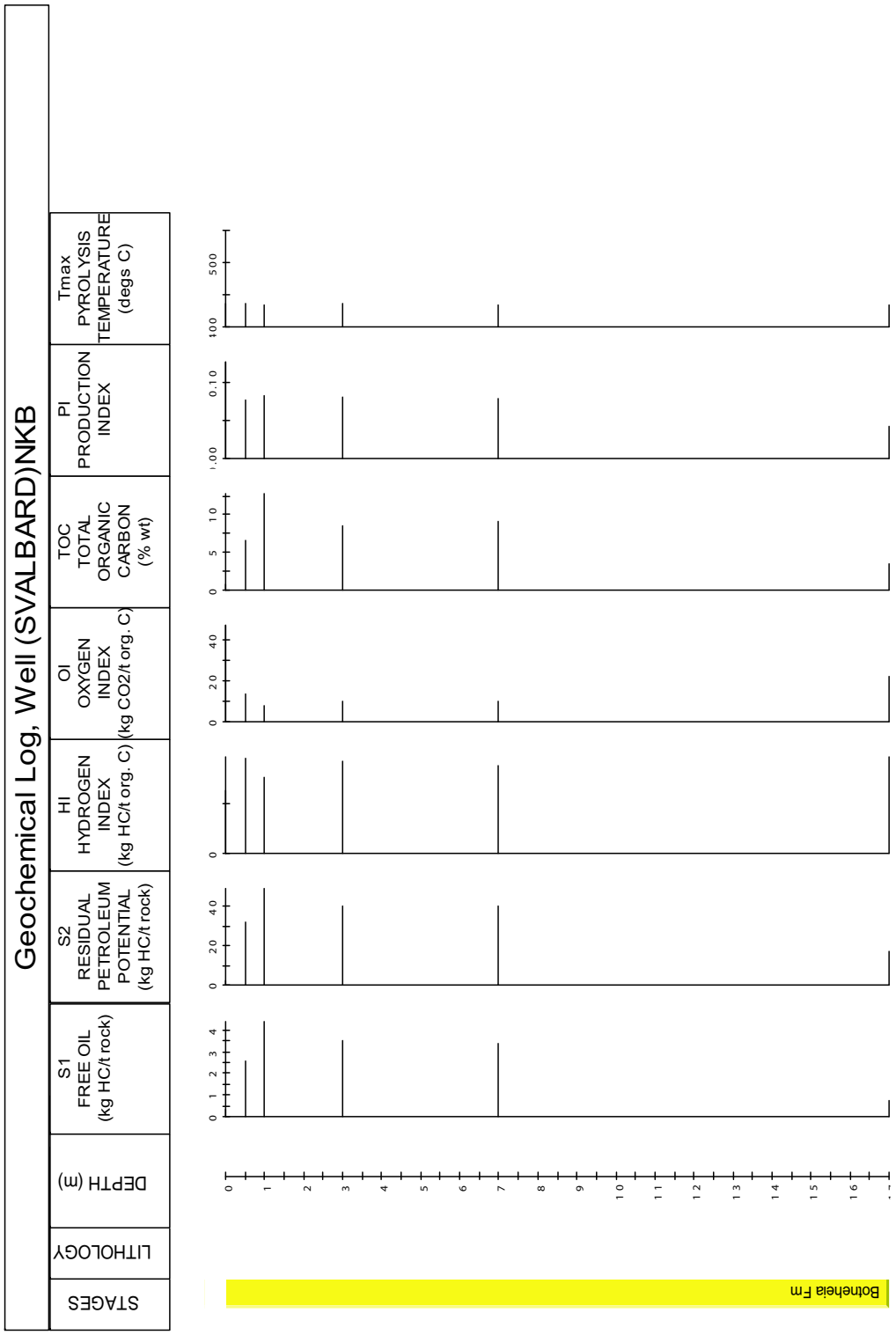

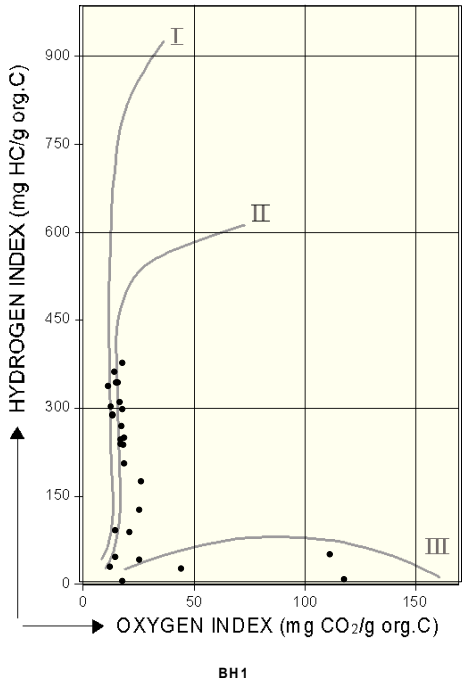

(a) Hydrogen Index against Oxygen Index

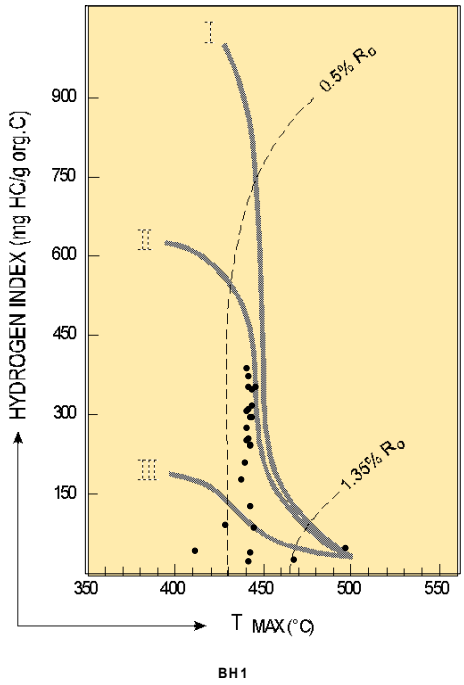

(b) Hydrogen Index against Tmax

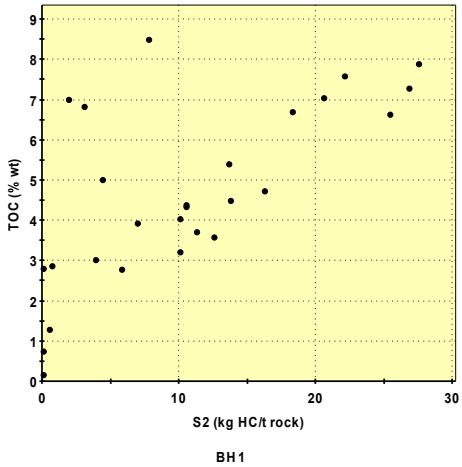

(c) TOC against S2

Figure A.10: *Maturity plots made from the Rock-Eval data Botneheia East, Central Spitsbergen. Profile with only a minor sill.*

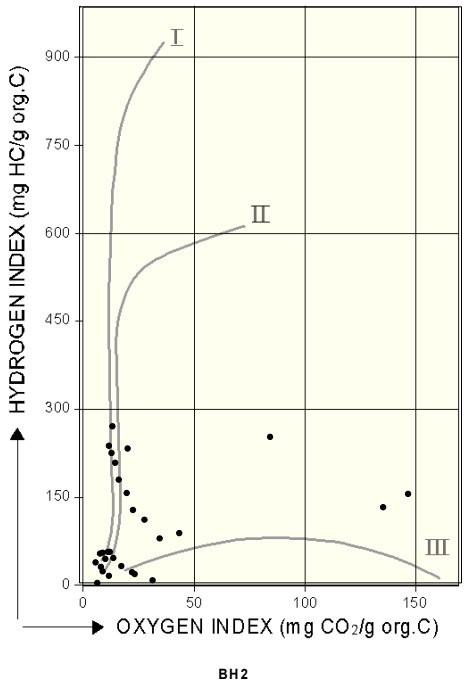

(a) Hydrogen Index against Oxygen Index

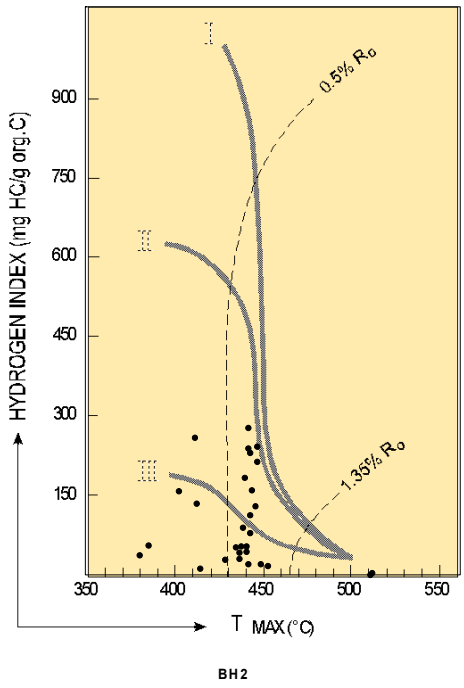

(b) Hydrogen Index against Tmax

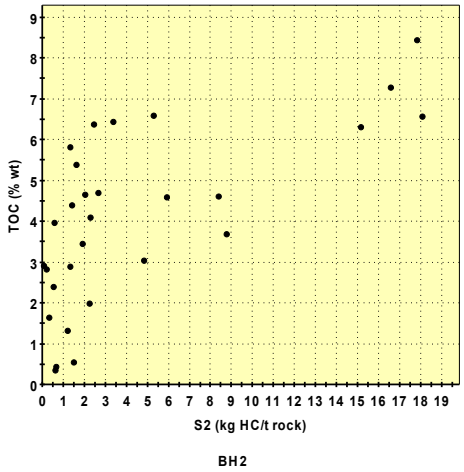

(c) TOC against S2

Figure A.11: *Maturity plots made from the Rock-Eval data Botneheia East, Central Spitsbergen. Profile above sill.*

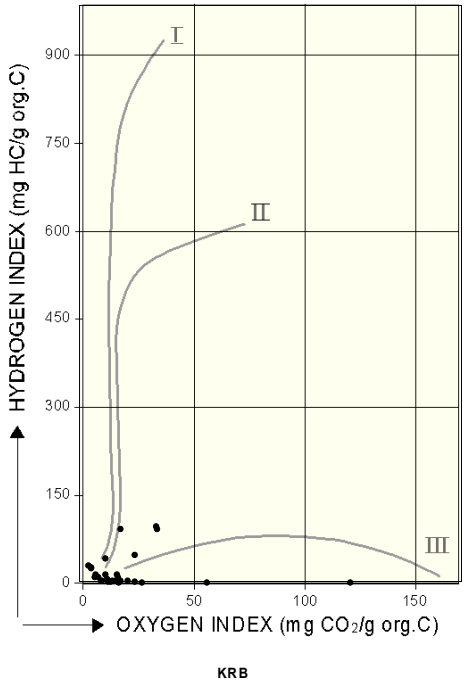

(a) Hydrogen Index against Oxygen Index

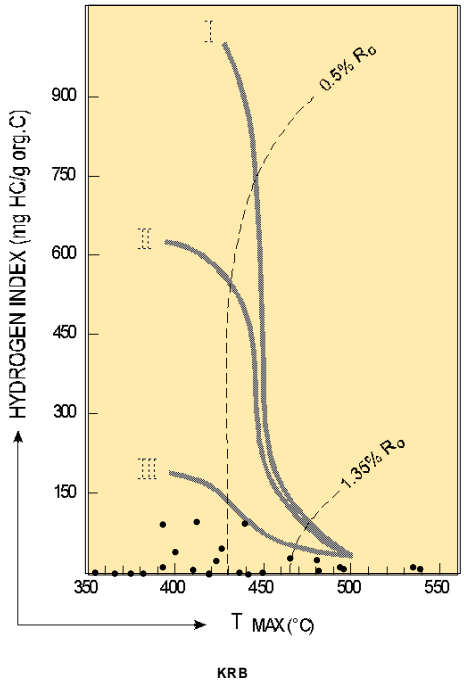

(b) Hydrogen Index against Tmax

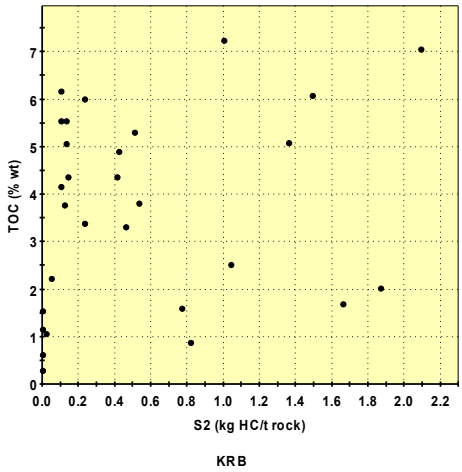

(c) TOC against S2

Figure A.12: *Maturity plots made from the Rock-Eval data Krefftberget, Barentsøya: Profile above sill.*

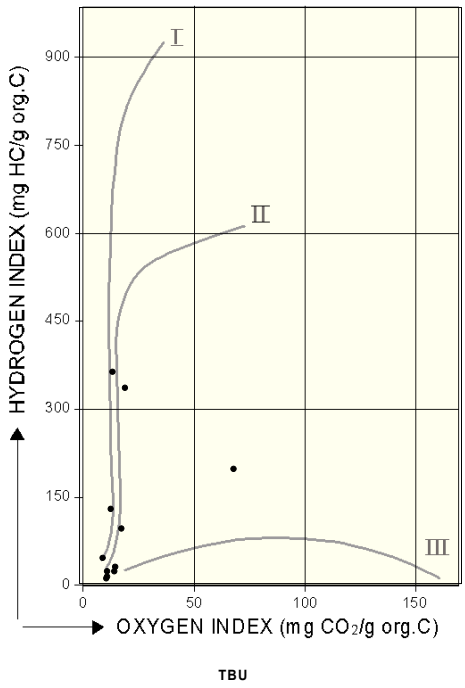

(a) Hydrogen Index against Oxygen Index

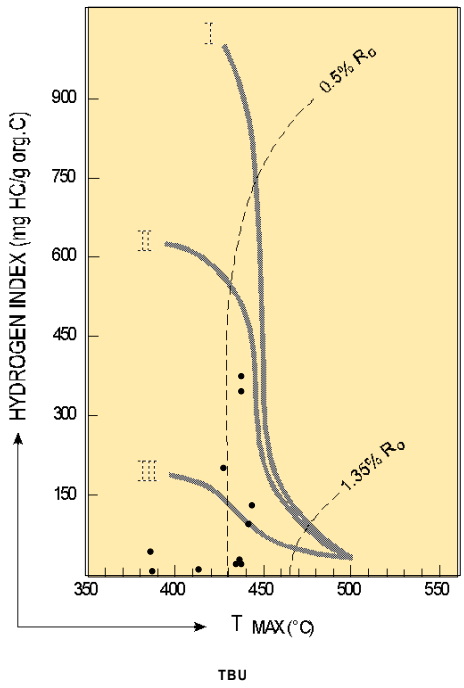

(b) Hydrogen Index against Tmax

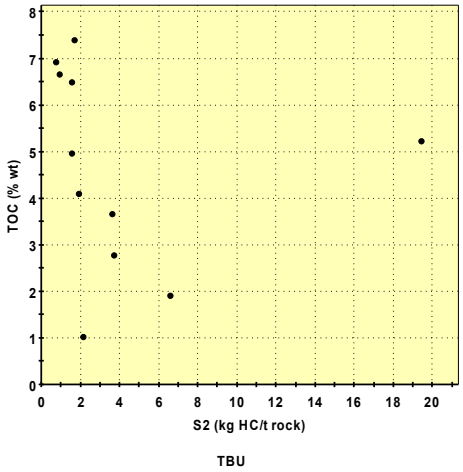

(c) TOC against S2

Figure A.13: *Maturity plots made from the Rock-Eval data Teistberget, Eastern Spitsbergen; Profile above sill.*

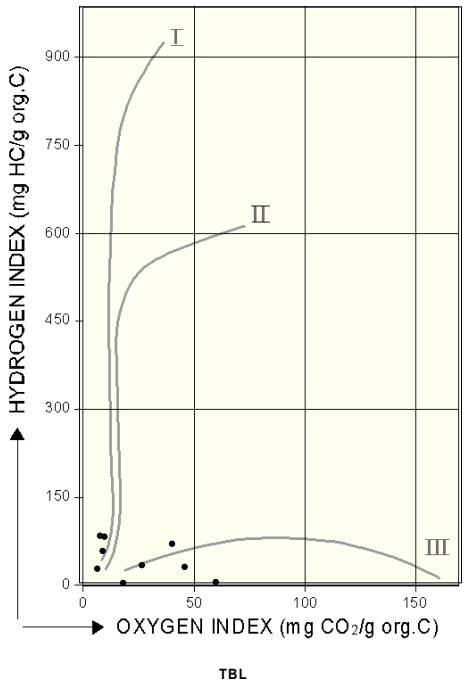

(a) Hydrogen Index against Oxygen Index

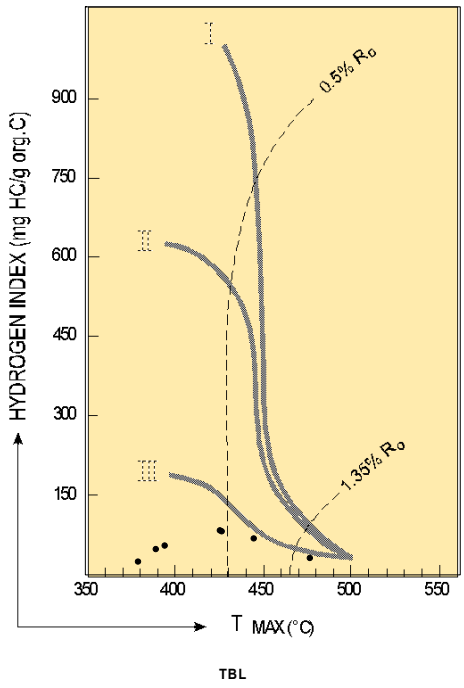

(b) Hydrogen Index against Tmax

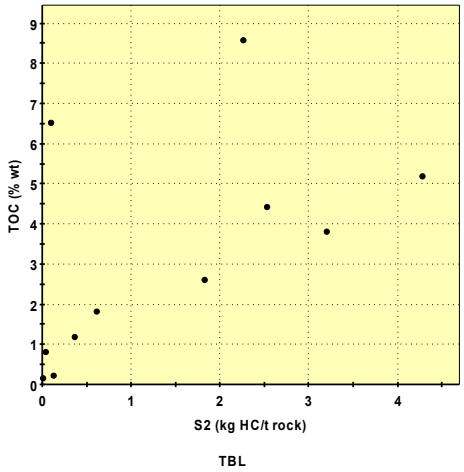

(c) TOC against S2

Figure A.14: *Maturity plots made from the Rock-Eval data Teistberget, Eastern Spitsbergen; Profile below sill.*

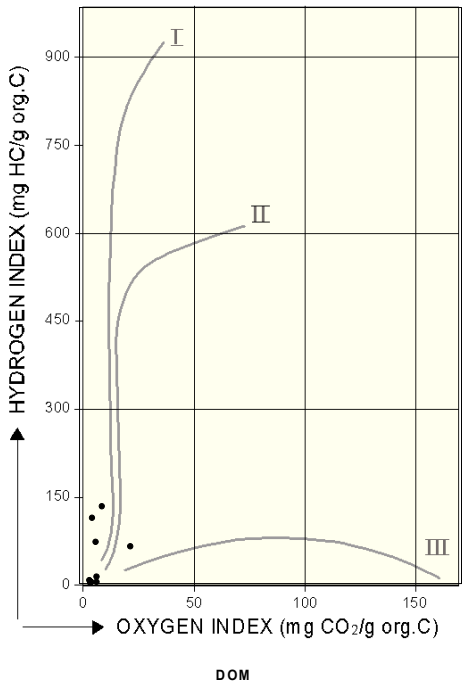

(a) Hydrogen Index against Oxygen Index

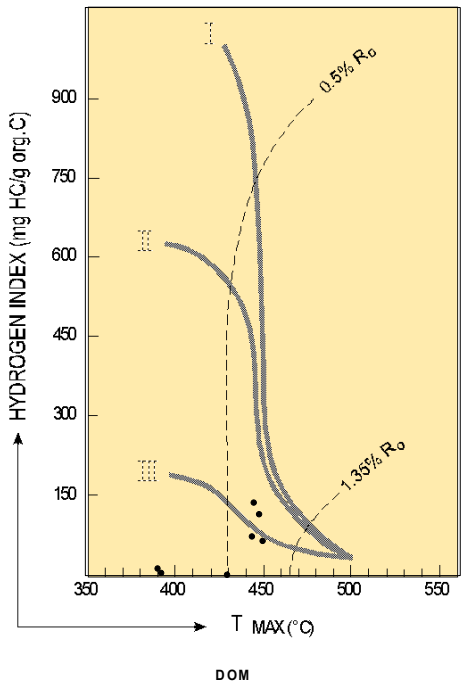

(b) Hydrogen Index against Tmax

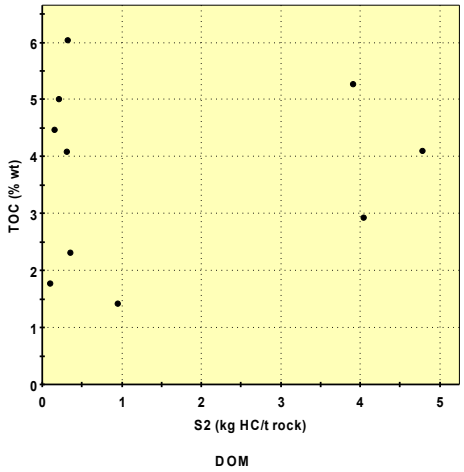

(c) TOC against S2

Figure A.15: *Maturity plots made from the Rock-Eval data Domen, Eastern Spitsbergen; Profile above sill.*

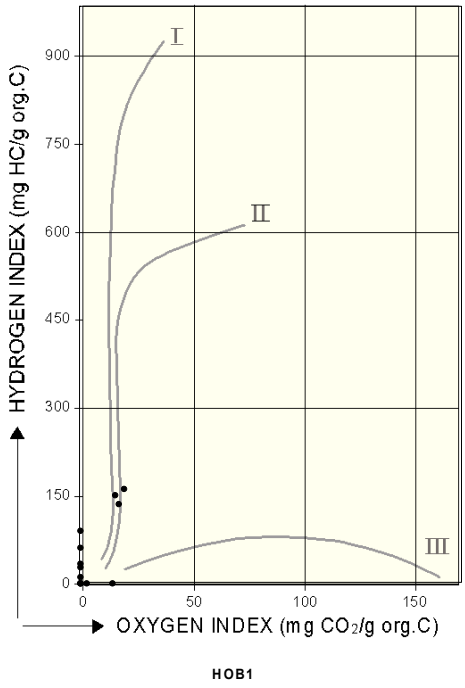

(a) Hydrogen Index against Oxygen Index

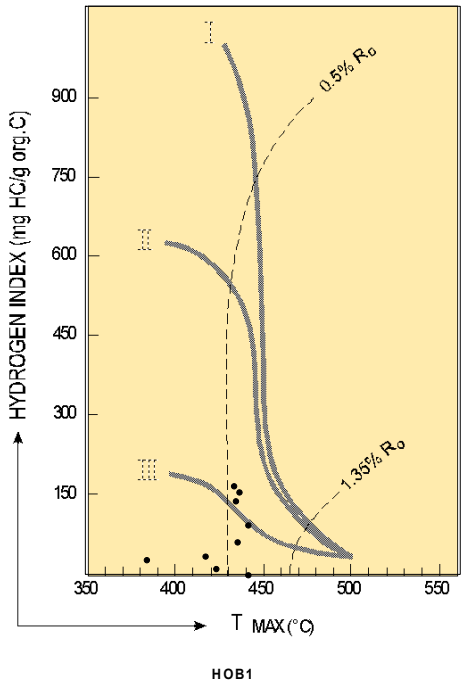

(b) Hydrogen Index against Tmax

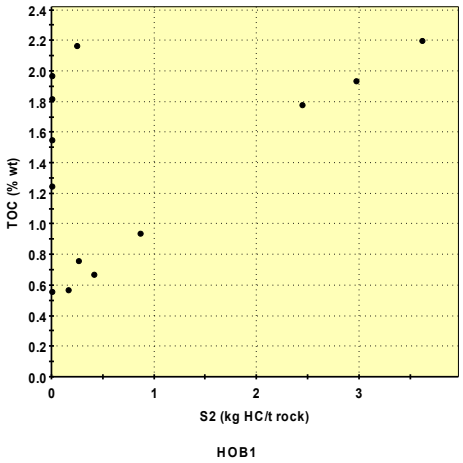

(c) TOC against S2

Figure A.16: *Maturity plots made from the Rock-Eval data Høgrinden South, Barentsøya. Series 1.*

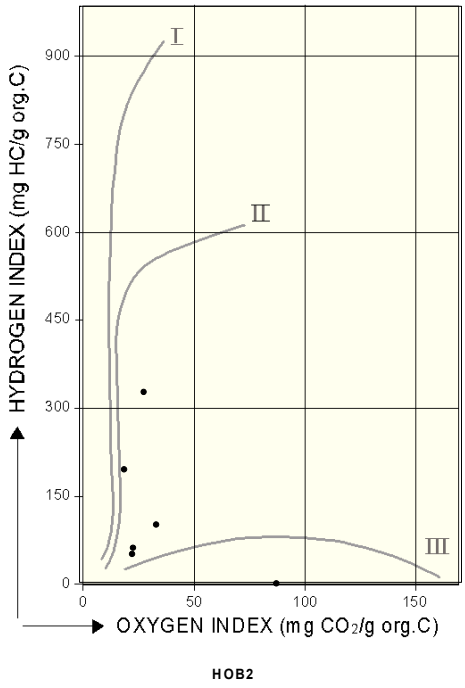

(a) Hydrogen Index against Oxygen Index

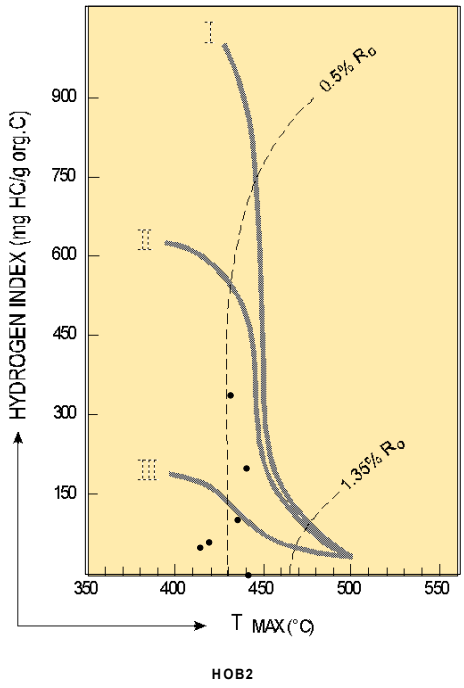

(b) Hydrogen Index against Tmax

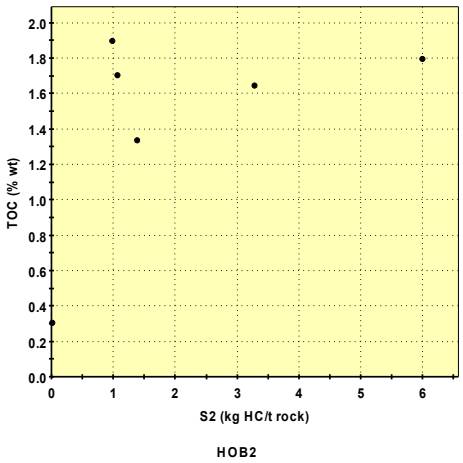

(c) TOC against S2

Figure A.17: *Maturity plots made from the Rock-Eval data Høgrinden South, Barentsøya. Series 2.*

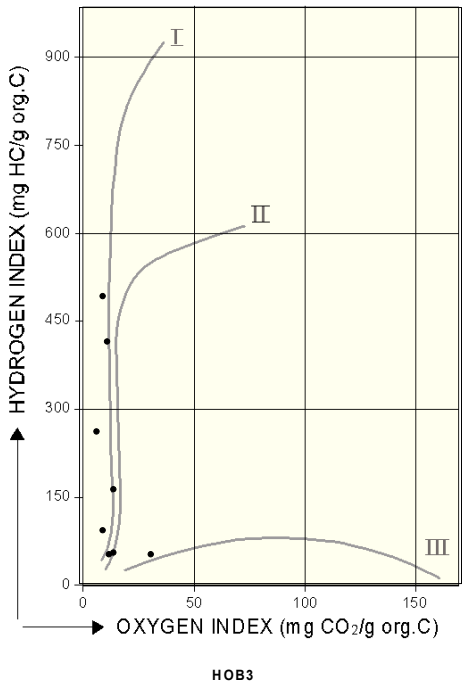

(a) Hydrogen Index against Oxygen Index

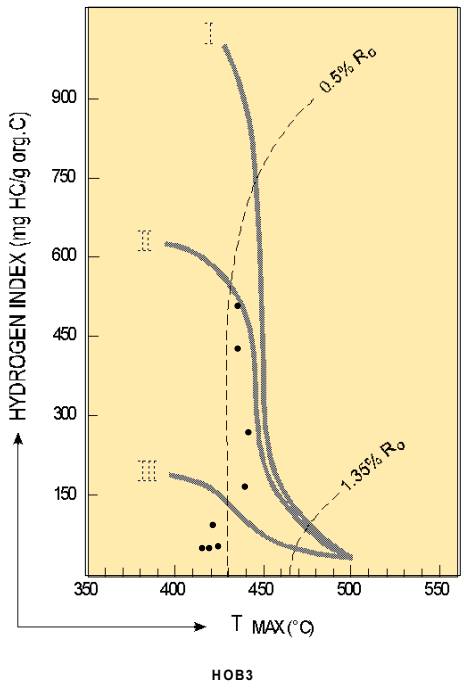

(b) Hydrogen Index against Tmax

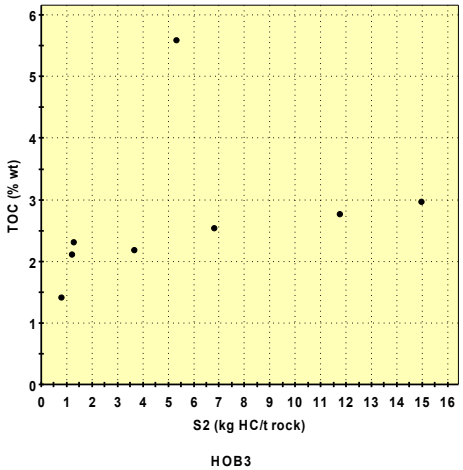

(c) TOC against S2

Figure A.18: *Maturity plots made from the Rock-Eval data Høgrinden South, Barentsøya. Series 3.; sampled laterally along a single horizon.*

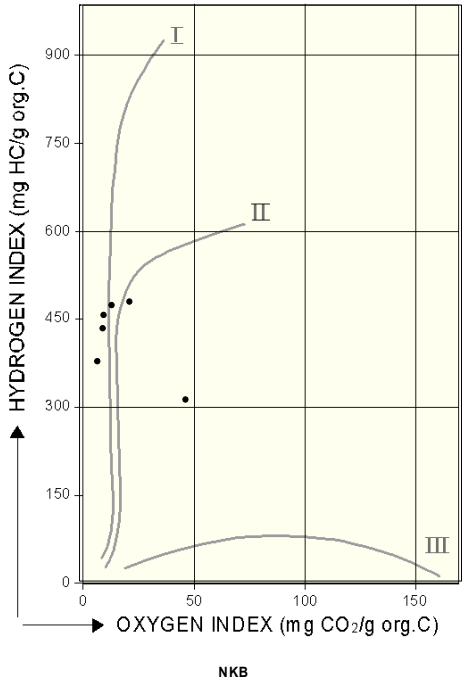

(a) Hydrogen Index against Oxygen Index

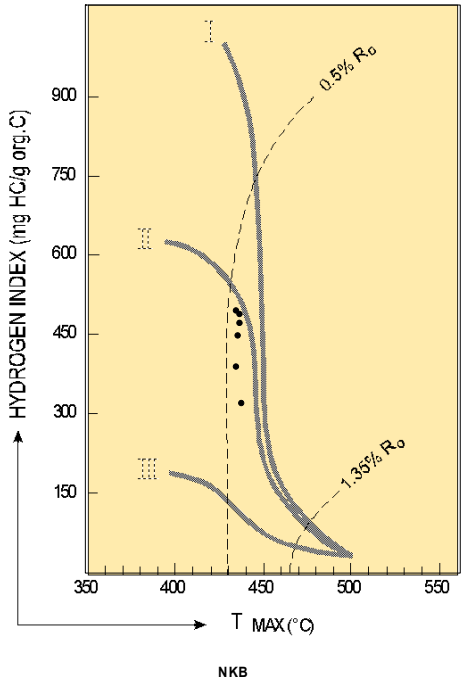

(b) Hydrogen Index against Tmax

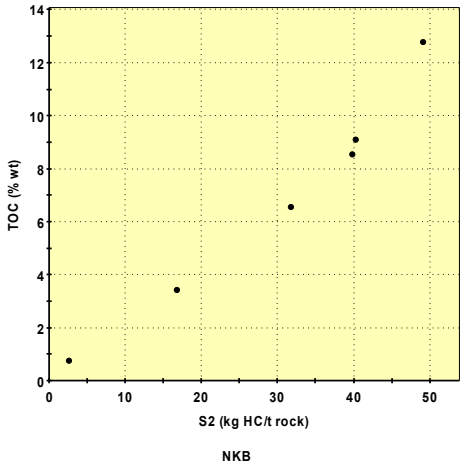

(c) TOC against S2

Figure A.19: *Maturity plots made from the Rock-Eval data Northern Kreftberget, Barentsøya; Profile without sill*

Appendix B

Iatroscan

Iatroscan analysis were performed at Institute for Geology, University of Oslo, Norway.

B.1 Analysis

The analytical equipment being used for the Iatroscan analysis was a Iatroscan TH-10, MK IV.

Iatroscan is the trade mark of a Thin-Layer Chromatography (TLC) analyser coupled with a Flame Ionisation Detector (FID) developed in Japan by Iatron.

Iatroscan analyses involves thin-layer chromatography and flame ionization detection (TLC-FID analyses) of petroleum fractions. It provides for a rapid and relatively accurate method for the quantification of saturated hydrocarbons, aromatic hydrocarbons and the polar fraction (resins and asphaltenes) in solvent extracts of petroleum source-rocks, reservoir rocks and crude oils (Karlsen and Larter, 1989). The varying proportions of saturated and aromatic hydrocarbons and polar compounds can be used to characterize the petroleum populations in the reservoir (Bhullar et al., 2000) and differentiate between migrated hydrocarbons, in-situ generated hydrocarbons and also diesel drilling fluids (Karlsen and Larter, 1989). This technique is suitable to screen large sample volumes from petroleum reservoirs to obtain information for selection of samples for high-resolution analyses.

Only small quantity of rock are required (50 mg to 2 g). In this study 172 extracted rock samples were analysed in addition to the standard oil NSO-1 by the Iatroscan TH-10 instrument equipped with a flame ionization detector (FID) and interfaced with an electric integrator (Perkin-Elmer LCI-100) used for rod scanning and quantification (see Karlsen and Larter (1989) for a description of the method). The components were separated using silica rods, type Chromarods-S III (pore diameter 60 Å, particle size $5\mu m$). The rock samples were crushed and the hydrocarbons extracted by adding 5 ml of DCM:MeOH (93:7 VOL%) in glass vials. The samples were placed in the dark for 2 weeks and shaken five times during the period. 3 μl of all of the samples were then systematically applied to a fixed point near the base of a chromarod. 8 out of 10 rods were used for the samples (2 rods pr. sample), as the remaining 2 were used for test runs, one with

the NSO-1 and the other blank. For separation along the Chromarods, solvents of different polarity were used to separate saturated hydrocarbons, aromatic hydrocarbons and polar compounds. The rods were placed in normalhexane (35 min) causing the saturated hydrocarbons to rise to the uppermost part of the rods. After air drying the rods were placed in toluene (12 min) causing the aromatic hydrocarbons to move to the middle of the rods. Then the Chromorods were placed in the Iatroscan instrument, the scanning speed was 30 sec/scan, and pure grade hydrogen (180 ml/min) and air (2.1 l/min) supplied by a pump were used for the detector.

B.2 Results

On the following pages the results from the Iatroscan analyses on the source-rock close to sills at Svalbard can be seen.

Table B.1: Iatroscan. Botneheia East, Central Spitsbergen; Profile with only a minor sill

Sample	*Mean Sat (mg/ml)*	*Mean Aro (mg/ml)*	*Mean Nso (mg/ml)*	*% Sat*	*% Aro*	*% Nso*	*mg Sat g rock*	*mg Aro g rock*	*mg Nso g rock*	*Sum HC g rock*	*Measured weight ba*
BH1-1	2.10	1.98	3.42	28.00	26.42	45.57	1.54	1.45	2.51	5.50	4.0891
BH1-2	1.54	1.21	4.37	21.61	16.99	61.40	1.13	0.89	3.20	5.22	4.0931
BH1-3	n.d.	n.d.	n.d.	n.d.	n.d.	n.d.	n.d.	n.d.	n.d.	n.d.	n.d.
BH1-4	3.22	1.36	4.97	33.73	14.28	51.99	2.25	0.95	3.47	6.67	4.2959
BH1-5	2.38	3.30	6.22	20.04	27.70	52.26	1.43	1.98	3.73	7.13	5.0044
BH1-6	1.73	1.86	9.62	13.12	14.07	72.81	1.29	1.39	7.18	9.86	4.0199
BH1-7	n.d.	n.d.	n.d.	n.d.	n.d.	n.d.	n.d.	n.d.	n.d.	n.d.	n.d.
BH1-8	n.d.	n.d.	n.d.	n.d.	n.d.	n.d.	n.d.	n.d.	n.d.	n.d.	n.d.
BH1-9	n.d.	n.d.	n.d.	n.d.	n.d.	n.d.	n.d.	n.d.	n.d.	n.d.	n.d.
BH1-10	2.38	3.30	6.22	20.04	27.70	52.26	1.27	1.75	3.31	6.33	5.6407
BH1-11	n.d.	n.d.	n.d.	n.d.	n.d.	n.d.	n.d.	n.d.	n.d.	n.d.	n.d.
BH1-12	n.d.	n.d.	n.d.	n.d.	n.d.	n.d.	n.d.	n.d.	n.d.	n.d.	n.d.
BH1-13	3.30	2.41	3.60	35.41	25.91	38.68	1.78	1.30	1.95	5.03	5.5569
BH1-14	1.18	1.88	1.09	28.39	45.36	26.25	0.63	1.01	0.58	2.23	5.5977
BH1-15	3.08	0.43	2.97	47.50	6.68	45.83	2.30	0.32	2.22	4.85	4.0065
BH1-16	n.d.	n.d.	n.d.	n.d.	n.d.	n.d.	n.d.	n.d.	n.d.	n.d.	n.d.
BH1-17	n.d.	n.d.	n.d.	n.d.	n.d.	n.d.	n.d.	n.d.	n.d.	n.d.	n.d.
BH1-18	n.d.	n.d.	n.d.	n.d.	n.d.	n.d.	n.d.	n.d.	n.d.	n.d.	n.d.
BH1-19	0.17	0.08	0.32	29.69	13.34	56.98	0.11	0.05	0.21	0.37	4.6505
BH1-20	3.80	1.97	3.66	40.27	20.91	38.82	2.76	1.43	2.66	6.85	4.1341
BH1-21	n.d.	n.d.	n.d.	n.d.	n.d.	n.d.	n.d.	n.d.	n.d.	n.d.	n.d.
BH1-22	n.d.	n.d.	n.d.	n.d.	n.d.	n.d.	n.d.	n.d.	n.d.	n.d.	n.d.
BH1-23	0.76	1.09	2.72	16.61	23.86	59.53	0.53	0.76	1.90	3.20	4.293
BH1-24	n.d.	n.d.	n.d.	n.d.	n.d.	n.d.	n.d.	n.d.	n.d.	n.d.	n.d.
BH1-25	n.d.	n.d.	n.d.	n.d.	n.d.	n.d.	n.d.	n.d.	n.d.	n.d.	n.d.
BHI-26	0.59	1.43	3.05	11.70	28.17	60.13	0.38	0.92	1.97	3.28	4.6372
BH1-27	n.d.	n.d.	n.d.	n.d.	n.d.	n.d.	n.d.	n.d.	n.d.	n.d.	n.d.

Table B.2: Iatroscan. Botneheia East, Central Spitsbergen; Profile above sill

Sample	*Mean Sat (mg/ml)*	*Mean Aro (mg/ml)*	*Mean Nso (mg/ml)*	*% Sat*	*% Aro*	*% Nso*	*mg Sat g rock*	*mg Aro g rock*	*mg Nso g rock*	*Sum HC g rock*	*Measured weight ba*
BH2-1	1.85	0.50	1.38	49.54	13.44	37.02	1.38	0.37	1.03	2.78	4.0299
BH2-2	n.d.	n.d.	n.d.	n.d.	n.d.	n.d.	n.d.	n.d.	n.d.	n.d.	n.d.
BH2-3	5.73	1.00	2.70	60.78	10.56	28.66	3.22	0.56	1.52	5.30	5.3411
BH2-4	n.d.	n.d.	n.d.	n.d.	n.d.	n.d.	n.d.	n.d.	n.d.	n.d.	n.d.
BH2-5	0.60	0.19	0.76	38.61	12.13	49.26	0.54	0.17	0.69	1.40	3.3285
BH2-6	n.d.	n.d.	n.d.	n.d.	n.d.	n.d.	n.d.	n.d.	n.d.	n.d.	n.d.
BH2-7	2.60	0.37	2.70	45.86	6.51	47.63	1.68	0.24	1.74	3.66	4.6364
BH2-8	2.20	0.96	1.55	46.76	20.36	32.88	1.43	0.62	1.00	3.05	4.6274
BH2-9	3.14	1.08	2.78	44.88	15.40	39.72	1.53	0.53	1.36	3.41	6.1573
BH2-10	1.56	0.23	2.22	38.95	5.64	55.41	1.13	0.16	1.61	2.90	4.1461
BH2-11	2.98	0.33	3.04	46.92	5.24	47.84	1.96	0.22	2.00	4.17	4.57
BH2-12	1.09	0.22	1.65	36.75	7.36	55.89	0.72	0.14	1.10	1.97	4.51
BH2-13	n.d.	n.d.	n.d.	n.d.	n.d.	n.d.	n.d.	n.d.	n.d.	n.d.	n.d.
BH2-14	0.37	0.11	1.21	22.00	6.53	71.46	0.28	0.08	0.90	1.26	4.0315
BH2-15	2.65	0.41	2.31	49.36	7.66	42.98	1.83	0.28	1.60	3.72	4.3363
BH2-16	n.d.	n.d.	n.d.	n.d.	n.d.	n.d.	n.d.	n.d.	n.d.	n.d.	n.d.
BH2-17	n.d.	n.d.	n.d.	n.d.	n.d.	n.d.	n.d.	n.d.	n.d.	n.d.	n.d.
BH2-18	6.32	3.17	3.48	48.72	24.42	26.86	4.31	2.16	2.38	8.85	4.3963
BH2-19	1.59	0.06	1.83	45.73	1.62	52.66	1.12	0.04	1.29	2.46	4.243
BH2-20	1.88	1.47	3.72	26.63	20.83	52.54	1.32	1.03	2.60	4.94	4.2952
BH2-21	1.19	1.25	3.26	20.82	21.94	57.24	0.87	0.91	2.39	4.17	4.101
BH2-22	1.51	3.16	4.94	15.69	32.93	51.39	1.08	2.27	3.55	6.90	4.1761
BH2-23	2.51	6.24	4.97	18.31	45.45	36.25	1.64	4.08	3.25	8.98	4.5868
BH2-24	1.07	2.76	4.74	12.44	32.25	55.31	0.60	1.55	2.66	4.82	5.3345
BH2-25	0.37	0.44	1.70	14.91	17.42	67.67	0.24	0.28	1.08	1.59	4.717
BH2-26	1.29	1.96	4.25	17.22	26.11	56.67	0.78	1.18	2.56	4.52	4.9843
BH2-27	1.65	0.56	1.69	42.17	14.46	43.38	0.99	0.34	1.02	2.34	4.9962
BH2-28	1.25	0.85	2.38	27.96	18.95	53.09	0.86	0.59	1.64	3.09	4.342
BH2-29	0.86	0.87	3.72	15.69	15.97	68.33	0.46	0.47	2.00	2.92	5.5972
BH2-30	1.30	2.40	5.30	14.48	26.70	58.82	0.82	1.52	3.34	5.68	4.7584

Table B.3: Iatroscan. Kreftberget, Barentsøya: Profile above sill

Sample	*Mean Sat (mg/ml)*	*Mean Aro (mg/ml)*	*Mean Nso (mg/ml)*	*% Sat*	*% Aro*	*% Nso*	*mg Sat g rock*	*mg Aro g rock*	*mg Nso g rock*	*Sum HC g rock*	*Measured weight ba*
KRB-1a	0.00	0.05	0.03	0.00	59.78	40.25	0.00	0.03	0.02	0.06	4.2067
KRB-1b	0.00	0.54	0.40	0.00	8.74	93.76	3.00	0.02	0.18	0.20	6.4638
KRB-3b(dupl)	0.00	0.03	0.08	0.00	0.00	140.00	0.03	0.10	0.05	0.05	4.7679
KRB-1c	2.66	1.06	2.37	43.67	14.46	38.87	1.53	0.61	1.36	3.50	9.2729
KRB-2	0.50	0.00	0.21	0.00	0.00	500.00	0.01	0.00	0.16	0.15	6.1437
KRB-3a	0.35	0.00	0.26	56.68	0.90	43.32	0.44	8.00	0.34	0.07	2.3669
KRB-3b	0.33	0.00	0.25	60.89	5.90	39.14	0.23	0.00	0.15	0.36	4.3335
KRB-4	n.d.	n.d.	n.d.	n.d.	n.d.	n.d.	n.d.	n.d.	n.d.	n.d.	n.d.
KRB-5	n.d.	n.d.	n.d.	n.d.	n.d.	n.d.	n.d.	n.d.	n.d.	n.d.	n.d.
KRB-6	n.d.	n.d.	n.d.	n.d.	n.d.	n.d.	n.d.	n.d.	n.d.	n.d.	n.d.
KRB-7	n.d.	n.d.	n.d.	n.d.	n.d.	n.d.	n.d.	n.d.	n.d.	n.d.	n.d.
KRB-8	1.25	5.02	0.21	84.20	1.39	14.41	0.87	0.01	0.85	1.04	4.2742
KRB-8(dupl)	1.95	5.07	0.28	84.57	3.19	12.23	1.24	0.05	0.18	1.46	4.7335
KRB-1	1.48	0.06	0.22	84.25	3.14	12.81	1.10	0.04	0.16	1.30	2.6556
KRB-10	1.52	0.06	0.17	86.99	3.47	9.54	0.78	0.03	0.09	0.90	9.8332
KRB-11	1.06	0.05	0.25	78.14	3.96	17.50	0.66	0.03	0.15	0.84	4.8984
KRB-32	0.51	0.03	0.26	42.22	5.79	52.00	0.12	0.02	0.14	0.27	5.4006
KRB-13	n.d.	n.d.	n.d.	n.d.	n.d.	n.d.	n.d.	n.d.	n.d.	n.d.	n.d.
KRB-14	0.18	0.03	0.17	46.65	8.73	44.62	0.11	0.02	0.10	0.23	4.9551
KRB-15	n.d.	n.d.	n.d.	n.d.	n.d.	n.d.	n.d.	n.d.	n.d.	n.d.	n.d.
KRB-16	n.d.	n.d.	0.09	n.d.	n.d.	n.d.	n.d.	n.d.	n.d.	n.d.	n.d.
KRB-17	0.00	0.00	0.10	0.00	0.00	100.00	0.00	0.00	0.07	0.07	4.1105
KRB-17(dupl)	0.00	0.05	0.23	0.00	17.60	82.40	0.00	0.03	0.13	0.15	5.5725
KRB-18a	n.d.	n.d.	n.d.	n.d.	n.d.	n.d.	n.d.	n.d.	n.d.	n.d.	n.d.
KRB-18b	0.12	0.09	0.20	28.86	21.44	49.70	0.07	0.05	0.11	0.23	5.2188
KRB-19	n.d.	n.d.	n.d.	n.d.	n.d.	n.d.	n.d.	n.d.	n.d.	n.d.	n.d.

Table B.4: B.3 cont.

Sample	*Mean Sat (mg/ml)*	*Mean Aro (mg/ml)*	*Mean Nso (mg/ml)*	*% Sat*	*% Aro*	*% Nso*	*mg Sat g rock*	*mg Aro g rock*	*mg Nso g rock*	*Sum HC g rock*	*Measured weight ba*
KRB-20	0.11	0.17	0.40	16.50	24.84	58.66	0.06	0.09	0.22	n.d.	5.5537
KRB-20(dupl)	0.11	0.18	0.47	14.69	23.35	61.96	0.08	0.12	0.33	0.53	4.2732
KRB-21	n.d.	n.d.	n.d.	n.d.	n.d.	n.d.	n.d.	n.d.	n.d.	n.d.	n.d.
KRB-22	1.92	0.39	0.54	67.24	13.72	19.04	0.92	0.19	0.26	1.36	6.2916
KRB-23	1.91	0.35	0.70	64.42	11.84	23.74	0.81	0.15	0.30	1.25	7.1213
KRB-24	2.26	0.90	1.03	53.82	21.52	24.66	1.59	0.63	0.73	2.95	4.2679
KRB-24(dupl)	1.77	0.71	1.04	50.29	20.23	29.48	1.03	0.42	0.61	2.05	5.1442
KRB-25	n.d.	n.d.	n.d.	n.d.	n.d.	n.d.	n.d	n.d.	n.d.	n.d.	n.d.
KRB-26	0.58	0.57	1.27	24.02	23.59	52.39	0.42	0.42	0.93	1.77	4.124

Table B.5: Iatroscan. Teistberget, Eastern Spitsbergen; Profile above sill

Sample	*Mean Sat (mg/ml)*	*Mean Aro (mg/ml)*	*Mean Nso (mg/ml)*	*% Sat*	*% Aro*	*% Nso*	*mg Sat g rock*	*mg Aro g rock*	*mg Nso g rock*	*Sum HC g rock*	*Measured weight ba*
TBU-1	0.27	0.15	0.33	36.34	19.32	44.33	0.18	0.09	0.22	0.49	4.6402
TBU-2	n.d.	n.d.	n.d.	n.d.	n.d.	n.d.	n.d.	n.d.	n.d.	n.d.	n.d.
TBU-3	0.36	0.10	0.97	25.31	7.14	67.55	0.21	0.06	0.55	0.81	5.3124
TBU-4	0.47	0.19	0.78	32.81	13.16	54.02	0.31	0.12	0.51	0.94	4.6042
TBU-4(dupl)	0.43	0.17	0.79	30.95	12.43	56.62	0.28	0.11	0.51	0.90	4.6315
TBU-5	n.d.	n.d.	n.d.	n.d.	n.d.	n.d.	n.d.	n.d.	n.d.	n.d.	n.d.
TBU-6	2.89	0.73	0.72	66.61	16.74	16.66	2.00	0.50	0.50	3.01	4.3292
TBU-7	3.07	2.62	2.95	35.60	30.28	34.12	1.74	1.48	1.67	4.90	5.2858
TBU-8	n.d.	n.d.	n.d.	n.d.	n.d.	n.d.	n.d.	n.d.	n.d.	n.d.	n.d.
TBU-9	2.78	0.24	2.39	51.34	4.42	44.24	1.92	0.17	1.65	3.74	4.3396
TBU-10	1.40	1.95	5.26	16.22	22.69	61.09	1.02	1.43	3.85	6.30	4.1008
TBU-11	n.d.	n.d.	n.d.	n.d.	n.d.	n.d.	n.d.	n.d.	n.d.	n.d.	n.d.

Table B.6: Iatroscan. Teistberget, Eastern Spitsbergen; Profile below sill

Sample	*Mean Sat (mg/ml)*	*Mean Aro (mg/ml)*	*Mean Nso (mg/ml)*	*% Sat*	*% Aro*	*% Nso*	*mg Sat g rock*	*mg Aro g rock*	*mg Nso g rock*	*Sum HC g rock*	*Measured weight ba*
TBL-1	0.61	0.09	1.60	26.55	4.03	69.42	0.31	0.05	0.81	1.17	5.9296
TBL-1(dupl)	0.53	0.13	1.18	28.73	7.02	64.24	0.27	0.07	0.60	0.93	5.9113
TBL-2	n.d.	n.d.	n.d.	n.d.	n.d.	n.d.	n.d.	n.d.	n.d.	n.d.	n.d.
TBL-3	0.55		0.50	52.42	0.00	47.58	0.35	0.00	0.31	0.66	4.755
TBL-4	2.05	0.41	0.78	63.23	12.55	24.22	1.58	0.31	0.60	2.50	3.8876
TBL-5	2.21	0.72	0.91	57.51	18.71	23.78	1.65	0.54	0.68	2.86	4.0239
TBL-6	2.13	0.36	0.85	63.76	10.87	25.37	1.34	0.23	0.53	2.10	4.7658
TBL-7	2.18	0.22	0.69	70.45	7.22	22.34	1.30	0.13	0.41	1.84	5.0394
TBL-8	n.d.	n.d.	n.d.	n.d.	n.d.	n.d.	n.d.	n.d.	n.d.	n.d.	n.d.
TBL-9	0.09	0.24	0.47	10.72	29.73	59.56	0.06	0.17	0.34	0.57	4.184
TBL-10	n.d.	n.d.	n.d.	n.d.	n.d.	n.d.	n.d.	n.d.	n.d.	n.d.	n.d.
TBL-11	n.d.	n.d.	n.d.	n.d.	n.d.	n.d.	n.d.	n.d.	n.d.	n.d.	n.d.

Table B.7: Iatroscan. Domen, Eastern Spitsbergen; Profile above sill

Sample	*Mean Sat (mg/ml)*	*Mean Aro (mg/ml)*	*Mean Nso (mg/ml)*	*% Sat*	*% Aro*	*% Nso*	*mg Sat g rock*	*mg Aro g rock*	*mg Nso g rock*	*Sum HC g rock*	*Measured weight ba*
DOM-1	n.d.	n.d.	n.d.	n.d.	n.d.	n.d.	n.d.	n.d.	n.d.	n.d.	n.d.
DOM-2	n.d.	n.d.	n.d.	n.d.	n.d.	n.d.	n.d.	n.d.	n.d.	n.d.	n.d.
DOM-3	0.93	0.21	0.35	62.07	14.27	23.66	0.65	0.15	0.25	1.05	4.2688
DOM-3(dupl)	0.98	0.20	0.45	60.34	11.97	27.69	0.64	0.15	0.29	1.08	4.6315
DOM-4	1.39	0.51	0.50	57.83	21.29	20.88	1.06	0.39	0.38	1.84	3.933
DOM-5	n.d.	n.d.	n.d.	n.d.	n.d.	n.d.	n.d.	n.d.	n.d.	n.d.	n.d.
DOM-6	0.05	0.08	0.22	14.09	22.79	63.12	0.03	0.05	0.14	0.22	4.6908
DOM-7	n.d.	n.d.	n.d.	n.d.	n.d.	n.d.	n.d.	n.d.	n.d.	n.d.	n.d.
DOM-8	n.d.	n.d.	n.d.	n.d.	n.d.	n.d.	n.d.	n.d.	n.d.	n.d.	n.d.
DOM-9a	0.58	0.89	1.65	18.71	28.43	52.86	0.39	0.59	1.09	2.07	4.5251
DOM-9b	n.d.	n.d.	n.d.	n.d.	n.d.	n.d.	n.d.	n.d.	n.d.	n.d.	n.d.
DOM-10	n.d.	n.d.	n.d.	n.d.	n.d.	n.d.	n.d.	n.d.	n.d.	n.d.	n.d.
DOM-11	1.96	2.80	3.63	23.39	33.38	43.23	1.32	1.89	2.44	5.65	4.4552

Table B.8: Iatroscan. Høgrinden South, Barentsøya

Sample	*Mean Sat (mg/ml)*	*Mean Aro (mg/ml)*	*Mean Nso (mg/ml)*	*% Sat*	*% Aro*	*% Nso*	*mg Sat g rock*	*mg Aro g rock*	*mg Nso g rock*	*Sum HC g rock*	*Measured weight ba*
HØB1-1	n.d.	n.d.	n.d.	n.d.	n.d.	n.d.	n.d.	n.d.	n.d.	n.d.	n.d.
HØB1-2	n.d.	n.d.	n.d.	n.d.	n.d.	n.d.	n.d.	n.d.	n.d.	n.d.	n.d.
HØB1-3	n.d.	n.d.	n.d.	n.d.	n.d.	n.d.	n.d.	n.d.	n.d.	n.d.	n.d.
HØB1-4	n.d.	n.d.	n.d.	n.d.	n.d.	n.d.	n.d.	n.d.	n.d.	n.d.	n.d.
HØB1-5	n.d.	n.d.	n.d.	n.d.	n.d.	n.d.	n.d.	n.d.	n.d.	n.d.	n.d.
HØB1-6	0.40	0.08	0.42	44.51	8.47	47.02	0.26	0.05	0.28	0.59	4.5442
HØB1-7	0.37	0.15	0.44	38.74	15.22	46.05	0.25	0.10	0.29	0.64	4.5419
HØB1-8	0.42	0.18	0.47	39.29	16.47	44.23	0.29	0.12	0.33	0.75	4.2637
HØB1-9	0.42	0.19	0.65	33.46	15.10	51.44	0.30	0.14	0.46	0.90	4.2364
HØB1-10	0.33	0.36	1.72	13.60	14.89	71.51	0.21	0.23	1.12	1.57	4.6019
HØB1-11	0.30	0.33	1.53	13.83	15.20	70.97	0.22	0.24	1.12	1.57	4.1172
HØB1-12	0.42	0.42	2.10	14.17	14.25	71.57	0.29	0.29	1.47	2.06	4.2812
HØB1-13	0.32	0.29	1.47	15.42	13.75	70.82	0.21	0.18	0.95	1.34	4.6716

Table B.9: Iatroscan. Høgrinden South, Barentsøya

Sample	*Mean Sat (mg/ml)*	*Mean Aro (mg/ml)*	*Mean Nso (mg/ml)*	*% Sat*	*% Aro*	*% Nso*	*mg Sat g rock*	*mg Aro g rock*	*mg Nso g rock*	*Sum HC g rock*	*Measured weight ba*
HØB2-1	n.d.	n.d.	n.d.	n.d.	n.d.	n.d.	n.d.	n.d.	n.d.	n.d.	n.d.
HØB2-2	n.d.	n.d.	n.d.	n.d.	n.d.	n.d.	n.d.	n.d.	n.d.	n.d.	n.d.
HØB2-3	n.d.	n.d.	n.d.	n.d.	n.d.	n.d.	n.d.	n.d.	n.d.	n.d.	n.d.
HØB2-4	0.63	0.10	0.96	37.04	6.16	56.79	0.46	0.08	0.71	1.25	4.0728
HØB2-5	0.99	0.28	1.47	36.05	10.39	53.57	0.67	0.19	0.99	1.85	4.4464
HØB2-6	0.47	0.25	0.71	32.94	17.42	49.63	0.28	0.15	0.43	0.86	4.9875
HØB2-7	0.43	0.26	1.80	17.42	10.45	72.13	0.30	0.18	1.25	1.73	4.3139
HØB2-8	1.14	0.54	2.47	27.36	13.09	59.55	0.80	0.38	1.74	2.91	4.2729
HØB3-1	n.d.	n.d.	n.d.	n.d.	n.d.	n.d.	n.d.	n.d.	n.d.	n.d.	n.d.

Table B.10: Iatroscan. Høgrinden South, Barentsøya; sampled laterally along a single horizon

Sample	*Mean Sat (mg/ml)*	*Mean Aro (mg/ml)*	*Mean Nso (mg/ml)*	*% Sat*	*% Aro*	*% Nso*	*mg Sat g rock*	*mg Aro g rock*	*mg Nso g rock*	*Sum HC g rock*	*Measured weight ba*
HØB3-2(dupl)	1.24	0.09	2.03	36.79	2.77	60.45	0.82	0.06	1.35	2.23	4.5304
HØB3-2	1.36	0.12	2.07	38.36	3.37	58.27	0.88	0.08	1.33	2.28	4.6626
HØB3-3	4.22	0.83	4.69	43.33	8.53	48.13	2.52	0.50	2.80	5.82	5.0235
HØB3-4	0.85	0.05	0.68	53.73	3.48	42.79	0.59	0.04	0.47	1.10	4.2856
HØB3-5	1.29	0.82	0.91	42.73	27.20	30.07	0.93	0.60	0.66	2.19	4.1378
HØB3-6	1.15	0.85	2.98	23.03	17.12	59.84	0.80	0.60	2.08	3.48	4.2939
HØB3-7	0.68	0.57	2.62	17.64	14.75	67.61	0.50	0.42	1.92	2.84	4.0913
HØB3-8	0.97	0.90	3.51	17.97	16.77	65.25	0.72	0.67	2.62	4.01	4.0262
HØB3-9	1.11	0.88	3.10	21.78	17.30	60.93	0.75	0.60	2.11	3.46	4.4047

Table B.11: Iatroscan. Northern Kreftberget, Barentsøya; Profile without sill

Sample	*Mean Sat (mg/ml)*	*Mean Aro (mg/ml)*	*Mean Nso (mg/ml)*	*% Sat*	*% Aro*	*% Nso*	*mg Sat g rock*	*mg Aro g rock*	*mg Nso g rock*	*Sum HC g rock*	*Measured weight ba*
NKB-1	0.23	0.14	1.04	16.18	9.93	73.89	0.15	0.09	0.69	0.93	4.5098
NKB-2	1.08	1.13	3.37	19.40	20.32	60.29	0.77	0.80	2.38	3.95	4.2469
NKB-3	2.63	7.87	10.31	12.64	37.83	49.53	1.62	4.86	6.36	12.84	4.8636
NKB-4	1.77	2.34	5.11	19.21	25.37	55.42	1.31	1.73	3.78	6.81	4.0593
NKB-5	1.77	2.11	4.07	22.29	26.48	51.22	1.19	1.41	2.73	5.34	4.4707
NKB-6	0.51	0.55	2.72	13.39	14.57	72.04	0.31	0.34	1.69	2.34	4.8431

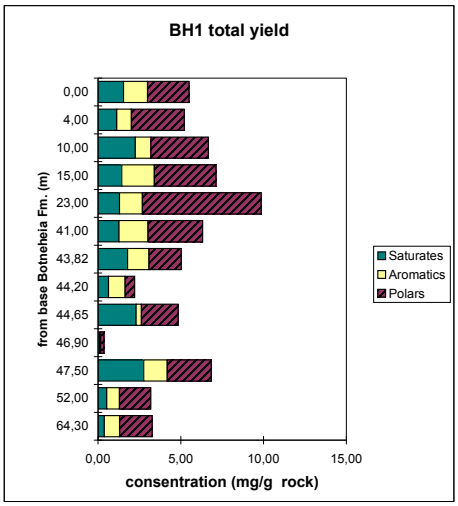

(a) Bar diagram showing the total yield. All units are reported in mg/ gram rock.

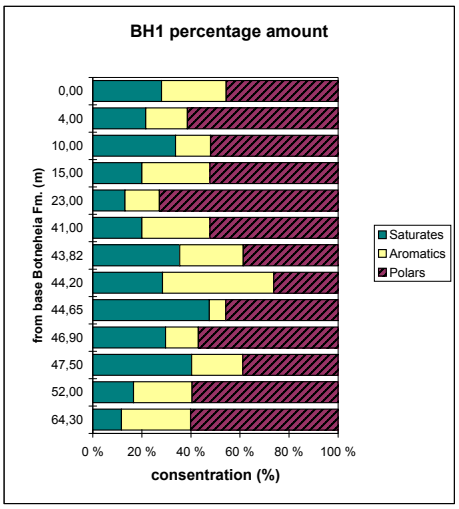

(b) Bar diagram showing the weight% of saturated hydrocarbones, aromatic hydrocarbones and polar compounds (resins and asphaltenes).

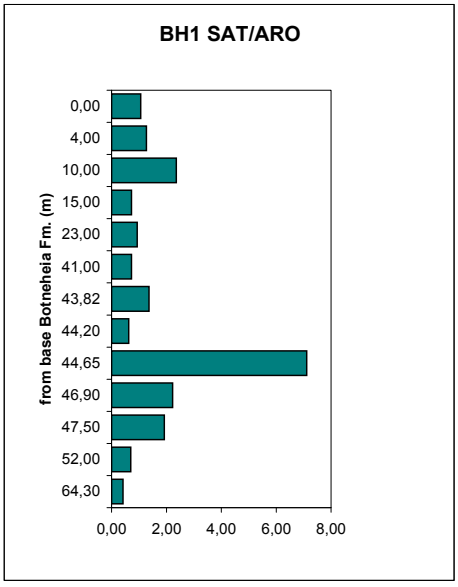

(c) Saturated hydrocarbons/aromatic hydrocarbons ratio (SAT/ARO). Reflecting the maturiy of the samples.

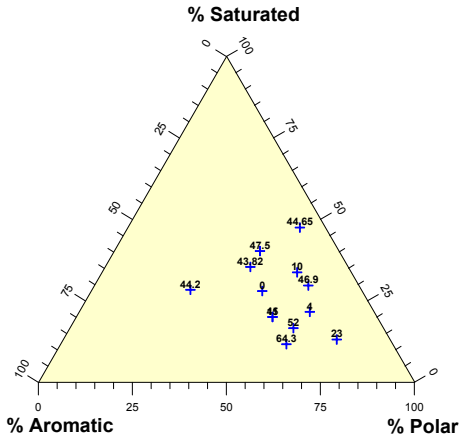

(d) A ternary plot of saturated, aromatic and polar compounds.

Figure B.1: *Plots made from the Iatroscan data Botneheia East, Central Spitsbergen. Profile with only a minor sill.*

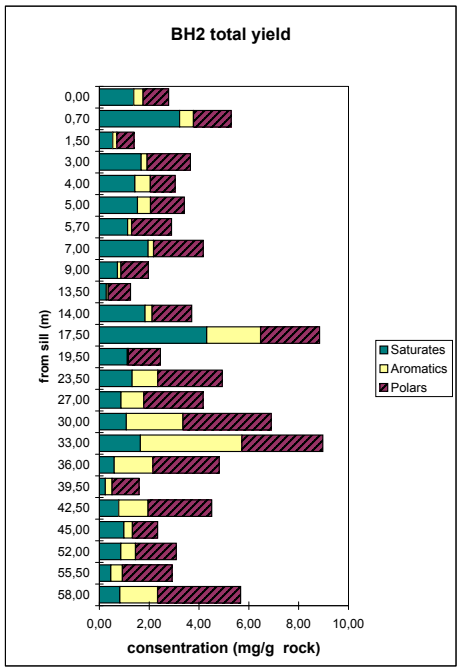

(a) Bar diagram showing the total yield. All units are reported in mg/ gram rock.

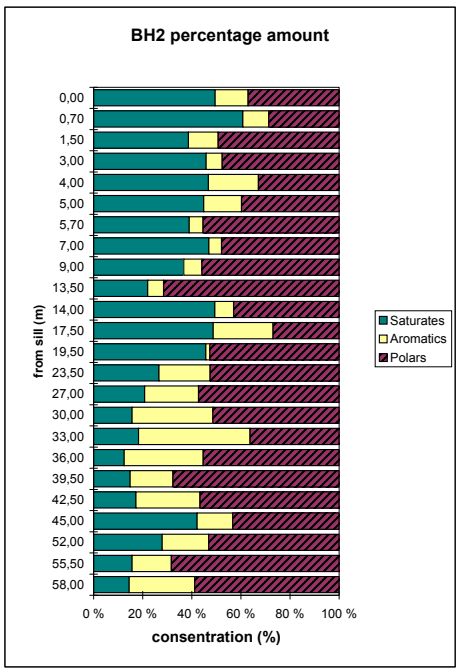

(b) Bar diagram showing the weight% of saturated hydrocarbones, aromatic hydrocarbones and polar compounds (resins and asphaltenes).

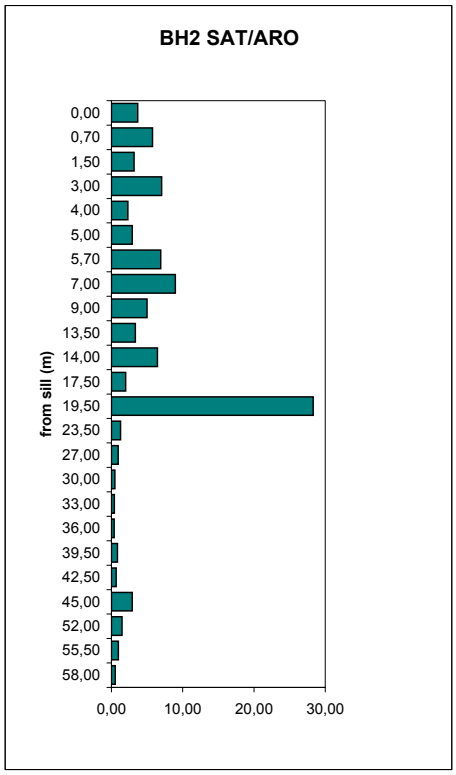

(c) Saturated hydrocarbons/aromatic hydrocarbons ratio (SAT/ARO). Reflecting the maturiy of the samples.

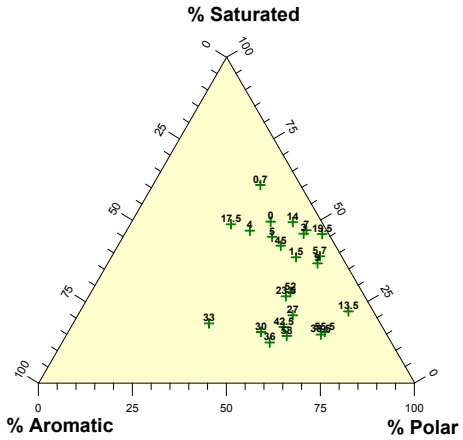

(d) A ternary plot of saturated, aromatic and polar compounds.

Figure B.2: *Plots made from the Iatroscan data Botneheia East, Central Spitsbergen. Profile above sill.*

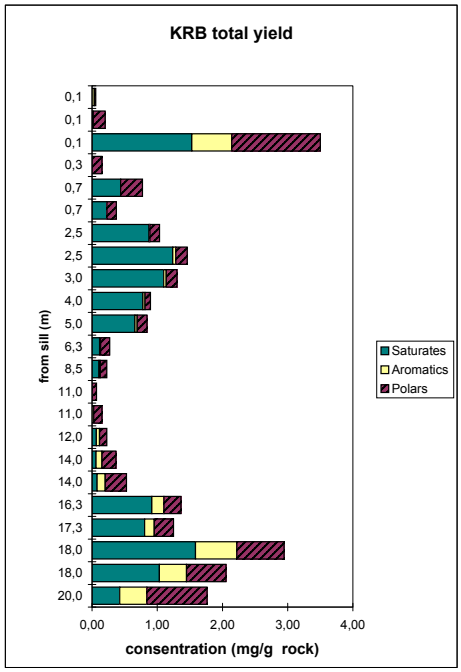

(a) Bar diagram showing the total yield. All units are reported in mg/ gram rock.

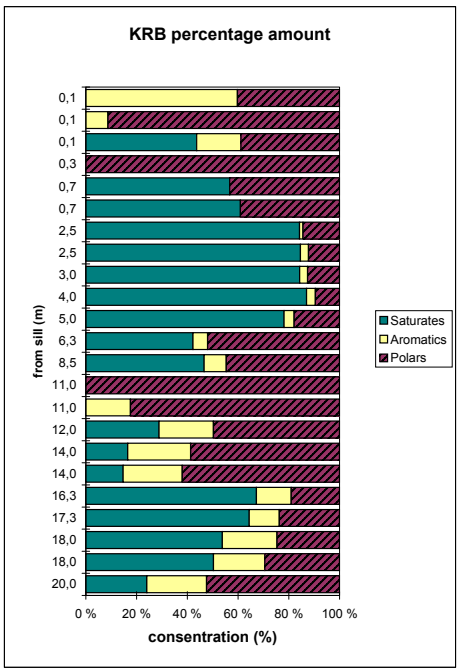

(b) Bar diagram showing the weight% of saturated hydrocarbones, aromatic hydrocarbones and polar compounds (resins and asphaltenes).

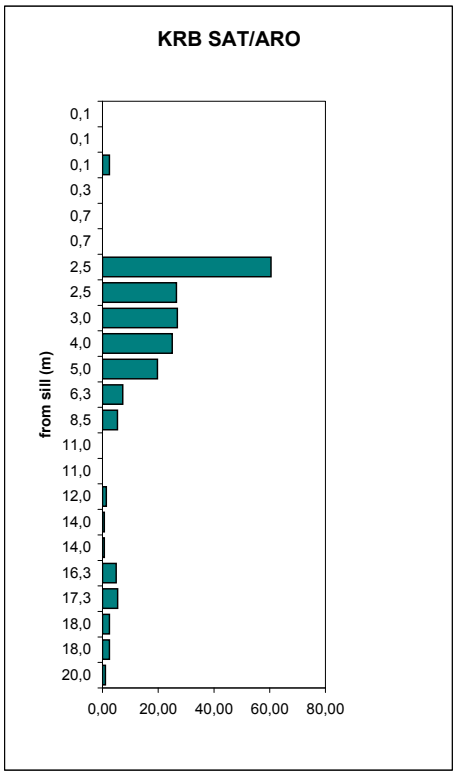

(c) Saturated hydrocarbons/aromatic hydrocarbons ratio (SAT/ARO). Reflecting the maturiy of the samples.

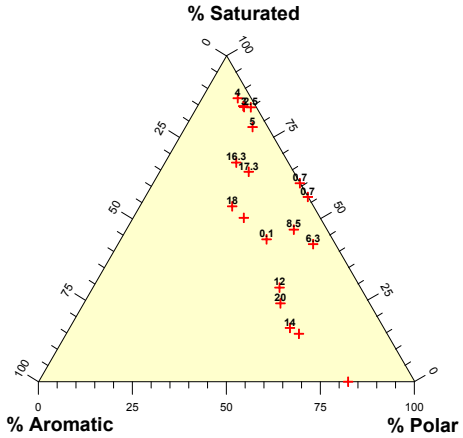

(d) A ternary plot of saturated, aromatic and polar compounds.

Figure B.3: *Plots made from the Iatroscan data Krefftberget, Barentsøya. Profile above sill.*

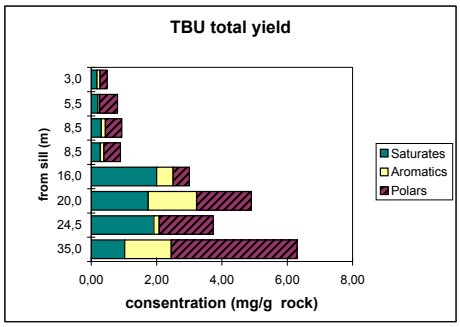

(a) Bar diagram showing the total yield. All units are reported in mg/ gram rock.

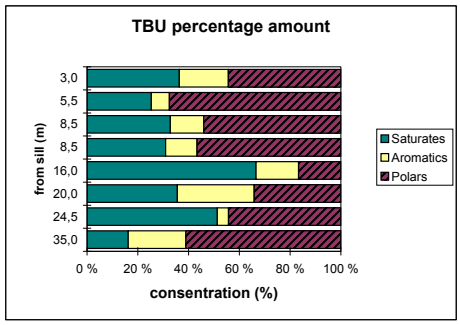

(b) Bar diagram showing the weight% of saturated hydrocarbones, aromatic hydrocarbones and polar compounds (resins and asphaltenes).

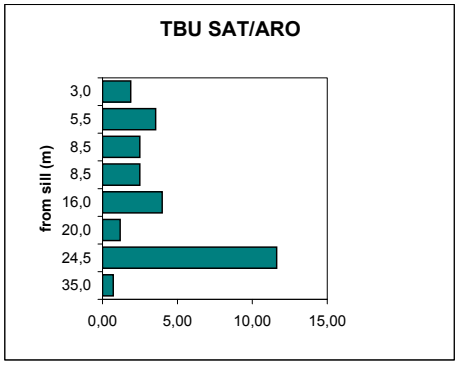

(c) Saturated hydrocarbons/aromatic hydrocarbons ratio (SAT/ARO). Reflecting the maturiy of the samples.

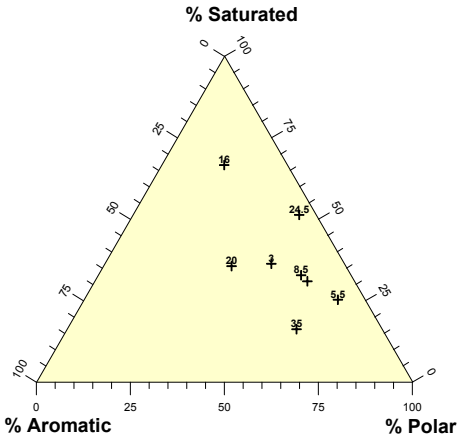

(d) A ternary plot of saturated, aromatic and polar compounds.

Figure B.4: *Plots made from the Iatroscan data Teistberget, Eastern Spitsbergen. Profile above sill.*

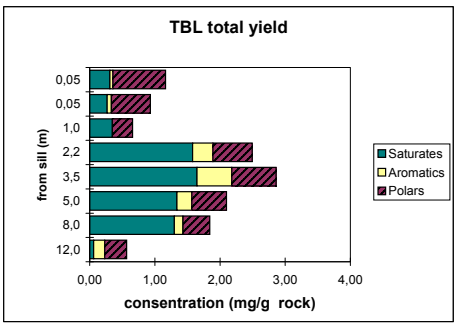

(a) Bar diagram showing the total yield. All units are reported in mg/ gram rock.

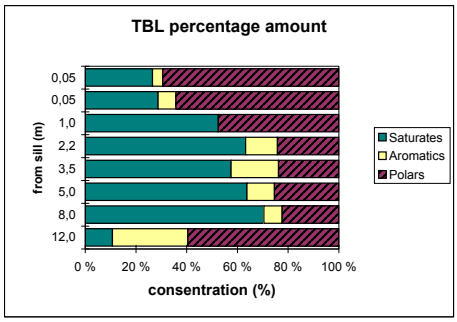

(b) Bar diagram showing the weight% of saturated hydrocarbones, aromatic hydrocarbones and polar compounds (resins and asphaltenes).

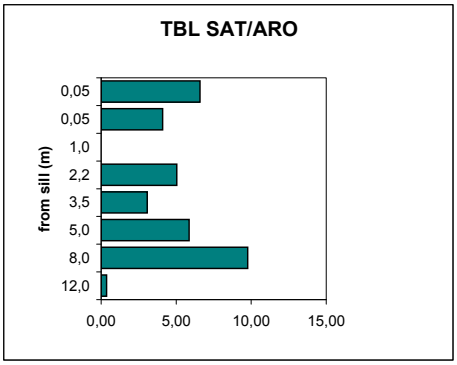

(c) Saturated hydrocarbons/aromatic hydrocarbons ratio (SAT/ARO). Reflecting the maturiy of the samples.

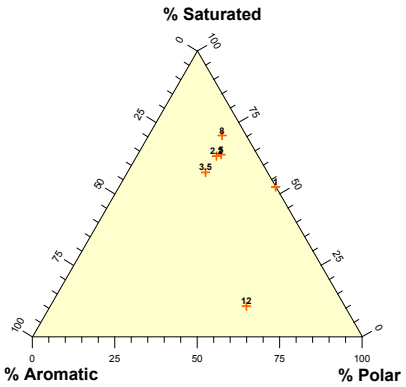

(d) A ternary plot of saturated, aromatic and polar compounds.

Figure B.5: *Plots made from the Iatroscan data Teistberget, Eastern Spitsbergen. Profile below sill.*

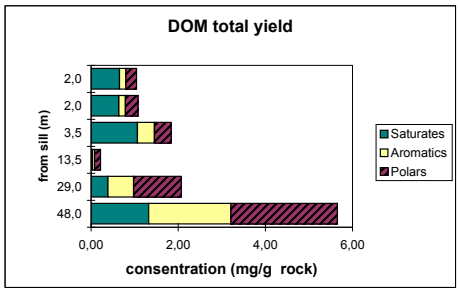

(a) Bar diagram showing the total yield. All units are reported in mg/ gram rock.

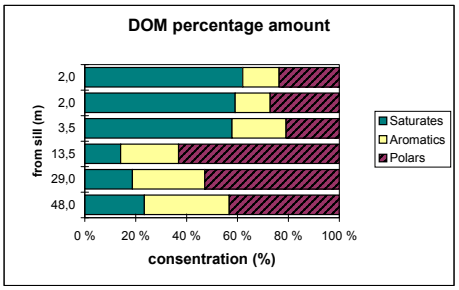

(b) Bar diagram showing the weight% of saturated hydrocarbones, aromatic hydrocarbones and polar compounds (resins and asphaltenes).

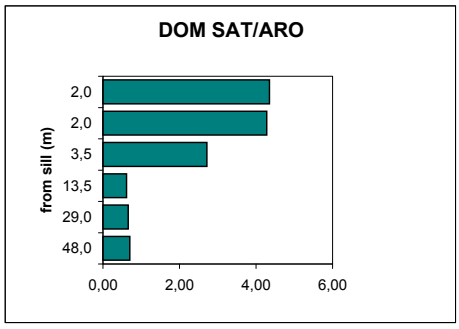

(c) Saturated hydrocarbons/aromatic hydrocarbons ratio (SAT/ARO). Reflecting the maturiy of the samples.

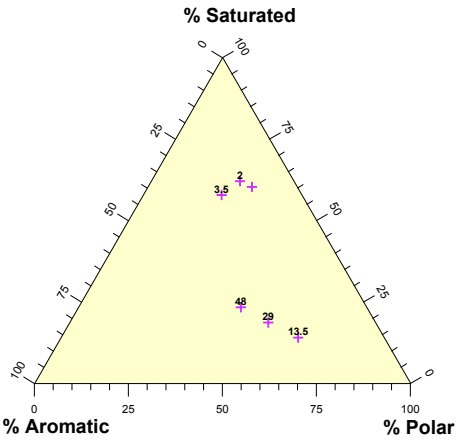

(d) A ternary plot of saturated, aromatic and polar compounds.

Figure B.6: *Plots made from the Iatroscan data Domen, Eastern Spitsbergen. Profile above sill.*

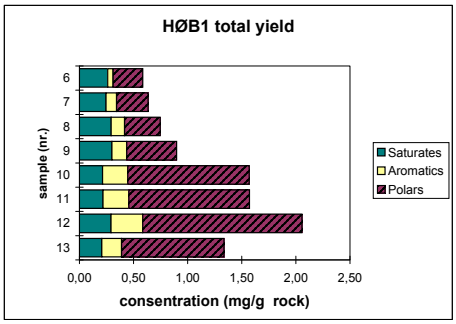

(a) Bar diagram showing the total yield. All units are reported in mg/ gram rock.

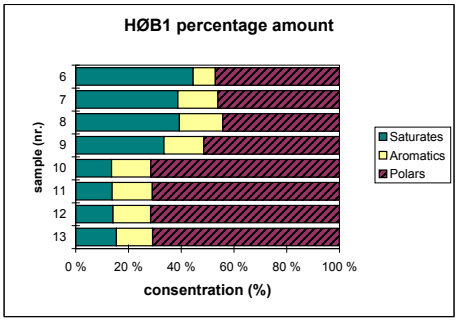

(b) Bar diagram showing the weight% of saturated hydrocarbones, aromatic hydrocarbones and polar compounds (resins and asphaltenes).

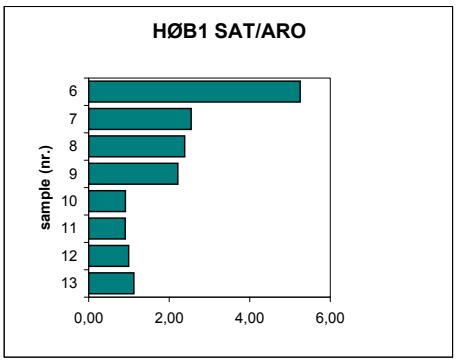

(c) Saturated hydrocarbons/aromatic hydrocarbons ratio (SAT/ARO). Reflecting the maturiy of the samples.

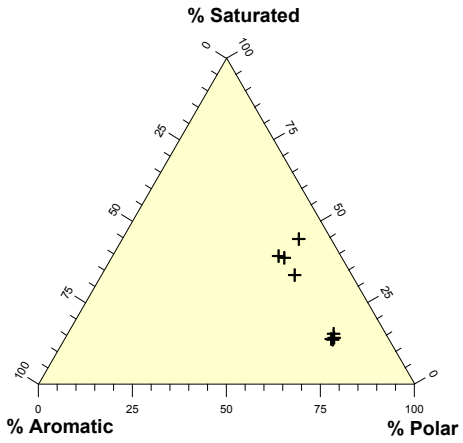

(d) A ternary plot of saturated, aromatic and polar compounds.

Figure B.7: *Plots made from the Iatroscan data Høgrinden South, Barentsøya. Series 1.*

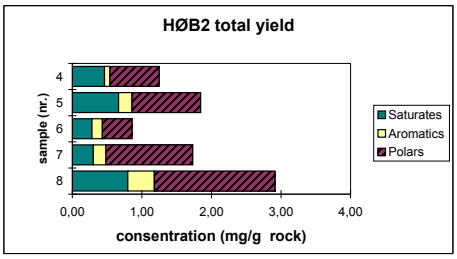

(a) Bar diagram showing the total yield. All units are reported in mg/ gram rock.

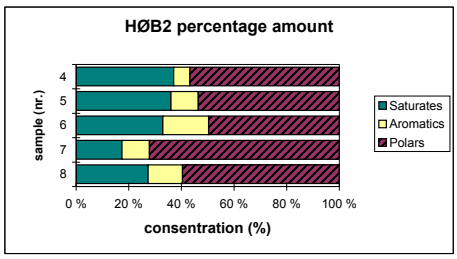

(b) Bar diagram showing the weight% of saturated hydrocarbones, aromatic hydrocarbones and polar compounds (resins and asphaltenes).

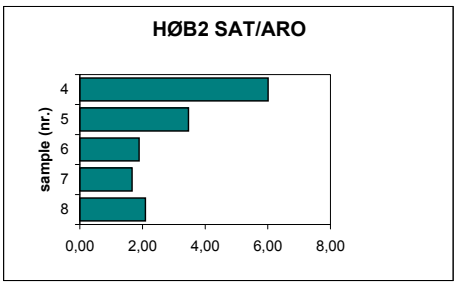

(c) Saturated hydrocarbons/aromatic hydrocarbons ratio (SAT/ARO). Reflecting the maturiy of the samples.

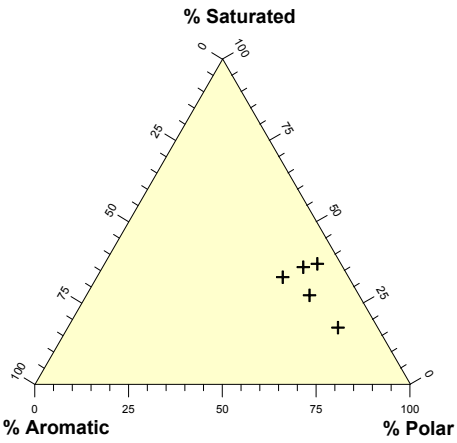

(d) A ternary plot of saturated, aromatic and polar compounds.

Figure B.8: *Plots made from the Iatroscan data Høgrinden South, Barentsøya. Series 2.*

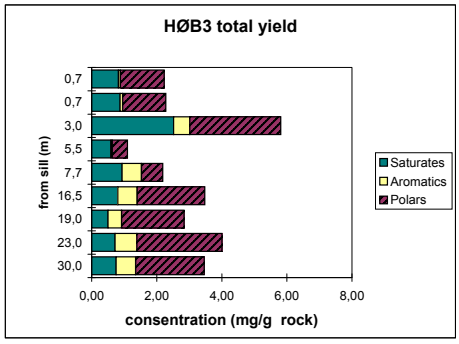

(a) Bar diagram showing the total yield. All units are reported in mg/ gram rock.

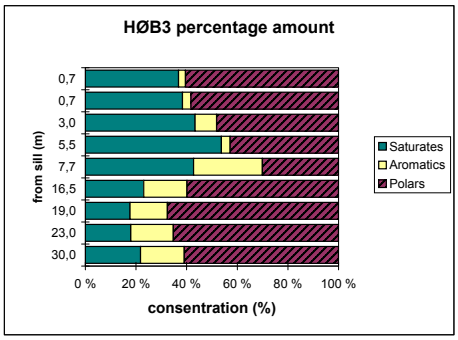

(b) Bar diagram showing the weight% of saturated hydrocarbones, aromatic hydrocarbones and polar compounds (resins and asphaltenes).

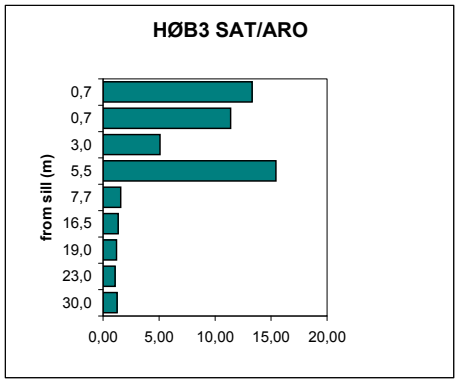

(c) Saturated hydrocarbons/aromatic hydrocarbons ratio (SAT/ARO). Reflecting the maturiy of the samples.

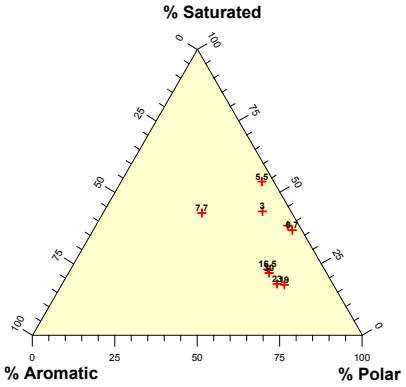

(d) A ternary plot of saturated, aromatic and polar compounds.

Figure B.9:
[Plots made from the Iatroscan data Høgrinden South, Barentsøya, sampled laterally along a single horizon. Series 3.]*Plots made from the Iatroscan data Høgrinden South, Barentsøya, sampled laterally along a single horizon. Series 3.*

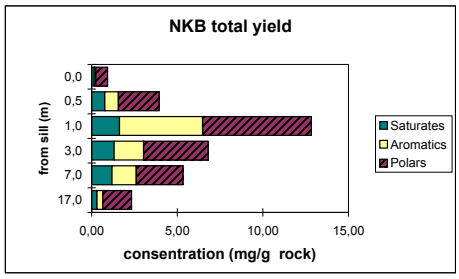

(a) Bar diagram showing the total yield. All units are reported in mg/ gram rock.

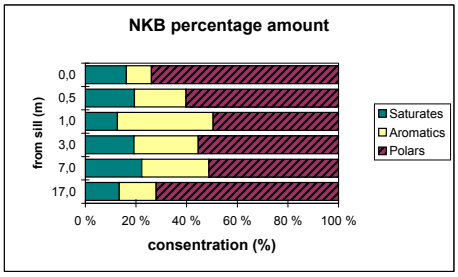

(b) Bar diagram showing the weight% of saturated hydrocarbones, aromatic hydrocarbones and polar compounds (resins and asphaltenes).

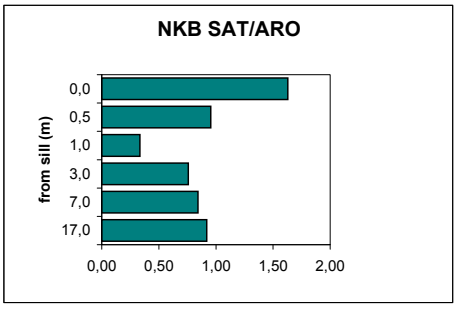

(c) Saturated hydrocarbons/aromatic hydrocarbons ratio (SAT/ARO). Reflecting the maturiy of the samples.

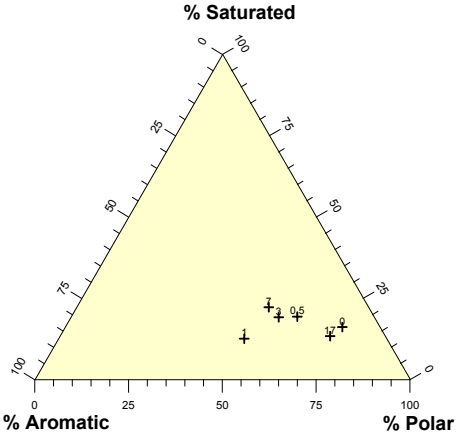

(d) A ternary plot of saturated, aromatic and polar compounds.

Figure B.10: *Plots made from the Iatroscan data Northern Kreftsberget, Central Spitsbergen. Profile without a sill.*

Appendix C

GC-FID

GC-FID analysis were carried out at Institute for Geology, University of Oslo, Norway.

Gas-chromatographic analyses is used for quantification of individual hydrocarbon components and is usually carried out on whole oils, total extracts or saturated and aromatic hydrocarbon fractions of crude oils and bitumens. The GC-FID instrument (Figure C.1) is used for geochemical screening of samples to obtain information about the n-alkanes and isoprenoid distributions. Information about "steranes" and "terpanes" may also in some cases be obtained.

Some of the most common parameters in organic petroleum geochemistry studies are based on data collected by the GC-FID. These parameters include:

- Carbon Preference Index (CPI) or Improved Odd Even Preference (OEP)
- pristane/n-C17
- phytane/n-C18
- pristane/phytane (Pr/Ph)

These parameters are mainly used as maturity and facies indicators, but GC-FID chromatograms may also provide a fingerprint of the total composition of the "stabilised" fluid (untopped, at ambient surface conditions, i.e. ~1 bar and ~15°C) (Weiss et al., 2004).

C.1 Analysis

The GC-FID instrument used in this study was a Varian Capillary Gas Chromatograph Model 3500 with a 50 m length HP Ultra-1 column, which had a 0.2 mm internal diameter and 0.33μm film thickness. Temperature programming was 80°C for 1 min, increasing 4.5°C/min to a final temperature of 320°C held for 20 min (total time 79.33 min). Pressure was 45 psi, the split flow through vent was 16 ml/min, the injector had a temperature of 300°C and the detector temperature was 330°C. The analysis was performed with nitrogen carrier gas and split injection.

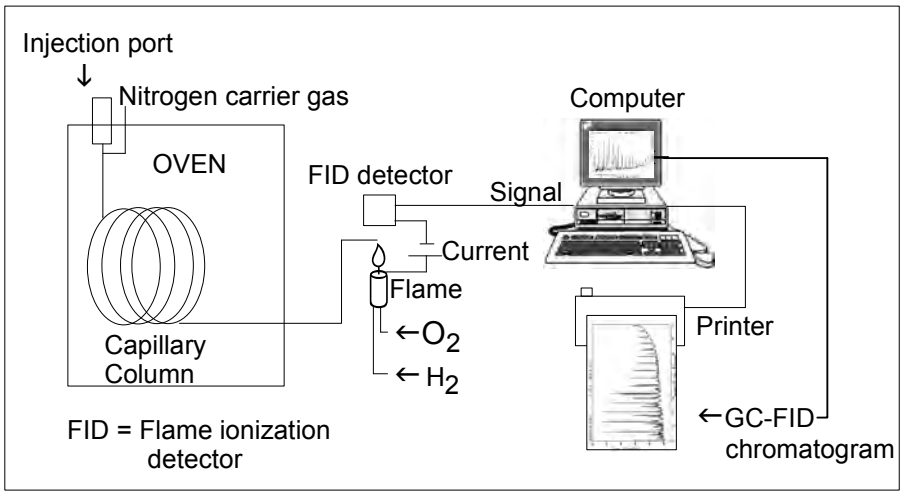

Figure C.1: *Principal sketch of the GC-FID instrument and its components with connected computer for data acquisition (Figure made by the author).*

C.2 Results

On the following pages can the results from the GC-FID analyses on source-rock samples close to sills at Svalbard be seen.

Abbreviations

- dil. = diluted
- n.d. = no data

Table C.1: GC-FID. Botneheia East, Central Spitsbergen; Profile with only a minor sill

Sample	nC17	nC18	Prist.	Phyt.	nC23	nC24	nC25	nC26	nC27	nC28	nC29	nC30	nC31	nC32
BH1-1	7.8	6.6	7.6	4.7	3.2	2.5	2.4	1.9	1.4	1.1	1	0.8	0.5	0.2
BH1-2	8.3	6.5	3.9	2.2	2.6	1.7	1.5	1.3	0.9	0.6	0.5	0.3	0.2	0.2
BH1-3	n.d.	n.d.	n.d.	n.d.	n.d.	n.d.	n.d.	n.d.	n.d.	n.d.	n.d.	n.d.	n.d.	n.d.
BH1-4	7.9	6.6	6.9	3.7	3.3	2.6	2.8	2	1.6	1.2	1	0.6	0.5	0.5
BH1-5	11.4	9	3.6	1.7	3.1	2.2	1.8	1.4	1	0.7	0.5	0.3	0.2	0.2
BH1-6	7.1	5.6	3.7	1.9	2.3	2.7	1.7	1.4	0.9	0.7	0.6	0.4	0.3	0.4
BH1-7	n.d.	n.d.	n.d.	n.d.	n.d.	n.d.	n.d.	n.d.	n.d.	n.d.	n.d.	n.d.	n.d.	n.d.
BH1-8	n.d.	n.d.	n.d.	n.d.	n.d.	n.d.	n.d.	n.d.	n.d.	n.d.	n.d.	n.d.	n.d.	n.d.
BH1-9	n.d.	n.d.	n.d.	n.d.	n.d.	n.d.	n.d.	n.d.	n.d.	n.d.	n.d.	n.d.	n.d.	n.d.
BH1-10	5.5	4.2	2.8	1.3	1.5	1.1	1	0.8	0.6	0.4	0.4	0.2	0.1	0.2
BH1-11	n.d.	n.d.	n.d.	n.d.	n.d.	n.d.	n.d.	n.d.	n.d.	n.d.	n.d.	n.d.	n.d.	n.d.
BH1-12	n.d.	n.d.	n.d.	n.d.	n.d.	n.d.	n.d.	n.d.	n.d.	n.d.	n.d.	n.d.	n.d.	n.d.
BH1-13	8.9	7.5	5	2.7	3.5	2.7	2.2	1.9	1.4	1.1	0.9	0.5	0.4	0.4
BH1-14	5.9	4.8	2	1.4	2	1.6	1.3	1.3	0.7	0.5	0.4	0.3	0.2	0.1
BH1-15	6	5.9	10.2	6.9	6.5	6.5	6.4	6.3	5.2	4	3.2	2.2	1.6	1.2
BH1-16	n.d.	n.d.	n.d.	n.d.	n.d.	n.d.	n.d.	n.d.	n.d.	n.d.	n.d.	n.d.	n.d.	n.d.
BH1-17	n.d.	n.d.	n.d.	n.d.	n.d.	n.d.	n.d.	n.d.	n.d.	n.d.	n.d.	n.d.	n.d.	n.d.
BH1-18	n.d.	n.d.	n.d.	n.d.	n.d.	n.d.	n.d.	n.d.	n.d.	n.d.	n.d.	n.d.	n.d.	n.d.
BH1-19	6.5	5.7	2.3	1.5	2.7	2.4	2.7	1.5	1.7	1.1	0.9	0.6	0.5	0.4
BH1-20	9.9	8.6	5.1	3	4.7	3.9	3.1	2.8	2	1.6	1.4	0.9	0.6	0.5
BH1-21	n.d.	n.d.	n.d.	n.d.	n.d.	n.d.	n.d.	n.d.	n.d.	n.d.	n.d.	n.d.	n.d.	n.d.
BH1-22	n.d.	n.d.	n.d.	n.d.	n.d.	n.d.	n.d.	n.d.	n.d.	n.d.	n.d.	n.d.	n.d.	n.d.
BH1-23	5.3	4.2	2.2	1.5	1.6	1	0.6	0.8	0.4	0.3	0.4	0.2	0.1	0.2
BH1-24	n.d.	n.d.	n.d.	n.d.	n.d.	n.d.	n.d.	n.d.	n.d.	n.d.	n.d.	n.d.	n.d.	n.d.
BH1-25	n.d.	n.d.	n.d.	n.d.	n.d.	n.d.	n.d.	n.d.	n.d.	n.d.	n.d.	n.d.	n.d.	n.d.
BH1-26	4.9	3.8	2	1.3	1.4	1	0.7	0.6	0.4	0.3	0.4	0.2	0.3	0.5
BH1-27	n.d.	n.d.	n.d.	n.d.	n.d.	n.d.	n.d.	n.d.	n.d.	n.d.	n.d.	n.d.	n.d.	n.d.

Table C.2: GC-FID. Botneheia East, Central Spitsbergen; Profile above sill

Sample	nC17	nC18	Prist.	Phyt.	nC23	nC24	nC25	nC26	nC27	nC28	nC29	nC30	nC31	nC32	nC33
BH2-1	13.5	13	10.1	6.5	10	8.5	7.3	6.8	6.1	4.8	4	3	2.4	1.8	1.3
BH2-2	n.d.	n.d.	n.d.	n.d.	n.d.	n.d.	n.d.	n.d.	n.d.	n.d.	n.d.	n.d.	n.d.	n.d.	n.d.
BH2-3	1.9	2.5	5.9	5.1	12.1	11.6	11	11.1	9.9	8.4	6.4	4.7	3.7	2.6	1.9
BH2-4	n.d.	n.d.	n.d.	n.d.	n.d.	n.d.	n.d.	n.d.	n.d.	n.d.	n.d.	n.d.	n.d.	n.d.	n.d.
BH2-5	3.6	3.6	7.2	4.5	2.3	2.2	2.4	2.5	2.6	2.4	2	1.4	1.1	0.6	0.5
BH2-6	n.d.	n.d.	n.d.	n.d.	n.d.	n.d.	n.d.	n.d.	n.d.	n.d.	n.d.	n.d	n.d.	n.d.	n.d.
BH2-7	dil.	dil.	dil.	dil.	dil.	dil.	dil.	dil.	dil.	dil.	dil.	dil.	dil.	dil.	dil.
BH2-8	dil.	dil.	dil.	dil.	dil.	dil.	dil.	dil.	dil.	dil.	dil.	dil.	dil.	dil.	dil.
BH2-9	dil.	dil.	dil.	dil.	dil.	dil.	dil.	dil.	dil.	dil.	dil.	dil.	dil.	dil.	dil.
BH2-10	dil.	dil.	dil.	dil.	dil.	dil.	dil.	dil.	dil.	dil.	dil.	dil.	dil.	dil.	dil.
BH2-11	dil.	dil.	dil.	dil.	dil.	dil.	dil.	dil.	dil.	dil.	dil.	dil.	dil.	dil.	
BH2-12	dil.	dil.	dil.	dil.	dil.	dil.	dil.	dil.	dil.	dil.	dil.	dil.	dil.	dil.	
BH2-13	n.d.	n.d.	n.d.	n.d.	n.d.	n.d.	n.d.	n.d.	n.d.	n.d.	n.d.	n.d.	n.d.	n.d.	
BH2-14	dil.	dil.	dil.	dil.	dil.	dil.	dil.	dil.	dil.	dil.	dil.	dil.	dil.	dil.	
BH2-15	4.5	3.5	11.3	6.9	2.1	1.8	1.6	2.8	3.3	3.1	2.5	1.6	1.2	1.1	
BH2-16	n.d.	n.d.	n.d.	n.d.	n.d.	n.d.	n.d.	n.d.	n.d.	n.d.	n.d.	n.d.	n.d.	n.d.	n.d.
BH2-17	n.d.	n.d.	n.d.	n.d.	n.d.	n.d.	n.d.	n.d.	n.d.	n.d.	n.d.	n.d.	n.d.	n.d.	n.d.
BH2-18	dil.	dil.	dil.	dil.	dil.	dil.	dil.	dil.	dil.	dil.	dil.	dil.	dil.	dil.	
BH2-19	dil.	dil.	dil.	dil.	dil.	dil.	dil.	dil.	dil.	dil.	dil.	dil.	dil.	dil.	
BH2-20	8	6.5	2.4	1.1	3	2.4	1.9	1.6	1.2	1	0.9	0.5	0.4	0.3	
BH2-21	4.5	3.5	1.4	0.9	1.2	0.9	0.7	0.6	0.4	0.4	0.3	0.3	0.2	0.2	
BH2-22	5.5	4.5	1.5	0.6	1.7	1.2	0.9	0.9	0.8	0.5	0.5	0.3	0.3	0.2	
BH2-23	dil.	dil.	dil.	dil.	dil.	dil.	dil.	dil.	dil.	dil.	dil.	dil.	dil.	dil.	
BH2-24	dil.	dil.	dil.	dil.	dil.	dil.	dil.	dil.	dil.	dil.	dil.	dil.	dil.	dil.	
BH2-25	dil.	dil.	dil.	dil.	dil.	dil.	dil.	dil.	dil.	dil.	dil.	dil.	dil.	dil.	
BH2-26	dil.	dil.	dil.	dil.	dil.	dil.	dil.	dil.	dil.	dil.	dil.	dil.	dil.	dil.	
BH2-27	8.8	8.2	4.6	3.6	4.8	4.1	3.2	3	2.9	2	1.8	1.2	1	0.8	
BH2-28	5	4.2	2.6	1.7	2	1.5	1.3	1.3	1	0.8	0.8	0.5	0.4	0.3	
BH2-29	4.4	3.7	2	1.2	1.3	1	0.9	0.9	0.7	0.5	0.5	0.3	0.4	0.3	
BH2-30	dil.	dil.	dil.	dil.	dil.	dil.	dil.	dil.	dil.	dil.	dil.	dil.	dil.	dil.	

Table C.3: GC-FID. Krefftberget, Barentsøya: Profile above sill

Sample	nC17	nC18	Prist.	Phyt.	nC23	nC24	nC25	nC26	nC27	nC28	nC29	nC30	nC31	nC32	nC33
KRB-1a	dil.	dil.	dil.	dil.	dil.	dil.	dil.	dil.	dil.	dil.	dil.	dil.	dil.	dil.	
KRB-1b	dil.	dil.	dil.	dil.	dil.	dil.	dil.	dil.	dil.	dil.	dil.	dil.	dil.	dil.	
KRB-1b(dupl)	dil.	dil.	dil.	dil.	dil.	dil.	dil.	dil.	dil.	dil.	dil.	dil.	dil.	dil.	
KRB-1c	11.8	11	4.1	2.1	5.7	4.6	3.6	3.1	2.4	1.8	1.4	1	0.9	0.9	
KRB-2	dil.	dil.	dil.	dil.	dil.	dil.	dil.	dil.	dil.	dil.	dil.	dil.	dil.	dil.	
KRB-3a	4.2	3.5	8.2	4.2	1.8	1.5	1.2	1.1	0.9	0.5	0.4	0.2	0.3	0.3	
KRB-3b	3.3	2.9	5.8	3.1	1.5	1.2	0.8	0.7	0.7	0.4	0.4	0.3	0.3		
KRB-4	n.d.	n.d.	n.d.	n.d.	n.d.	n.d.	n.d.	n.d.	n.d.	n.d.	n.d.	n.d.	n.d.	n.d.	
KRB-5	n.d.	n.d.	n.d.	n.d.	n.d.	n.d.	n.d.	n.d.	n.d.	n.d.	n.d.	n.d.	n.d.	n.d.	
KRB-6	n.d.	n.d.	n.d.	n.d.	n.d.	n.d.	n.d.	n.d.	n.d.	n.d.	n.d.	n.d.	n.d.	n.d.	
KRB-7	n.d.	n.d.	n.d.	n.d.	n.d.	n.d.	n.d.	n.d.	n.d.	n.d.	n.d.	n.d.	n.d.	n.d.	
KRB-8	9.8	7.6	14.9	8.2	3.1	2.2	1.5	1.1	0.7	0.2	0.3	0.2	0.2	0.2	
KRB-8(dupl)	8.7	6.9	13.8	7.5	3	2.1	1.6	1.1	0.7	0.3	0.2	0.2	0.3	0.2	
KRB-9	8.3	6.7	10.7	5.8	2.1	1.4	0.8	0.4	0.3	0.1	0.1	0.1	0.1	0.1	
KRB-10	n.d.	n.d.	n.d.	n.d.	n.d.	n.d.	n.d.	n.d.	n.d.	n.d.	n.d.	n.d.	n.d.	n.d.	
KRB-11	7.8	5.6	6.5	3.3	0.5	0.2	0.5	0.1	0.2	0.1	0.1	0.1	0.1	0.1	
KRB-12	2.3	1.6	4.8	2.3	0.2	0.1	0.2	0.1	0.2	0.1	0.1	0.1	0.2	0.2	
KRB-13	n.d.	n.d.	n.d.	n.d.	n.d.	n.d.	n.d.	n.d.	n.d.	n.d.	n.d.	n.d.	n.d.	n.d.	
KRB-14	n.d.	n.d.	n.d.	n.d.	n.d.	n.d.	n.d.	n.d.	n.d.	n.d.	n.d.	n.d.	n.d.	n.d.	
KRB-15	n.d.	n.d.	n.d.	n.d.	n.d.	n.d.	n.d.	n.d.	n.d.	n.d.	n.d.	n.d.	n.d.	n.d.	
KRB-16	n.d.	n.d.	n.d.	n.d.	n.d.	n.d.	n.d.	n.d.	n.d.	n.d.	n.d.	n.d.	n.d.	n.d.	
KRB-17															
KRB-17(dupl)															
KRB-18a	n.d.	n.d.	n.d.	n.d.	n.d.	n.d.	n.d.	n.d.	n.d.	n.d.	n.d.	n.d.	n.d.	n.d.	
KRB-18b															
KRB-19	n.d.	n.d.	n.d.	n.d.	n.d.	n.d.	n.d.	n.d.	n.d.	n.d.	n.d.	n.d.	n.d.	n.d.	
KRB-20															
KRB-20(dupl)															

Table C.4: C.3 on the page before cont.

Sample	nC17	nC18	Prist.	Phyt.	nC23	nC24	nC25	nC26	nC27	nC28	nC29	nC30	nC31	nC32	nC33
KRB-21	n.d.	n.d.	n.d.	n.d.	n.d.	n.d.	n.d.	n.d.	n.d.	n.d.	n.d.	n.d.	n.d.	n.d.	
KRB-22	11.5	10.2	2.2	1.2	5.9	4.9	4.2	3.7	3	2.4	1.8	1.4	1	0.7	
KRB-23	12.7	11.4	3.2	1.8	6.2	5.3	4.4	4.1	3.2	2.6	2	1.6	1.1	0.7	
KRB-24	12.6	11.2	4.2	2.2	6.3	5.2	4.3	4	3.1	2.4	2	1.3	1.1	0.6	
KRB-24(dupl)	10.4	9.6	3.6	1.8	5.2	4.6	3.8	3.4	2.6	2.2	1.6	1.1	0.8	0.6	
KRB-25	n.d.	n.d.	n.d.	n.d.	n.d.	n.d.	n.d.	n.d.	n.d.	n.d.	n.d.	n.d.	n.d.	n.d.	
KRB-26	7.1	6	2.6	1.2	3.2	2.6	2.4	1.9	1.4	1	0.7	0.5	0.5	0.3	

Table C.5: GC-FID. Teistberget, Eastern Spitsbergen; Profile above sill

Sample	nC17	nC18	Prist.	Phyt.	nC23	nC24	nC25	nC26	nC27	nC28	nC29	nC30	nC31	nC32	nC33
TBU-1	2.4	1.9	0.4	0.4	1.2	1.5	1.6	2.2	3	3.5	3.5	2.9	2.5	2.8	1.3
TBU-2	n.d.	n.d.	n.d.	n.d.	n.d.	n.d.	n.d.	n.d.	n.d.	n.d.	n.d.	n.d.	n.d.	n.d.	n.d.
TBU-3	2.5	1.9	0.7	0.6	1.4	1.8	2.3	3.2	4.2	5.2	5.2	4.2	3.4	2.2	1.7
TBU-4	2.6	1.8	0.4	0.3	0.6	0.7	1	2.5	3.6	4.2	3.7	2.8	2.1	1.4	0.9
TBU-4(dupl)	3.2	2.3	0.6	0.5	0.9	0.9	3.1	2.7	4.5	5.2	4.7	3.5	2.7	1.9	1.1
TBU-5	n.d.	n.d.	n.d.	n.d.	n.d.	n.d.	n.d.	n.d.	n.d.	n.d.	n.d.	n.d.	n.d.	n.d.	
TBU-6	9.7	8.5	1.4	0.6	4.5	3.5	3.1	2.6	2.1	1.6	1.3	0.9	0.7	0.4	0.2
TBU-7	7.8	6.8	4.4	2.8	4	3.4	2.5	2.6	2.1	1.8	1.2	0.9	0.7	0.4	0.3
TBU-8	n.d.	n.d.	n.d.	n.d.	n.d.	n.d.	n.d.	n.d.	n.d.	n.d.	n.d.	n.d.	n.d.	n.d.	
TBU-9	0.6	0.6	5.8	4.5	1.4	2.4	3.3	4.1	4.3	3.8	2.8	1.9	1.5	1.2	0.8
TBU-10	3.7	3	2	1.4	1.1	0.8	0.6	0.6	0.4	0.4	0.3	0.2	0.4	0.5	0.2
TBU-11	n.d.	n.d.	n.d.	n.d.	n.d.	n.d.	n.d.	n.d.	n.d.	n.d.	n.d.	n.d.	n.d.	n.d.	

Table C.6: GC-FID. Teistberget, Eastern Spitsbergen; Profile below sill

Sample	nC17	nC18	Prist.	Phyt.	nC23	nC24	nC25	nC26	nC27	nC28	nC29	nC30	nC31	nC32	nC33
TBL-1	dil.	dil.	dil.	dil.	dil.	dil.	dil.	dil.	dil.	dil.	dil.	dil.	dil.	dil.	
TBL-1(dupl)	dil.	dil.	dil.	dil.	dil.	dil.	dil.	dil.	dil.	dil.	dil.	dil.	dil.	dil.	
TBL-2	n.d.	n.d.	n.d.	n.d.	n.d.	n.d.	n.d.	n.d.	n.d.	n.d.	n.d.	n.d.	n.d.	n.d.	
TBL-3	7.9	8.4	5	3.2	9.2	8.4	7.8	6.9	6	4.9	3.6	2.4	1.9	1.2	
TBL-4	12.3	11.9	8.9	5.6	9.8	8.4	7.6	6.9	5.7	5	3.9	3.9	2.4	1.5	
TBL-5	9.9	9.3	8.7	6.5	9.7	8.4	7.7	7.3	7	4.8	3.6	2.4	2	1.4	
TBL-6	10.2	9	11.1	6.6	5.2	4.4	3.6	3.6	3	2.2	1.6	1.1	0.9	0.5	
TBL-7	6.9	6.1	11.2	7	4.2	3.7	3.2	3.2	2.4	2	1.3	0.9	0.6	0.4	
TBL-8	4.7	4.2	7.2	4.7	3.3	3	2.4	2.3	1.8	1.4	1.1	0.7	0.6	0.4	
TBL-9	dil.	dil.	dil.	dil.	dil.	dil.	dil.	dil.	dil.	dil.	dil.	dil.	dil.	dil.	
TBL-10	n.d.	n.d.	n.d.	n.d.	n.d.	n.d.	n.d.	n.d.	n.d.	n.d.	n.d.	n.d.	n.d.	n.d.	
TBL-11	n.d.	n.d.	n.d.	n.d.	n.d.	n.d.	n.d.	n.d.	n.d.	n.d.	n.d.	n.d.	n.d.	n.d.	

Table C.7: GC-FID. Domen, Eastern Spitsbergen; Profile above sill

Sample	nC17	nC18	Prist.	Phyt.	nC23	nC24	nC25	nC26	nC27	nC28	nC29	nC30	nC31	nC32	nC33
DOM-1	n.d.	n.d.	n.d.	n.d.	n.d.	n.d.	n.d.	n.d.	n.d.	n.d.	n.d.	n.d.	n.d.	n.d.	
DOM-2	n.d.	n.d.	n.d.	n.d.	n.d.	n.d.	n.d.	n.d.	n.d.	n.d.	n.d.	n.d.	n.d.	n.d.	
DOM-3	8.1	7.4	6.8	2.8	6.4	5.7	5.2	4.4	4.3	3.2	2.9	1.6	1.2	0.7	
DOM-3(dupl)	9.2	8.4	7.6	3.3	7.2	6.2	6	4.9	4.6	3.5	3.2	1.8	1.4	0.8	
DOM-4	8.1	7.4	9.5	4.4	7.4	6.8	6.2	5.5	5.4	4.2	4.2	2.3	1.9	1.1	
DOM-5	n.d.	n.d.	n.d.	n.d.	n.d.	n.d.	n.d.	n.d.	n.d.	n.d.	n.d.	n.d.	n.d.	n.d.	
DOM-6	dil.	dil.	dil.	dil.	dil.	dil.	dil.	dil.	dil.	dil.	dil.	dil.	dil.	dil.	
DOM-7	n.d.	n.d.	n.d.	n.d.	n.d.	n.d.	n.d.	n.d.	n.d.	n.d.	n.d.	n.d.	n.d.	n.d.	
DOM-8	n.d.	n.d.	n.d.	n.d.	n.d.	n.d.	n.d.	n.d.	n.d.	n.d.	n.d.	n.d.	n.d.	n.d.	
DOM-9a	2.4	2.1	3.1	0.9	1.8	1.5	1.5	1.2	1.2	0.6	0.8	0.5	0.3	0.2	
DOM-9b	n.d.	n.d.	n.d.	n.d.	n.d.	n.d.	n.d.	n.d.	n.d.	n.d.	n.d.	n.d.	n.d.	n.d.	
DOM-10	n.d.	n.d.	n.d.	n.d.	n.d.	n.d.	n.d.	n.d.	n.d.	n.d.	n.d.	n.d.	n.d.	n.d.	
DOM-11	5.8	5.4	2.4	1.6	4	4	3.5	3.8	3.5	3.4	3.2	2.8	2	1.5	

Table C.8: GC-FID. Høgrinden South, Barentsøya

Sample	nC17	nC18	Prist.	Phyt.	nC23	nC24	nC25	nC26	nC27	nC28	nC29	nC30	nC31	nC32	nC33
HØB1-1	n.d.	n.d.	n.d.	n.d.	n.d.	n.d.	n.d.	n.d.	n.d.	n.d.	n.d.	n.d.	n.d.	n.d.	
HØB1-2	n.d.	n.d.	n.d.	n.d.	n.d.	n.d.	n.d.	n.d.	n.d.	n.d.	n.d.	n.d.	n.d.	n.d.	
HØB1-3	n.d.	n.d.	n.d.	n.d.	n.d.	n.d.	n.d.	n.d.	n.d.	n.d.	n.d.	n.d.	n.d.	n.d.	
HØB1-4	n.d.	n.d.	n.d.	n.d.	n.d.	n.d.	n.d.	n.d.	n.d.	n.d.	n.d.	n.d.	n.d.	n.d.	
HØB1-5	n.d.	n.d.	n.d.	n.d.	n.d.	n.d.	n.d.	n.d.	n.d.	n.d.	n.d.	n.d.	n.d.	n.d.	
HØB1-6	4.4	3.9	5.7	3	2.5	2.1	1.7	1.5	1.4	0.6	0.9	0.4	0.3	0.5	
HØB1-7	4.3	3.7	5.1	2.6	2.2	1.8	1.1	1.2	0.8	0.6	0.5	0.4	0.3	0.4	
HØB1-8	1.7	1.4	5.2	2.7	0.9	0.7	0.6	0.7	0.8	0.7	0.6	0.4	0.3	0.4	
HØB1-9	10.1	8.2	11.1	5.6	4.4	3.7	2.4	2.4	1.8	1.2	1.3	0.8	0.6	0.9	
HØB1-10	8.1	6.8	7.4	4	3	2.4	1.5	1.6	1.4	0.8	0.9	0.4	0.8	0.6	
HØB1-11	8.1	6.2	7.3	3.9	2.7	2.4	1.7	1.4	1.2	0.9	0.8	0.5	0.5	0.6	
HØB1-12	7	5.4	7.3	3.5	2.5	2	1.3	1.2	1	0.7	0.6	0.5	0.5	0.6	
HØB1-13	3.7	3.1	3.7	1.8	1.4	1	0.7	0.6	0.6	0.4	0.5	0.3	0.3	0.4	

Table C.9: GC-FID. Høgrinden South, Barentsøya

Sample	nC17	nC18	Prist.	Phyt.	nC23	nC24	nC25	nC26	nC27	nC28	nC29	nC30	nC31	nC32	nC33
HØB2-1	n.d.	n.d.	n.d.	n.d.	n.d.	n.d.	n.d.	n.d.	n.d.	n.d.	n.d.	n.d.	n.d.	n.d.	
HØB2-2	n.d.	n.d.	n.d.	n.d.	n.d.	n.d.	n.d.	n.d.	n.d.	n.d.	n.d.	n.d.	n.d.	n.d.	
HØB2-3	n.d.	n.d.	n.d.	n.d.	n.d.	n.d.	n.d.	n.d.	n.d.	n.d.	n.d.	n.d.	n.d.	n.d.	
HØB2-4	n.d.	n.d.	n.d.	n.d.	n.d.	n.d.	n.d.	n.d.	n.d.	n.d.	n.d.	n.d.	n.d.	n.d.	
HØB2-5	4.60	4.4	9	4.9	3.6	3.2	2.7	2.4	2	1.7	1.3	0.7	0.5	0.4	
HØB2-6	4.9	4.2	6.8	3.4	2.7	2.4	1.7	1.7	1.1	0.9	0.9	0.6	0.5	0.5	
HØB2-7	5.3	4.2	6.2	2.9	2.2	1.9	1.4	1.2	0.9	0.7	0.6	0.4	0.4	0.4	
HØB2-8	5.9	5.1	9.1	4.6	3.4	3.2	2.4	2.3	1.8	1.6	1.2	0.8	0.6	0.5	

Table C.10: GC-FID. Høgrinden South, Barentsøya; sampled laterally along a single horizon

Sample	nC17	nC18	Prist.	Phyt.	nC23	nC24	nC25	nC26	nC27	nC28	nC29	nC30	nC31	nC32	nC33
HØB3-1	n.d.	n.d.	n.d.	n.d.	n.d.	n.d.	n.d.	n.d.	n.d.	n.d.	n.d.	n.d.	n.d.	n.d.	
HØB3-2(dupl)	1.6	1.1	3.1	2	0.5	0.6	0.8	1.2	1.5	2	3.2	2.5	2.6	2.1	1.3
HØB3-2	1.6	1.2	3.1	2	0.5	0.8	0.4	1.2	1.5	2	2.9	2.3	2.5	1.9	1.3
HØB3-3	1.8	1.4	2.1	0.6	0.5	0.6	0.6	0.5	0.4	0.4	1.3	0.2	0.9	1.5	1
HØB3-4	1.5	1.2	6.1	4	1	1.1	1.1	2.3	2.5	2.7	2.4	1.1	1.2	1.1	0.7
HØB3-5	2.6	2.3	12.4	7	2.6	2.7	2.5	2.6	2	1.7	1.4	0.9	0.6	0.4	0.3
HØB3-6	9.8	8.5	12.3	6	5	4.5	3	2.7	2	1.5	1.2	0.7	0.5	0.5	0.3
HØB3-7	7.5	6	7.7	3.7	3	2.4	1.6	1.3	0.7	0.6	0.5	0.3	0.2	0.2	0.1
HØB3-8	8.6	7.2	10	4.4	4.2	3.4	2.4	2.1	1.4	1.1	0.9	0.6	0.4	0.6	0.2
HØB3-9	8.8	7.2	8.5	3.8	3.8	3.1	2.2	1.9	1.2	0.9	0.8	0.4	0.3	0.5	0.2

Table C.11: GC-FID. Northern Kreftberget, Barentsøya; Profile without sill

Sample	nC17	nC18	Prist.	Phyt.	nC23	nC24	nC25	nC26	nC27	nC28	nC29	nC30	nC31	nC32	nC33
NKB-1	8.4	6.7	10.5	5.1	3.4	2.8	2.2	1.7	1.3	1.1	0.9	0.6	0.8	0.5	0.3
NKB-2	6.8	5.4	7.8	3.5	2.8	2.2	1.5	1.3	0.8	0.7	0.5	0.4	0.2	0.3	0.1
NKB-3	5.3	4	8.5	4.3	2.1	1.8	1.1	1.1	0.7	0.7	0.7	0.5	0.4	0.6	0.4
NKB-4	6.2	5	9.6	5.1	3.1	2.6	1.7	1.7	1.2	1	0.7	0.7	0.5	0.6	0.3
NKB-5	7.2	6	10.4	5.6	3.9	3.4	2.4	2.2	1.4	1.1	1.1	0.9	0.4	0.7	0.3
NKB-6	7	5.2	7.9	3.6	2.6	2.2	1.6	1.4	0.9	0.7	0.9	0.5	0.6	0.6	0.3

Appendix D

Parameters, calculated from GC-FID data

D.1 Analysis

Pristane and phytane According to the traditional view, these molecules are inherited from phytol, a side chain of the chlorophyll molecule that separates from the porphyrine structure after deposition (Tissot and Welte, 1984). More recently, it has been suggested that pristane and phytane also may have a bacterial origin (Peters and Moldowan, 1993). The depositional environment determines the further fate of phytol (Figure D.1). The pristane/phytane ratio (Pr/Ph) indicates the organic facies of the depositional environment. Pr/Ph < 1 indicates hypersaline, anoxic or carbonate setting, Pr/Ph > 3 is typical of hydrocarbons from deltaic organic matter or humic dominated sediments, while intermediate values directs the attention to "normal" marine sediments. Plots made of these calculated parameters must be supported by other data to be conclusive.

Pr/n-C_{17} and Ph/n-C_{18} are additional parameters helping to pinpoint the source-rock facies, maturity and the level of biodegradation of petroleum. During maturation, the Pr/n-C_{17} and Ph/n-C_{18} ratios will become depressed due to the thermal breakdown of isoprenoids (Pr and Ph) before n-alkanes (Tissot and Welte, 1984).

CPI The Carbon Preference Index (CPI) can be used to deduce if an oil or extract is thermally immature (values considerably deviating 1.0). A hypersaline or carbonate environment may cause a value below 1.0, while a silisiclastic lithology generally gives a CPI > 1 until a maturity of about 0.8% Ro, at which stage unity is approached. Most mature oils will have CPI = 1.0 (Peters and Moldowan, 1993).

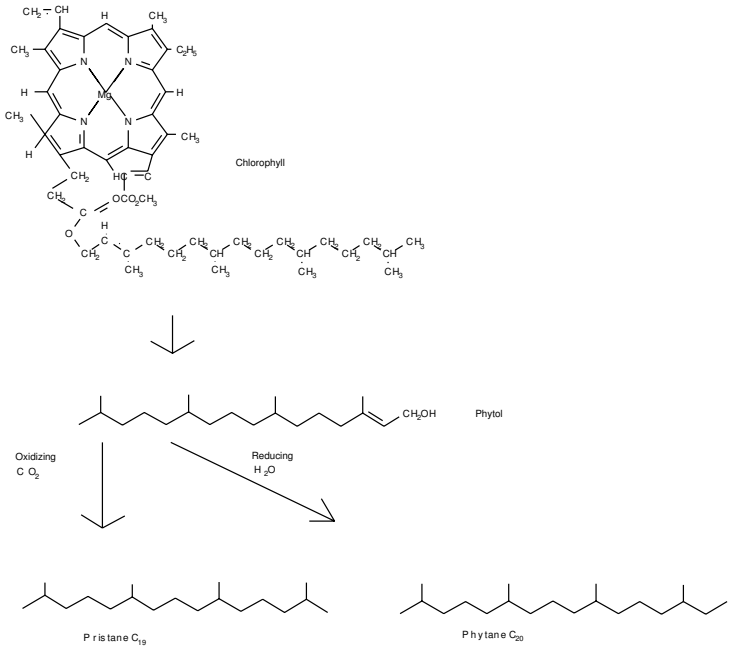

Figure D.1: *Pristane and phytane originates generally from chlorophyll via phytol (Peters and Moldowan, 1993), (Figure made by the author).*

D.2 Results

The results for parameters calculated on the basis of the GC-FID data, can be viewed on the following pages.

Table D.1: Parameters, GC-FID. Botneheia East, Central Spitsbergen; Profile with only a minor sill

Sample	nC17/nC18	Prist/nC17	Phyt/nC18	Prist/Phyt	CPI	$CPI_{Philipi}$	CPI_1	CPI_2	nC17/nC31
BH1-1	1.18	0.97	0.71	1.62	1.08	1.05	1.27	1.38	15.60
BH1-2	1.28	0.47	0.34	1.77	1.04	1.11	1.37	1.45	41.50
BH1-3	n.d.	n.d.	n.d.	n.d.	n.d.	n.d	n.d.	n.d.	n.d.
BH1-4	1.20	0.87	0.56	1.86	1.15	1.11	1.33	1.35	15.80
BH1-5	1.27	0.32	0.19	2.12	1.05	1.00	1.36	1.42	57.00
BH1-6	1.27	0.52	0.34	1.95	0.94	1.09	0.98	1.20	23.67
BH1-7	n.d.	n.d.	n.d.	n.d.	n.d.	n.d.	n.d.	n.d.	n.d.
BH1-8	n.d.	n.d.	n.d.	n.d.	n.d.	n.d.	n.d.	n.d.	n.d.
BH1-9	n.d.	n.d.	n.d.	n.d.	n.d.	n.d.	n.d.	n.d.	n.d.
BH1-10	1.31	0.51	0.31	2.15	1.08	1.33	1.32	1.38	55.00
BH1-11	n.d.	n.d.	n.d.	n.d.	n.d.	n.d.	n.d.	n.d.	n.d.
BH1-12	n.d.	n.d.	n.d.	n.d.	n.d.	n.d.	n.d.	n.d.	n.d.
BH1-13	1.19	0.56	0.36	1.85	1.02	1.13	1.24	1.35	22.25
BH1-14	1.23	0.34	0.29	1.43	0.94	1.00	1.14	1.44	29.50
BH1-15	1.02	1.70	1.17	1.48	1.03	1.03	1.01	1.35	3.75
BH1-16	n.d.	n.d.	n.d.	n.d.	n.d.	n.d.	n.d.	n.d.	n.d.
BH1-17	n.d.	n.d.	n.d.	n.d.	n.d.	n.d.	n.d.	n.d.	n.d.
BH1-18	n.d.	n.d.	n.d.	n.d.	n.d.	n.d.	n.d.	n.d.	n.d.
BH1-19	1.14	0.35	0.26	1.53	1.32	1.06	1.38	1.48	13.00
BH1-20	1.15	0.52	0.35	1.70	1.00	1.12	1.16	1.33	16.50
BH1-21	n.d.	n.d.	n.d.	n.d.	n.d.	n.d.	n.d.	n.d.	n.d.
BH1-22	n.d.	n.d.	n.d.	n.d.	n.d.	n.d.	n.d.	n.d.	n.d.
BH1-23	1.26	0.42	0.36	1.47	0.83	1.60	1.31	1.10	53.00
BH1-24	n.d.	n.d.	n.d.	n.d.	n.d.	n.d.	n.d.	n.d.	n.d.
BH1-25	n.d.	n.d.	n.d.	n.d.	n.d.	n.d.	n.d.	n.d.	n.d.
BH1-26	1.29	0.41	0.34	1.54	0.99	1.60	1.31	1.10	16.33
BH1-27	n.d.	n.d.	n.d.	n.d.	n.d.	n.d.	n.d.	n.d.	n.d.

Table D.2: Parameters, GC-FID. Botneheia East, Central Spitsbergen; Profile above sill

Sample	nC17/nC18	Prist/nC17	Phyt/nC18	Prist/Phyt	CPI	$CPI_{Philipi}$	CPI_1	CPI_2	nC17/nC31
BH2-1	1.04	0.75	0.50	1.55	1.03	1.03	1.13	1.30	5.63
BH2-2	n.d.	n.d.	n.d.	n.d.	n.d.	n.d.	n.d.	n.d.	n.d.
BH2-3	0.76	3.11	2.04	1.16	1.01	0.98	1.02	1.27	0.51
BH2-4	n.d.	n.d.	n.d.	n.d.	n.d.	n.d.	n.d.	n.d.	n.d.
BH2-5	1.00	0.50	1.60	1.96	1.06	1.05	1.00	1.30	3.27
BH2-6	n.d.	n.d.	n.d.	n.d.	n.d.	n.d.	n.d.	n.d.	n.d.
BH2-7	n.d.	n.d.	n.d.	n.d.	n.d.	n.d.	n.d.	n.d.	n.d.
BH2-8	n.d.	n.d.	n.d.	n.d.	n.d.	n.d.	n.d.	n.d.	n.d.
BH2-9	n.d.	n.d.	n.d.	n.d.	n.d.	n.d.	n.d.	n.d.	n.d.
BH2-10	n.d.	n.d.	n.d.	n.d.	n.d.	n.d.	n.d.	n.d.	n.d.
BH2-11	n.d.	n.d.	n.d.	n.d.	n.d.	n.d.	n.d.	n.d.	n.d.
BH2-12	n.d.	n.d.	n.d.	n.d.	n.d.	n.d.	n.d.	n.d.	n.d.
BH2-13	n.d.	n.d.	n.d.	n.d.	n.d.	n.d.	n.d.	n.d.	n.d.
BH2-14	n.d.	n.d.	n.d.	n.d.	n.d.	n.d.	n.d.	n.d.	n.d.
BH2-15	1.29	2.51	1.97	1.64	0.96	1.06	0.80	1.21	3.75
BH2-16	n.d.	n.d.	n.d.	n.d.	n.d.	n.d.	n.d.	n.d.	n.d.
BH2-17	n.d.	n.d.	n.d.	n.d.	n.d.	n.d.	n.d.	n.d.	n.d.
BH2-18	n.d.	n.d.	n.d.	n.d.	n.d.	n.d.	n.d.	n.d.	n.d.
BH2-19	n.d.	n.d.	n.d.	n.d.	n.d.	n.d.	n.d.	n.d.	n.d.
BH2-20	1.23	0.30	0.17	2.18	1.05	1.20	1.23	1.39	20.00
BH2-21	1.29	0.31	0.26	1.56	0.90	0.86	1.27	1.00	22.50
BH2-22	1.22	0.27	0.13	2.50	1.09	1.25	1.24	1.60	18.33
BH2-23	n.d.	n.d.	n.d.	n.d.	n.d.	n.d.	n.d.	n.d.	n.d.
BH2-24	n.d.	n.d.	n.d.	n.d.	n.d.	n.d.	n.d.	n.d.	n.d.
BH2-25	n.d.	n.d.	n.d.	n.d.	n.d.	n.d.	n.d.	n.d.	n.d.
BH2-26	n.d.	n.d.	n.d.	n.d.	n.d.	n.d.	n.d.	n.d.	n.d.
BH2-27	1.07	0.52	0.44	1.28	1.07	1.13	1.13	1.43	8.80
BH2-28	1.19	0.52	0.40	1.53	1.03	1.23	1.18	1.38	12.50
BH2-29	1.19	0.45	0.32	1.67	1.09	1.25	1.16	1.45	11.00
BH2-30	n.d.	n.d.	n.d.	n.d.	n.d.	n.d.	n.d.	n.d.	n.d.

Table D.3: Parameters, GC-FID. Krefftberget, Barentsøya: Profile above sill

Sample	nC17/nC18	Prist/nC17	Phyt/nC18	Prist/Phyt	CPI	$CPI_{Philipi}$	CPI_1	CPI_2	nC17/nC31
KRB-1a	n.d.	n.d.	n.d.	n.d.	n.d.	n.d.	n.d.	n.d.	n.d.
KRB-1b	n.d.	n.d.	n.d.	n.d.	n.d.	n.d.	n.d.	n.d.	n.d.
KRB-1b(dupl)	n.d.	n.d.	n.d.	n.d.	n.d.	n.d.	n.d.	n.d.	n.d.
KRB-1c	1.07	0.35	0.19	1.95	1.01	1.00	1.21	1.27	13.11
KRB-2	n.d.	n.d.	n.d.	n.d.	n.d.	n.d.	n.d.	n.d.	n.d.
KRB-3a	1.20	1.95	1.20	1.95	1.09	1.14	1.15	1.60	14.00
KRB-3b	1.14	1.76	1.07	1.87	1.21	1.14	1.21	2.00	11.00
KRB-4	n.d.	n.d.	n.d.	n.d.	n.d.	n.d.	n.d.	n.d.	n.d.
KRB-5	n.d.	n.d.	n.d.	n.d.	n.d.	n.d.	n.d.	n.d.	n.d.
KRB-6	n.d.	n.d.	n.d.	n.d.	n.d.	n.d.	n.d.	n.d.	n.d.
KRB-7	n.d.	n.d.	n.d.	n.d.	n.d.	n.d.	n.d.	n.d.	n.d.
KRB-8	1.29	1.52	1.08	1.82	1.16	1.50	1.39	2.00	49.00
KRB-8(dupl)	1.26	1.59	1.09	1.84	1.16	0.80	1.44	1.71	29.00
KRB-9	1.24	1.29	0.87	1.84	1.25	1.00	1.61	1.67	83.00
KRB-10	n.d.	n.d.	n.d.	n.d.	n.d.	n.d.	n.d.	n.d.	n.d.
KRB-11	1.39	0.83	0.59	1.97	2.03	1.00	3.33	1.33	78.00
KRB-12	1.44	2.09	1.44	2.09	1.58	1.00	2.00	1.25	11.50
KRB-13	n.d.	n.d.	n.d.	n.d.	n.d.	n.d.	n.d.	n.d.	n.d.
KRB-14	n.d.	n.d.	n.d.	n.d.	n.d.	n.d.	n.d.	n.d.	n.d.
KRB-15	n.d.	n.d.	n.d.	n.d.	n.d.	n.d.	n.d.	n.d.	n.d.
KRB-16	n.d.	n.d.	n.d.	n.d.	n.d.	n.d.	n.d.	n.d.	n.d.
KRB-17	n.d.	n.d.	n.d.	n.d.	n.d.	n.d.	n.d.	n.d.	n.d.
KRB-17(dupl)	n.d.	n.d.	n.d.	n.d.	n.d.	n.d.	n.d.	n.d.	n.d.
KRB-18a	n.d.	n.d.	n.d.	n.d.	n.d.	n.d.	n.d.	n.d.	n.d.
KRB-18b	n.d.	n.d.	n.d.	n.d.	n.d.	n.d.	n.d.	n.d.	n.d.
KRB-19	n.d.	n.d.	n.d.	n.d.	n.d.	n.d.	n.d.	n.d.	n.d.

Table D.4: D.3 cont.

Sample	nC17/nC18	Prist/nC17	Phyt/nC18	Prist/Phyt	CPI	$CPI_{Philipi}$	CPI_1	CPI_2	nC17/nC31
KRB-20	n.d.	n.d.	n.d.	n.d.	n.d.	n.d.	n.d.	n.d.	n.d.
KRB-20(dupl)	n.d.	n.d.	n.d.	n.d.	n.d.	n.d.	n.d.	n.d.	n.d.
KRB-21	n.d.	n.d.	n.d.	n.d.	n.d.	n.d.	n.d.	n.d.	n.d.
KRB-22	1.13	0.19	0.12	1.83	1.01	0.95	1.17	1.29	11.50
KRB-23	1.11	0.25	0.16	1.78	0.99	0.95	1.13	1.29	11.55
KRB-24	1.13	0.33	0.20	1.91	1.04	1.08	1.15	1.44	11.45
KRB-24(dupl)	1.08	0.35	0.19	2.00	0.99	0.97	1.13	1.28	13.00
KRB-25	n.d.	n.d.	n.d.	n.d.	n.d.	n.d.	n.d.	n.d.	n.d.
KRB-26	1.18	0.37	0.20	2.17	1.09	0.93	1.24	1.44	14.20

Table D.5: Parameters, GC-FID. Teistberget, Eastern Spitsbergen; Profile above sill

Sample	nC17/nC18	Prist/nC17	Phyt/nC18	Prist/Phyt	CPI	$CPI_{Philipi}$	CPI_1	CPI_2	nC17/nC31
TBU-1	1.26	0.17	0.21	1.00	0.99	1.09	0.76	0.98	0.96
TBU-2	n.d.	n.d.	n.d.	n.d.	n.d.	n.d.	n.d.	n.d	n.d.
TBU-3	1.32	0.28	0.32	1.17	1.03	1.11	0.74	1.10	0.74
TBU-4	1.44	0.15	0.17	1.33	0.99	1.06	0.50	1.12	1.24
TBU-4(dupl)	1.39	0.19	0.22	1.20	1.17	1.08	1.11	1.12	1.19
TBU-5	n.d.	n.d.	n.d.	n.d.	n.d.	n.d.	n.d.	n.d	n.d
TBU-6	1.14	0.14	0.07	2.33	1.07	1.04	1.25	1.41	13.86
TBU-7	1.15	0.56	0.41	1.57	0.94	0.89	1.08	1.29	11.14
TBU-8	n.d.	n.d.	n.d.	n.d.	n.d.	n.d.	n.d.	n.d	n.d
TBU-9	1.00	9.67	7.50	1.29	1.03	0.98	0.72	1.25	0.40
TBU-10	1.23	0.54	0.47	1.43	0.93	1.00	1.21	1.00	9.25
TBU-11	n.d.	n.d.	n.d.	n.d.	n.d.	n.d.	n.d.	n.d	n.d

Table D.6: Parameters, GC-FID. Teistberget, Eastern Spitsbergen; Profile below sill

Sample	nC17/nC18	Prist/nC17	Phyt/nC18	Prist/Phyt	CPI	$CPI_{Philipi}$	CPI_1	CPI_2	nC17/nC31
TBL-1	n.d.	n.d.	n.d.	n.d.	n.d.	n.d.	n.d.	n.d.	n.d.
TBL-1(dupl)	n.d.	n.d.	n.d.	n.d.	n.d.	n.d.	n.d.	n.d.	n.d.
TBL-2	n.d.	n.d.	n.d.	n.d.	n.d.	n.d.	n.d.	n.d.	n.d.
TBL-3	0.94	0.63	0.38	1.56	1.05	0.99	1.11	1.35	4.16
TBL-4	1.03	0.72	0.47	1.59	0.97	0.88	1.14	1.15	5.13
TBL-5	1.06	0.88	0.70	1.34	1.08	1.00	1.11	1.47	4.95
TBL-6	1.13	1.09	0.73	1.68	1.02	0.97	1.10	1.45	11.33
TBL-7	1.13	1.62	1.15	1.60	0.96	0.90	1.07	1.30	11.50
TBL-8	1.12	1.53	1.12	1.53	1.01	1.05	1.08	1.40	7.83
TBL-9	n.d.	n.d.	n.d.	n.d.	n.d.	n.d.	n.d.	n.d.	n.d.
TBL-10	n.d.	n.d.	n.d.	n.d.	n.d.	n.d.	n.d.	n.d.	n.d.
TBL-11	n.d.	n.d.	n.d.	n.d.	n.d.	n.d.	n.d.	n.d.	n.d.

Table D.7: Parameters, GC-FID. Domen, Eastern Spitsbergen; Profile above sill

Sample	nC17/nC18	Prist/nC17	Phyt/nC18	Prist/Phyt	CPI	$CPI_{philipi}$	CPI_1	CPI_2	nC17/nC31
DOM-1	n.d.	n.d.	n.d.	n.d.	n.d.	n.d.	n.d.	n.d.	n.d.
DOM-2	n.d.	n.d.	n.d.	n.d.	n.d.	n.d.	n.d.	n.d.	n.d.
DOM-3	1.09	0.84	0.38	2.43	1.14	1.21	1.15	1.53	6.75
DOM-3(dupl)	1.10	0.83	0.39	2.30	1.15	1.21	1.19	1.51	6.57
DOM-4	1.09	1.17	0.59	2.16	1.15	1.29	1.11	1.51	4.26
DOM-5	n.d.	n.d.	n.d.	n.d.	n.d.	n.d.	n.d.	n.d.	n.d.
DOM-6	n.d.	n.d.	n.d.	n.d.	n.d.	n.d.	n.d.	n.d.	n.d.
DOM-7	n.d.	n.d.	n.d.	n.d.	n.d.	n.d.	n.d.	n.d.	n.d.
DOM-8	n.d.	n.d.	n.d.	n.d.	n.d.	n.d.	n.d.	n.d.	n.d.
DOM-9a	1.14	1.29	0.43	3.44	1.26	1.45	1.22	1.77	8.00
DOM-9b	n.d.	n.d.	n.d.	n.d.	n.d.	n.d.	n.d.	n.d.	n.d.
DOM-10	n.d.	n.d.	n.d.	n.d.	n.d.	n.d.	n.d.	n.d.	n.d.
DOM-11	1.07	0.41	0.30	1.50	0.97	1.03	0.96	1.13	2.90

Table D.8: Parameters, GC-FID. Høgrinden South, Barentsøya

Sample	nC17/nC18	Prist/nC17	Phyt/nC18	Prist/Phyt	CPI	$CPI_{Philipi}$	CPI_1	CPI_2	nC17/nC31
HØB1-1	n.d.	n.d.	n.d.	n.d.	n.d.	n.d.	n.d.	n.d.	n.d.
HØB1-2	n.d.	n.d.	n.d.	n.d.	n.d.	n.d.	n.d.	n.d.	n.d.
HØB1-3	n.d.	n.d.	n.d.	n.d.	n.d.	n.d.	n.d.	n.d.	n.d.
HØB1-4	n.d.	n.d.	n.d.	n.d.	n.d.	n.d.	n.d.	n.d.	n.d.
HØB1-5	n.d.	n.d.	n.d.	n.d.	n.d.	n.d.	n.d.	n.d.	n.d.
HØB1-6	1.13	1.30	0.77	1.90	1.18	1.80	1.17	1.73	14.67
HØB1-7	1.16	1.19	0.70	1.96	0.86	1.00	1.10	1.14	14.33
HØB1-8	1.21	3.06	1.93	1.93	0.98	1.09	1.07	1.13	5.67
HØB1-9	1.23	1.10	0.68	1.98	0.95	1.30	1.11	1.28	16.83
HØB1-10	1.19	0.91	0.59	1.85	1.12	1.50	1.13	1.72	10.13
HØB1-11	1.31	0.90	0.63	1.87	1.02	1.14	1.16	1.25	16.20
HØB1-12	1.30	1.04	0.65	2.09	0.95	1.00	1.19	1.17	14.00
HØB1-13	1.19	1.00	0.58	2.06	1.07	1.43	1.31	1.27	12.33

Table D.9: Parameters, GC-FID. Høgrinden South, Barentsøya

Sample	nC17/nC18	Prist/nC17	Phyt/nC18	Prist/Phyt	CPI	$CPI_{Philipi}$	CPI_1	CPI_2	nC17/nC31
HØB2-1	n.d.	n.d.	n.d.	n.d.	n.d.	n.d.	n.d.	n.d.	n.d.
HØB2-2	n.d.	n.d.	n.d.	n.d.	n.d.	n.d.	n.d.	n.d.	n.d.
HØB2-3	n.d.	n.d.	n.d.	n.d.	n.d.	n.d.	n.d.	n.d.	n.d.
HØB2-4	n.d.	n.d.	n.d.	n.d.	n.d.	n.d.	n.d.	n.d.	n.d.
HØB2-5	1.05	1.96	1.11	1.84	1.03	1.08	1.13	1.36	9.20
HØB2-6	1.17	1.39	0.81	2.00	0.94	1.20	1.07	1.25	9.80
HØB2-7	1.26	1.17	0.69	2.14	1.00	1.09	1.16	1.27	13.25
HØB2-8	1.16	1.54	0.90	1.98	0.96	1.00	1.05	1.24	9.83

Table D.10: Parameters, GC-FID. Høgrinden South, Barentsøya; sampled laterally along a single horizon

Sample	nC17/nC18	Prist/nC17	Phyt/nC18	Prist/Phyt	CPI	$CPI_{Philipi}$	CPI_1	CPI_2	nC17/nC31
HØB3-1	n.d.	n.d.	n.d.	n.d.	n.d.	n.d.	n.d.	n.d.	n.d.
HØB3-2(dupl)	1.45	1.94	1.82	1.55	1.16	1.42	0.72	1.11	0.61
HØB3-2	1.33	1.94	1.67	1.55	1.07	1.35	0.45	1.11	0.64
HØB3-3	1.29	1.17	0.43	3.50	1.56	4.33	1.00	1.24	2.00
HØB3-4	1.25	4.07	3.33	1.53	1.00	1.26	0.62	1.24	1.25
HØB3-5	1.13	4.77	3.04	1.77	0.99	1.08	0.96	1.33	4.33
HØB3-6	1.15	1.26	0.71	2.05	0.98	1.09	1.11	1.37	19.60
HØB3-7	1.25	1.03	0.62	2.08	0.95	1.11	1.24	1.27	37.50
HØB3-8	1.19	1.16	0.61	2.27	0.93	1.06	1.20	1.17	21.50
HØB3-9	1.22	0.97	0.53	2.24	0.97	1.23	1.20	1.28	29.33

Table D.11: Parameters, GC-FID. Northern Kreftberget, Barentsøya; Profile without sill

Sample	nC17/nC18	Prist/nC17	Phyt/nC18	Prist/Phyt	CPI	$CPI_{Philipi}$	CPI_1	CPI_2	nC17/nC31
NKB-1	1.25	1.25	0.76	2.06	1.09	1.06	1.24	1.36	10.50
NKB-2	1.26	1.15	0.65	2.23	0.88	0.91	1.23	1.07	34.00
NKB-3	1.33	1.60	1.08	1.98	0.85	1.17	1.10	1.00	12.40
NKB-4	1.24	1.55	1.02	1.88	0.85	0.82	1.12	1.04	18.00
NKB-5	1.20	1.44	0.93	1.86	0.89	1.10	1.13	1.07	13.25
NKB-6	n.d.	1.13	0.69	2.19	1.04	1.50	1.17	1.33	11.67

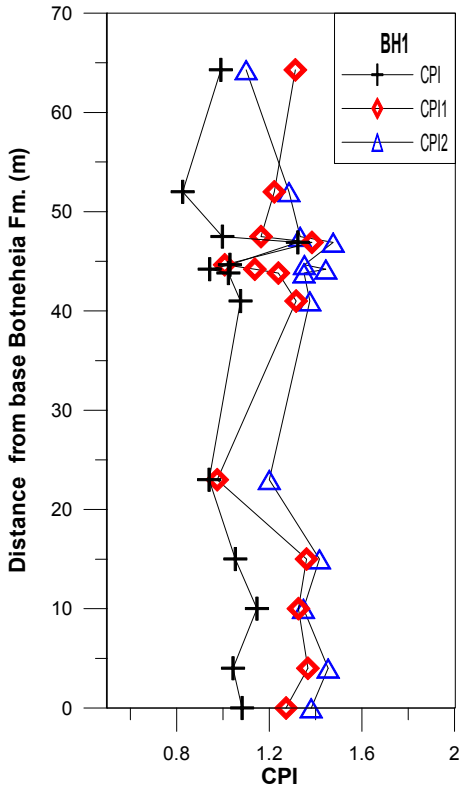

(a) CPI values

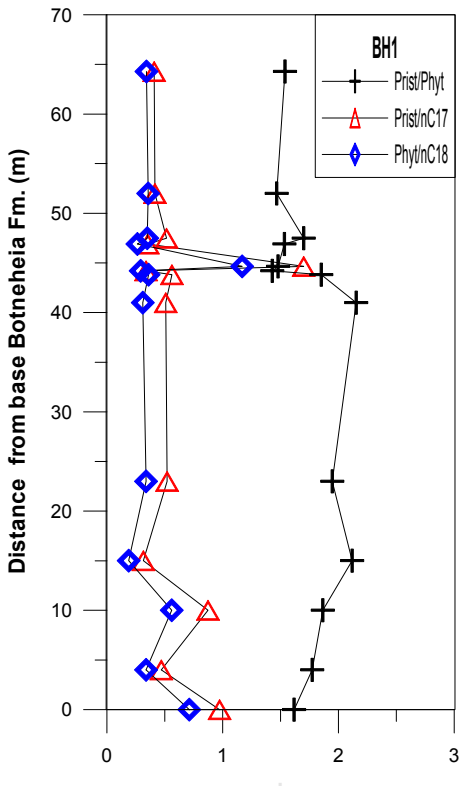

(b) Pristan, Phytan, n-C_{17} and n-C_{18}

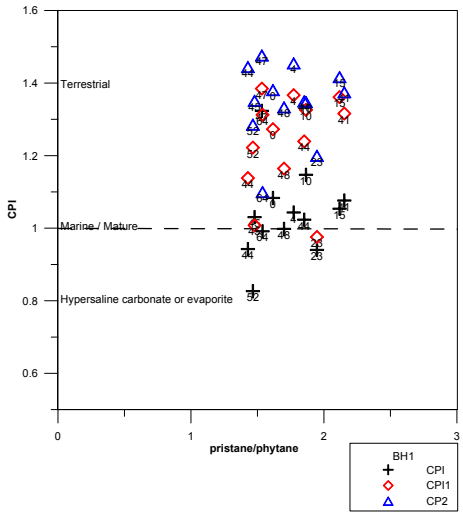

(c) CPI versus Pristan/Phytan. Number below each sample representation is the distance to base Botneheia Fm. in meter.

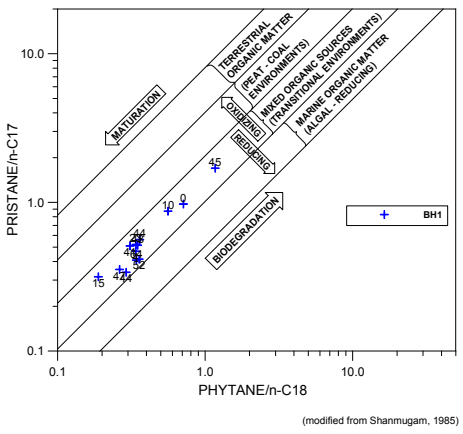

(d) Pristane/n-C_{17} versus Phytan/n-C_{18}. Number below each sample representation is the distance to base Botneheia Fm. in meter.

Figure D.2: *GC data from Botneheia East, Central Spitsbergen. Profile with only a minor sill at ca. 45 meter from base Botneheia.*

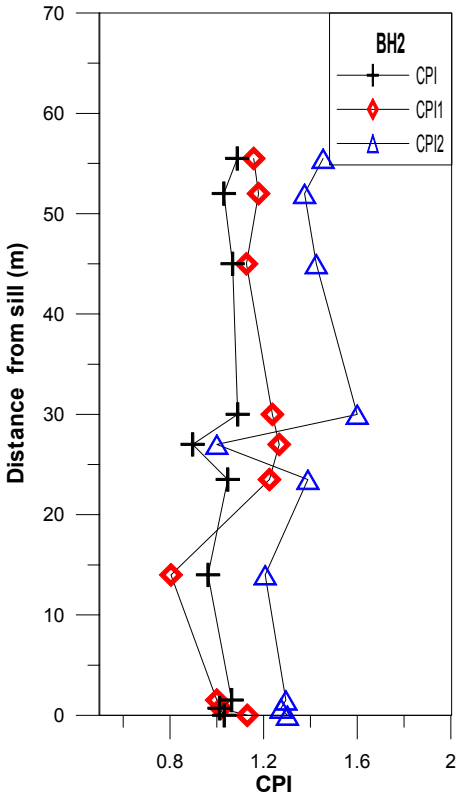

(a) CPI values

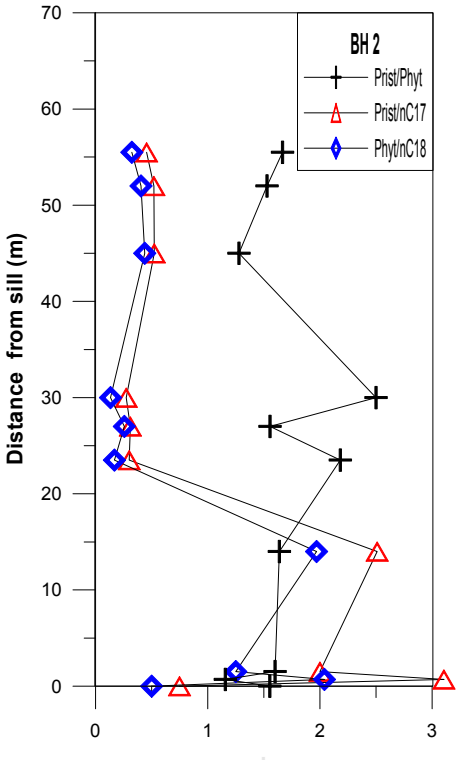

(b) Pristan, Phytan, n-C_{17} and n-C_{18}

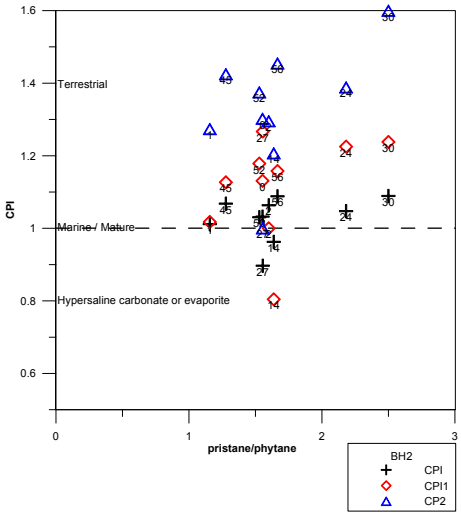

(c) CPI versus Pristan/Phytan. Number below each sample representation indicate the distance to the sill in meter.

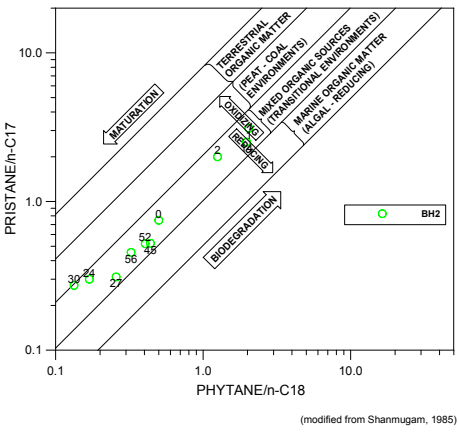

(d) Pristane/n-C_{17} versus Phytan/n-C_{18}. Number below each sample representation indicate the distance to the sill in meter.

Figure D.3: *GC data from Botneheia East, Central Spitsbergen. Profile above sill.*

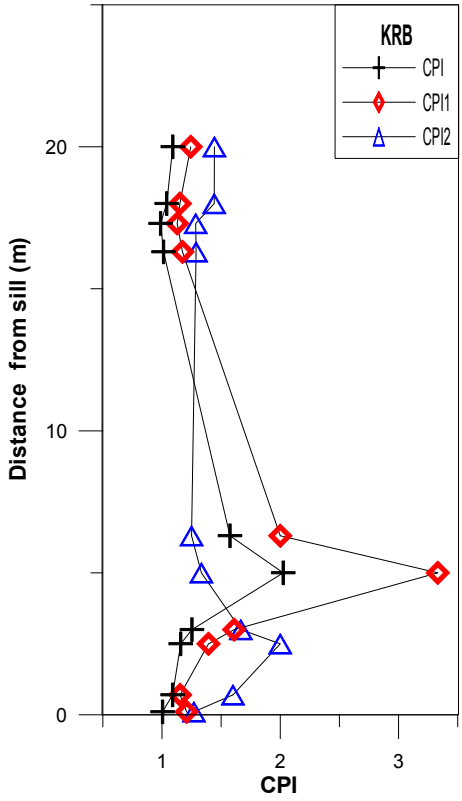

(a) CPI values

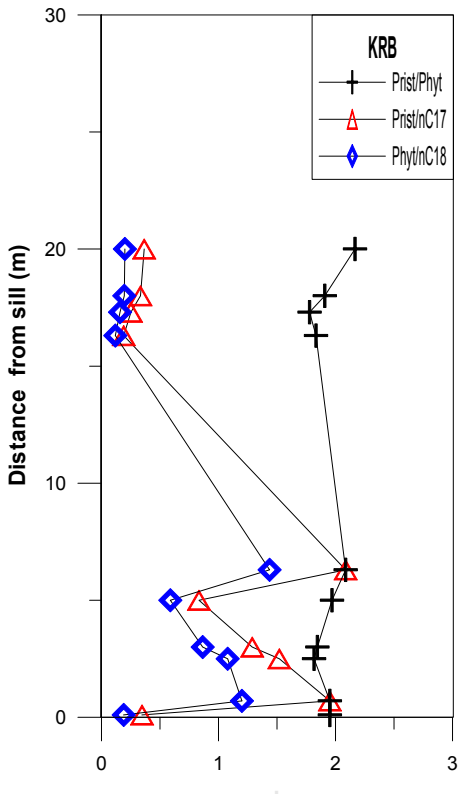

(b) Pristan, Phytan, n-C_{17} and n-C_{18}

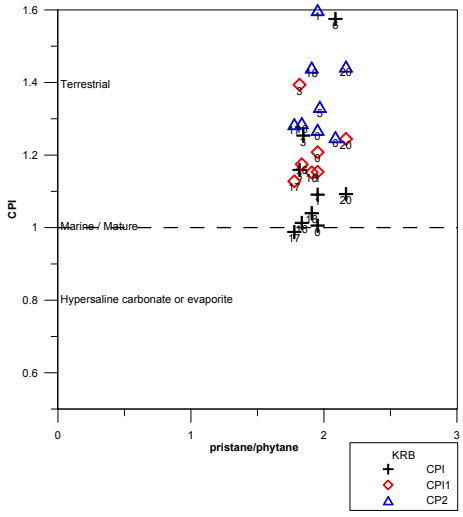

(c) CPI versus Pristan/Phytan. Number below each sample representation indicate the distance to the sill in meter.

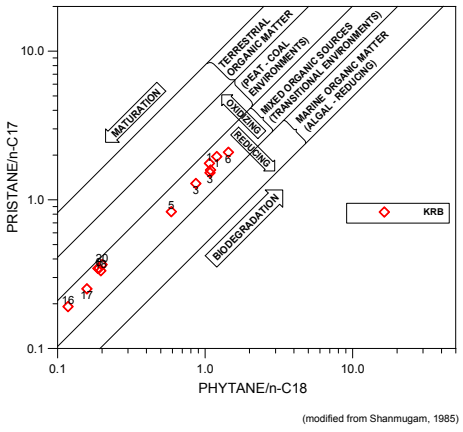

(d) Pristane/n-C_{17} versus Phytan/n-C_{18}. Number below each sample representation indicate the distance to the sill in meter.

Figure D.4: *GC data from Kreftberget, Barentsøya. Profile above sill.*

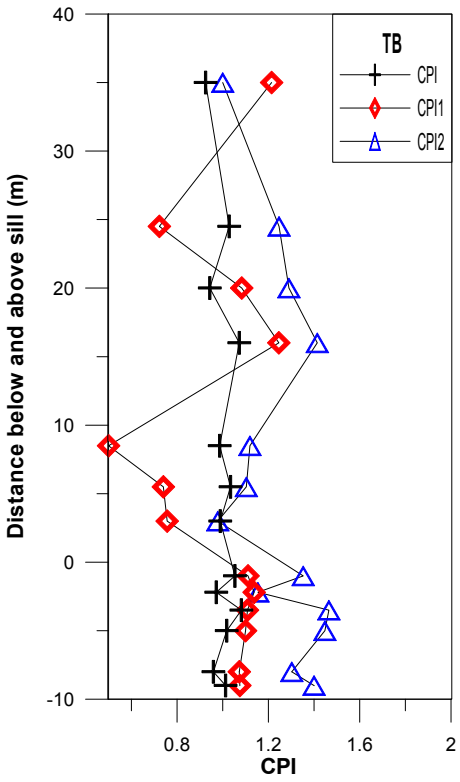

(a) CPI values

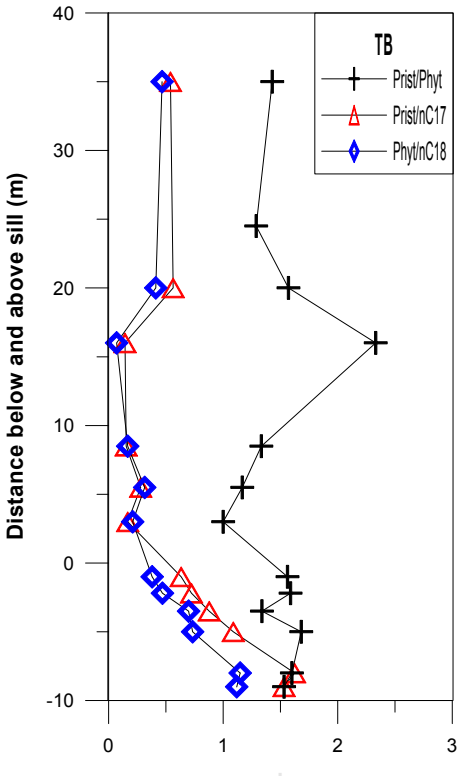

(b) Pristan, Phytan, n-C_{17} and n-C_{18}

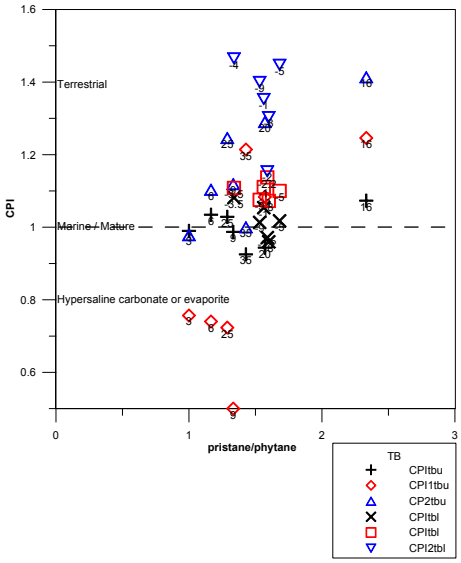

(c) CPI versus Pristan/Phytan. Number below each sample representation indicate the distance to the sill in meter.

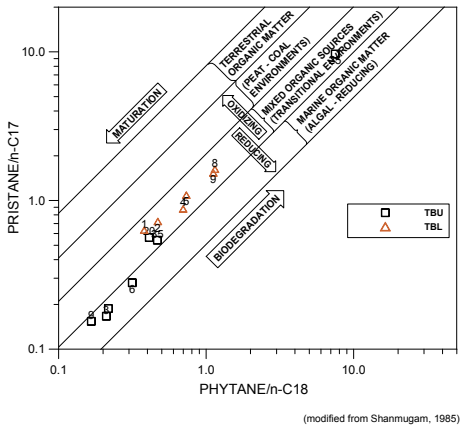

(d) Pristane/n-C_{17} versus Phytan/n-C_{18}. Number below each sample representation indicate the distance to the sill in meter.

Figure D.5: *GC data from Teistberget, Eastern Spitsbergen.*

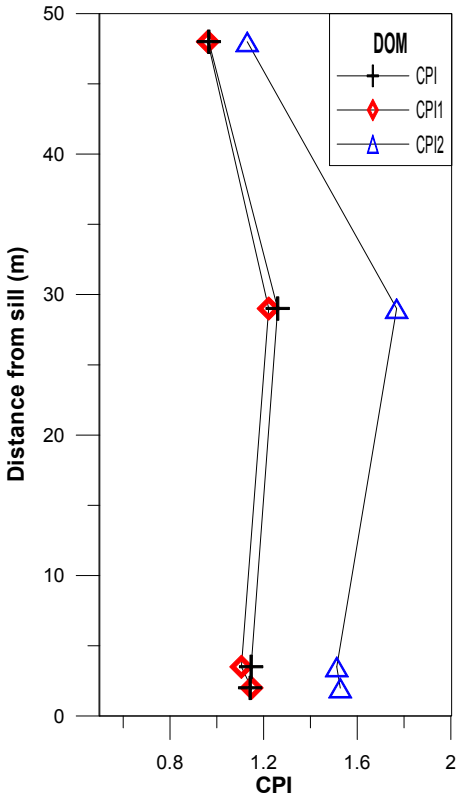

(a) CPI values

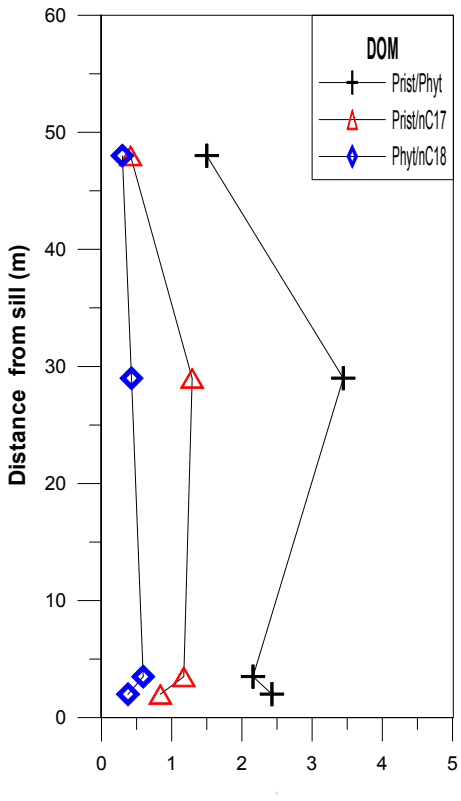

(b) Pristan, Phytan, n-C_{17} and n-C_{18}

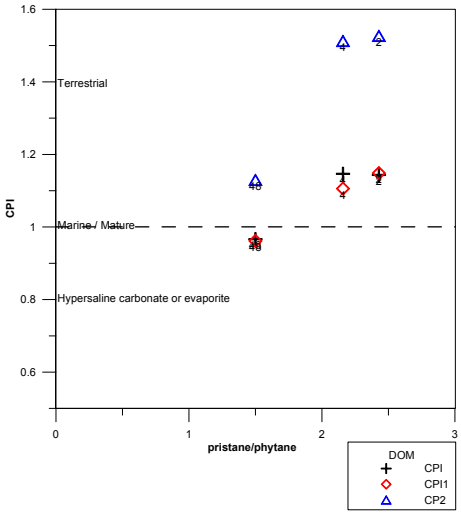

(c) CPI versus Pristan/Phytan. Number below each sample representation indicate the distance to the sill in meter.

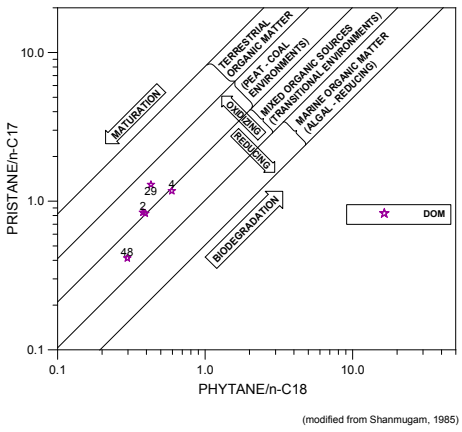

(d) Pristane/n-C_{17} versus Phytan/n-C_{18}. Number below each sample representation indicate the distance to the sill in meter.

Figure D.6: *GC data from Domen, Eastern Spitsbergen. Profile above sill.*

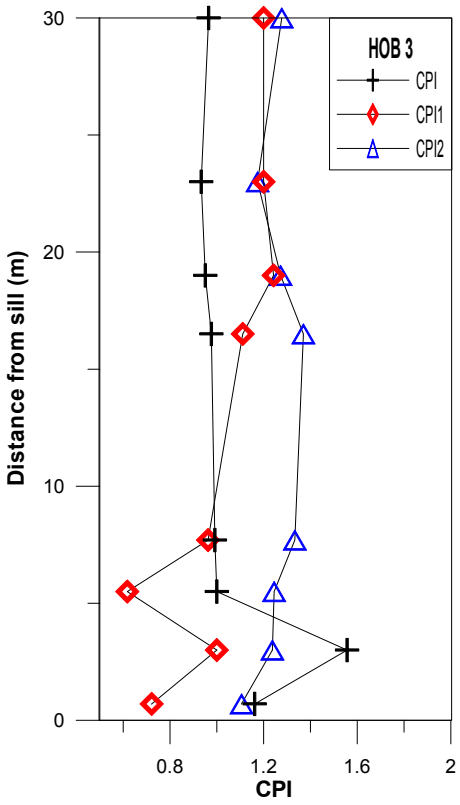

(a) CPI values

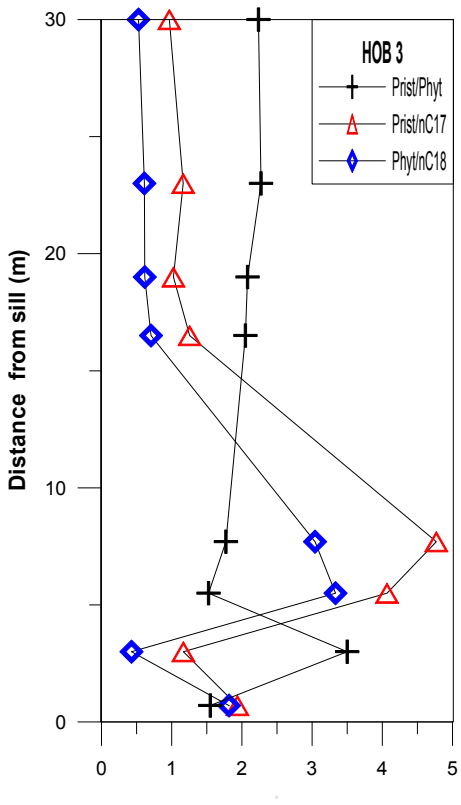

(b) Pristan, Phytan, n-C_{17} and n-C_{18}

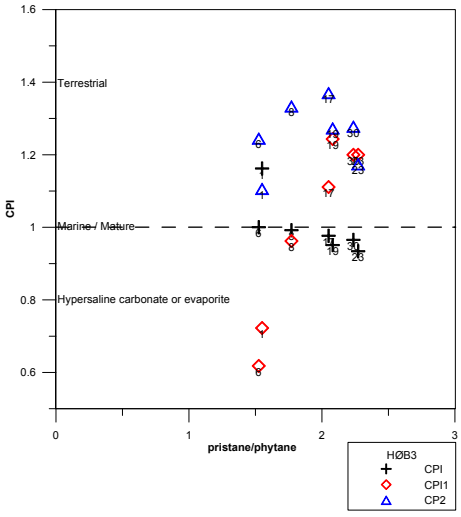

(c) CPI versus Pristan/Phytan. Number below each sample representation indicate the distance to the sill in meter.

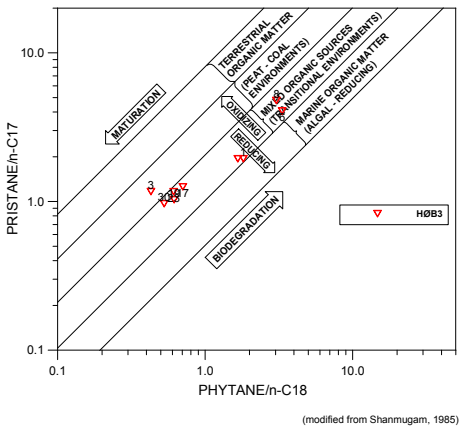

(d) Pristane/n-C_{17} versus Phytan/n-C_{18}. Number below each sample representation indicate the distance to the sill in meter.

Figure D.7: *GC data from Høgrinden South, Barentsøya; samples sampled laterally along a single horizon.*

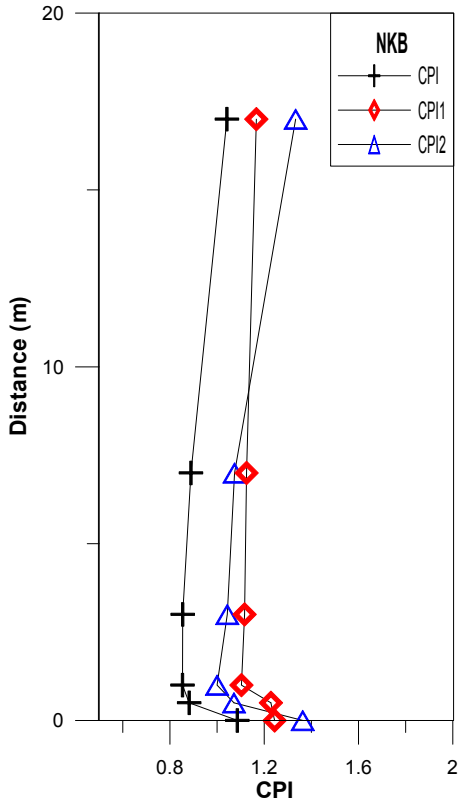

(a) CPI values

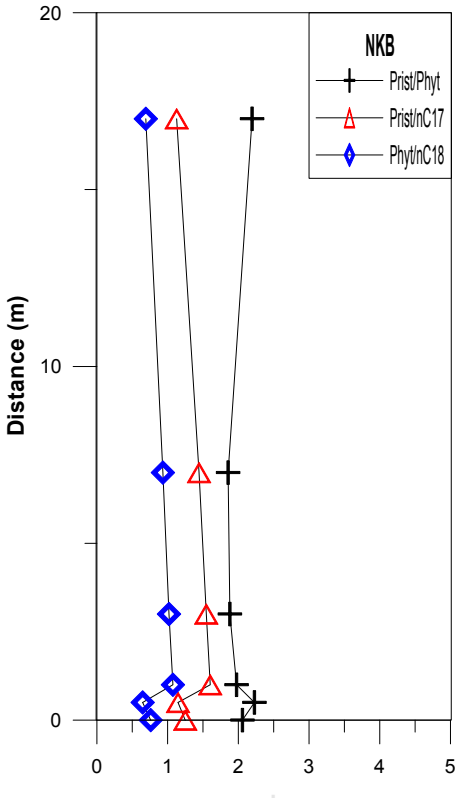

(b) Pristan, Phytan, n-C_{17} and n-C_{18}

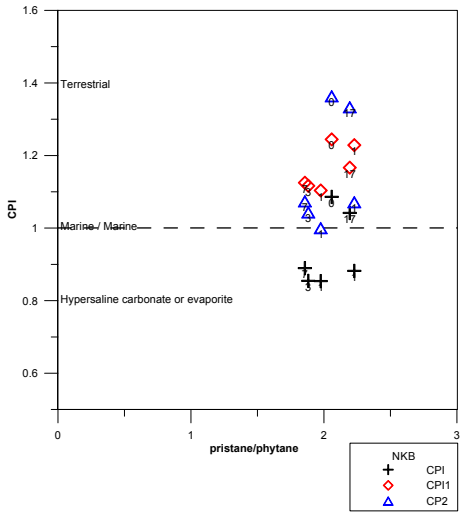

(c) CPI versus Pristan/Phytan

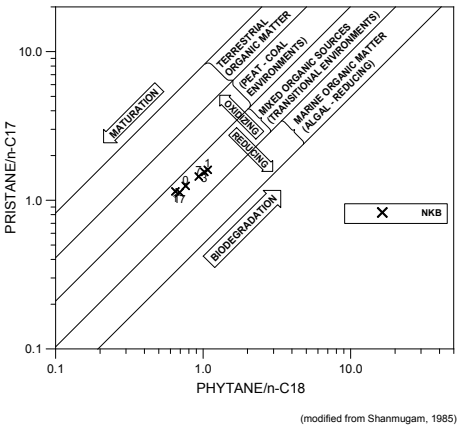

(d) Pristane/n-C_{17} versus Phytan/n-C_{18}

Figure D.8: *GC data from Northern Kreftsberget, Barentsøya; Profile without sill.*

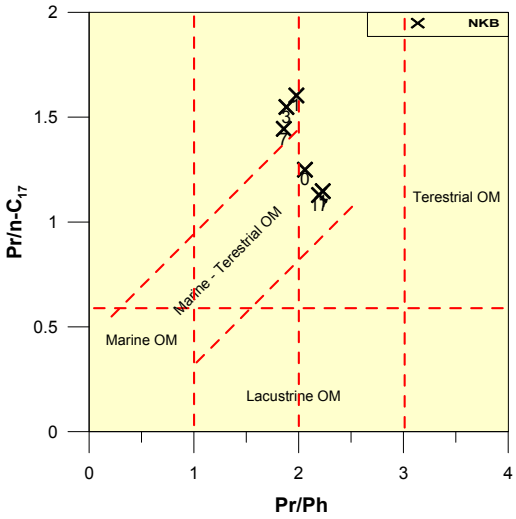

(a) NKB

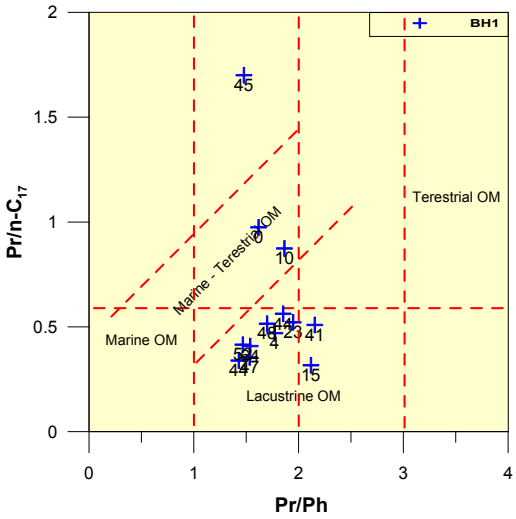

(b) BH1

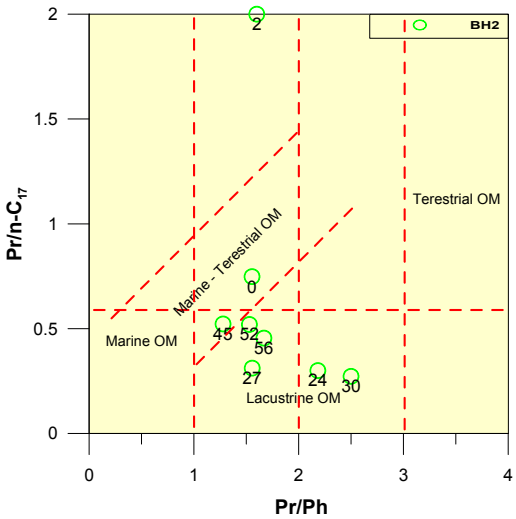

(c) BH2

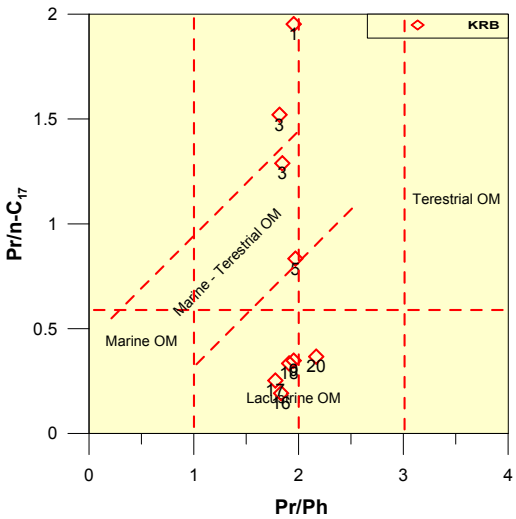

(d) KRB

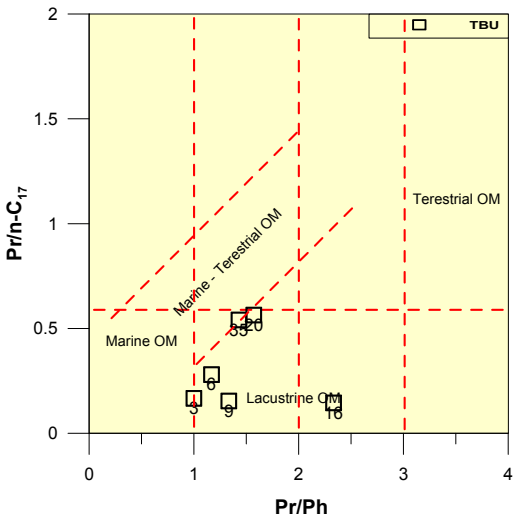

(e) TBU

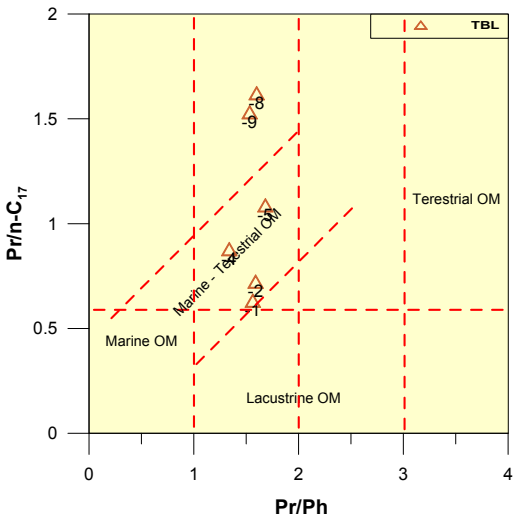

(f) TBL

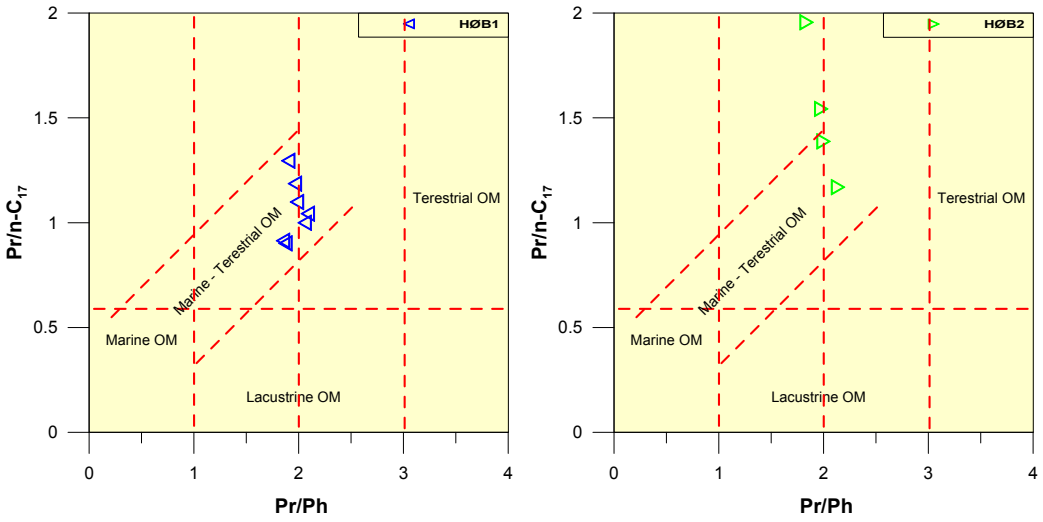

(g) HØB1

(h) HØB2

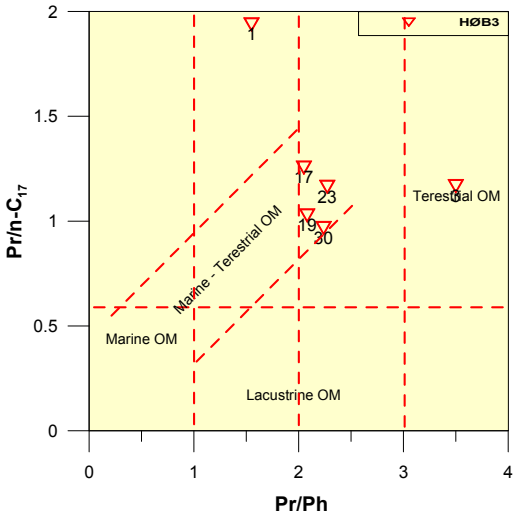

(i) HØB3

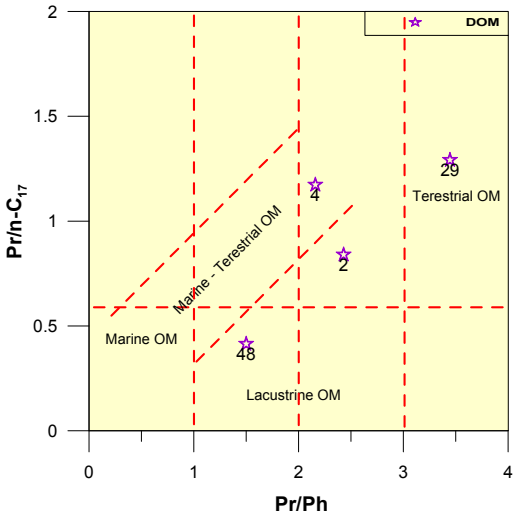

(j) DOM

Figure D.9: *Pristane/nC_{17} versus Pristane/Phytane for each sample series*

Appendix E

Stable isotopes

Stable-isotopes analyses was carried out at Institute for Energy Technology, Kjeller, Norway. The description of the analytical method below comes from their report.

The stable isotope results are listed in Tables E.1 to E.13.

Some analyses are repeated and the results from both analyses are then reported in the tables.

The PeGIS software (Dahl and Rasmussen, 2003) was used to produce Figures E.1 to E.8.

E.1 Analysis

Stable-isotopes on total extract (EOM)

Soxhlet extraction Total extracts (EOM) are obtained by Soxhlet extraction with 7% (volume)$MeOH$ in dichloromethane (DCM). Each extraction thimble is pre-extracted at least for one hour before being used for sample extraction.

5 - 7 g of fine crushed rock samples are weighed into extraction thimbles and extracted for 20 - 24 hours. The solvent is removed to near dryness by a rotary evaporator. The remaining solvent is transferred to a small pre-weighed vial and the solvent is allowed to evaporate at room temperature to constant weight.

The amount of EOM extracted from the diffrent rock samples is included in Table E.1 to E.13.

Stable isotopes The total extracts are dissolved in a known amount of dichloromethane, and aliquots of 2 - 4 mg (or as much as possible) are put into Pyrex glass tubes. The solvent is evaporated for one hour at 60°C or at room temperature overnight, and CuO is added to the glass tubes together with some small pieces of $Ag(s)$. The tubes are evacuated, sealed with a torch and combusted for 1 hour at 550°C (Sofer, 1980). The combustion products CO_2 and H_2O are separated and the $^{13}C/^{12}C$ isotope ratios determined on the separated CO_2.

The isotopic measurements are performed on a Finnigan MAT 251 dual inlet, triple collector, isotope ratio mass spectrometer and a VG Optima dual inlet, triple collector, isotope ratio mass spectrometer.

Stable-isotopes on isolated kerogen About 5 mg of isolated kerogen is put into quarts tubes, and CuO is added together with some small pieces of $Ag(s)$. The tubes are evacuated, sealed with a torch and combusted for 2 minutes at 900°C. The combustion products CO_2 and H_2O are separated and the $^{13}C/^{12}C$ isotope ratios determined on the separated CO_2.

The isotopic measurements are performed on a Finnigan MAT 251 dual inlet, triple collector, isotope ratio mass spectrometer and a VG Optima dual inlet, triple collector, isotope ratio mass spectrometer.

Stable-isotopes on carbonates (calcite/dolomite) 25 to 300 mg of the residue from the Soxhlet extraction (25 to 300 mg in order to get about 510 mg carbonate) is transferred to a glass container. 2 ml 100% H_3PO_4 acid is added and evacuated to 5x 10-3 mbar. The reaction is controlled in a water bath at 25.0°C for 2 hours. The produced CO_2 gas (calcite fraction) is then cleaned through a cooling trap at -80°C and the $^{13}C/^{12}C$ and $^{18}O/^{16}O$ isotope ratios determined on the cleaned CO_2.

The glass container is put back into the water bath for another 100 hours reaction and trated as above. (The produced CO_2 gas (dolomite fraction) is then cleaned through a cooling trap at -80°C and the $^{13}C/^{12}C$ and $^{18}O/^{16}O$ isotope ratios determined on the cleaned CO_2).

The isotopic measurements are performed on a Finnigan MAT 251 dual inlet, triple collector, isotope ratio mass spectrometer and a VG Optima dual inlet, triple collector, isotope ratio mass spectrometer.

E.2 Results

Table E.1: Stable-isotopes. Botneheia East, Central Spitsbergen; Profile with only a minor sill

Sample	m from sill	Calsite Delta 13C ‰PDB	Calsite Delta 18O ‰PDB	Dolomite Delta 13C ‰PDB	Dolomite Delta 18O ‰PDB	Kerogen Delta 13C ‰PDB	EOM Delta 13C ‰PDB	mgEOM g rock
BH1-27	67.00	-2.2	-8.7	-2.3	-10.3	-30.9	-32.1	0.7
BH1-26	64.30	-2.2	-9.4	-3.0	-13.2	-30.5	-30.6	3.8
BH1-25	59.00	-3.2	-8.8	-2.6	-10.0	-30.4	-31.8	3.0
BH1-24	55.00	-3.1	-8.4	-2.3	-8.8	-31.1	-31.2	2.8
BH1-23	52.00	-3.2	-9.2	-3.0	-10.0	-31.2	-31.4	3.3
BH1-22	50.80	-3.2	-8.7	-3.6	-11.2	-30.6	-31.2	3.4
		-3.1	-9.1					
BH1-21	48.80	-6.1	-10.4	-6.5	-11.1	-31.1	-31.6	4.2
BH1-20	47.50	-4.7	-10.5	-6.2	-16.5	-30.6	-31.2	11.2
BH1-19	46.90	-13.9	-13.7	-14.4	-16.1	-30.0	-31.4	0.9
		-14.3	-13.9	-14.2	-16.0	-29.5		
BH1-18	46.82	-18.2	-17.9	-17.4	-18.9	-27.2	-31.1	0.4
BH1-17	44.96	-16.6	-14.4	-15.8	-15.5	-27.9	-31.8	0.6
BH1-16	44.90	-15.9	-15.0	-15.7	-16.0	-30.2	-30.8	1.1
BH1-15	44.65	-14.5	-13.8	-15.0	-16.7	-31.0	-31.3	4.8
BH1-14	44.20	-8.9	-10.9	-10.7	-15.5	-30.9	-314	3.5
BH1-13	43.82	-7.0	-11.4	-9.6	-13.8	-31.2	-31.3	5.0
BH1-12	43.00	-6.4	-10.5	-5.6	-11.9	-30.9	-31.0	4.3
BH1-11	42.00	-7.7	-10.9	-5.5	-12.4	-31.1	-31.5	7.1
BH1-10	41.00	-5.5	-10.9	-4.7	-14.1	-31.1	-30.9	6.3
BH1-9	37.50	-5.1	-10.6	-4.9	-15.6	-31.2	-31.3	4.6
BH1-8	31.00	-4.6	-9.8	-3.4	-11.0	-30.5	-31.2	4.7
BH1-7	28.50	-5.8	-9.6	-1.3	-6.2	-31.4	-30.9	4.8
BH1-6	23.00	-4.3	-11.8	-3.2	-15.6	-30.9	-30.9	4.5
BH1-5	15.00	-3.0	-11.3	-2.6	-14.7	-31.8	-31.6	4.6
BH1-4	10.00	-3.5	-11.9	-1.8	-14.1	-31.6	-31.0	4.6
BH1-3	7.00	-4.3	-10.3	-2.6	-11.3	-31.7	-31.5	3.3
BH1-2	4.00	-3.5	-11.4	-3.1	-15.0	-31.6	-31.4	5.8
BH1-1	0.00	-4.4	-9.0	-3.7	-10.6	-31.9	-31.6	4.9

Table E.2: Stable-isotopes. Botneheia 2, Central Spitsbergen; Profile above sill

Sample	m from sill	Calsite Delta 13C ‰PDB	Calsite Delta 18O ‰PDB	Dolomite Delta 13C ‰PDB	Dolomite Delta 18O ‰PDB	Kerogen Delta 13C ‰PDB	EOM Delta 13C ‰PDB	mgEOM g rock
BH2-30	58.00	-3.2	-9.9	-2.6	-11.0	-30.6	-30.7	5.1
							-31.2	
BH2-29	55.50	-3.1	-12.2	-2.6	-12.5	-30.4	-30.6	3.0
BH2-28	52.00	-3.2	-13.2	-3.3	-13.4	-30.5	-30.3	3.3
BH2-27	45.00	-3.0	-11.2	-2.9	-11.4	-30.9	-31.5	2.3
BH2-26	42.50	-3.5	-10.4	-3.9	-13.4	-31.1	-31.7	4.2
BH2-25	39.50	-2.6	-9.6	-2.9	-10.1	-30.8	-31.3	1.6
BH2-24	36.00	-5.3	-11.3	-5.9	-16.4	-31.0	-31.8	5.1
BH2-23	33.00	-5.5	-12.7	-5.6	-15.3	-30.8	-31.0	7.1
							-30.4	
BH2-22	30.00	-5.4	-11.9	-5.7	-14.8	-30.7	-31.2	7.2
BH2-21	27.00	-5.0	-11.1	-4.9	-12.4	-30.4	-30.6	3.6
BH2-20	23.50	-5.4	-11.6	-5.3	-14.3	-30.4	-30.5	4.6
BH2-19	19.50	-	-	-1.4	-13.7	-30.3	-30.5	3.1
BH2-18	17.50	-	-	-	-	-30.8	-31.1	6.2
BH2-17	16.80	-	-	-	-	-29.9	-30.5	0.4
							-30.4	
BH2-16	14.50	-15.2	-15.9	-2.5	-14.7	-25.5	-30.0	0.0
						-32.7		
						-28.6		
BH2-15	14.00	-	-	-	-	-30.2	-31.4	4.1
BH2-14	13.50	-4.3	-3.3	-5.3	-15.0	-29.3	-31.1	1.1
BH2-13	11.00	-5.5	-12.1	-6.2	-17.1	-29.8	-30.4	0.4
BH2-12	9.00	-5.0	-2.5	-	-	-30.2	-30.5	1.8

Table E.3: E.2 cont.

Sample	m from sill	Calsite Delta 13C ‰PDB	Calsite Delta 18O ‰PDB	Dolomite Delta 13C ‰PDB	Dolomite Delta 18O ‰PDB	Kerogen Delta 13C ‰PDB	EOM Delta 13C ‰PDB	mgEOM g rock
BH2-11	7.000	-14.8	-30.9		-15.2	-30.4	-30.7	2.8
BH2-10	5.70	-5.1	-8.2	-	-	-29.9	-30.5	2.4
BH2-9	5.00	-4.1	-19.8	-	-	-30.4	-30.9	2.1
BH2-8	4.00	-	-	-	-	-31.0	-31.3	3.1
BH2-7	3.00	-	-	-	-	-29.8	-31.2	2.2
BH2-6	2.00	-5.0	-14.0	-5.8	-15.9	-30.4	-30.1	0.5
BH2-5	1.50	-7.6	-12.6	-5.3	-18.4	-29.8	-29.9	0.6
BH2-4	1.00	0.3	-9.9	-3.9	-11.6	-29.8	-30.5	0.7
BH2-3	0.70	-6.9	-17.6	-6.7	-17.0	-30.2	-31.1	3.6
BH2-2	0.30	-7.6	-17.5	-7.9	-19.3	-30.9	-31.0	2.5
BH2-1	0.00	-8.2	-17.9	-8.4	-20.0	-31.1	-31.1	3.0

Table E.4: Stable-isotopes. Krefftberget, Barentsøya: Profile above sill

Sample	m from sill	Calsite Delta 13C ‰PDB	Calsite Delta 18O ‰PDB	Dolomite Delta 13C ‰PDB	Dolomite Delta 18O ‰PDB	Kerogen Delta 13C ‰PDB	EOM Delta 13C ‰PDB	mgEOM g rock
KRB-36		-2.4	-14.2	-	-	-24.3	-25.6	0.7
KRB-35		-3.5	-17.0	-3.2	-17.6	-25.4	-26.7	0.6
					-1.5	-24.3		
KRB-34		-2.0	-15.3	-2.2	-18.6	-24.0	-26.1	0.4
KRB-33		-1.3	-14.3	-2.6	-17.5	-24.1	-25.1	0.4
						-24.3		
KRB-32		-5.0	-17.9	-1.9	-19.1	-24.2	-25.9	0.4
		1.3	9.5	1.3	-17.0			
KRB-31		-3.3	-17.4	-1.4	-14.9	-24.3	-25.7	0.6
KRB-30		-6.7	-14.5	-6.3	-15.5	-26.0	-27.6	0.7
KRB-29		-5.9	-14.3	-	-	-24.2	-26.2	0.3
KRB-28		-2.4	-12.4	-2.2	-19.0	-24.8	-28.0	0.5
KRB-27		-1.7	-9.1	-	-	-28.4	-30.1	2.3
						-28.4		
KRB-26	20.0	-4.1	-13.9	-4.3	-15.1	-28.4	-29.3	1.7
KRB-25	19.0	-2.8	-9.2	-3.1	-11.4	-30.0	-30.6	6.1
						-30.0		
KRB-24	18.0	-2.7	-9.0			-30.2	-30.7	2.7
		-2.8	-9.0	-2.5	-10.5			
KRB-23	17.3	-4.9	-8.7	-5.3	-11.2	-29.R	-30.3	2.4
KRB-22	16.3	-4.4	-8.3	-4.9	-11.4	-30.5	-29.9	1.9
						-29.9	-29.9	
KRB-21	15.0	-4.3	-10.0	-4.1	-11.2	-29.8	-29.2	0.8

Table E.5: Table E.4 Cont.

Sample	m from sill	Calsite Delta 13C ‰PDB	Calsite Delta 18O ‰PDB	Dolomite Delta 13C ‰PDB	Dolomite Delta 18O ‰PDB	Kerogen Delta 13C ‰PDB	EOM Delta 13C ‰PDB	mgEOM g rock
KRB-20	14.0	-4.0	-9.6	-5.0	-12.8	-30.5	-29.1	0.7
KRB-19	13.0	-4.2	10.2	-4.5	-14.8	-30.3	-29.3	0.3
KRB-18A	12.0	-4.9	-11.4	-5.8	-15.8	-29.9	-28.9	0.3
KRB-18B	12.0	-4.6	-11.2	-5.5	-15.9	-30.1	-28.8	0.2
KRB-17	11.0	-5.2	-12.2	-5.4	-16.3	-30.0	-29.4	0.1
KRB-16	10.0	-5.6	-13.2	-5.8	-16.8	-30.2	-28.8	0.1
KRB-15	9.3	-5.4	-13.4	-5.9	-16.5	-30.4	-28.9	0.2
KRB-14	8.5	-5.0	-15.4	-1.8	-14.0	-30.3	-29.6	0.2
		-5.0	-14.9	-4.7	-15.4	-30.3		
KRB-13	7.3	-4.9	-13.5	-4.6	-17.8	-30.1	-29.8	0.2
						-29.5	-29.7	
KRB-12	6.3	-	-	-4.7	-13.5	-29.6	-30.5	0.2
KRB-11	5.0	-	-	-7.6	-17.4	-30.5	-32.0	1.3
KRB-10	4.0	-	-	-15.2	-16.1	-30.2	-32.0	1.6
KRB-9	3.0	-	-	-	-	-30.g	-31.4	1.6
KRB-8	2.5	-	-	-	-	-30.7	-31.3	1.5
KRB-7	2.0	-7.1	-8.1	-6.3	-12.1	-30.9	-31.1	1.0
KRB-6	1.6	-	-	-	-	-30.7	-30.9	0.9
					-1.5	-29.1		
KRB-5	1.4	-7.9	-9.2	-8.2	-9.9	-29.2	-30.9	0.5
KRB-4	1.0			-11.1	-10.3	-29.5	-30.9	0.3
KRB-3A	0.7	-8.5	-11.5	-8.3	-12.1	-31.2	-31.6	0.7
KRB-3B	0.7	-7.7	-16.0	-9.3	-22.4	-30.0	-31.5	0.3
KRB-2	0.3	-5.7	-10.7	-5.8	-12.1	-	-28.7	0.1
KRB-1A	0.1	-6.0	-10.7	-6.2	-12.5	-29.2	-30.7	0.3
KRB-1B	0.1	-6.8	-11.7	-6.7	-12.9	-	-	0.1
KRB-1C	0.1	-13.8	-17.0	-13.9	-16.5	-	-	0.0

Table E.6: Stable-isotopes. Teistberget, Eastern Spitsbergen; Profile above sill

Sample	m from sill	Calsite Delta 13C ‰PDB	Calsite Delta 18O ‰PDB	Dolomite Delta 13C ‰PDB	Dolomite Delta 18O ‰PDB	Kerogen Delta 13C ‰PDB	EOM Delta 13C ‰PDB	mgEOM g rock
TBU-11	38.0	-4.3	-7.0	-4.8	-4.8	-30.8	-31.5	3.1
TBU-10	35.0	-3.1	-7.9	-2.5	-10.0	-31.4	-31.8	5.3
TBU-9	24.5	-3.4	-9.2	-2.3	-7.9	-31.0	-31.3	2.9
TBU-8	23.0	-6.5	-7.5	-5.7	-8.2	-30.5	-31.3	3.3
TBU-7	20.0	-3.3	-7.9	-3.7	-9.9	-30.4	-31.1	5.9
TBU-6	16.0	-4.3	-10.1	-4.7	-12.2	-30.2	-30.3	3.9
TBU-5	11.5	-4.3	-12.8	-5.6	-13.8	-30.0	-31.0	1.0
TBU-4	8.5	-5.5	-12.7	-5.9	-16.5	-30.4	-30.9	1.0
		-5.3	-12.8	-5.6				
TBU-3	5.5	-	-	-5.6	-13.3	-30.1	-30.4	1.1
TBU-2	4.1	-1.7	-12.7	-	-	-30.0	-30.8	1.1
TBU-1	3.0	-	-	-	-	-29.8	-30.7	0.5

Table E.7: Stable-isotopes. Teistberget, Eastern Spitsbergen; Profile below sill

Sample	m from sill	Calsite Delta 13C ‰PDB	Calsite Delta 18O ‰PDB	Dolomite Delta 13C ‰PDB	Dolomite Delta 18O ‰PDB	Kerogen Delta 13C ‰PDB	EOM Delta 13C ‰PDB	mgEOM g rock
TBL-1	0.05	-7.5	-7.5	-	-	-25.8	-29.1	1.3
							-30.1	
TBL-2	0.4	-11.2	-14.7	-10.8	-14.2	-29.5	-30.8	1.9
TBL-3	1.0	-	-	1.7	-2.3	-30.6	-30.2	0.6
						-30.3		
TBL-4	2.2	-	-	1.1	-10.3	-30.1	-30.7	0.0
TBL-5	3.5	-	-	-	-	-29.7	-31.6	3.2
TBL-6	5.0	-	-	-	-	-30.3	-31.2	3.0
TBL-7	8.0	-	-	-4.3	-12.9	-30.3	-31.2	1.7
TBL-8	9.0	-7.3	-14.2	-6.7	-15.0	-30.2	-31.7	1.8
TBL-9	12.0	-	-	-	-	-31.0	-29.7	2.4
						-30.6	-28.7	
TBL-10	17.0	-3.2	-7.8	-1.1	-6.4	-29.3	-30.5	3.0
TBL-11	22.0	-4.2	-9.7	-4.2	-12.4	-29.1	-28.3	0.2

Table E.8: Stable-isotopes. Domen, Eastern Spitsbergen; Profile above sill

Sample	m from sill	Calsite Delta 13C ‰PDB	Calsite Delta 18O ‰PDB	Dolomite Delta 13C ‰PDB	Dolomite Delta 18O ‰PDB	Kerogen Delta 13C ‰PDB	EOM Delta 13C ‰PDB	mgEOM g rock
DOM-11	48.0	-	-	-	-	-27.1	-27.8	4.6
DOM-10	38.0	-13.8	-12.5	-14.2	-14.4	-26.2	-27.0	1.0
DOM-9A	29.0	-	-	-	-	-26.0	-27.3	2.1
DOM-9B	29.0	-	-	-	-	-26.1	-27.2	3.2
DOM-8	15.0	-7.3	-12.7	-	-	-26.2	-27.0	0.5
DOM-7	13.5	-	-	-	-	-25.8	-27.7	0.3
DOM-6	13.5	-	-	-	-	-26.0	-27.7	0.3
DOM-5	10.5	-	-	-	-	-26.1	-28.3	0.4
DOM-4	3.5	-	-	-	-	-26.4	-29.5	1.9
DOM-3	2.0	-9.3	-10.2	-10.9	-8.5	-26.0	-29.4	1.5
DOM-2	0.2	-14.0	-16.0	-15.2	-17.2	-26.0	-28.7	0.1
DOM-1	0.0	-13.4	-15.8	-15.4	-17.7	-29.6	-	0.1
		-13.2	-15.9	-15.4	-17.7			

Table E.9: Stable-isotopes. KMB-C

Sample	m from sill	Calsite Delta 13C ‰PDB	Calsite Delta 18O ‰PDB	Dolomite Delta 13C ‰PDB	Dolomite Delta 18O ‰PDB	Kerogen Delta 13C ‰PDB	EOM Delta 13C ‰PDB	mgEOM g rock
KMB-C 1		-4.5	-16.7	-		-	-28.9	0.1
KMB-C 2		-	-	-		-26.2	-30.1	0.1
KMB-C 3		-	-	-		-24.3	-27.7	0.1
KMB-C 4		-	-	-		-23.7	-25.6	0.2
KMB-C 5		-	-	-		-24.2	-26.5	0.0

Table E.10: Stable-isotopes. KMB-D

Sample	m from sill	Calsite Delta 13C ‰PDB	Calsite Delta 18O ‰PDB	Dolomite Delta 13C ‰PDB	Dolomite Delta 18O ‰PDB	Kerogen Delta 13C ‰PDB	EOM Delta 13C ‰PDB	mgEOM g rock
KMB-D 1		-4.9	-14.3	-5.1	-16.1	-	-29.1	0.1
KMB-D 2		-2.5	-17.9	-2.9	-19.6	-29.1	-28.0	0.2
KMB-D 3		-4.0	-13.3	-4.6	-14.3	-24.4	-30.5	0.2
KMB-D 4		-6.9	-11.8	-7.0	-13.4	-24.0	-29.3	0.2
KMB-D 5		-2.2	-11.7	-23	-13.0	-24.4	-27.0	0.1
KMB-D 6		-0.2	-10.8	-0.8	-12.4	-24.0	-27.5	0.2

Table E.11: Stable-isotopes. Høgrinden South, Barentsøya; sampled laterally along a single horizon

Sample	m from sill	Calsite Delta 13C ‰PDB	Calsite Delta 18O ‰PDB	Dolomite Delta 13C ‰PDB	Dolomite Delta 18O ‰PDB	Kerogen Delta 13C ‰PDB	EOM Delta 13C ‰PDB	mgEOM g rock
HØB3-1	0.0	-13.0	-18.4	-12.2	-14.8	-29.8	-28.1	0.2
		-13.0	-18.0	-12.3	-15.8			
HØB3-2	0.7	-11.6	-18.8	-10.4	-15.0	-29.3	-31.8	3.3
HØB3-3	3.0	-11.3	-16.0	-11.3	-13.9	-30.6	-31.8	6.6
HØB3-4	5.5	-9.8	-15.1	-11.4	-14.1	-29.6	-31.7	1.6
		-9.5	-15.2					
HØB3-5	7.7	-9.5	-15.2	-9.6	-16.0	30.0	-31.7	2.6
HØB3-6	16.5	-4.9	-9.6	-6.4	-11.9	-30.1	-31.9	3.6
		-4.9	-9.3	-6.4	-12.0			
HØB3-7	19.0	-3.5	-7.4	-4.5	-8.9	-30.6	-32.1	3.7
HØB3-8	23.0	-2.8	-6.7	-3.0	-5.2	-31.1	-31.8	3.8
HØB3-9	30.0	-3.0	-7.5	-3.8	-8.1	-30.7	-32.2	3.8

Table E.12: Stable-isotopes. Northern Kreftberget, Barentsøya; Profile without sill

Sample	m from sill	Calsite Delta 13C ‰PDB	Calsite Delta 18O ‰PDB	Dolomite Delta 13C ‰PDB	Dolomite Delta 18O ‰PDB	Kerogen Delta 13C ‰PDB	EOM Delta 13C ‰PDB	mgEOM g rock
NKB-14		-2.6	-15.0	-4.3	-21.6	-24.4	-26.0	0.2
						-24.5		
NKB-13		-3.8	-11.7	-3.9	-13.5	-24.9	-26.1	0.7
NKB-12		-0.5	-14.8	-2.4	-16.0	-24.7	-26.2	0.2
NKB-11		1.9	-16.3	-2.8	-17.9	-24.2	-25.7	0.6
NKB-10		-4.6	-11.6	-5.2	-13.6	-24.6	-26.5	0.2
NKB-9		0.6	-13.4	-6.2	-16.3	-24.6	-26.1	0.8
NKB-8		0.6	-13.2	-3.9	-18.0	-24.4	-26.1	0.5
							-25.6	
NKB-7		-1.0	-7.2	-1.5	-11.6	-30.6	-28.8	0.5
							-28.4	
							-31.9	
NKB-6	17.0	-2.6	-6.3	-2.6	-8.1	-30.9	-31.4	3.7
NKB-5	1.0	-5.8	-9.9	-4.4	-12.2	-30.7	-31.7	6.7
NKB-4	7.0	-6.0	-9.7	-4.7	-13.5	-30.8	-31..4	6.6
NKB-3	3.0	-5.1	-11.0	-3.8	-15.1	-30.9	-31.3	11.1
NKB-2	0.5	-4.0	-e .7	-3.3	-12.1	-30.2	-31.5	5.3
NKB-1	0.0	-3.1	-6.5	0.1	-5.0	-30.3	-31.6	1.7
		-2.9	-6.2	0.3	-5.2			

Table E.13: Stable-isotopes. NPD Standard samples

Sample	m from sill	Calsite Delta 13C ‰PDB	Calsite Delta 18O ‰PDB	Dolomite Delta 13C ‰PDB	Dolomite Delta 18O ‰PDB	Kerogen Delta 13C ‰PDB	EOM Delta 13C ‰PDB	mgEOM g rock
JR-1.	-6.4	-8.2	-5.0	-10.1	-32.1	-32.1	16.7	
aliqout #13	-6.4	-8.4	-4.9	-9.7	-32.2	-32.0		
SR-1.	-3.2	-7.8	-2.0	-6.8	-32.9	-33.1	5.7	
aliqout #13	-3.4	-8.0	-1.9	-6.6	-33.1	-33.3		

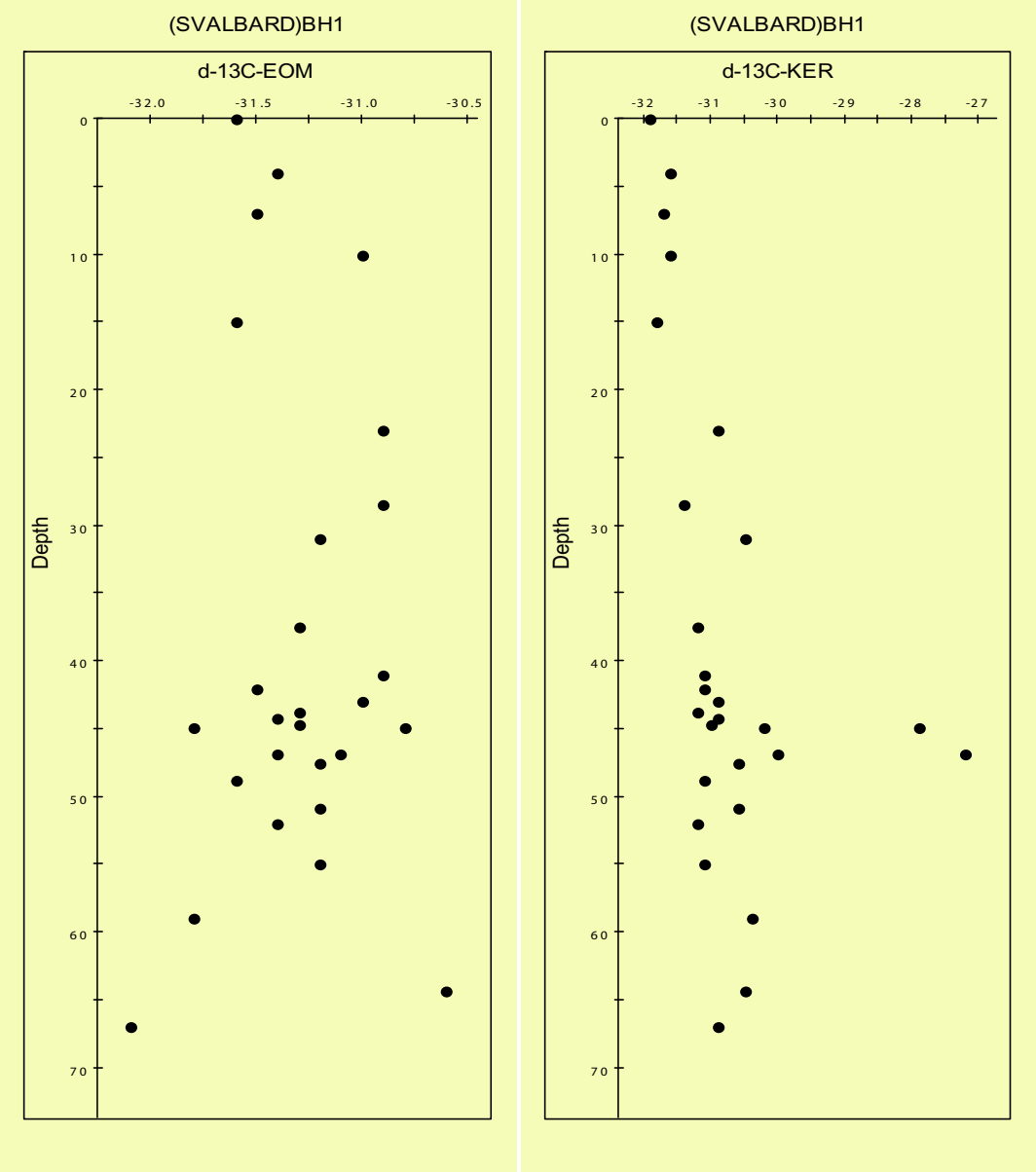

Figure E.1: *δ^{13} EOM and δ^{13}C Kerogen ploted against distance from base Botneheia Fm. Botneheia East, Central Spitsbergen; Profile with only a minor sill*

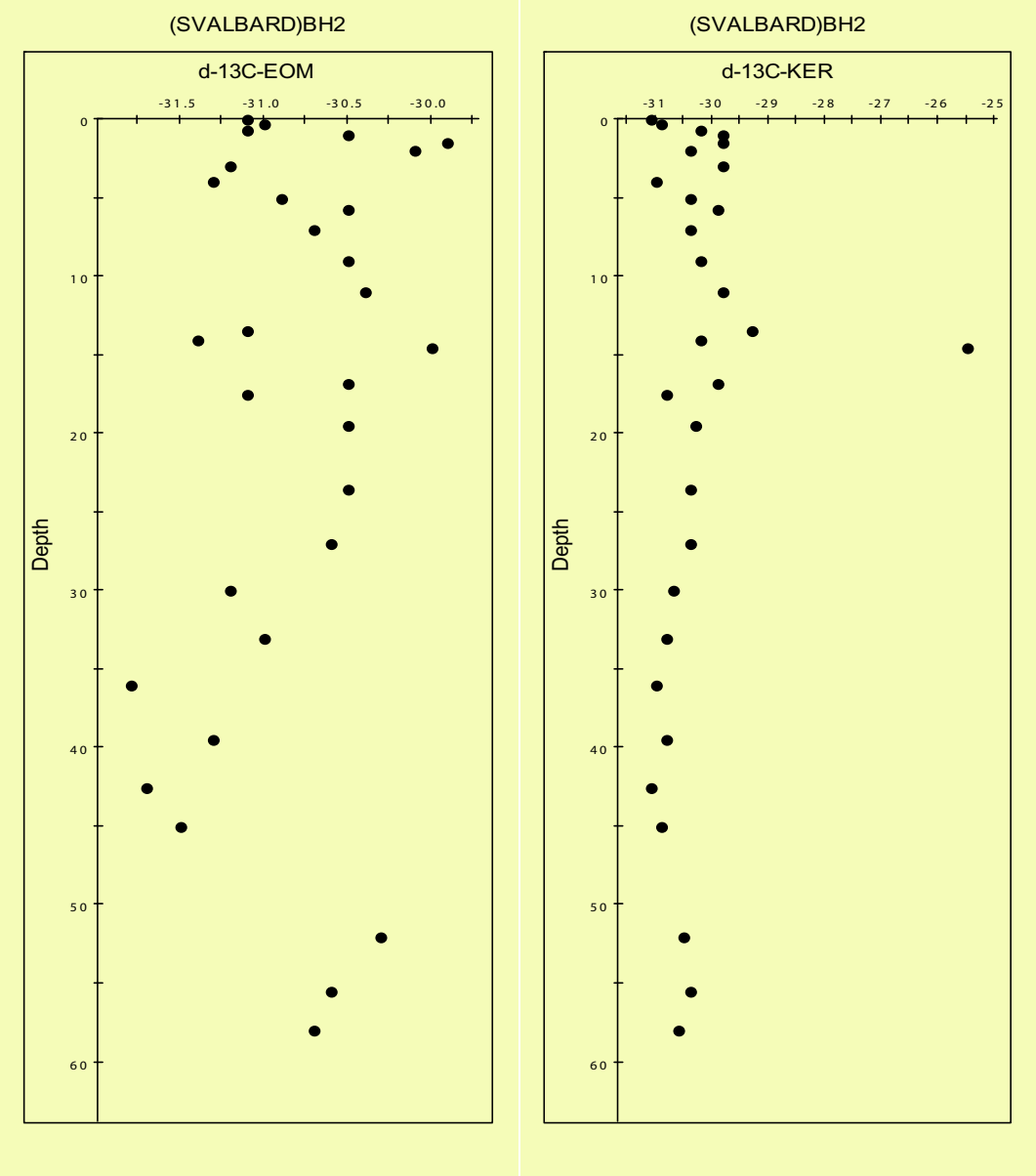

Figure E.2: *$\delta^{13}C$ EOM and $\delta^{13}C$ Kerogen ploted against distance from sill. Botneheia 2, Central Spitsbergen; Profile above sill*

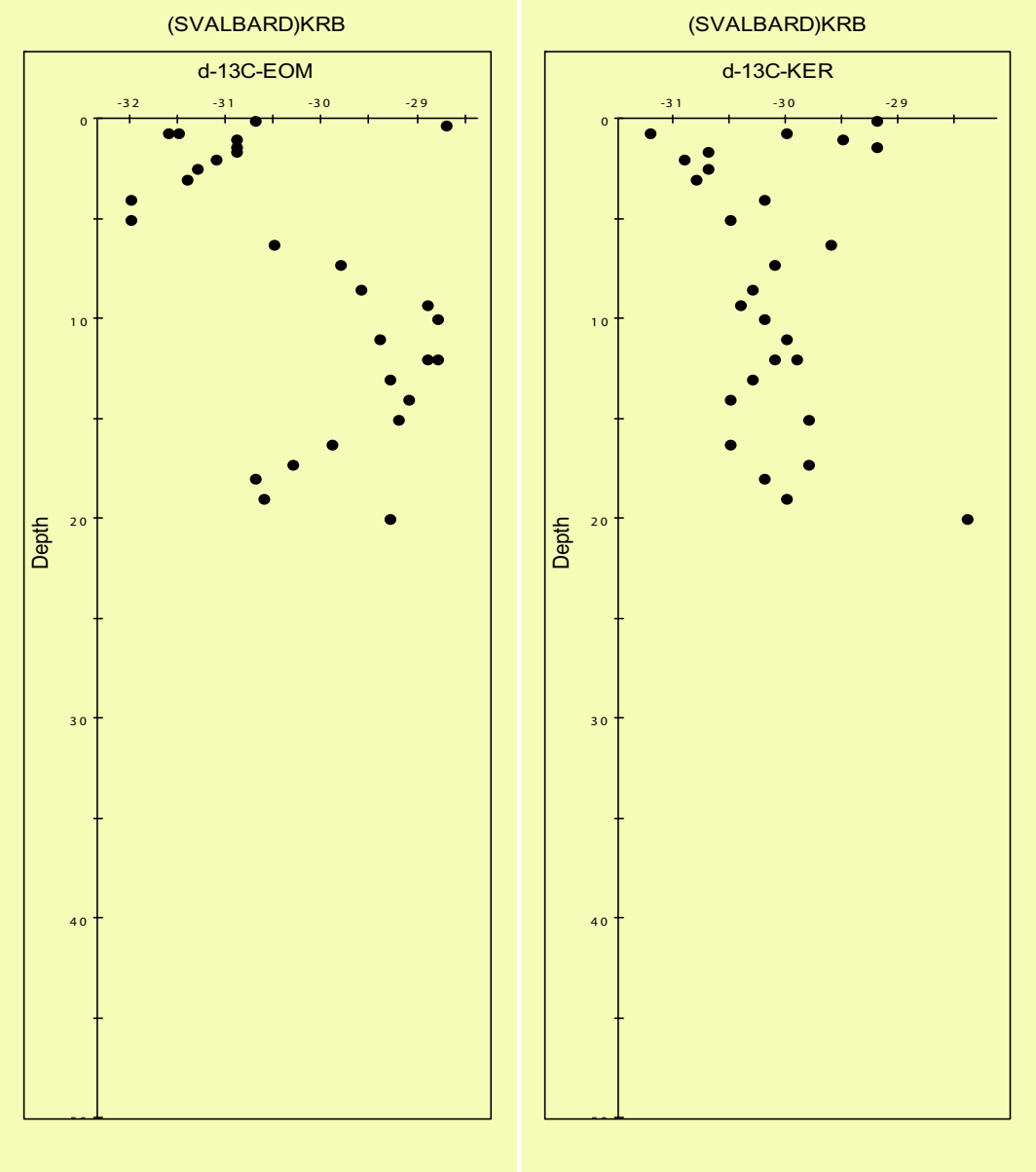

Figure E.3: *$\delta^{13}C$ EOM and $\delta^{13}C$ Kerogen ploted against distance from sill. Krefft-berget, Barentsøya: Profile above sill*

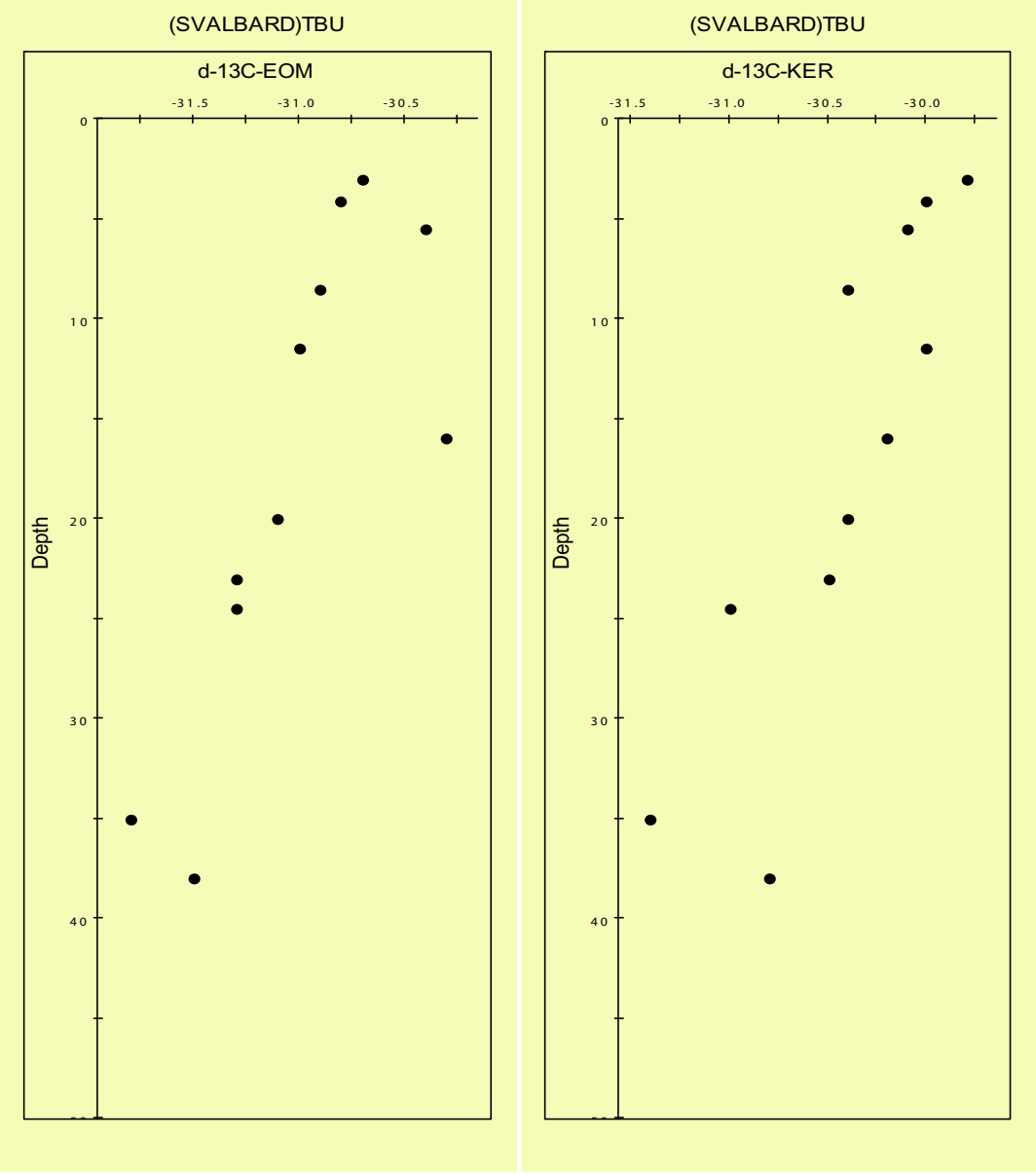

Figure E.4: *$\delta^{13}C$ EOM and $\delta^{13}C$ Kerogen ploted against distance from sill. Teistberget, Eastern Spitsbergen; Profile above sill*

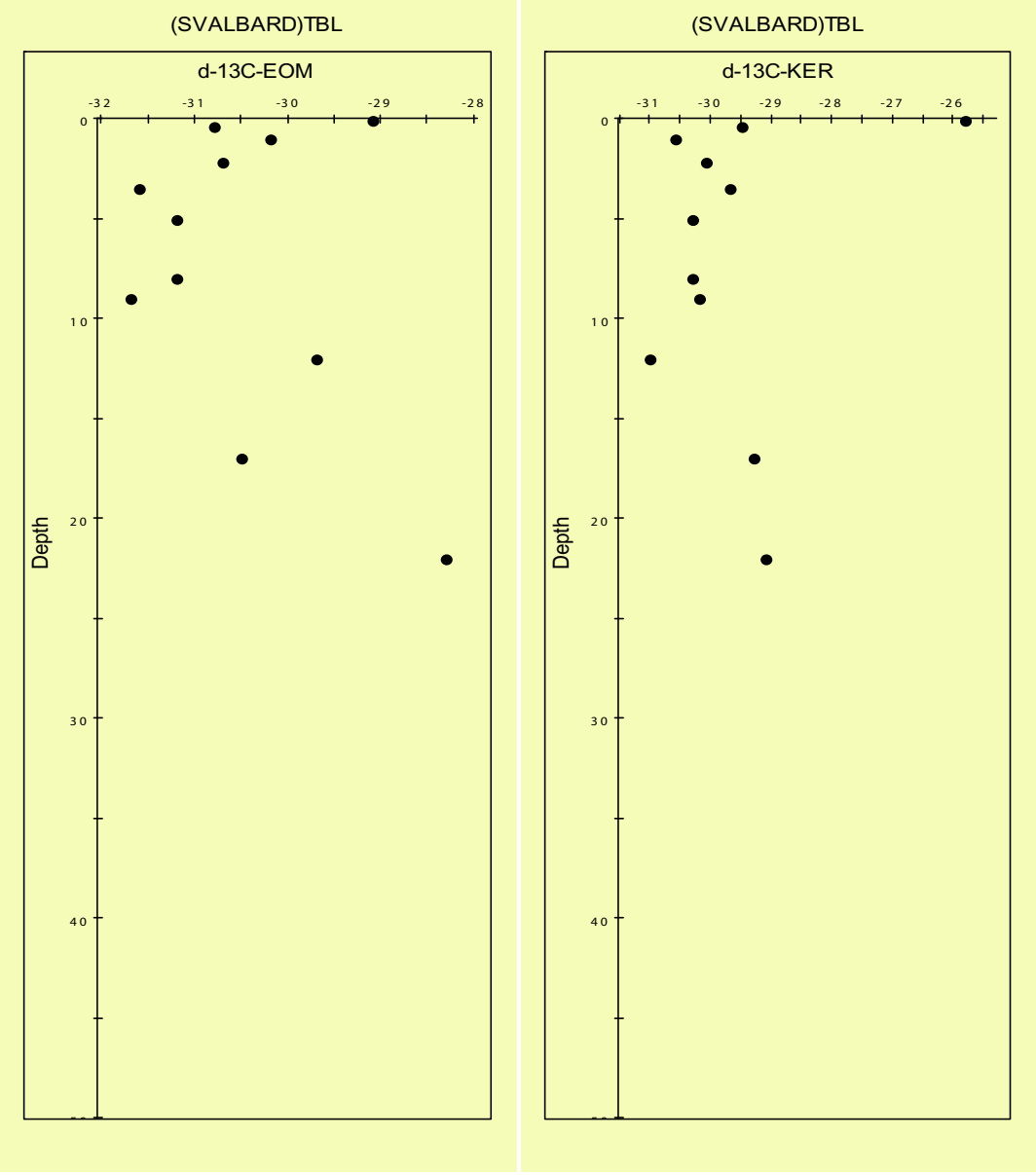

Figure E.5: $\delta^{13}C$ *EOM and* $\delta^{13}C$ *Kerogen ploted against distance from sill. Teistberget, Eastern Spitsbergen; Profile below sill*

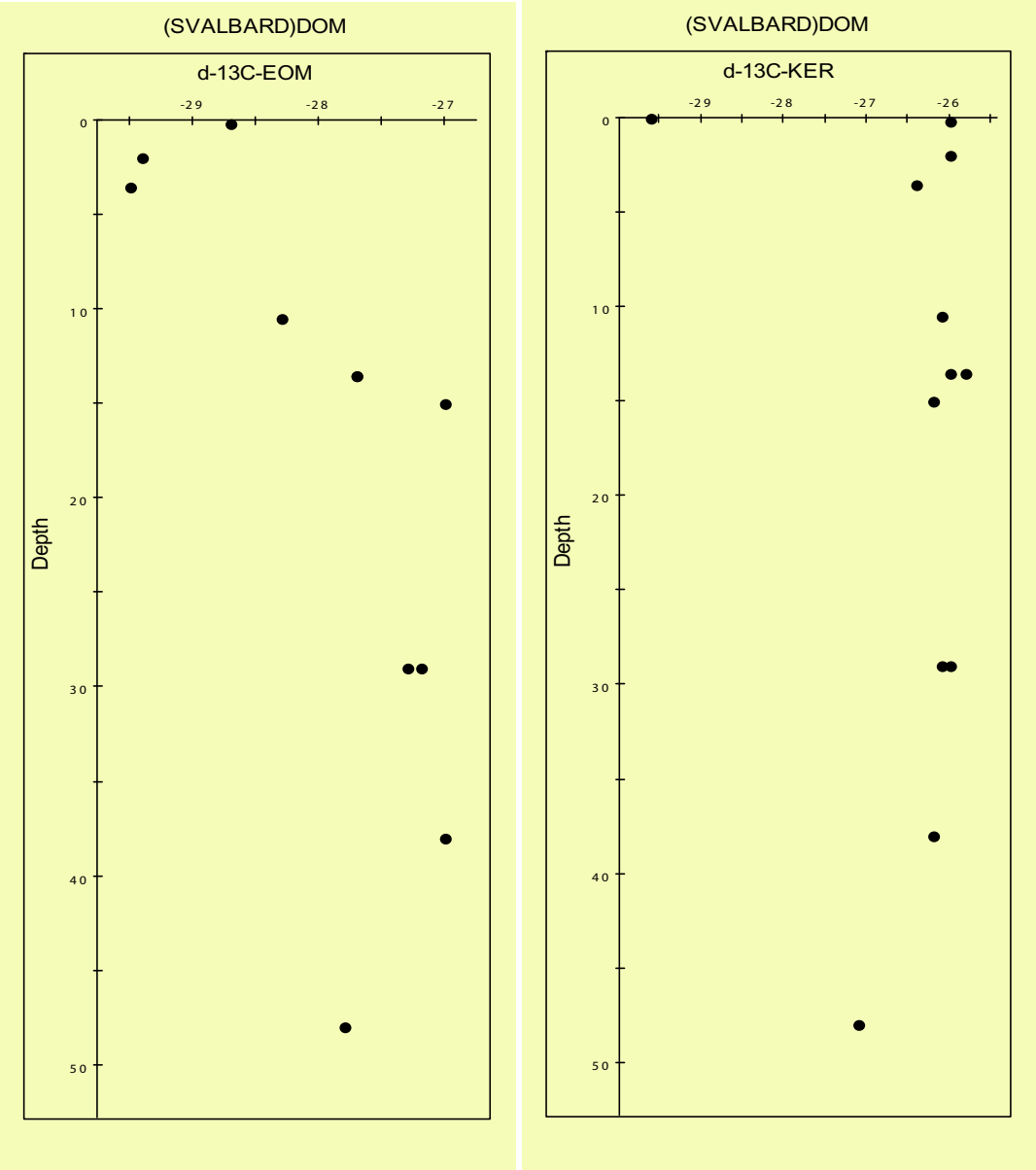

Figure E.6: *$\delta^{13}C$ EOM and $\delta^{13}C$ Kerogen ploted against distance from sill. Domen, Eastern Spitsbergen; Profile above sill*

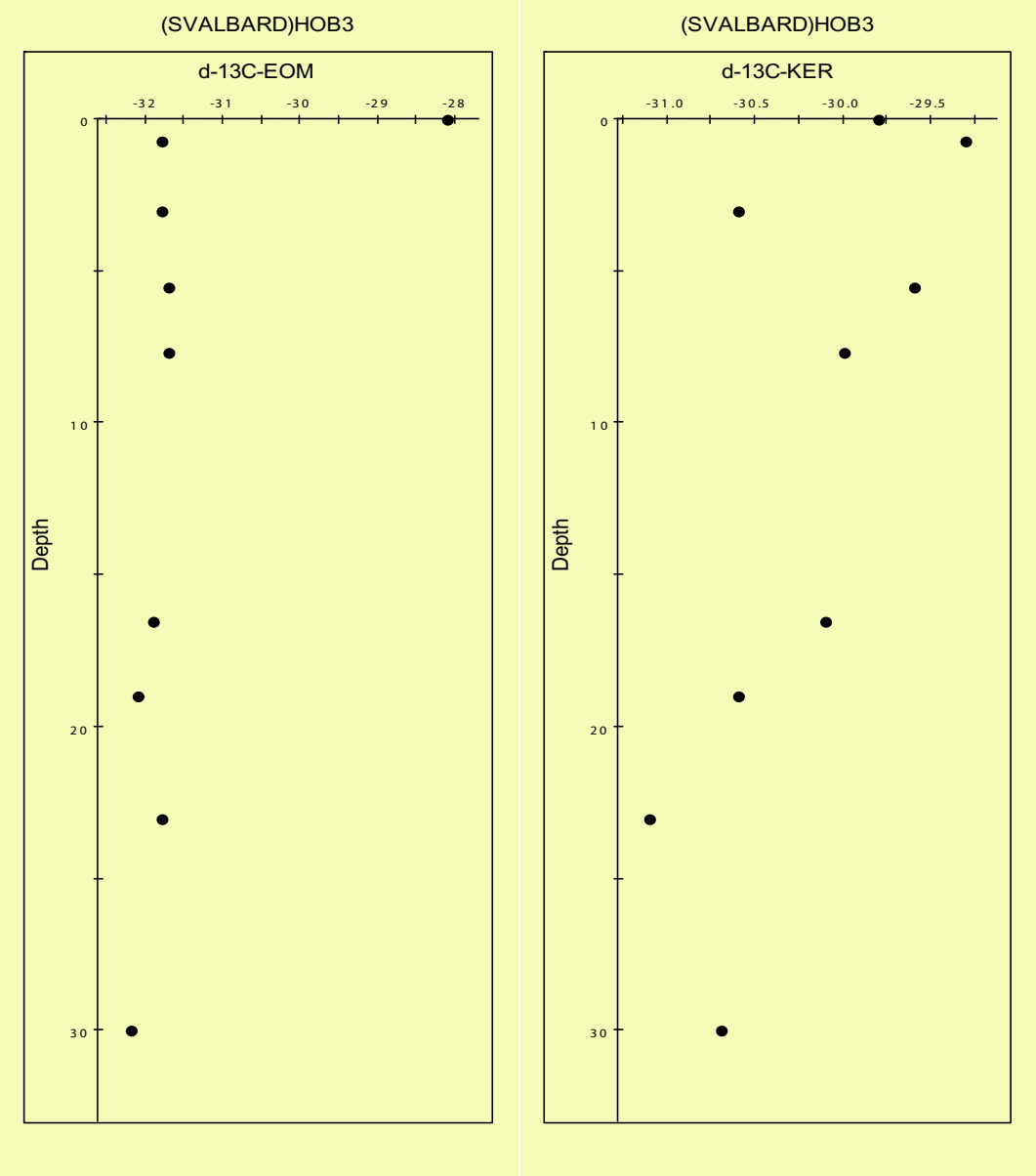

Figure E.7: *$\delta^{13}C$ EOM and $\delta^{13}C$ Kerogen ploted against distance from sill. Høgrinden South, Barentsøya; sampled laterally along a single horizon*

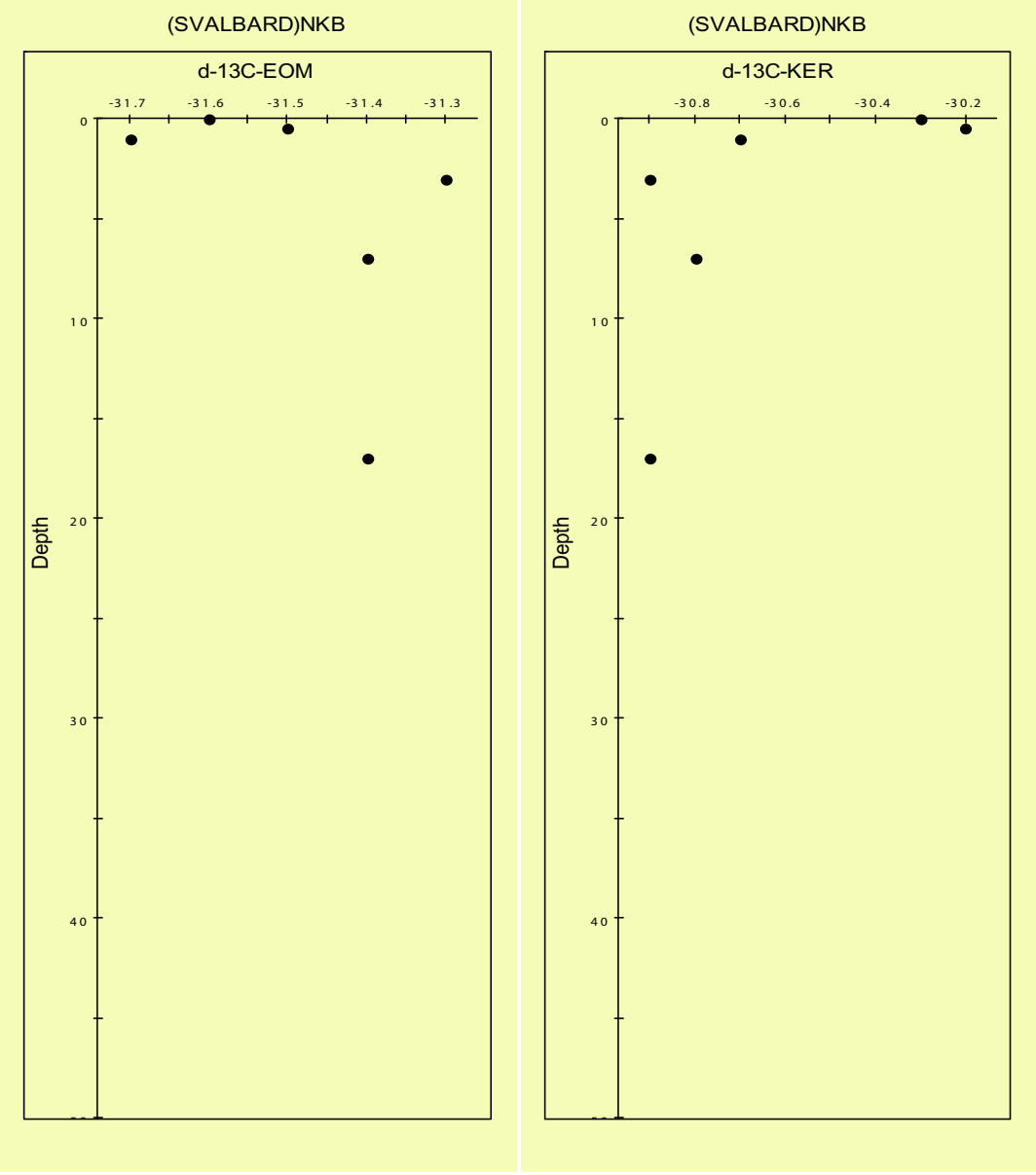

Figure E.8: *$\delta^{13}C$ EOM and $\delta^{13}C$ Kerogen Northern Kreftberget, Barentsøya; Profile without sill*

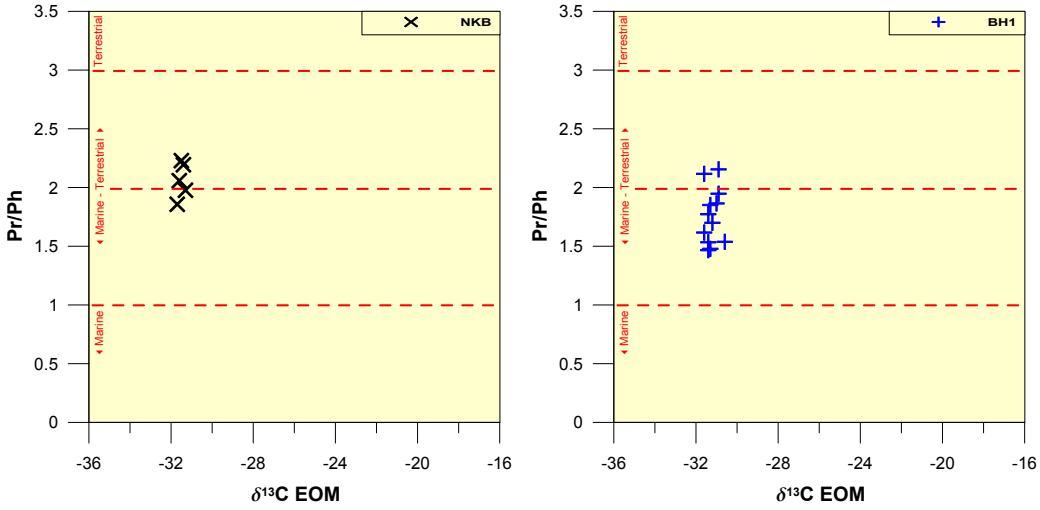

(a) NKB

(b) BH1

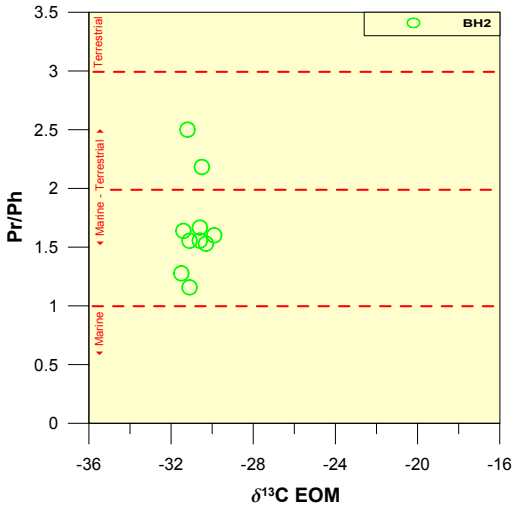

(c) BH2

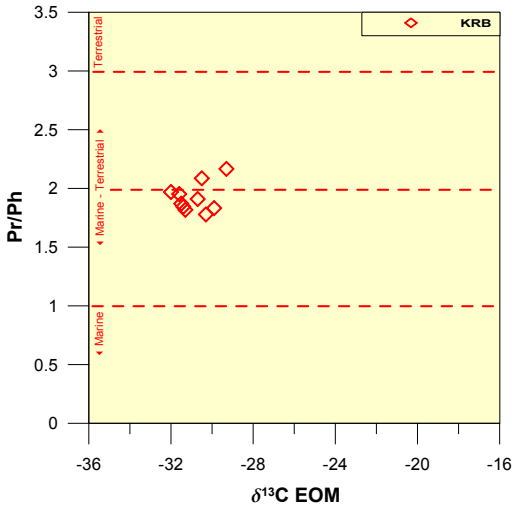

(d) KRB

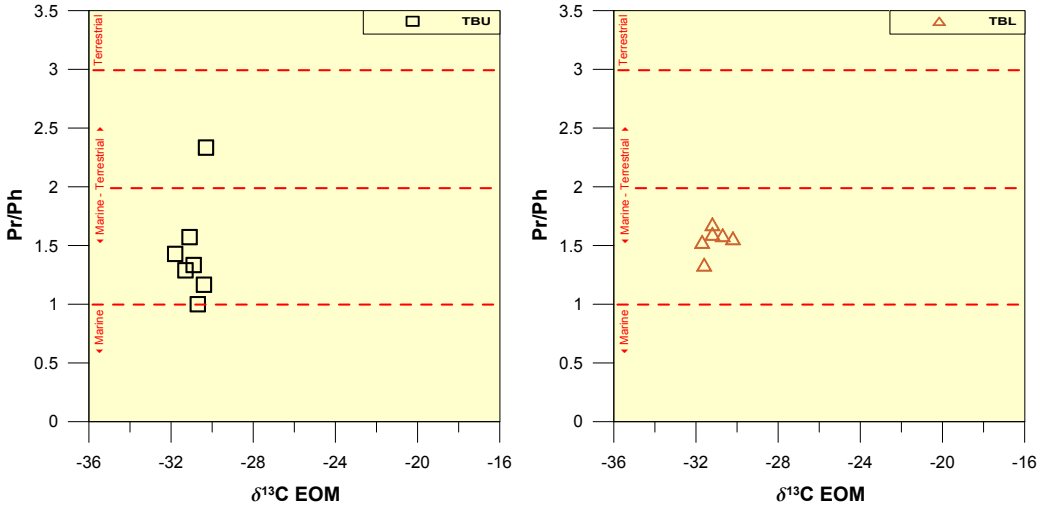

(e) TBU

(f) TBL

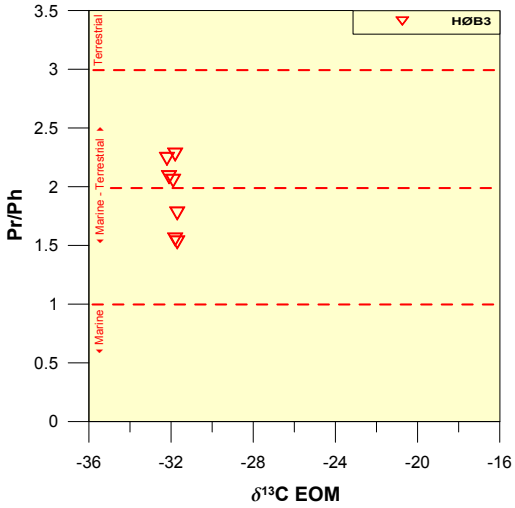

(g) HØB3

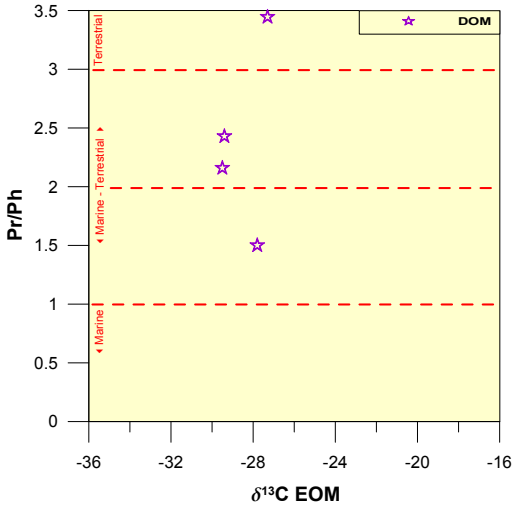

(h) DOM

Figure E.9: *Pristane/Phytane versus $\delta^{13}C$ EOM for each sample series*

Appendix F

Vitrinite reflectance

Vitrinite reflectance analyses was carried out at Institute for Energy Technology, Kjeller, Norway. The description of the analytical method below comes from their report.

Vitrinite reflectance determinations were conducted to identify the probable position of the "oil window" (zone of maximum bitumen generation), and the background maturity level of each locality.

F.1 Analysis

The analytical equipment being used for the vitrinite reflectance analysis was a Zeis MPM 03 photometer microscope equipped with an Epiplan-Neofluar 40/0.90 oil objective. The sensitive measuring spot was kept constant for all measurements at about 2.5 micron in diameter. The measurements were made through a green band pass filter (546 nm) and in oil immersion (refractive index 1.515 at 18°C).

The readings were made without a polarizer and using a stationary stage. This procedure is called measurements of random reflectance (%Rm). The photometer is calibrated daily against a standard of known reflectance (%Rm=0.588) and routinely (daily) checked against two other standards of significant different reflectances (% Rm=0.879 and 1.696). A deviation from these values of less than ±0.01 and ±0.02 respectively is considered as acceptable. The calibration is routinely checked during the course of measurements at least every hour, and a deviation of less than ±0.005 is considered acceptable.

For each sample at least 20 points were measured if possible, and quality ratings are given to various important aspects, which may affect the measurements. The aspects are abundance of vitrinite, uncertainties in the identification of indigenous vitrinite, type of vitrinite, particle size, particle surface quality and abundance of pyrite.

F.2 Results

The raw data from the measurements are presented here for each sample both as tabulated data and histograms. A true vitrinite population is selected among the readings based on observations made during the measurements, and arithmetic mean values are calculated for this population and other populations. A quality rating is given to the true population. The results are listed in Tables F.1 to F.11.

The PeGIS software (Dahl and Rasmussen, 2003) was used to produce Figures F.1 to F.8.

Figures On the figures I have not subdivided between “Good” and “Medium” samples, they are both plotted in the same series: “Pop1”, “Poor” is plotted as “Pop2”.

Table F.1: Vitrinite reflectance. Botneheia East, Central Spitsbergen; Profile with only a minor sill

Sample	m from base of Botneheia	Vitrinite reflectance VR	STD	Nb of meas	Sample quality
BH1-27	67.00	0.45	0.07	14	M
BH1-26	64.30	0.51	0.06	20	M
BH1-25	59.00	0.39	0.06	21	M
BH1-24	55.00	0.39	0.07	24	M
BH1-23	52.00	0.39	0.04	23	G
BH1-22	50.80	0.49	0.06	23	M
BH1-21	48.80	0.47	0.05	7	P
BH1-20	47.50	0.71	0.12	13	P
BH1-19	46.90	1.35	0.19	10	P
BH1-18	46.82	barren			
BH1-17	44.96	1.29	0.19	6	P
BH1-16	44.90	1.33	0.02	2	P
BH1-15	44.65	0.68	0.13	22	P
BH1-14	44.20	1.61	0.39	29	P
BH1-13	43.82	1.23	0.11	21	M
BH1-12	43.00	0.43	0.04	24	G
BH1-11	42.00	0.4	0.04	10	M
BH1-10	41.00	0.47	0.06	21	M
BH1-9	37.50	0.47	0.05	20	P
BH1-8	31.00	0.39	0.06	23	M
BH1-7	28.50	0.41	0.04	10	M
BH1-6	23.00	0.47	0.07	24	M
BH1-5	15.00	0.43	0.04	24	M
BH1-4	10.00	0.46	0.06	24	M
BH1-3	7.00	0.45	0.05	25	M
BH1-2	4.00	0.44	0.05	25	M
BH1-1	0.00	0.44	0.05	22	M

Table F.2: Vitrinite reflectance. Botneheia 2, Central Spitsbergen; Profile above sill

Sample	m from base of Botneheia	Vitrinite reflectance VR	STD	Nb of meas	Sample quality
BH2-30	58.00	0.41	0.06	20	M
BH2-29	55.50	0.45	0.08	17	P
BH2-28	52.00	0.5	0.09	5	P
BH2-27	45.00	0.56	0.07	5	P
BH2-26	42.50	0.51	0.06	20	M
BH2-25	39.50	0.57	0.06	14	M
BH2-24	36.00	0.55	0.05	20	M
BH2-23	33.00	0.6	0.05	23	M
BH2-22	30.00	0.57	0.03	19	M
BH2-21	27.00	0.85	0.04	6	P
BH2-20	23.50	0.89	0.04	6	P
BH2-19	19.50	4.5	0.26	20	P
BH2-18	17.50	4.52	0	1	P
BH2-17	16.80	2.7	0.26	5	P
BH2-16	14.50	5.56	0.46	17	M
BH2-15	14.00	3.11	0.36	19	P
BH2-14	13.50	4.83	0.37	7	P
BH2-13	11.00	2.48/3.24	0.28/0.15	23/6	M
BH2-12	9.00	2.65/3.87	0.53/0.19	6/8	P
BH2-11	7.00	2.11/3.50	0.40/0.30	8/7	P
BH2-10	5.70	2.32/5.19	0.47/0.09	22/3	P
BH2-9	5.00	2.22/4.64	0.26/0.35	21/3	P
BH2-8	4.00	2.06/4.15	0.27/0.46	19/6	P
BH2-7	3.00	2.22/3.98	0.38/0.18	21/7	P
BH2-6	2.00	2.22/3.95	0.40/0.30	24/5	P
BH2-5	1.50	2.31/3.37	0.28/0.15	20/8	P
BH2-4	1.00	2.45/1.25	0.31/0	26/1	P
BH2-3	0.70	barren			
BH2-2	0.30	barren			
BH2-1	0.00	1.06	0	1	M

Table F.3: Vitrinite reflectance. Krefftberget, Barentsøya, Profile above sill

Sample	m from sill	Vitrinite reflectance			
		VR	STD	Nb of meas	Sample quality
KRB-36		0.51	0.05	22	M
KRB-35		0.61	0.05	21	M
KRB-34		0.59	0.04	22	M
KRB-33		0.66	0.05	20	M
KRB-32		0.66	0.05	21	M
KRB-31		0.63	0.04	21	M
KRB-30		0.58	0.07	20	M
KRB-29		0.65	0.05	21	M
KRB-28		0.59	0.07	14	M
KRB-27		0.58	0.06	23	M
KRB-26	20.0	0.87	0.06	11	P
KRB-25	19.0	0.73	0.02	4	P
KRB-24	18.0	1.66	0.16	18	P
KRB-23	17.3	1.69	0.3	18	P
KRB-22	16.3	1.86	0.11	19	P
KRB-21	15.0	2.23	0.27	25	P
KRB-20	14.0	2.11	0.21	25	P
KRB-19	13.0	2.48	0.17	20	P
KRB-18A	12.0	2.88	0.19	22	P
KRB-18B	12.0	2.9	0.3	25	P
KRB-17	11.0	3.16	0.4	25	P
KRB-16	10.0	3.57	0.3	20	P
KRB-15	9.3	3.8	0.27	24	P
KRB-14	8.5	4.22	0.35	28	P
KRB-13	7.3	4.89	0.43	25	P
KRB-12	6.3	5.27	0.27	23	P
KRB-11	5.0	4.52	0.39	22	P
KRB-10	4.0	4.42	0.39	24	P
KRB-9	3.0	3.61	0.16	25	P
KRB-8	2.5	3.08	0.19	22	P
KRB-7	2.0	2.01	0.16	23	P
KRB-6	1.6	1.48	0.14	21	P
KRB-5	1.4	0.62/1.37	0.12/0.01	8/10/2	
KRB-4	1.0	0.68/1.04	0.02/0.12	3/9	
KRB-3A	0.7	1.33	0.19	22	M
KRB-3B	0.7	1.3	0.14	22	G
KRB-2	0.3	1.44	0.06	2	P
KRB-lA	0.1	barren			
KRB-1B	0.1	barren			
KRB-1C	0.1	barren			

Table F.4: Vitrinite reflectance. Teistberget, Eastern Spitsbergen, Profile above sill

Sample	m from sill	Vitrinite reflectance			
		VR	STD	Nb of meas	Sample quality
TBU-11	38.0	0.4	0.04	4	P
TBU-10	35.0	0.4	0.06	28	M
TBU-9	24.5	0.87	0.05	5	P
TBU-8	23.0	1.24	0.1	19	M
TBU-7	20.0	1.49	0.11	20	M
TBU-6	16.0	2	0.14	23	M
TBU-5	11.5	3.74	0.26	23	P
TBU-4	8.5	4.03	0.25	25	P
TBU-3	5.5	4.89	0.27	23	P
TBU-2	4.1	4.73	0.2	14	P
TBU-1	3.0	4.45	0.28	24	P

Table F.5: Vitrinite reflectance. Teistberget, Eastern Spitsbergen, Profile below sill

Sample	m from sill	Vitrinite reflectance			
		VR	STD	Nb of meas	Sample quality
TBL-1	0.05	barren			
TBL-2	0.4	barren			
TBL-3	1.0	0.75/1.13	0.07/0.09	9/12	P
TBL-4	2.2	1.84/2.46	0.13/0.22	17/9	P
TBL-5	3.5	4.2	0.57	22	M
TBL-6	5.0	4.61	0.25	21	P
TBL-7	8.0	4.19	0.32	18	P
TBL-8	9.0	3.95	0.48	19	M
TBL-9	12.0	3.03	0.21	22	M
TBL-10	17.0	2.23	0.18	21	G
TBL-11	22.0	1.55	0.18	19	M

Table F.6: Vitrinite reflectance. Domen, Eastern Spitsbergen, Profile above sill

Sample	m from sill	Vitrinite reflectance			
		VR	STD	Nb of meas	Sample quality
DOM-11	48.0	0.56	0.08	18	M
DOM-10	38.0	0.68	0.06	24	M
DOM-9A	29.0	0.67	0.05	20	M
DOM-9B	29.0	0.73	0.06	23	G
DOM-8	15.0	2.59	0.14	22	G
DOM-7	13.5	2.85	0.33	29	M
DOM-6	13.5	3.15	0.23	23	M
DOM-5	10.5	4.25	0.26	26	P
DOM-4	3.5	3.41	0.27	22	P
DOM-3	2.0	2.96	0.33	23	P
DOM-2	0.2	0.73/1.10	0.06/0.13	9/8	P
DOM-1	0.0	0.61/1.19	0.02/0.11	5110	P

Table F.7: Vitrinite reflectance. KMB-C

Sample	m from sill	Vitrinite reflectance			
		VR	STD	Nb of meas	Sample quality
KMB-C-1		barren			
KMB-C-2		1.19	0.32	4	P
KMB-C-3		1.60	0.16	11	P
KMB-C-4		4.99	0.28	26	P
KMB-C-5		4.84	0.36	21	P

Table F.8: Vitrinite reflectance. KMB-D

Sample	m from sill	Vitrinite reflectance			
		VR	STD	Nb of meas	Sample quality
KMB-D-1		2.92	0.04	3	P
KMB-D-2		baren			
KMB-D-3		2.18	0.22	7	P
KMB-D-4		2.40	0.20	13	P
KMB-D-5		2.72	0.36	6	P
KMB-D-6		2.58	0.31	8	P

Table F.9: Vitrinite reflectance. Høgrinden South, Barentsøya, sampled laterally along a single horizon

Sample	m from sill	Vitrinite reflectance			
		VR	STD	Nb of meas	Sample quality
HØB3-1	0.0	barren			
HØB3-2	0.7	0.95	0.05	13	P
HØB3-3	3.0	3.76	0.25	22	P
HØB3-4	5.5	5.11	0.33	25	P
HØB3-5	7.7	3.82	0.32	20	P
HØB3-6	16.5	1.18	0.10	9	M
HØB3-7	19.0	0.54	0.06	22	M
HØB3-8	23.0	0.35	0.08	10	M
HØB3-9	30.0	0.30	0.07	3	P

Table F.10: Vitrinite reflectance. Northern Krefftberget, Barentsøya, Profile without sill

Sample	m from start	Vitrinite reflectance			
		VR	STD	Nb of meas	Sample quality
NKB-14		1.73	0.14	21	G
NKB-13		0.48	0.02	4	P
NKB-12		0.55	0.04	18	M
NKB-11		0.58	0.06	25	M
NKB-10		0.55	0.05	19	M
NKB-9		0.54	0.04	22	M
NKB-8		0.6	0.07	24	M
NKB-7		0.49	0.05	19	M
NKB-6	17.0	0.38	0.04	9	M
NKB-5	1.0	0.45	0.05	20	M
NKB-4	7.0	0.28	0.02	19	M
NKB-3	3.0	0.29	0.03	23	M
NKB-2	0.5	0.34	0.06	23	M
NKB-1	0.0	0.34	0.08	5	P

Table F.11: Vitrinite reflectance. NPD standard source-rocks

Sample	m from sill	Vitrinite reflectance			
		VR	STD	Nb of meas	Sample quality
JR-1, aliquot #13		0.22/0.42	0.04/0.03	8/10	P
SR-1, aliquot #13		0.31	0.03	29	M

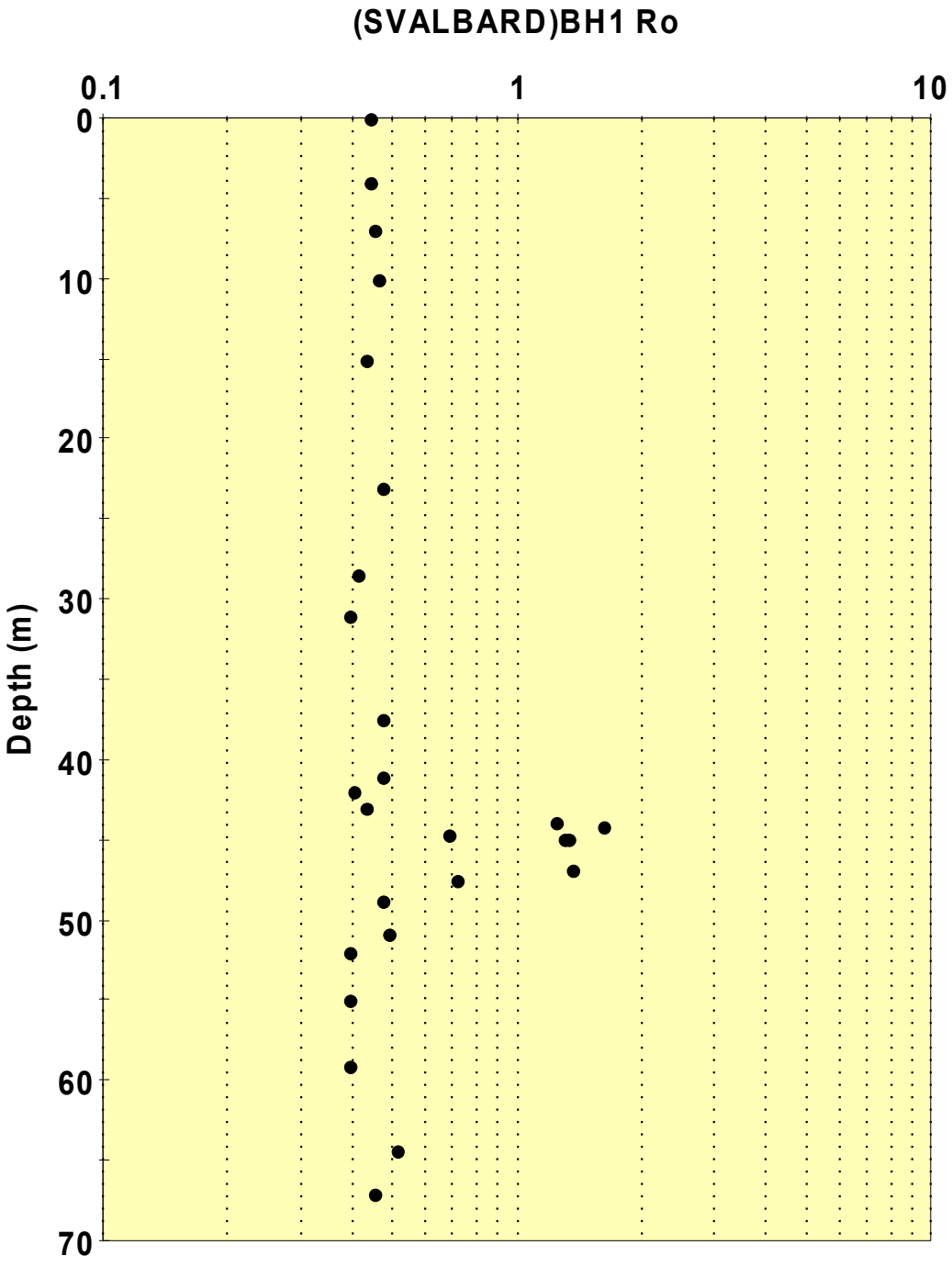

Figure F.1: *Vitrinite reflectance plotted against distance from base Botneheia Fm. Botneheia East, Central Spitsbergen; Profile with only a minor sill*

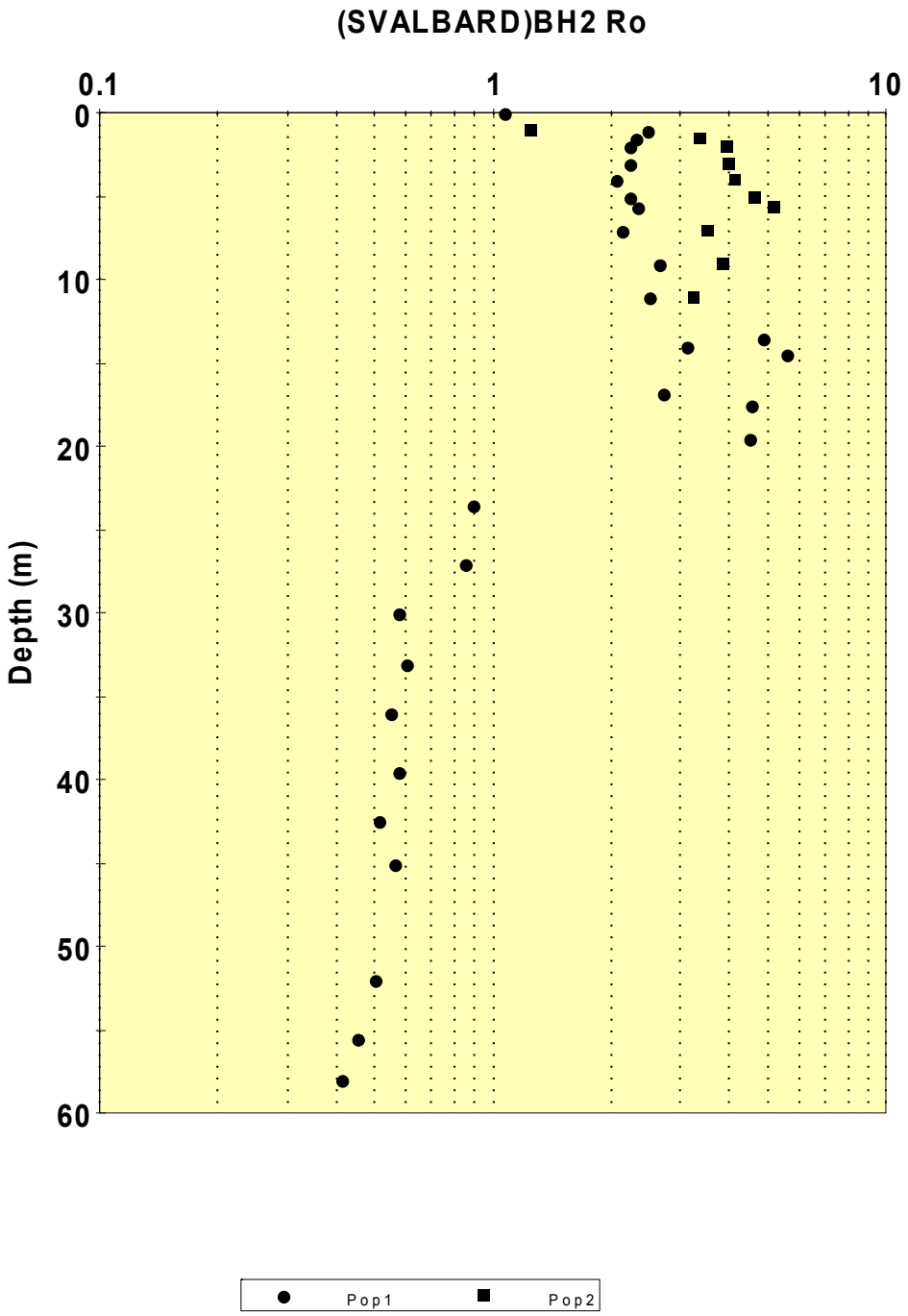

Figure F.2: *Vitrinite reflectance plotted against distance from sill. Botneheia 2, Central Spitsbergen; Profile above sill*

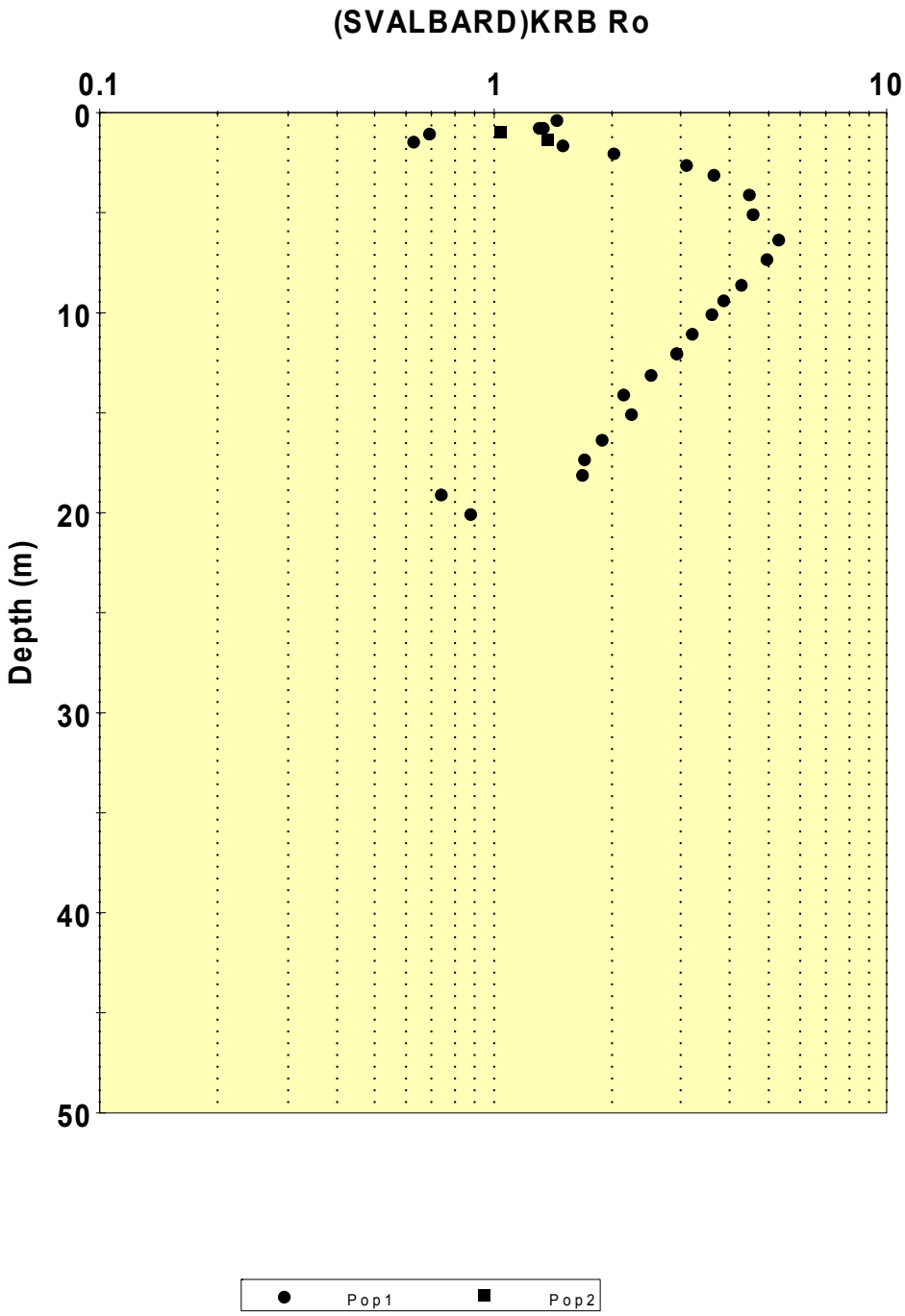

Figure F.3: *Vitrinite reflectance plotted against distance from sill. Krefftberget, Barentsøya: Profile above sill*

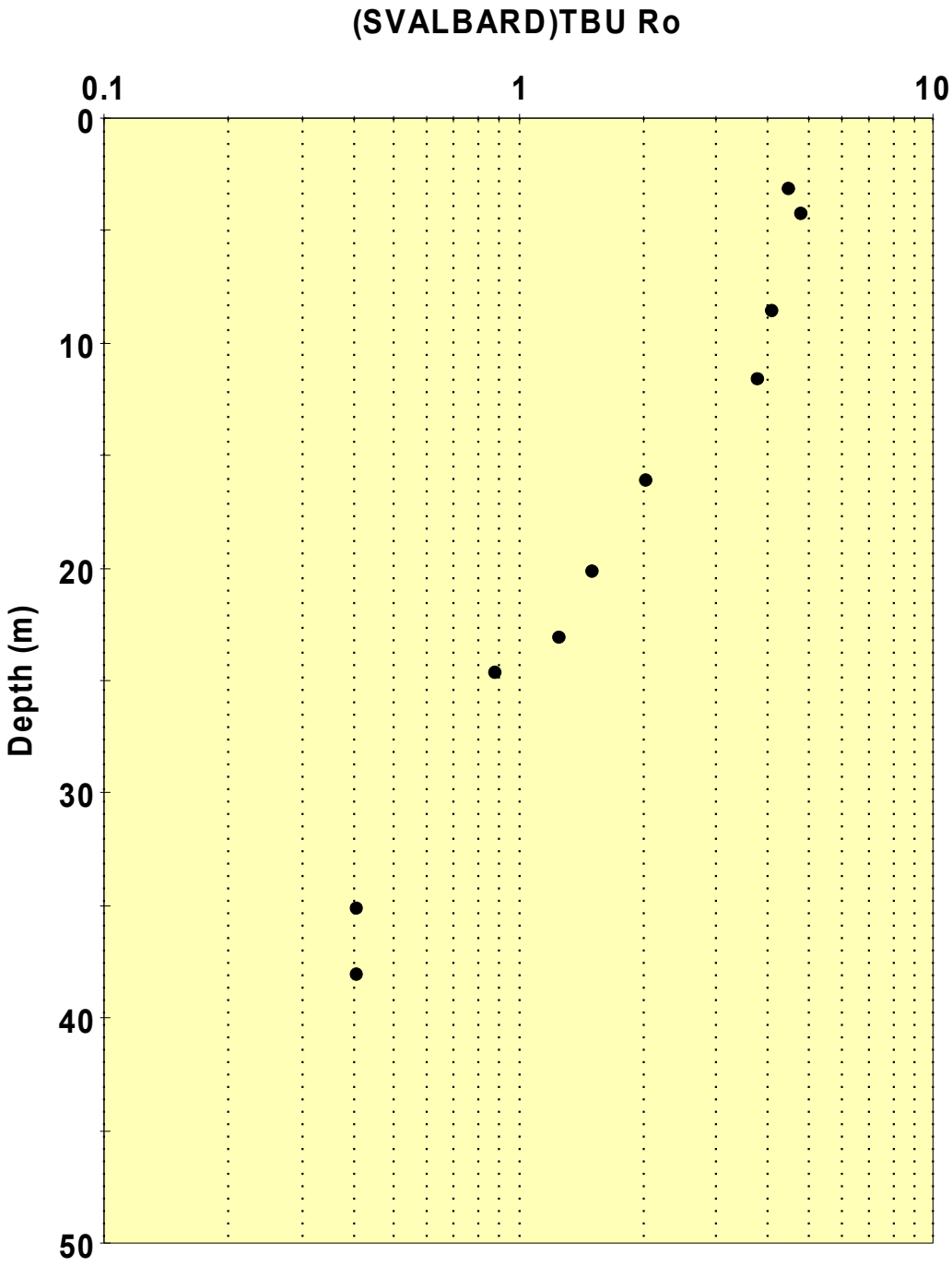

Figure F.4: *Vitrinite reflectance plotted against distance from sill. Teistberget, Eastern Spitsbergen; Profile above sill*

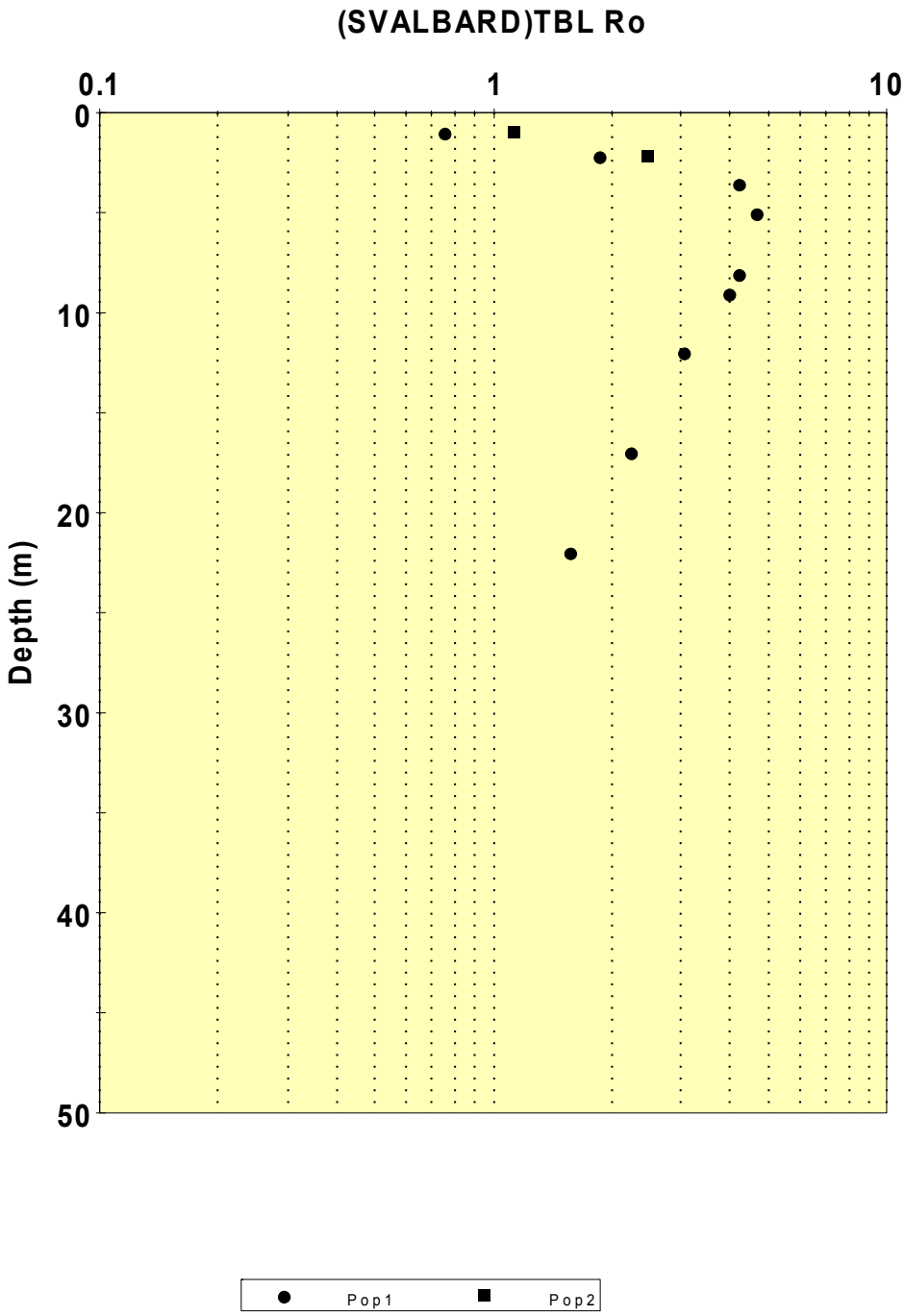

Figure F.5: *Vitrinite reflectance plotted against distance from sill. Teistberget, Eastern Spitsbergen; Profile below sill*

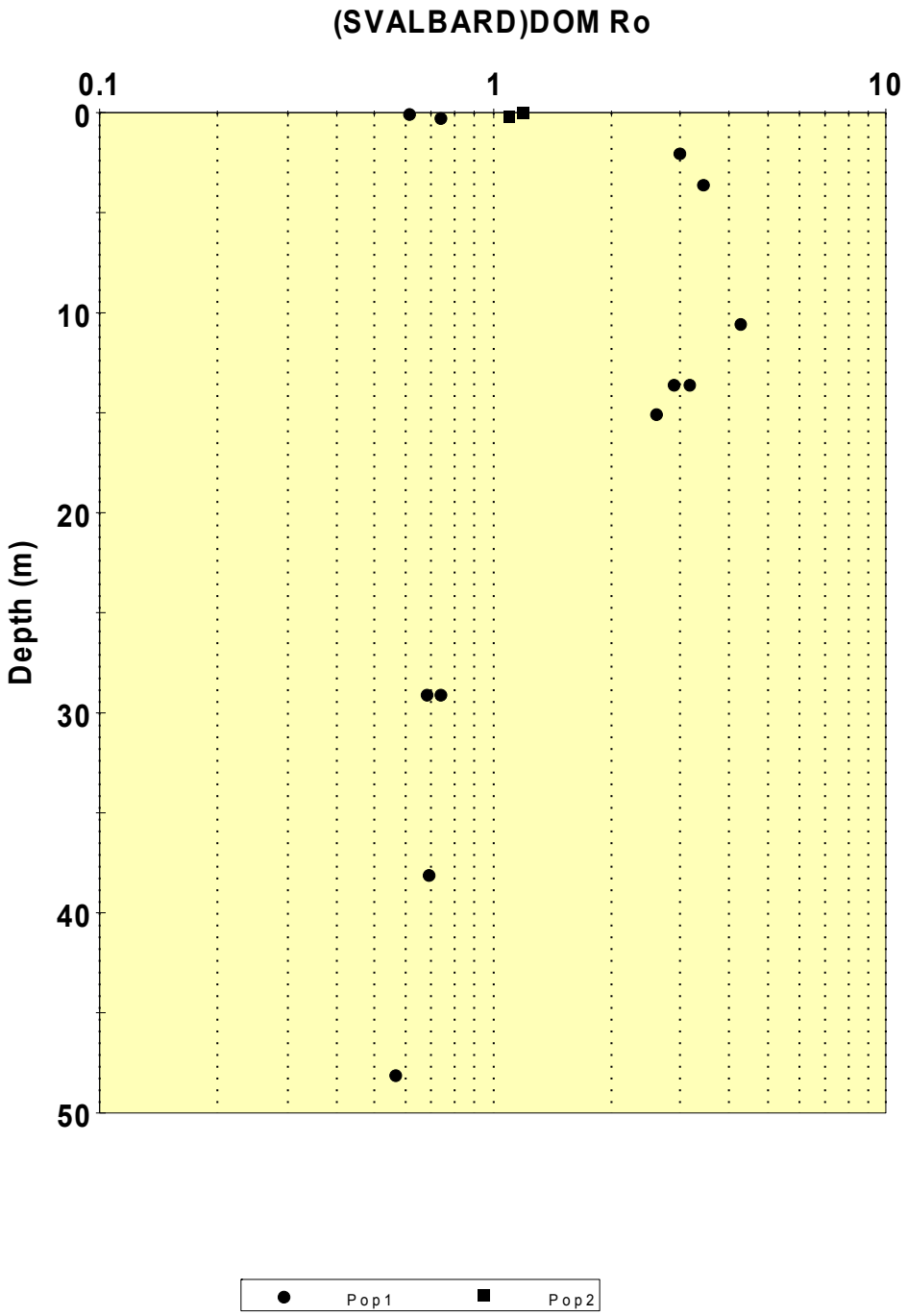

Figure F.6: *Vitrinite reflectance plotted against distance from sill. Domen, Eastern Spitsbergen; Profile above sill*

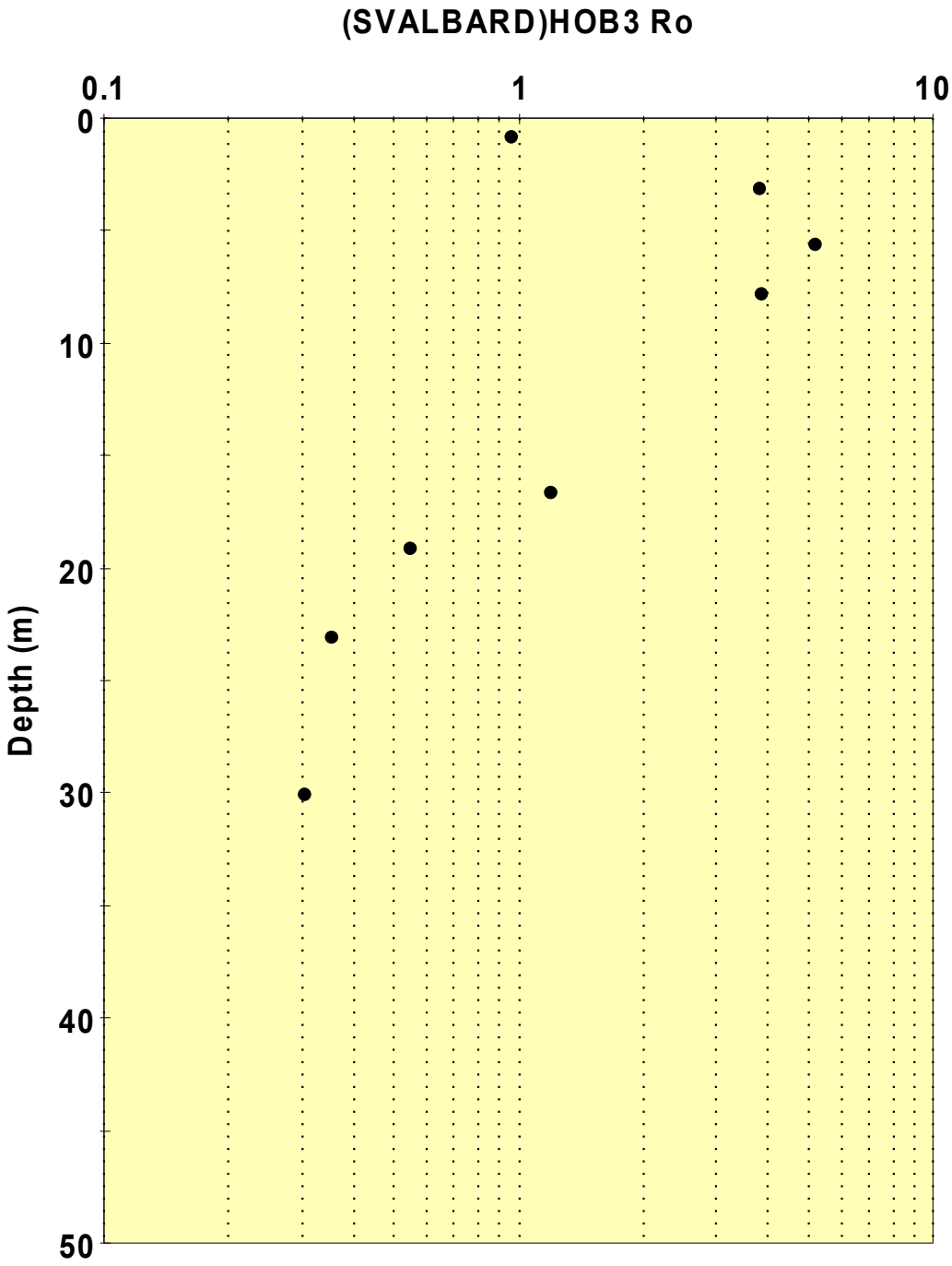

Figure F.7: *Vitrinite reflectance plotted against distance from sill Høgrinden South, Barentsøya. Sampels sampled laterally along a single horizon*

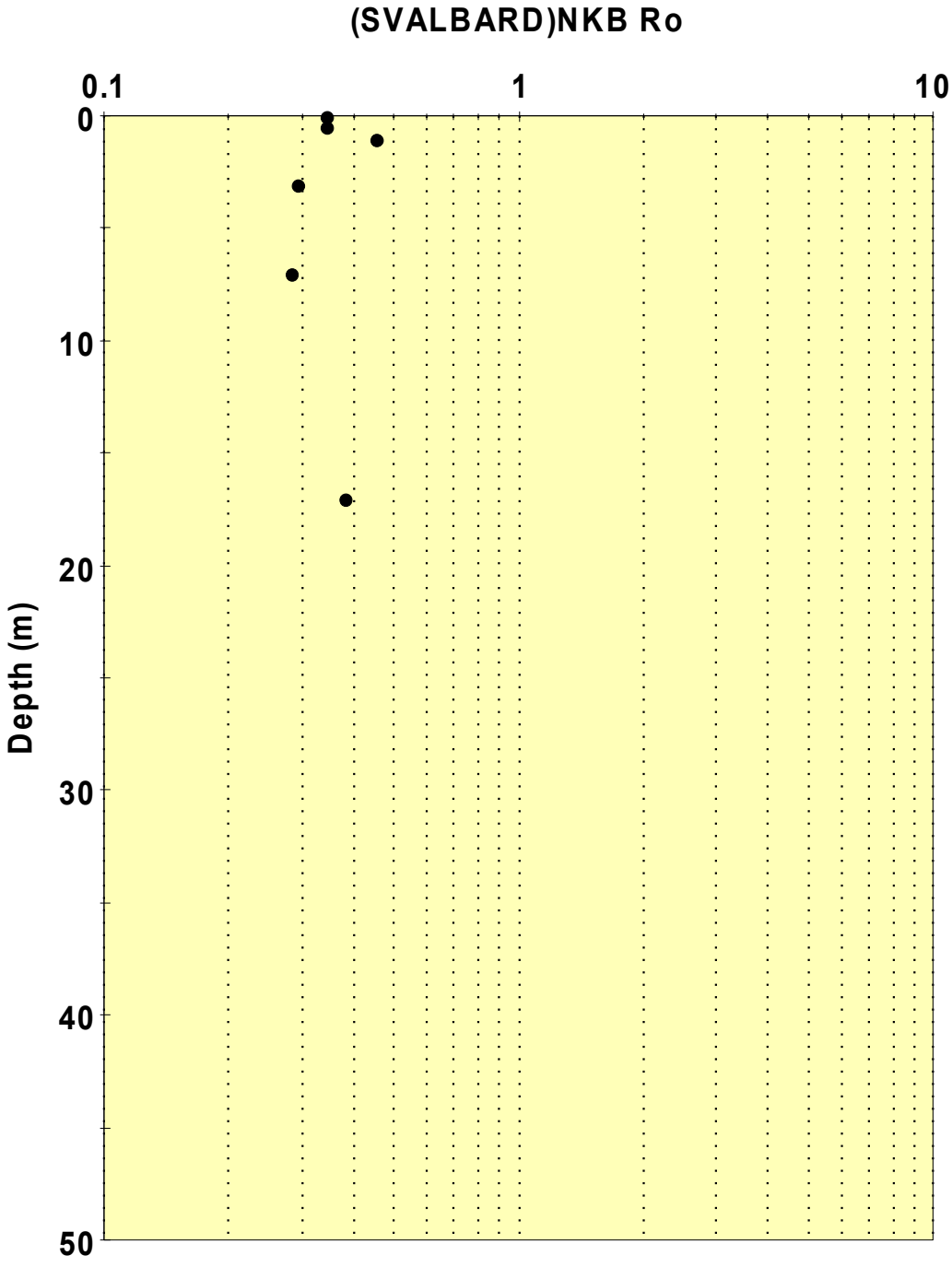

Figure F.8: *Vitrinite reflectance. Northern Kreftberget, Barentsøya; Profile without sill*

Appendix G

Kerogen description

The kerogen descriptions was performed at Institute for Energy Technology, Kjeller, Norway. The description of the analytical method below comes from their report.

G.1 Analyses

The analytical equipment being used was a Zeiss MPM 03 photometer microscope equipped for transmitted white light and incident blue light. The observations were made through a Neofluar 10/0.30 dry objective and a Neofluar 40/0.75 O.D. dry objective. The white light source of the microscope, a 100W tungsten lamp, was set to 7V. As source for the blue light, a HBO 100W/2 mercury lamp, was used.

The samples are described by sorting the organic material found into six main groups by percent. These groups are: Fluoramorphinite (FA), Hebamorphinite (HA), Algal organic matter (AL), Herbaceous organic matter (HE), Woody organic matter (WO) and Coaly organic matter (CO).

The kerogen composition is reported to a precision ± 10% and the values are reported as integers. The results are listed in Table G.1 on the following page to Table G.12 on page 270.

G.2 Results

On the following pages, the results from the Kerogen description analyses can be seen. The values in Table G.1 to Table G.12 from the Ife report. Figure G.1 and G.2 was made by the author.

Table G.1: Botneheia East, Central Spitsbergen; Profile with only a minor sill

Sample	m from base of Botneheia	Kerogen description FA(%)	HA(%)	AL(%)	HE(%)	WO(%)	CO(%)
BH1-27	67.0	35	30	0	10	10	15
BH1-26	64.3	60	15	0	10	5	10
BH1-25	59.0	55	25	0	10	5	5
BH1-24	55.0	50	25	0	15	0	10
BH1-23	52.0	30	15	5	10	10	35
BHl-22	50.8	5	45	0	10	0	40
BH1-21	48.8	0	65	0	5	0	30
BH1-20	47.5	0	5	0	0	0	95
BH1-19	46.9	0	50	0	5	0	45
BH1-18 Poor sample	46.8	0	0	0	0	0	100
BH1-17 Poor sample	45.0	0	0	0	0	0	100
BH1-16	44.9	0	5	0	0	0	95
BH1-15	44.7	0	10	0	0	0	90
BH1-14	44.2	0	20	0	0	0	80
BH1-13	43.8	5	45	0	5	5	40
BH1-12	43.0	5	45	5	5	5	35
BH1-11	42.0	5	55	5	5	0	30
BH1-10	41.0	5	55	10	5	0	25
BH1-9	37.5	30	15	15	10	0	30
BH1-8	31.0	20	65	0	15	0	15
BH1-7	28.5	20	60	0	10	0	20
BH1-6	23.0	10	65	0	10	0	15
BH1-5	15.0	20	35	20	15	0	10
BH1-4	10.0	30	50	0	10	0	10
BH1-3	7.0	30	35	0	20	5	10
BH1-2	4.0	20	35	0	15	0	30
BH1-1	0.0	20	35	0	20	5	20

Table G.2: Botneheia 2, Central Spitsbergen; Profile above sill

Sample	m from base of Botneheia	Kerogen description FA(%)	HA(%)	AL(%)	HE(%)	WO(%)	CO(%)
BH2-30	58.0	35	30	0	10	S	20
BH2-29	55.5	25	30	0	10	5	30
BH2-28	52.0	0	70	0	10	0	20
BH2-27	45.0	0	35	0	15	0	50
BH2-26	42.5	0	45	0	10	5	40
BH2-25	39.5	0	35	0	15	10	40
BH2-24	36.0	0	55	0	0	5	40
BH2-23	33.0	0	50	0	0	5	45
BH2-22	30.0	0	35	0	0	30	35
BH2-21	27.0	0	40	0	0	15	45
BH2-20	23.5	0	60	0	0	10	30
BH2-19	19.5	0	10	0	0	0	90
BH2-18	17.5	0	0	0	0	0	100
BH2-17	16.8	0	0	0	0	0	100
BH2-16	14.5	0	10	0	0	0	90
BH2-15	14.0	0	5	0	0	0	95
BH2-14	13.5	0	5	0	5	0	90
BH2-13	11.0	0	20	0	5	0	75
BH2-12	9.0	0	10	0	5	0	85
BH2-11	7.0	0	10	0	0	0	90
BH2-10	5.7	0	5	0	0	0	95
BH2-9	5.0	0	0	0	0	0	100
BH2-8	4.0	0	0	0	0	0	100
BH2-7	3.0	0	0	0	0	0	100
BH2-6	2.0	0	0	0	0	0	100
BH2-5	1.5	0	0	0	0	0	100
BH2-4	1.0	0	70	0	0	0	30
BH2-3	0.7	50	10	0	10	0	30
BH2-2 Poor sample	0.3	0	60	0	0	0	40
BH2-1 Poor sample	0.0	0	60	0	0	0	40

Table G.3: Kreftsberget, Barentsøya, Profile above sill

Sample	m from sill	Kerogen description FA(%)	HA(%)	AL(%)	HE(%)	WO(%)	CO(%)
KRB-36		30	15	0	5	25	25
Possible content of algae		15	15	15	5	25	25
KRB-35		25	5	0	5	25	40
Possible content of algae		15	5	10	5	25	40
KRB-34		35	10	0	5	20	30
Possible content of algae		15	10	20	5	20	30
KRB-33		30	10	0	10	20	30
Possible content of algae		15	10	15	10	20	30
KRB-32		10	10	0	20	20	40
KRB-31		20	10	0	20	10	40
Possible content of algae		5	10	15	20	10	40
KRB-30		35	5	0	30	10	20
KRB-29		35	15	0	10	10	30
KRB-28		20	25	10	15	10	20
Certain recognition of dinocysts							
KRB-27		10	55	5	20	0	10
Certain recognition of dinocysts							
KRB-26	20.0	5	30	0	15	0	50
KRB-25	19.0	20	40	0	10	0	30
KRB-24	18.0	10	30	0	20	0	40
KRB-23 Poor sample	17.3	5	25	0	20		50
KRB-22 Poor sample	16.3	0	50	0	0	0	50
KRB-21	15.0	0	75	0	5	0	20
KRB-20	14.0	5	60	0	15	0	20
KRB-19	13.0	0	80	0	5	0	15
KRB-18A	12.0	0	50	0	0	0	50
KRB-18B	12.0	5	45	0	0	0	50
KRB-17	11.0	0	25	0	0	0	75
KRB-16	10.0	0	50	0	15	5	30
KRB-15	9.3	0	15	0	0	0	85
KRB-14	8.5	0	10	0	0	0	90
KRB-13	7.3	0	5	0	0	0	95
KRB-12	6.3	0	5	0	0	0	95
KRB-11	5.0	0	0	0	0	0	100
KRB-10	4.0	0	0	0	0	0	100
KRB-9	3.0	0	0	0	0	0	100
KRB-8	2.5	0	0	0	0	0	100
KRB-7	2.0	0	0	0	0	0	100
KRB-6	1.6	0	0	0	0	0	100
KRB-5	1.4	0	0	0	0	0	100
KRB-4	1.0						
KRB-3A	0.7	0	0		0	0	100

Table G.4: Table G.3 cont.

Sample	m from sill	Kerogen description FA(%)	HA(%)	AL(%)	HE(%)	WO(%)	CO(%)
KRB-2 Poor sample	0.3	0	0		0	0	100
KRB-1A Poor sample	0.1	0	0	0	0	0	100
KRB-1B Poor sample	0.1	0	0	0	0	0	100
KRB-1C Poor sample	0.1						

Table G.5: Northern Kreftsberget, Barentsøya, Profile without sill

Sample	m from sill	Kerogen description FA(%)	HA(%)	AL(%)	HE(%)	WO(%)	CO(%)
NKB-14		5	50	0	10	15	20
NKB-13		0	10	0	5	20	65
NKB-12		10	25	0	15	15	35
NKB-11		10	25	10	15	20	20
NKB-10		15	20	15	10	10	30
NKB-9		20	20	5	10	15	30
Dinocysts/acritarchs							
NKB-8		20	20	0	10	20	30
NKB-7		30	25	5	15	15	10
Acritarchs							
NKB-6	17.0	75	5	0	5	5	10
Possible content of algae		60	5	15	5	5	10
NKB-5	1.0	80	0	0	10	5	5
NKB-4	7.0	90	0	0	5	0	5
NKB-3	3.0	95	0	0	5	0	0
NKB-2	0.5	80	0	0	10	5	5
NKB-1	0.0	60	0	20	10	0	10

Table G.6: Høgrinden South, Barentsøya, sampled laterally along a single horizon

Sample	m from sill	Kerogen description FA(%)	HA(%)	AL(%)	HE(%)	WO(%)	CO(%)
HØB3-1 Poor sample	0.0	0	10	0	0	0	90
HØB3-2	0.7	0	20	0	0	0	80
HØB3-3	3.0	0	0	0	0	0	100
HØB3-4	5.5	0	35	0	15	0	50
HØB3-5	7.7	0	60	0	10	0	30
HØB3-6	16.5	35	20	0	20	5	20
Possible content of algae		15	20	20	20	5	20
HØB3-7	19.0	40	10	0	30	5	15
HØB3-8	23.0	50	10	0	20	5	15
Possible content of algae		20	10	20	20	5	15
HØB3-9	30.0	70	0	0	20	0	10
Possible content of algae		50	0	20	20	0	10

Table G.7: Teistberget, Eastern Spitsbergen, Profile above sill

Sample	m from sill	Kerogen description FA(%)	HA(%)	AL(%)	HE(%)	WO(%)	CO(%)
TBU-11 Poor sample	38.0	35	20	20	10	5	10
TBU-10	35.0	5	75	0	5	5	10
TBU-9 Poor sample	24.5	0	60	0	0	0	40
TBU-8	23.0	0	60	0	10	0	30
TBU-7	20.0	0	65	0	5	0	30
TBU-6	16.0	0	60	0	0	0	40
TBU-5	11.5	0	30	0	0	0	70
TBU-4	8.5	0	10	0	0	0	90
TBU-3	5.5	0	5	0	0	0	95
TBU-2	4.1	5	0	0	0	0	95
TBU-1	3.0	5	45	0	0	0	50

Table G.8: Teistberget, Eastern Spitsbergen, Profile below sill

Sample	m from sill	Kerogen description FA(%)	HA(%)	AL(%)	HE(%)	WO(%)	CO(%)
TBL-1 Poor sample	0.1		0	0	0	0	100
TBL-2	0.4	20	20	0	0	0	60
TBL-3	1.0	0	0	0	0	0	100
TBL-4	2.2	0	5	0	0	0	95
TBL-5	3.5	0	5	0	5	0	90
TBL-6	5.0	0	5	0	5	0	90
TBL-7	8.0	0	5	0	5	0	90
TBL-8	9.0	0	30	0	5	0	65
TBL-9	12.0	0	25	0	0	5	70
TBL-10	17.0	5	65	0	5	5	20
TBL-11	22.0	25	40	0	10	5	20

Table G.9: Domen, Eastern Spitsbergen, Profile above sill

Sample	m from sill	Kerogen description FA(%)	HA(%)	AL(%)	HE(%)	WO(%)	CO(%)
DOM-11	48.0	0	65	0	20	5	10
DOM-10	38.0	35	30	0	10	10	15
DOM-9A	29.0	20	30	0	20	15	15
DOM-9B	29.0	20	30	0	20	15	15
DOM-8	15.0	0	55	0	5	0	40
DOM-7	13.5	0	50	0	10	10	30
DOM-6	13.5	0	50	0	5	5	40
DOM-5	10.5	0	40	0	5	5	50
DOM-4	3.5	0	65	0	0	5	30
DOM-3	2.0	0	65	0	0	5	30
DOM-2 Poor sample	0.2	0	40	0	0	0	60
DOM-1 Poor sample	0.0	0	0	0	0	0	100

Table G.10: KMB-C

Sample	m from sill	Kerogen description FA(%)	HA(%)	AL(%)	HE(%)	WO(%)	CO(%)
KMB-C-1		0	55	0	5	0	40
KMB-C-2		0	40	0	20	5	35
KMB-C-3		10	30	0	0	0	60
KMB-C-4		0	20	0	0	0	80
KMB-C-5		0	0	0	0	0	100

Table G.11: KMB-D

Sample	m from sill	Kerogen description FA(%)	HA(%)	AL(%)	HE(%)	WO(%)	CO(%)
KMB-D-1 Poor sample		0	15	0	5	0	80
KMB-D-2 Poor sample		0	50	0	0	0	50
KMB-D-3 Poor sample		0	40	0	10	0	50
KMB-D-4 Poor sample		10	30	0	10	10	40
KMB-D-5 Poor sample		10	40	0	20	0	30
KMB-D-6 Poor sample		10	30	0	30	0	30

Table G.12: NPD standard source-rocks

Sample	m from sill	Kerogen description FA(%)	HA(%)	AL(%)	HE(%)	WO(%)	CO(%)
JR-1, aliqout #13		40	0	45	5	0	10
SR-1, aliquot #13		10	35	25	15	5	10

Table G.13: Legend to table G.1 - G.12 and the kerogen description figures in this appendix and in chapter 5

FA	Fluorescing amorphous material
HA	Non-fluorescing amorphous material
AL	Algal material and dinocysts
HE	Herbacaous material, spores, pollen, cuticles
WO	Woody material
CO	Coal

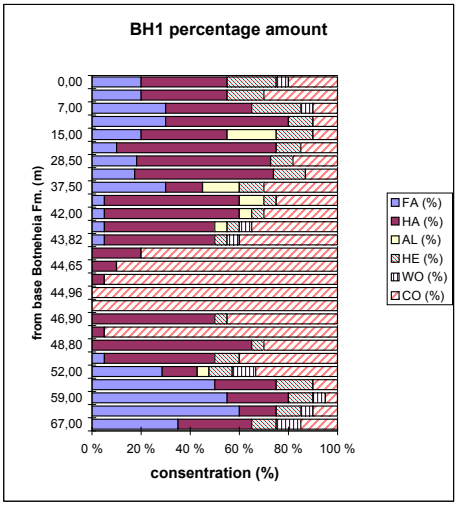

(a) BH1

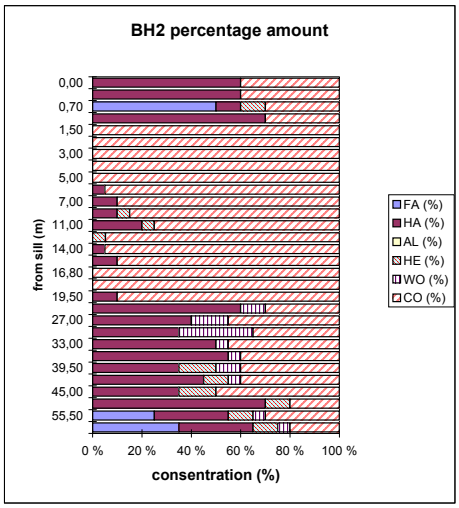

(b) BH2

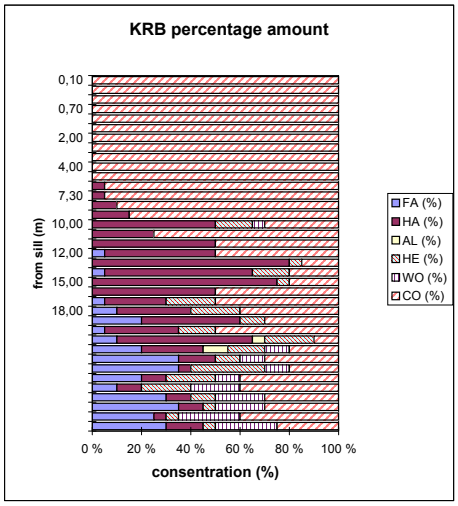

(c) KRB

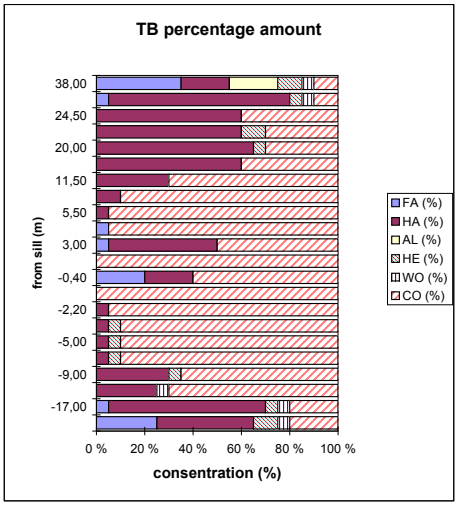

(d) TB

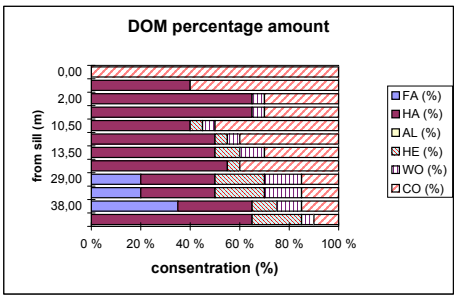

(e) DOM

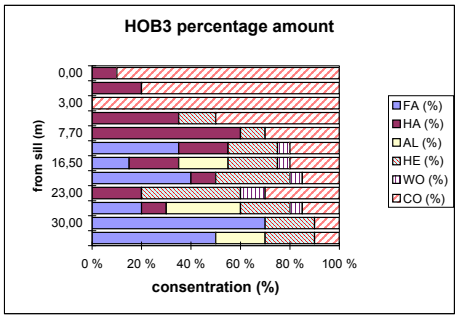

(f) HØB3

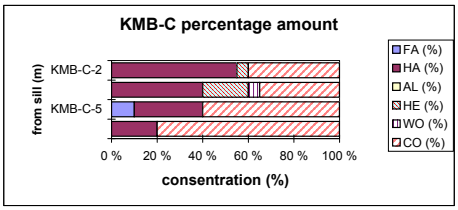

(g) KMB-C

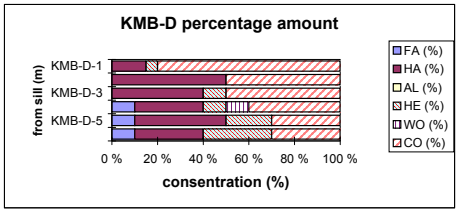

(h) KMB-D

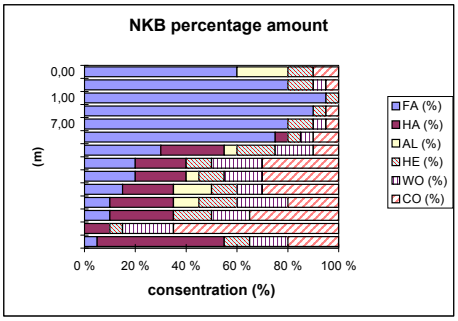

(i) NKB

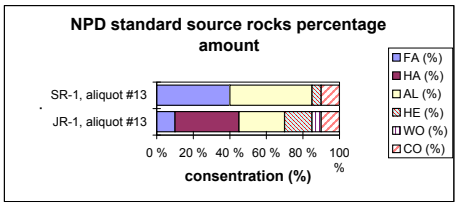

(j) NPD

Figure G.1: *% distribution of the kerogen content*

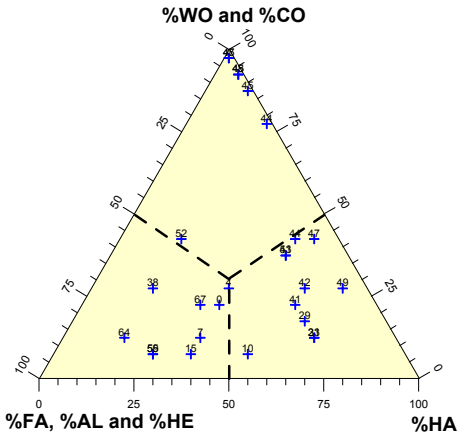

(a) BH1

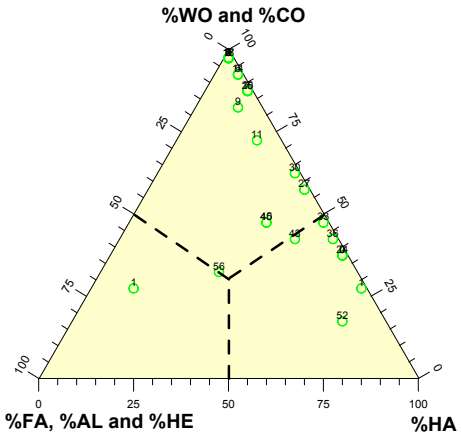

(b) BH2

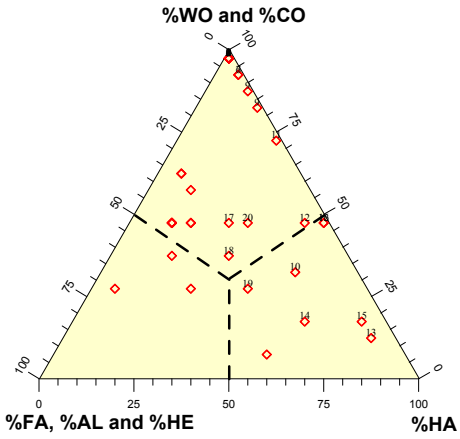

(c) KRB

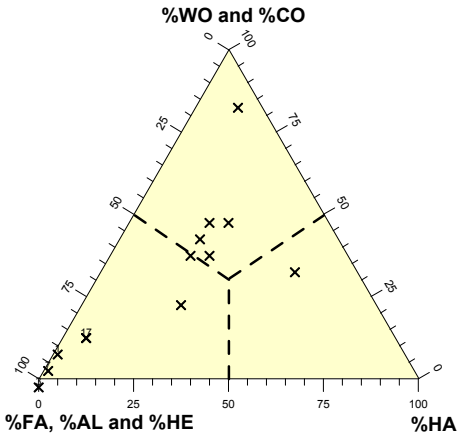

(d) NKB

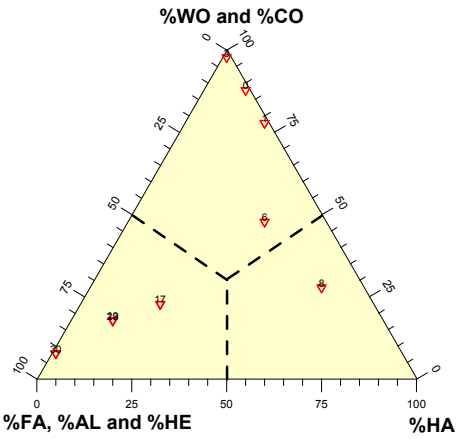

(e) HOB3

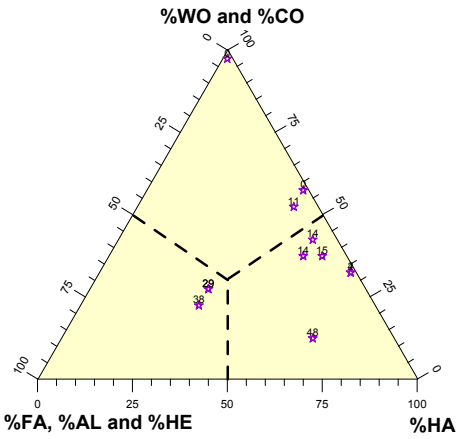

(f) DOM

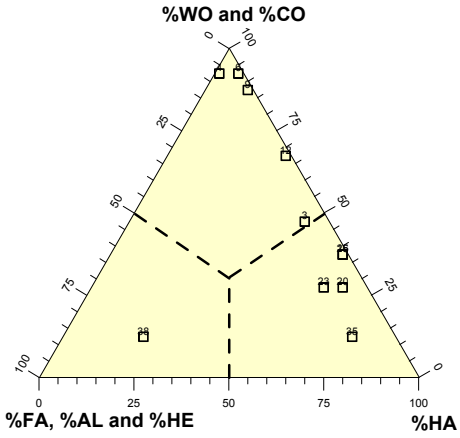

(g) TBU

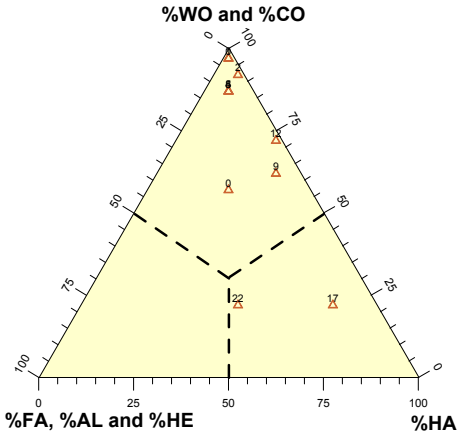

(h) TBL

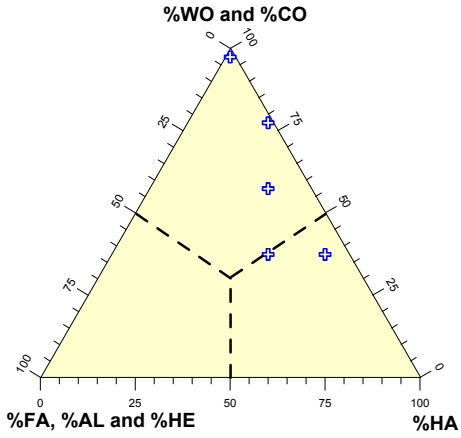

(i) KMB-C

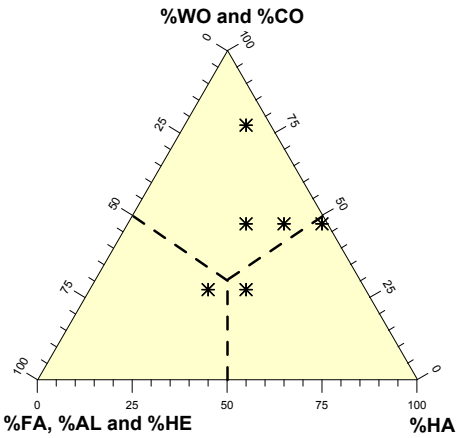

(j) KMB-D

Figure G.2: *Ternary Plots made from the Vitrinite description data from all sampled series. The number above each sample mark represent the distance from sill.*

Appendix H

Mathematica Source Code

On the next to pages I have included the sorce code for the termperature plots presented in Chapter 5.

The plots have been calculated using Equation 5.5 on page 99.

The thickness of the sill in this theoretical plots is 30 meter. Magma temperature is 1000°C assuming instantaneous intrusion of the sill into source-rock.

The rock to be intruded by a sill (the country rock) is assumed to be at 1500 meter depth. Two temperatures have been used, in order to account for both areas with a normal geothermal gradient (30°C pr. km), and for areas with high volcanic activity (60°C pr. km). At 1500 meter depth this gives an start temperature of 45°C and 90°C respectively.

For further details, see source code.

```
Temp[t_, x_, Tm_, T0_]:=Block[{κ, τ, L, arg1, arg2},
κ = 10^-6;
L = 15;
τ = t * 365.25 * 24 * 3600;
arg1 = (L-(L+x))/(2√(κτ));
arg2 = (L+(L+x))/(2√(κτ));
T0 + (Tm-T0)/2 (Erf[arg1] + Erf[arg2])]
$TextStyle = {FontFamily → "Times", FontSize → 20, FontWeight->"Normal"};
plot1 = Plot[{Temp[t, 1, 1000, 45], Temp[t, 5, 1000, 45], Temp[t, 10, 1000, 45], Temp[t, 20, 1000, 45
Temp[t, 40, 1000, 45]}, {t, 0, 30}, PlotRange → {{0, 30}, {44, 500}},

Background → RGBColor[1, 1, 1],
PlotStyle → {{Thickness[0.004], RGBColor[0, 1, 1]}, {Thickness[0.004], RGBColor[1, 0, 1]}, {Thickne
{Thickness[0.004], RGBColor[1, 0, 0]},
{Thickness[0.004], RGBColor[0, 0, 1]}, {Thickness[0.004], RGBColor[0, 0, 0]}},
Axes → False, Frame → True, FrameStyle → Thickness[0.004], FrameLabel → {None, None, None, Non
FrameTicks → {{5, 10, 15, 20, 25, 30}, {45, 150, 300, 450, 600}, None, None}]
```

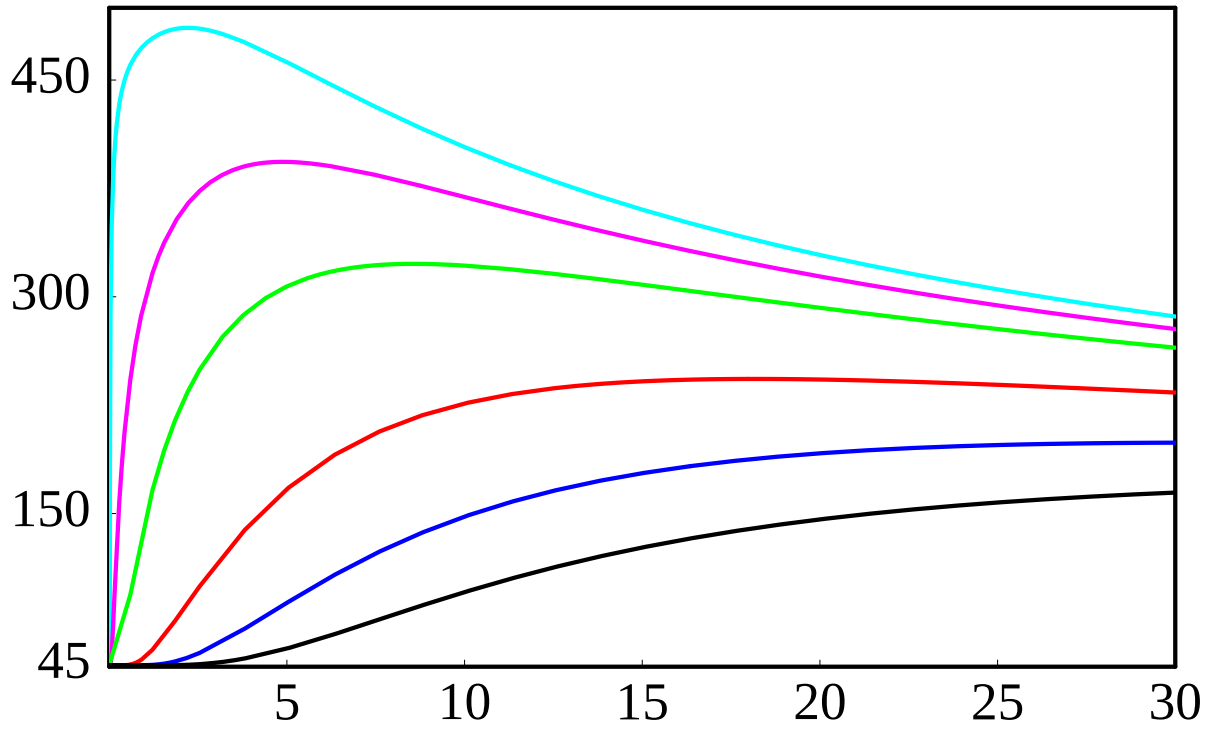

−Geothermal gradient 30° per kilometer−

```
Export["plott45_2.eps", plot1, ImageSize → 72 * 8.5]
```

plott45_2.eps

```
$TextStyle = {FontFamily → "Times", FontSize → 20, FontWeight->"Normal"};
plot2 = Plot[{Temp[t, 1, 1000, 90], Temp[t, 5, 1000, 90], Temp[t, 10, 1000, 90], Temp[t, 20, 1000, 90
Temp[t, 40, 1000, 90]}, {t, 0, 30}, PlotRange → {{0, 30}, {85, 600}},

Background → RGBColor[1, 1, 1],
```

```
PlotStyle → {{Thickness[0.004], RGBColor[0, 1, 1]}, {Thickness[0.004], RGBColor[1, 0, 1]}, {Thickne
{Thickness[0.004], RGBColor[1, 0, 0]},
{Thickness[0.004], RGBColor[0, 0, 1]}, {Thickness[0.004], RGBColor[0, 0, 0]}},
Axes → False, Frame → True, FrameStyle → Thickness[0.004], FrameLabel → {None, None, None, Non
FrameTicks → {{5, 10, 15, 20, 25, 30}, {90, 150, 300, 450, 600}, None, None}]
```

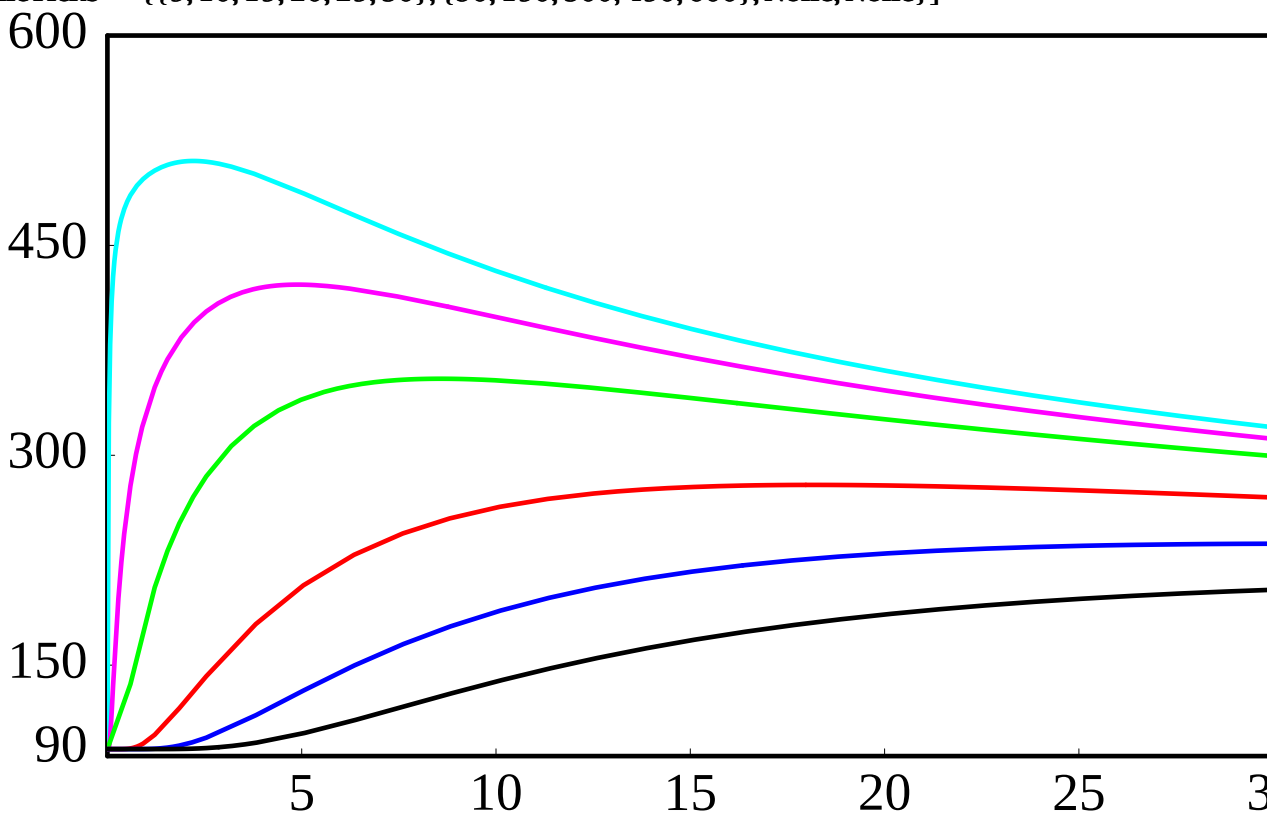

−Geothermal gradient 60° per kilometer−

```
Export["plott90_2.eps", plot2, ImageSize → 72 * 8.5]
```

plott90_2.eps

Appendix I

Accepted abstract for poster presented at the 22 IMOG Meeting

On the next two pages is my abstract for a poster submitted to the 22nd International Meeting on Organic Geochemistry 12-16th September 2005 Seville, Spain.

POS1-6: Thermal effects of basaltic sill emplacement into source rocks on maturity & hydrocarbon generation

J.H. Hubred[1], D.A. Karlsen[1], S. Dahlgren[2]

1) Department of Geosciences P.O.Box 1047, Blindern, N-0316 Oslo, Norway (e-mail: jornar@geo.uio.no)
2) Norwegian Petroleum Directorate, P.O.Box 600, N-4001 Stavanger, Norway Present address: County councils of Buskerud, Telemark and Vestfold, Svend Foynsgt. 9 Fylkeshuset, N-3110 Tønsberg, Norway

In sedimentary basins sills have a tendency to become emplaced in litholgies of lower mechanical competence, like shales, which can possess source rock qualities.

In this study we have been investigating the thermal effects of thick sills on sedimentary rock units at Svalbard, Norway. We believe this study to be directly relevant for sills in large scale sedimentary basins. If sills were emplaced in contact with the source rocks at great burial depth a "source rock on a hot plate" type of situation could arise with a temperature-heat history quite unlike that of small dykes in shallow, water-rich sediments. An additional effect could be related to a regional increase in heat flow if the sills are in a sense "symptoms" of massive ingenious activity as known from other regions.

It is well proven that thin sills and dykes can locally mature source rocks, increase biomarker ratio in extractable compounds and at the same time cause systematic increases in kerogen maturity parameters. Since few organic geochemistry results on large scale sills have been published it was not clear to us if massive sills simply could be viewed as a upscalling phenomena of the smaller dyke and sill systems..

Samples were collected from eight different profiles with sills. The Triassic Botneheia black shale source rock formation, with dominantly marine kerogen, were collected from the hills of Botneheia (Central Spitsbergen), Teistberget (eastern Central Spitsbergen), Krefftberget and Høgrinden (Barentsøya Island). Samples were also collected from the Jurassic Janusfjellet black shale (with dominantly terrestrial kerogen) from Domen (eastern Central Spitsbergen) and the Wilhelmøya Island. Samples from identical black shale units in nearby sections not thermally affected by the sills were also collected and used for comparison.

Organic petrographical descriptions, vitrinite reflectance, Rock Eval, TC and TOC were determined on all 170 samples, whereas metamorphic phase petrology, EOM, Iatroscan TLC-FID, GC-FID, GC-MS and isotopic studies of C and O (in carbonates, kerogen and extracts) were conducted on 48 selected samples.

The vitrinite reflectance (%R_o) profiles show the typical inverted profile closer to the sills i.e. the vitrinite values are as low as 1.5 at 2m from a 23m thick sill, 5 at 5m, decreasing

to 3.5 at 10 meters before reaching the background value of 0.8 at about 20m distance from the sill.

However, no trends in biomarker maturity of the extracts could be detected over the same profile. These results were in the beginning difficult to understand but lead us to suggest that the generative process caused violent mobilization of water, at the same time as generation of light hydrocarbons took place, transporting these light hydrocarbons away. Low maturity biomarkers have at a later stage back diffused from the lower maturity, unaffected shales into the thermally affected shales following cooling of the intrusions. The composition of generated hydrocarbons extracted from the rock samples indicates that hydrocarbon generation by sills may be a less than perfect analogue for "normal" hydrocarbon generation in subsiding basins.

Results from this study would not only be relevant for sill intruded sedimentary basins but would possibly also be relevant for deep water exploration e.g. the Atlantic volcanic margin were sediments have experienced increased heat flows due to magmatic underplating.

Appendix J

Poster presented at the 22 IMOG Meeting

On the next page is my poster presenting the results from this study at the 22nd International Meeting on Organic Geochemistry 12-16th September 2005 Seville, Spain. I am afraid it would be difficult to read it here in my thesis since the original poster is scaled down from A0 to less than A4 to be viewed on one page here in the thesis.

THERMAL EFFECTS OF BASALTIC SILL EMPLACEMENT

Jørnar Heggsum Hubred[1,2)], Dag A. Karlsen[1)] and Sven Dahlgren[3)]

1) Department of Geosciences P.O.Box 1047, Blindern, N-0316 Oslo, Norway 2) jornar@geo.uio.no 3) Norwegian Petroleum Directorate, P.O.Box 600, N-4001 Stavanger, Norway Present address: County councils of Buskerud, Telemark and Vestfold, Svend Foynsgt. 9 Fylkeshuset, N-3110 Tønsberg, Norway

1 Introduction

It is well proven that thin sills and dykes can locally mature source rocks, increase biomarker ratio in extractable compounds and at the same time cause systematic increases in kerogen maturity parameters. Since few organic geochemistry results on large scale sills have been published it was not clear to us if massive sills simply could be viewed as a upscalling phenomena of the smaller dyke and sill systems usually considered.

Samples were collected from eight different profiles with sills. The Triassic Botneheia black shale source rock formation, with dominantly marine kerogen, were collected from the hills of Botneheia (Central Spitsbergen), Teistberget (eastern Central Spitsbergen), Kreftberget and Høgrinden (Barentsøya Island). Samples were also collected from the Jurassic Janusfjellet black shale (with dominantly terrestrial kerogen) from Domen (eastern Central Spitsbergen) and the Wilhelmøya Island.

Organic petrographical descriptions, vitrinite reflectance, Rock Eval, TC and TOC were determined on all 170 samples, whereas EOM, Iatroscan TLC-FID, GC-FID, GC-MS and isotopic studies of C and O (in carbonates, kerogen and extracts) were conducted on 48 selected samples.

2 Results

2.1 Microscope investigations

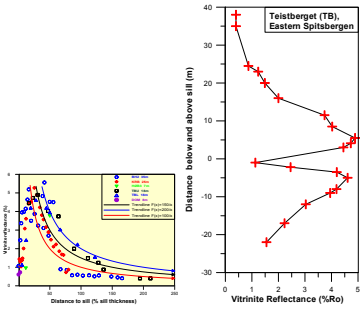

(a) Vitrinite (b) Vitrinite below and above Teistberget 18m thick sill

Figure 1: The response of vitrinite reflectance towards an intrusion contact seems to follow a general pattern. At 25-50% sill thickness from contact, vitrinite seems to reach maximum reflectance. Closer to the contact, vitrinite reflectance drops significantly. A explanation may be a reaction between organic matter and steam at the contact, which results in formation of carbon monoxide. This reaction may be associated with the vitrinite reflectance reversal (Bishop and Abbott 1995).

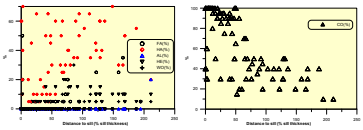

(a) Kerogen types (b) Coaly kerogen

Figure 2: Kerogen description/types against distance to sill in %sill thickness. Coaly kerogen increases on the expense of other types

2.2 Rock Eval

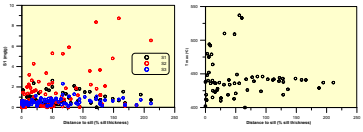

(a) S_1, S_2 and S_3 (b) T_{max} (°C)

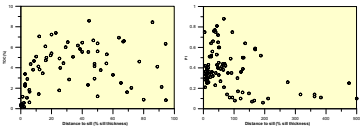

(c) TOC (d) Production index

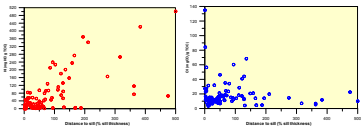

(e) Hydrogen index (f) Oxygen index

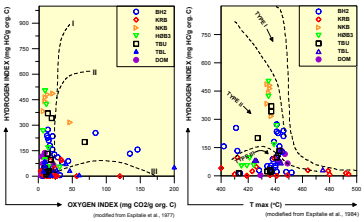

(g) Hydrogen Index - Oxygen Index (h) Hydrogen Index - T_{max}

Figure 3: a) to e); Rock Eval results against distance to sill in %sill thickness. S_2 decreases, S_1 and S_3 unaffected. HI decreases already at 200% sill thickness away from sill. TOC is rather scattered in the samples but seems to be unaffected until 20% sill thickness away from sill were it drops to values below 0.5% at the sill contact. Figures f); HI versus OI and g); HI versus T_{max} show that the kerogen mainly evolved by thermal maturation along the oil-prone Type II pathway. Samples approach higher levels of thermal maturity nearer origo of the plot.

2.3 Composition of hydrocarbons

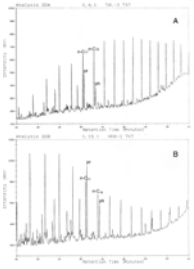

Figure 4: Typical GC-Fid traces for the Botneheia close to sill sample extracts: A; close to sill , B; Far from sill. Close to the sill(s) the GC-FID chromatograms are biased; concentration of n-alkanes dominate on the high carbon number side, like figure 4(A). Far away from the sill, were the sill has not affected the samples, or at places were no sill is present the n-alkane pattern shows a decrease in peak height with increasing carbon number, creating a concave curve in the chromatogram like in figure 4(B).

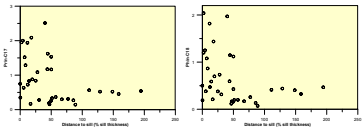

(a) Pristane/n-C_{17} (b) Phytane/n-C_{18}

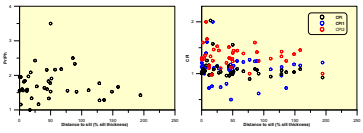

(c) Pristan/Phytan (d) CPI

Figure 5: Parameters calculated from GC-FID results against distance to sill in %sill thickness. Pristane, figure 5(a) predominate over the n-C_{18} from contact at a distance of 50% sill thickness. For phytane figure 5(b) the trend is a little less clear but also here we find samples with a predominance of phytane at distances less than 50% sill thickness. Isoprenoids are among the first compounds to be produced during thermal degradation of kerogen (Burnham et al. 1982). The Pr/Ph ratio of the unaffected sediments is approximately 1.5, figure 5(c). This ratio shows no trend in variation due to the thermal effects of the sill, but results are scattered towards higher and lower values between 90 and 0% sill thickness. Some thermal-related variation is noticeable due to the sill heating but there is no consistent trend within the zone of alteration. In figure 5(d) three different CPI is plotted. The first one CPI is the normal CPI calculated on C_{24} to C_{32}. To evaluate if the extracts had the same odd/even distribution for both short- and longer chained n-alkanes two more CPI values were calculated. CPI1 for the short chained and CPI2 for the long chained. The plot of the different CPI parameters calculated shows differences in value. A possible explanation is that the kerogen is a mixture of marine algal type II kerogen and terestrial type III kerogen.

2.4 Isotope study -lack of trends

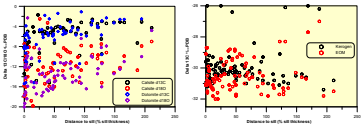

(a) Calsite and Dolomite (b) Kerogen and EOM

Figure 6: Isotope values against distance to sill in %sill thickness. There is a lot of scatter in the data but the values seems to become lighter as the contact is approached.

2.5 Temperature calculations -cooling model

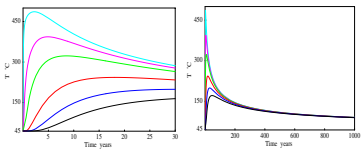

(a) 30 years (b) 1000 years

Figure 7: Calculated theoretical temperatures against time for 6 different distances away from a 30 meter thick sill at 1500 meter depth. Both figures are the same plot. The uppermost curve in both plots is for a distance 1 meter (m) from the sill. The following curves represent respectively 5m, 10m, 20m 30m and 40m away from the sill. It is clear that sill emplacement is a short lived heating event.

3 Conclusions

Contact metamorphism affects the maturity of the intruded rocks to a distance that depends on various factors including temperature differences between the sill and the invaded rock, water content of the sediment, rate of cooling and depth of emplacement.

Vitrinite reflectance indicate maturation of the source rock up to 1.5 times sill thickness away from sill. Hydrocarbon generation was however restricted to 2/3 times sill thickness away from sill. The relatively small volumes of thermally altered source rock prevent the occurrence of commercial quantities of petroleum connected with sill emplacement into source rocks.

Rapid heating of organic matter at these 8 locations at Svalbard resulted in changes which are not directly comparable to those of slow burial maturation. E.g. did vitrinite reflectance respond more rapidly than bitumen composition at high temperatures over a short time.

Figure J.1: *Poster presented at the IMOG 2005 meeting on Organic Geochemistry*

Appendix K

Second poster

On the next page is the draft for yet another poster. This poster is not yet finished but is intended to present the data on the hydrocarbons within the Botneheia sill. Hopefully I will be able to finish this study at some later time.

As with the poster presented in Seville, Spain I am afraid it would be difficult to read it here in my thesis since the original poster is scaled down from A0 to less than A4 to be viewed on one page here in the thesis.

EVIDENCES OF OIL IN SPITSBERGEN CRETACEOUS SILL

Jørnar Heggsum Hubred[1,2)] and Dag A. Karlsen[1)]

1) Department of Geosciences P.O.Box 1047, Blindern, N-0316 Oslo, Norway 2) jornar@geo.uio.no

1 Introduction

A sample collected of the Botneheia sill, intruded into the Botnehia source rock formation at Spitsbergen, Svalbard is proved to contain oil. This oil is probably migrated only a few meters from the intruded Botneheia source rock after the sill cooled down. Extracts on samples from the source rock will be compared to the sill extracts. Extracts will also be compared with oils from the North sea.

The Botneheia Fm is promising as a source rock for the Barents sea because of its widespread distribution throughout the area.

Figure 1: Picture showing the Botneheia source rock covered with snow, the dark pronounced cliff is the sill emplaced into the lithologically weak shale of the Botneheia, Botneheia Spitsbergen. (Photo by the author, 2002)

2 Botneheia source rock

The Botneheia Formation itself forms a coarsening upward succession where basal mudstones grade into siltstone. The formation consists mainly of black shale with abundant small phosphate nodules. Thin to medium thick carbonaceous siltstone beds occur throughout the unit. The upper part is highly calcitic due to numerous thin-shelled bivalves, and these beds form a staking out cliff (Blanknuten Member). The top is marked by a siltstone bed with phosphate nodules, and overlain by grey shale with purple weathering siderite nodules of the Tschermarkfjellet Formation.

The Botneheia Formation is interpreted as a deltaic influenced, regressive shelf deposit, with partly restricted environments in terms of water circulation (Mørk et al. 1982; Mørk et al. 1999).

3 Sill age

Publications on the geology of Svalbard usually speculate on the time of intrusion. Before K-Ar dating of the dolerites were done in the late 1960's Nathorst (1911) among others suggested that the intrusions were Late Jurasic-Early Cretaceous in age, while another group among them Harland (1961) dated them as Late Cretaceous.

Isotopic determinations were first attempted by Gayer et al. (1970) but with to little precision to have stratigraphic significance. The principal study by Burov et al. (1975) yielded 45 determinations from Isfjorden, Storfjorden, Barentsøya, Edgeøya, Wilhelmsøya and Nordaustlandet. Quartz-dolerites are typical of ages around 140Ma and younger olivine-dolerites range around 110 Ma. Burov et al. (1975) concluded two maxima at 144±5 and 105±5 Ma and their plot showing older intrusion to be in Spitsbergen and the Younger on eastern Svalbard.

I can of course not be absolutely sure that the samples used for the time measurements is taken from the same sills as in this study. What is certain is that the sill of this study and the sill sampled for Burov et al. (1975) study, is that the sills are located in the same areas. Burov et al. (1975) study also shows that the sills located in the same areas on Svalbard shows approximately the same time readings. I therefore feel confident that the times for sill emplacement at botneheia is early late Cretaceous at 90±15. Sample nr. in Burov et al. (1975): 2865.

4 Results

4.1 Microscope investigations

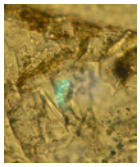

Figure 2: Photograph showing that there is liquid hydrocarbons present within the sill.

4.2 Gas sample

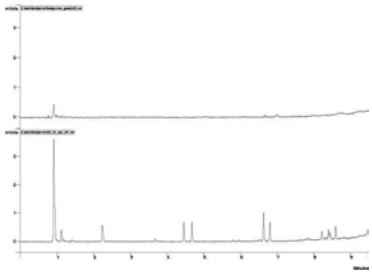

Figure 3: **Topp:** Air sample run through the GC Fid showing the background values of HC at the laboratory the same day as the sill gas sample were run. **Botom:** Sill gas sample showing a clear hydrocarbon signature. Gas sample obtained by crushing a sill rock sample into a airtight mill, grinding chamber.

4.3 Extracts

205g sill rock were crushed using a motorized grinding chamber. Sample were extracted for 48 hours in 200 ml diclormethane (DCM). Extract were slowly evaporated to 5 ml, from which a GC-MS samples were taken.

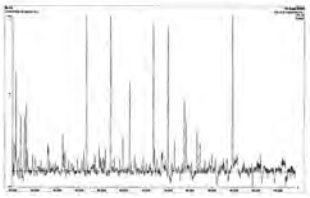

Figure 4: GC-MS 191

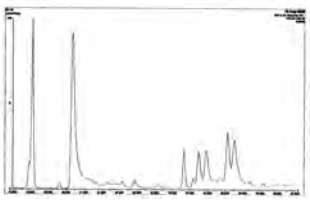

Figure 5: GC-MS 192

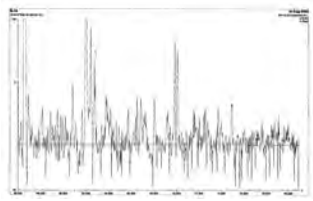

Figure 6: GC-MS 218

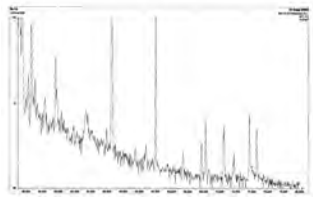

Figure 7: GC-MS 231

5 Conclusions

This is the first results of this study. The GC-MS results contains a lot of contaminants. This would be tried avoided with further evaporating of the extract. From what then is left a new GC-MS run would be tried and a sample wold also be runed through the GC-Fid. When this is done the suggested comparison would be done.

References

Burov, J. P., s. A. A. Krasil, D. V. Firsov, and B. A. Klubov (1975). The age of spitsbergen dolerites (from isotopic dating). *Årbok - Norsk Polarinstitutt 1975*, 101–108.

Gayer, R. A., D. C. Gee, W. B. Harland, J. A. Miller, H. R. Spall, R. H. Wallis, and T. S. Wisnes (1970). *Radiometric age determinations on rocks from Spitsbergen*, Volume 137 of *Norsk Polarinstitutt Skrifter*. Oslo, Norway: Norsk Polarinstitutt.

Harland, W. B. (1961). An outline structural history of spitsbergen. *Geology of the Artic 1*, 68–132.

Mørk, A., W. K. Dallmann, H. Dypvik, E. P. Johannessen, G. B. Larssen, J. Nagy, A. Nottvedt, S. Olaussen, T. M. Pcelina, D. Worsley, and e. Stratigrafic Commitee for Svalbard (1999). Mesozoic lithostratigraphy. In W. K. Dallmann, K. Birkenmajer, H. Dypvik, G. Gjelberg John, B. Keilen Hilde, A. Mørk, J. Nagy, A. Nottvedt, M. Pcelina Tatjana, J. Steel Ron, and D. Worsley (Eds.), *Lithostratigraphic lexicon of Svalbard; review and recommendations for nomenclature use; upper Palaeozoic to Quaternary bedrock.*, pp. 127–214. Tromsø, Norway: Norsk Polarinstitutt.

Mørk, A., R. Knarud, and D. Worsley (1982). Depositional and diagenetic environments of the Triassic and Lower Jurassic succession of Svalbard. In F. Embry Ashton and R. Balkwill Hugh (Eds.), *Arctic geology and geophysics; proceedings of the Third international symposium on Arctic geology.*, Volume 8 of *Memoir*, pp. 371–398. Calgary, AB, Canada: Canadian Society of Petroleum Geologists.

Nathorst, A. G. (1911). Beitraege zur geologie der baeren-insel, spitzbergens und des koenig-karl-landes. *Bulletin - Uppsala Universitet, Mineralogisk-geologiska Institut 10*, 261–415.

Figure K.1: *Poster to be presented at a meeting in the future*

Appendix L

Semester paper

This appendix contain my semesterpaper written autumn 2003. The semesterpaper is a summary on the development of organic geochemistry and a discussion of how organic geochemistry results can be utilized in basin modeling, which at that time were believed to be an important part of my thesis.

The Semester Paper is only included in the printed version of the Thesis.